

**FUNCTIONAL METALLODENDRIMERS:
FROM SOLUTION ENSEMBLES
TO SURFACE-CONFINEMENT**

PROEFSCHRIFT

ter verkrijging van
de graad van doctor aan de Universiteit Twente,
op gezag van de rector magnificus,
prof. dr. F. A. van Vught,
volgens besluit van het College voor Promoties
in het openbaar te verdedigen
op vrijdag 28 september 2001 te 15.00 uur.

door

Hendrik Willem Johan van Manen

geboren op 31 december 1972
te Veenendaal

Dit proefschrift is goedgekeurd door:

Promotor Prof. dr. ir. D. N. Reinhoudt

Copromotor Dr. ir. F. C. J. M. van Veggel

Cover:

The cover displays a *snow crystal* (diameter 1.2 mm) that has been grown artificially from an electric needle (shown out of focus behind the crystal on the right side) in the laboratory of professor Kenneth G. Libbrecht (California Institute of Technology, United States). The highly branched structure is obtained by employing the right set of growth conditions (temperature, humidity, etc.). *Dendrimers*, the macromolecules which form the subject of this thesis, are also characterized by a highly branched architecture. They have typical dimensions that are 100,000-1,000,000 times smaller than the snow crystal displayed on the cover.

“It is a staggeringly small world that is below”

Richard Feynman, 1959

Aan mijn ouders

The research described in this thesis was financially supported by the Council for Chemical Sciences of the Netherlands Organization for Scientific Research (CW-NWO).

ISBN 90-365-1629-3

Contents

Chapter 1

General introduction	1
----------------------	---

Chapter 2

Non-covalent synthesis of metallodendrimers	5
2.1 Introduction	6
2.2 Metals in the dendrimer core	7
2.2.1 Introduction	7
2.2.2 Encapsulated metal clusters	7
2.2.3 Dendrimers containing Ru(II)-bipyridine units as cores	9
2.2.4 Dendrimers containing metal-terpyridine units as cores	11
2.2.5 Coordination of dendrons to metalloporphyrins	12
2.2.6 Other “metals as cores” dendrimers	14
2.2.7 Concluding remarks	15
2.3 Metals as dendrimer branching units	15
2.3.1 Introduction	15
2.3.2 Metallodendrimers based on Ru(II)- and Os(II)-polypyridine complexes	16
2.3.3 Conclusions	21
2.4 Metals as connectors between dendritic building blocks	21
2.4.1 Introduction	21
2.4.2 Organometallic Pt ^{II} /Pt ^{IV} -containing dendrimers	22
2.4.3 Dendrimers based on metal-terpyridine complexes	24
2.4.4 Dendrimers based on metal-acetylide complexes	27
2.4.5 Metallodendrimers based on SCS Pd ^{II} pincer moieties	30
2.4.6 Conclusions	34
2.5 Concluding remarks	34
2.6 References and notes	35

Chapter 3

The coordination chemistry of SCS Pd ^{II} pincers	41
3.1 Introduction	42
3.2 Pincer systems in supramolecular chemistry and transition metal catalysis	42
3.2.1 PCP pincer systems	43
3.2.2 NCN pincer systems	45
3.2.3 SCS pincer systems	48
3.3 Aim and scope of this chapter	50
3.4 Results and discussion	50
3.4.1 Synthesis and characterization of model SCS Pd ^{II} pincer complexes	50
3.4.2 X-ray structure of 7	52
3.4.3 Substitution of the labile MeCN ligand by pyridines	52
3.4.4 Coordination of triphenylphosphine to SCS Pd ^{II} pincers	57
3.4.5 X-ray crystal structure of 10 ·(PPh ₃) ₂	57
3.4.6 Stability of coordinated PPh ₃ complexes	58
3.4.7 Coalescence temperatures of different SCS Pd ^{II} pincer complexes	59
3.4.8 Coordination of other phosphorus-containing ligands	60
3.4.9 Coordination of sulfur-containing ligands	61
3.5 Conclusions	61
3.6 Experimental Section	62
3.7 References and notes	65

Chapter 4

Convergent synthesis of nanosize, layer-block metallodendrimers	69
4.1 Introduction	70
4.2 Coordination chemistry in self-assembly	70
4.2.1 Latticed motifs	70
4.2.2 Cyclic motifs	72
4.2.3 Filamentous motifs	74
4.2.4 Interlaced motifs	75
4.2.5 Mixed-motif complexes	78
4.3 Aim and scope of this chapter	79
4.4 Results and discussion	79
4.4.1 Synthesis of covalent phosphine-functionalized dendritic wedges	79
4.4.2 Coordination of phosphine wedges to SCS Pd ^{II} pincer systems	80
4.4.3 Convergent metallodendrimer growth starting from	

	phosphine wedge G_1^{phos}	82
4.4.4	Convergent metallodendrimer growth starting from phosphine wedge BrG_2^{phos}	85
4.4.5	Characterization of $BrG_2^{\text{phos}}-G_{3,\text{conv}}^{\text{Me}}$ and measurements of methyl proton relaxation rate constants	86
4.4.6	MALDI-TOF mass spectrometry of metallodendrimers	86
4.5	Conclusions	88
4.6	Experimental Section	88
4.7	References and notes	92

Chapter 5

Fluorescent metallodendrimers:

	Toward switchable single molecules	95
5.1	Introduction	96
5.2	Aim and scope of this chapter	99
5.3	Results and discussion	99
5.3.1	Synthesis of rhodamine B-cored metallodendrimers	99
5.3.2	Characterization by NMR spectroscopy and mass spectrometry	101
5.3.3	Switching of rhodamine B-cored metallodendrimers	103
5.3.3.1	UV-Vis spectroscopic studies	103
5.3.3.2	Fluorescence spectroscopic studies	106
5.3.4	AFM measurements on rhodamine B metallodendrimers	108
5.4	Conclusions	109
5.5	Experimental Section	110
5.6	References and notes	111

Chapter 6

	Water-soluble, non-covalent Pd^{II} pincer assemblies	115
6.1	Introduction	116
6.2	Aim and scope of this chapter	120
6.3	Results and discussion	120
6.3.1	Synthesis of water-solubilizing ligands	120
6.3.2	Coordination of water-solubilizing ligands to SCS Pd^{II} pincers	123
6.3.2.1	Complexes with ligand 4	123
6.3.2.2	Complexes with ligand 5	124
6.3.2.3	Complexes with ligand 6	127

6.3.3	Convergent metallodendrimer synthesis starting from ligand 6	128
6.3.4	MALDI-TOF mass spectrometry of water-soluble assemblies	129
6.4	Conclusions	130
6.5	Experimental Section	130
6.6	References and notes	132

Chapter 7

Single molecules on a gold surface:

Isolation, visualization, and coordination chemistry	135
--	-----

7.1	Introduction	136
7.2	Aim and scope of this chapter	138
7.3	Results and discussion	139
7.3.1	Spatial isolation of single dendrimers on a gold surface	139
7.3.1.1	Synthesis of metallodendritic adsorbates	139
7.3.1.2	Isolation of metallodendrimers in SAMs on gold	140
7.3.1.3	Synthesis of a covalent dendritic adsorbate	142
7.3.1.4	Isolation of covalent dendritic adsorbates in SAMs on gold	143
7.3.2	Coordination chemistry on single SCS Pd ^{II} pincers on a gold surface	144
7.3.2.1	Synthesis of adsorbates and solution studies	144
7.3.2.2	Spatial isolation of individual dendrons on gold	147
7.4	Conclusions	149
7.5	Experimental Section	149
7.6	References and notes	152

Chapter 8

Chemistry on isolated, surface-confined dendrimers	157
--	-----

8.1	Introduction	158
8.2	Aim and scope of this chapter	158
8.3	Results and discussion	159
8.3.1	Synthesis of dendritic adsorbate 1	159
8.3.2	Synthesis of a dendritic wedge containing an SCS Pd ^{II} pincer group	162
8.3.3	Coordination chemistry of dendritic wedge 13 in solution	163
8.3.4	Coordination chemistry of pyridine-terminated adsorbate 1 inserted into decanethiol SAMs	164
8.3.5	Covalent growth reactions	166
8.4	Conclusions	169

8.5	Experimental Section	169
8.6	References and notes	173
	Summary	175
	Samenvatting	179
	Dankwoord	183
	Curriculum vitae	185

Chapter 1

General introduction

Nanotechnology, a word already coined in 1974 by Taniguchi, nowadays is thought to lead to the next industrial revolution.^{1,2} In a recent report of the National Science and Technology Council (USA), it has been stated that “nanotechnology’s impact on the health, wealth, and security of the world’s people is expected to be at least as significant as the combined influences in the twentieth century of antibiotics, the integrated circuit, and human-made polymers.”³ In its broadest sense, nanotechnology concerns the (controlled) manipulation of matter at a level of 0.1 nm (the dimension of an atom) to roughly 100 nm (the smallest computer chip line widths at present). Miniaturization of technological devices is one of the major challenges in nanotechnology, the most obvious beneficiary being the microelectronics industry. The last four decades have witnessed a dramatic decrease in computer chip feature sizes, following a trend known as Moore’s law.⁴ Using a “top down” approach, these sizes have been reduced from 15 μm to 0.13 μm ⁵ by conventional techniques such as optical, X-ray, and extreme ultraviolet lithography. However, such methods will reach the limits of technological and economical feasibility in the near future. Therefore, scientific attention is gradually shifting toward a “bottom up” approach that ultimately will allow the fabrication of molecular nanoscale devices from atoms and molecules.^{6,7} Such an approach was already foreseen in 1959 by Richard Feynman in his now famous lecture “There’s plenty of room at the bottom”, in which he stated that “...the principles of physics, as far as I can see, do not speak against the possibility of maneuvering things atom by atom”.⁸ He was proven right when in 1990 scientists at IBM reported the positioning of individual xenon atoms at a nickel surface to write the name of their employer.⁹

It is anticipated that *self-assembly* will play a vital role in applications of nanotechnology. Self-assembly has been defined by George Whitesides as “...the spontaneous association of molecules under equilibrium conditions into stable, structurally well-defined aggregates joined by non-covalent bonds”.¹⁰ In *supramolecular chemistry*¹¹ (the “chemistry of molecular assemblies and of the intermolecular bond”¹²), research efforts are increasingly being directed toward the use of self-assembly as the *Aufbau* principle in the formation of molecular architectures of nanosize dimensions.¹³ The most important types of non-covalent interactions available in self-assembly are van der Waals, hydrophobic, and charge transfer interactions, aromatic π - π stacking, hydrogen bonds, and coordination bonds (arranged in order of increasing

binding strength). In Nature such non-covalent interactions are extensively applied in the formation of complex nanosize structures composed of smaller subunits. Fascinating examples include viruses such as the Tobacco Mosaic Virus (in which more than 2000 identical proteins self-assemble), ribosomes (the cell's machinery for the production of proteins), and double-stranded DNA (in which two nucleotide strands form a double helix held together by hydrogen bonds and aromatic stacking interactions).

Among the non-covalent interactions available to the supramolecular chemist, the metal-ligand coordination bond is increasingly being utilized in the creation of complex, discrete structures of nanosize dimensions.¹⁴ Functionalization of such assemblies is exploited in order to introduce properties that allow them to be addressed individually (*e.g.* by photons, electrons, etc.). The goal is to eventually obtain controllable functional machines at the molecular level.¹⁵ One particular class of molecules that might fulfil these foreseen applications are *dendrimers*, highly branched globular macromolecules of low polydispersity that emanate from a central functionality (the core). *Metallo-dendrimers* form an intensively studied subclass of dendrimers, due to either interesting photoactive or redoxactive properties of the metals themselves or to their coordination chemistry which often facilitates their synthesis, *e.g. via* self-assembly. This thesis will discuss the synthesis of functional metallo-dendrimers in which the coordination of ligands to SCS Pd^{II} pincers (Figure 1.1) is employed as the assembly motif.



Figure 1.1. The SCS Pd(II) pincer system. The fourth coordination site shown on the right is the anchoring position for dendritic building blocks (represented by the sphere labeled “ligand”).

The field of metallo-dendrimers is reviewed in chapter 2. Only dendrimers in which the metal is indispensable for keeping the dendritic structure intact are discussed. Emphasis will be placed on specific properties that may lead to future applications.

In chapter 3 the coordination chemistry of SCS Pd^{II} pincer systems will be discussed in detail. The relative coordination strengths of several ligands have been determined, and the knowledge gathered from this work forms the basis of the metallo-dendrimer syntheses described in subsequent chapters.

The construction of hybrid covalent-noncovalent “layer block” metallo-dendrimers is described in chapter 4. In this work, metallo-dendrimers have been decorated at their periphery

with a hydrophobic layer of covalent Fréchet dendrons, and this greatly enhances their solubility in apolar solvents.

With the knowledge gained from the work discussed in chapter 4, a fluorescent dye has been encapsulated by a metallodendritic architecture. Interestingly, the fluorescence of the core can be switched on and off by iterative treatment with acid and base. The rate of switching is dependent on the size of the dendritic shell around the fluorophore. These results will be described in chapter 5.

Water-soluble, non-covalent Pd^{II} pincer assemblies form the subject of chapter 6. Both carbohydrate and tetraethyleneglycol chains have been employed as peripheral ligands for the SCS Pd^{II} pincer moiety, resulting in water-soluble polyelectrolytes. These might be of interest as recyclable, water-soluble catalysts, to be separated from reaction mixtures *via* nanofiltration methods.

Chapters 7 and 8 describe a strategy for the insertion of isolated dendritic molecules into preformed self-assembled monolayers of alkylthiols on a gold surface. A prerequisite for surface-confinement is the presence of a dialkylsulfide chain that acts as the anchoring moiety for the substrate. Individual, nanometer-sized dendritic molecules can be visualized by atomic force microscopy. Coordination chemistry on isolated dendrimers allow them to be grown on the surface into even larger structures (chapter 8).

References and notes

- ¹ Nanotechnology, a C&EN special report. *Chem. & Eng. News* **2000**, 78 (42), 25.
- ² For comprehensive websites devoted to nanotechnology, see: a) www.zyvex.com/nano/; b) planet-hawaii.com/nanozine; c) www.foresight.org.
- ³ Nanotechnology Research Directions: Interagency Working Group on Nanoscience, Engineering and Technology (IWGN) Workshop Report; Roco, M. C.; Williams, R. S.; Alivisatos, P., Eds.; September 1999. Available on the internet at: <http://itri.loyola.edu/nano/IWGN.Research.Directions/>.
- ⁴ Moore's law states that the number of transistors that can be fabricated on a silicon integrated circuit – and therefore the computing speed of such a circuit – is doubling every 18 to 24 months.
- ⁵ Although the commercial Pentium[®] 4 1.5 GHz microprocessor, introduced in November 2000, is built on 0.18 μm technology, a microprocessor based on 0.13 μm technology was recently fabricated by Intel. See for more information: <http://www.intel.com/research/silicon/index.htm>.
- ⁶ For a review on artificial molecular machines, see: Balzani, V.; Credi, A.; Raymo, F. M.; Stoddart, J. F. *Angew. Chem. Int. Ed.* **2000**, 39, 3348.
- ⁷ For a bottom-up approach to molecular computers, see: Dagani, R. *Chem. & Eng. News* **2000**, 78 (42), 27.
- ⁸ Reprinted in Caltech's Engineering and Science, February 1960, p. 22 and available on the internet at: <http://www.zyvex.com/nanotech/feynman.html>.
- ⁹ "Positioning Single Atoms with a Scanning Tunnelling Microscope"; Eigler, D. M.; Schweizer, E. K. *Nature* **1990**, 344, 524.

- ¹⁰ Whitesides, G. M.; Mathias, J. P.; Seto, C. T. *Science* **1991**, *254*, 1312.
- ¹¹ *Supramolecular Chemistry*; Steed, J. W.; Atwood, J. L.; Wiley: Chichester, 2000.
- ¹² Lehn, J.-M. *Angew. Chem. Int. Ed. Engl.* **1988**, *27*, 89.
- ¹³ Templating, Self-assembly, and Self-organization. *Comprehensive Supramolecular Chemistry*; Lehn, - M., Chair Ed.; Atwood, J. L., Davis, J. E. D., MacNicol, D. D., Vögtle, F., Exec. Eds.; Pergamon: Oxford, UK, 1987-1996; Vol. 9.
- ¹⁴ Chambron, J.-C.; Dietrich-Buchecker, C. O.; Sauvage, J.-P. Transition Metals as Assembling and Templating Species: Synthesis of Catenanes and Molecular Knots. In *Comprehensive Supramolecular Chemistry*; Lehn, J.-M., Chair Ed.; Atwood, J. L., Davis, J. E. D., MacNicol, D. D., Vögtle, F., Exec. Eds.; Pergamon: Oxford, UK, 1987-1996; Vol. 9, Chapter 2. Baxter, P. N. W. Metal Ion Directed Assembly of Complex Architectures and Nanostructures. *ibid.*; Vol. 9, Chapter 5. Constable, E. C. Polynuclear Transition Metal Helicates. *ibid.*; Vol. 9, Chapter 6. Fujita, M. Self-assembled Macrocycles, Cages, and Catenanes Containing Transition Metals in Their Backbones. *ibid.*; Vol. 9, Chapter 7.
- ¹⁵ a) Balzani, V.; Credi, A.; Raymo, F. M.; Stoddart, J. F. *Angew. Chem. Int. Ed.* **2000**, *39*, 3348; b) Gómez-López, M.; Stoddart, J. F. Molecular and Supramolecular Nanomachines. In *Handbook of Nanostructured Materials and Nanotechnology*; Nalwa, H. S., Ed.; Academic Press: London, UK, 2000; Vol. 5, Chapter 3.

Chapter 2

Non-covalent synthesis of metallodendrimers[#]

The field of dendrimers has undergone an explosive growth since the first dendritic structures were reported two decades ago. These three-dimensional, highly branched macromolecules have attracted interest from such diverse areas as polymeric, organic, inorganic, biomedical, theoretical, and physical chemistry. From an application point of view, the incorporation of a range of metals into the dendritic framework is of particular interest. The resulting metallodendrimers might be applied in fields such as catalysis, sensors, medical diagnosis, light-harvesting devices, and nanoparticles. In this chapter, metallodendrimers are discussed in which the metals are essential for creating and maintaining the dendritic structure. This means that all the dendrimers described are assembled non-covalently using coordination chemistry. Where possible, emphasis is placed on the specific behavior and the characterization methods of the dendrimers, because characterization is of utmost importance in establishing their often complicated three-dimensional structure. Finally, it is emphasized that their properties may lead to future applications.

[#] This chapter has been published: van Manen, H.-J.; van Veggel, F. C. J. M.; Reinhoudt, D. N. *Top. Curr. Chem.* **2001**, 217, in press.

2.1 Introduction

After the early theoretical and experimental work by Flory in the 1940s on three-dimensional branched macromolecules,¹ Vögtle *et al.*² described in 1978 the first example of an iterative synthetic methodology towards well-defined branched architectures, now commonly referred to as *dendrimers*. In the mid 1980s, research on these fascinating fractal-like polymers was heavily intensified by the groups of Tomalia³ and Newkome.⁴

A common definition of dendrimers is that they are globular, monodisperse, highly branched macromolecules of well-defined size and shape, that are constructed *via* an iterative sequence of reaction steps. Two main approaches are usually distinguished in their synthesis, *i.e.* the *divergent* (from the core to the outside) and *convergent* (from the periphery inwards) dendritic growth.⁵

The combination of dendrimer chemistry with the specific properties of (transition) metals is very interesting from the point of view of possible applications. Materials with new catalytic, optical, magnetic, electro- and photochemical, and biomedical properties might be created by the combination of dendritic structures and metals. This combines the fields of organic, inorganic, supramolecular, and polymer chemistry into a highly interdisciplinary field of research.

Virtually all positions in the dendritic framework are amenable to metal incorporation. This chapter will focus on metallodendrimers in which the metals are essential for creating the dendritic structure, *i.e.* the metals serve as the structural units “glueing” the organic building blocks together. This narrows the metallodendrimer field to three different classes:

- Dendrimers containing metals as cores;
- Dendrimers containing metals as branching units;
- Dendrimers containing metals as connectors between building blocks.

A consequence of this restriction is that metallodendrimers in which the metals have been positioned at the periphery (*e.g.* ferrocenes,⁶ catalytic sites,⁷ etc.) or have been incorporated as structural auxiliaries (site-specific⁸ or random⁹ inclusion) will not be covered. The reader is referred to some excellent reviews and monographs about (metallo)dendrimers for in-depth information about these and other topics.^{5,6,10} There are also review articles devoted to other specific classes of dendrimers, *e.g.* heteroatom-containing (Si, P, B, Ge, or Bi) dendrimers,¹¹ chiral dendrimers,¹² carbohydrate-containing dendrimers,¹³ light-harvesting dendrimers,¹⁴ dendronized polymers,¹⁵ and dendrimers in diagnostics.¹⁶

In this chapter, most dendritic structures are depicted with one dendron arm fully drawn, whereas the other arms, identical to the one drawn, are represented by cones.

2.2 Metals in the dendrimer core

2.2.1 Introduction

The incorporation of metals at the core of dendrimers may serve a number of purposes. In general, research in this area is aimed at tailoring the properties of the core metal as a function of the type and generation (size) of the organic dendrons folded around it. The shielding of the dendritic core from the environment is a well-known phenomenon and has been under investigation since the first report of core encapsulation by Fréchet *et al.* in 1993.¹⁷ A review about this topic has recently appeared.¹⁸

2.2.2 Encapsulated metal clusters

The encapsulation of electroactive moieties is important in understanding electron transfer found in biological systems¹⁹ (e.g. cytochromes) and also in the construction of molecular electronic devices.²⁰ By attaching dendrons to a porphyrin core, enzyme mimics have been prepared in which electron transfer to or from the porphyrin is affected by the bulkiness of the dendrons and the microenvironment they create around the porphyrin.²¹

Iron-sulfur clusters serve in nature as electron transfer and storage sites, and as structure-enforcing units in enzymes.¹⁹ Gorman and coworkers have placed dendritic wedges (G1-G4) around electroactive iron-sulfur clusters of the form $[\text{Fe}_4\text{S}_4(\text{SR})_4]^{2-}$, resulting in new hybrid inorganic/organic dendritic architectures.²² The dendrimers were prepared by a ligand exchange reaction of aromatic thiol-substituted dendrons on $(n\text{-Bu}_4\text{N})_2[\text{Fe}_4\text{S}_4(\text{S}\text{-}t\text{-Bu})_4]$. The second generation dendrimer is shown in Figure 2.1.

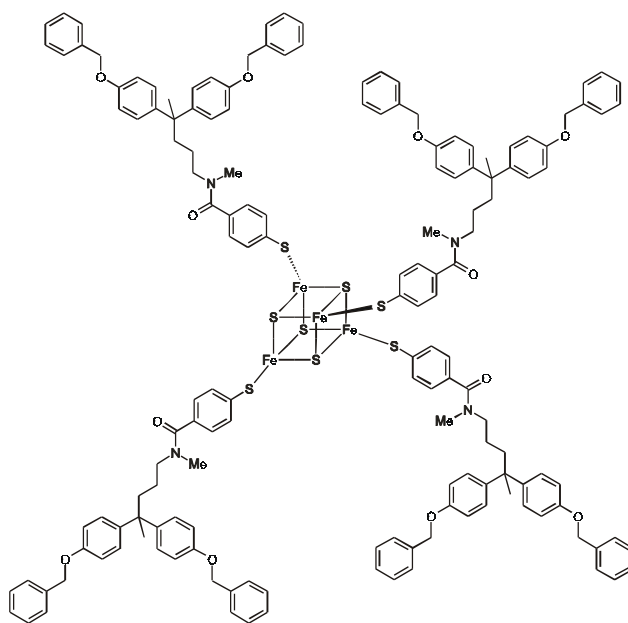


Figure 2.1. Second generation dendrimer containing an iron-sulfur cluster as a core.

In the ^1H NMR spectrum, a substantial broadening and change in chemical shifts of the thiolate aromatic ring protons close to the paramagnetic iron-sulfur cluster was observed. The small longitudinal relaxation time constants (T_1) of these protons confirmed their fast relaxation, which is expected for protons in close proximity to a paramagnetic group. In a subsequent study,²³ a dramatic decrease in T_1 values for the protons in the dendrimers containing a paramagnetic iron-sulfur core was found in comparison with similar dendrimers that contained a diamagnetic tetraphenylmethane core. This observation led the authors to conclude that protons in each generation of the dendrimers must approach the core of the molecule closely in order to experience the attenuation of T_1 values. This conclusion is consistent with radial density distributions of different dendritic generations, as calculated from molecular dynamics simulations.

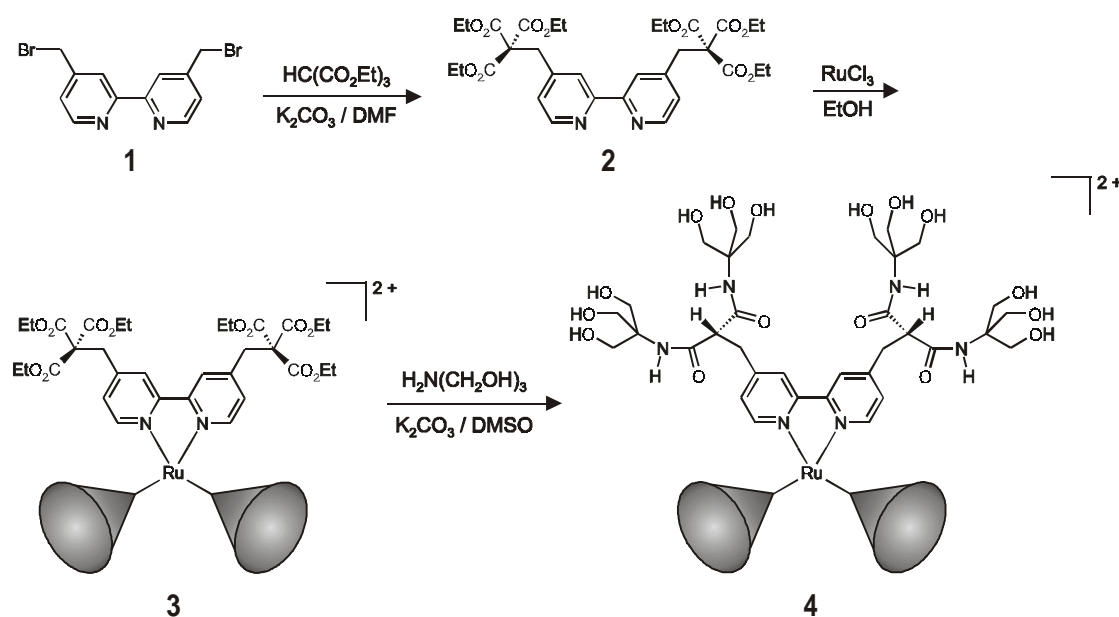
The insulating effects of increasing steric bulk of the dendritic ligands on the electrochemical properties of the iron-sulfur core were demonstrated by cyclic voltammetry. Going from G0 to G4, increasingly more negative reduction potentials $E_{1/2}$ were observed. Moreover, G0-G3 displayed increasingly larger voltage differences between the current maxima of the reduction and return oxidation waves (ΔE), which indicates an increasing kinetic difficulty of reduction/oxidation. In the dendritic zinc porphyrins reported by Diederich *et al.*,^{21a} the increasingly electron-rich microenvironment created by the dendritic branches around the core hinders reduction and facilitates oxidation of the porphyrin ring, which is reflected in more negative reduction potentials and less positive oxidation potentials, respectively, with increasing generation. Apparently, electronic effects rather than steric effects primarily determine the redox potentials of the core. Clearly, the type of dendrimer positioned around the core has a profound influence on its electrochemical properties. This was recently confirmed by Gorman *et al.*,²⁴ who compared iron-sulfur dendrimers containing rigid phenylacetylene-type dendrons with the flexible iron-sulfur dendrimers described above. Diffusion coefficients and corresponding hydrodynamic radii of the dendrimers in dilute solution were determined by pulsed field gradient spin-echo NMR and chronoamperometry. For both the flexible and rigid series, both techniques showed that increasing the dendrimer generation results in a decrease in diffusion coefficient and thus an increase in hydrodynamic radius. Whereas the flexible series of dendrimers displayed a large dependence of the hydrodynamic radius on the solvent, the rigid dendrimers showed little change in radius as a function of solvent. This observation is consistent with the rigid and “shape persistent”²⁵ nature of these dendrimers. Heterogeneous electron-transfer rate constants indicate that the rigid dendrimers attenuated more effectively the electron transfer rate than the flexible ones. These results were rationalized using computational conformational searching which indicated an off-center “mobile” iron-sulfur core in the flexible series and a central and relatively immobile core in the rigid series.

Recently, other metal clusters have also served as inorganic dendritic cores. Dendrimers $\text{Mo}_6(\mu_3\text{-Cl})_8(\text{OR})_6$ (R = dendrons, G0-G2) were constructed by Gorman *et al.* from triflate- or methoxy-capped pseudo-octahedral clusters $[\text{Mo}_6\text{Cl}_8(\text{X})_6]^{2-}$, X = OTf or OMe) by ligand

exchange reactions with dendrons containing focal phenoxide groups.²⁶ Similarly, exchange of labile acetonitrile ligands in the hexanuclear $[\text{Re}_6\text{Se}_8(\text{MeCN})_6](\text{SbF}_6)_2$ cluster for pyridine-functionalized dendrons (G1) produced the corresponding dendrimers in high yields after chromatography.²⁷ Both these hybrid organic/inorganic dendrimers were characterized by electrospray mass spectrometry, which clearly showed the molecular ion peaks.

2.2.3 Dendrimers containing Ru(II)-bipyridine units as cores

Since the complexes of the $[\text{Ru}(\text{bpy})_3]^{2+}$ family (bpy = 2,2'-bipyridine) show a unique combination of photophysical and redox properties,²⁸ incorporation of these moieties as cores into dendritic frameworks offers the possibility of modifying their properties as a function of the dendritic generation. This was investigated by Vögtle, Balzani, and their coworkers,²⁹ who synthesized dendritic ligands by a divergent strategy, starting from 4,4'-functionalized 2,2'-bipyridines. Following procedures reported by Newkome *et al.*,³⁰ 4,4'-bis(bromomethyl)-2,2'-bipyridine **1** was alkylated with triethyl methanetricarboxylate to obtain the dendritic hexaester **2** shown in Scheme 2.1. Three of these ligands were subsequently coordinated to Ru^{II} to give complex **3**, which was finally converted into the hydrophilic hydroxyl-containing Ru^{II} -dendrimer **4** by amidation with tris(hydroxymethyl)aminomethane.



Scheme 2.1. Synthesis of a first generation, hydrophilic metallodendrimer based on the $[\text{Ru}(\text{bpy})_3]^{2+}$ -motif.

Unfortunately, dendritic growth beyond generation one was not possible by this synthetic method. Therefore, a slightly different methodology was pursued based on dendrimer chemistry developed by Diederich and coworkers.³¹ The second generation Ru^{II} dendrimer **5** (containing 54 peripheral esters) prepared in this manner is depicted in Figure 2.2.

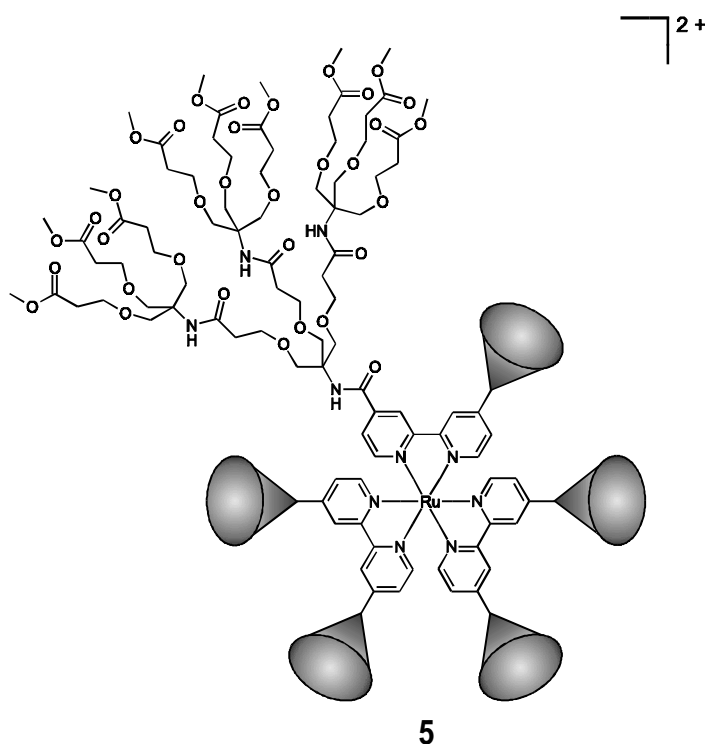


Figure 2.2. Second generation Ru(II)-containing metallodendrimer **5**.

The absorption and emission spectra of complexes **4** and **5** are similar to those of the unsubstituted parent Ru^{II}-bipyridine complexes. However, the large dendritic complexes exhibited a more intense emission and a longer excited-state lifetime than [Ru(bpy)₃]²⁺ in aerated solutions. This is due to the shielding effect of the dendritic branches on the Ru^{II}-bipyridine core, thereby limiting the quenching effect of dioxygen (for **5** the rate constant of dioxygen quenching is twelve times smaller than for [Ru(bpy)₃]²⁺). The authors emphasize the importance of long-lived luminescent excited states in immunoassay applications, since the label signal can be read after the decay of the sample background fluorescence.

Combining the [Ru(bpy)₃]²⁺ core with peripheral naphthyl units, Vögtle and Balzani *et al.*³² also reported that very efficient energy transfer takes place from the potentially fluorescent excited states of the aromatic moieties of the dendritic wedges (naphthyl-functionalized Fréchet-type aryl ether dendrons were used in this case) to the Ru^{II} dendritic core. This antenna effect, potentially useful in harvesting sunlight,³³ was again accompanied by reduced dioxygen quenching of the core luminescence, although the effect was smaller than reported for complex **5** (Figure 2.2).

Recently, Vögtle, De Cola, Balzani, and their coworkers extended the work on Ru^{II}-dendrimers by decorating the periphery of Ru^{II}-bipyridine aryl ether dendrimers with either benzyl or 4'-*tert*-butylphenoxy groups.³⁴ All dendrimers showed the characteristic luminescence of the [Ru(bpy)₃]²⁺-type core, and a similar protection of the luminescent excited state of the core from dioxygen quenching was observed as discussed above. For the compounds containing the 4'-*tert*-butylphenoxy peripheral units, the electrochemical behavior and the

excited-state electron-transfer quenching by cationic (methyl viologen dication, MV^{2+}), neutral (tetrathiafulvalene, TTF), and anionic (anthraquinone-2,6-disulfonate anion) quenchers, which quench³⁵ the 3MLCT excited state of $[Ru(bpy)_3]^{2+}$, were investigated. The core of the largest dendrimer (24 peripheral 4'-*tert*-butylphenoxy groups) showed an electrochemical behavior typical of encapsulated electroactive units. The quenching rate constants, obtained by Stern-Volmer kinetic analysis, decreased with increasing number and size (= generation) of the dendritic branches for each quencher. The magnitude of this effect depends on the quencher and is largest for MV^{2+} and smallest for TTF.

2.2.4 Dendrimers containing metal-terpyridine units as cores

Whereas dendritic *growth* based on metal terpyridines is well-developed (see section 2.4.3), the *encapsulation* of terpyridine complexes has received less attention, particularly in comparison with metal *bipyridine* complexes (*vide supra*). This might be due to the absence of room temperature luminescence of $[Ru(terpy)_2]^{2+}$, which renders terpyridine-based assemblies less suitable for practical applications involving light-induced processes. However, there are a few exceptions. In a first attempt to mimick redox proteins, Chow *et al.* synthesized aryl ether dendrons (G1-G3) containing a focal terpyridine and they studied the redox properties of the corresponding iron(II) complexes.³⁶ The encapsulation was indicated by a decreasing reversibility of the metal redox centers with increasing dendritic generation. These cyclic voltammetry results were rationalized by the steric hindrance caused by the bulky dendritic shell, hindering the metal complexes from approaching the electrode surface. Similar effects due to shielding of the redox center are well known for cytochrome *c* and other electron-transfer proteins.^{37,38} The dendritic iron(II) complexes were further characterized by X-ray photoelectron spectroscopy (XPS), which showed that the solid-state coordinating environments of the iron(II) of different generations were very similar.

A methodology for preparing bis-dendrimers, developed by Newkome and coworkers,³⁹ also utilized the metal complexation ability of terpyridines. Starting from a carboxylic acid-functionalized terpyridine, divergent dendritic growth (G1-G4) followed by complexation of the terpyridine with $RuCl_3$ led to the first half of the bis-dendrimer (Figure 2.3a). Subsequent connection of the second terpyridine dendrimer (using 4-ethylmorpholine as the reducing agent) provided the Ru^{II} bis-dendrimers (Figure 2.3b) in yields of around 60%.

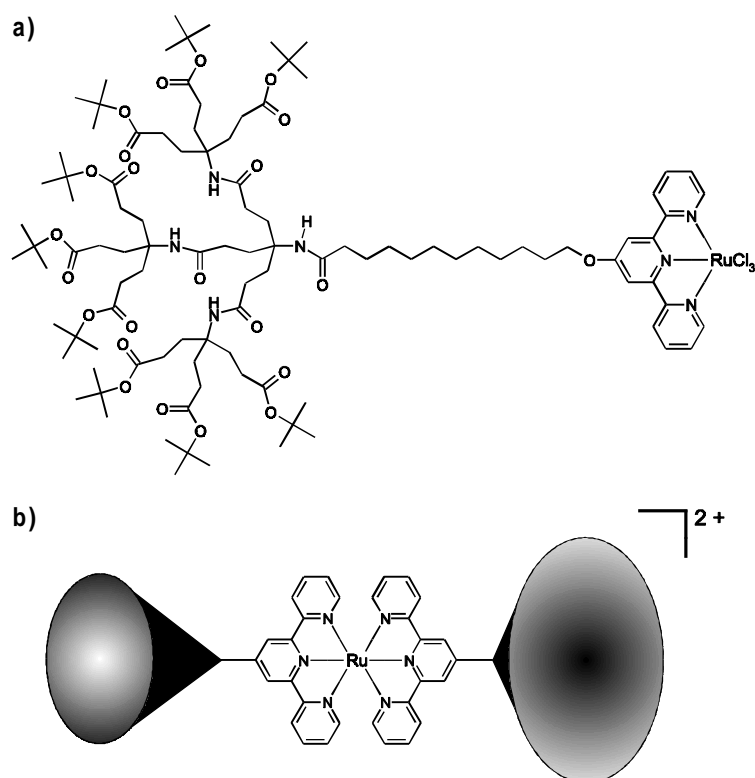


Figure 2.3. Half (a) and complete (b) bis-dendrimers containing Ru(II)-terpyridine units.

Cyclic voltammetry showed that for the low generation bis-dendrimers both the cationic and anionic scans display electrochemically and chemically reversible processes. However, for the sterically congested bis-dendrimers irreversible behavior (both electrochemically and chemically) was found, similar to the results of Chow *et al.* (*vide supra*). Moreover, hardly any potential shifts were found. Interestingly, the sequential growth of the bis-dendrimer allows the two halves to differ in size, structure, and properties. In the reported examples the two halves only differ in generation (Figure 2.3b).

2.2.5 Coordination of dendrons to metalloporphyrins

There are a few porphyrin-containing dendrimers in which coordination of dendritic ligands to the porphyrin metal is exploited in the growth of larger dendritic structures. Aida *et al.* used zinc porphyrins decorated with four aryl ether dendrons (Figure 2.4) to study the interpenetrating interaction of imidazole-functionalized dendrons with the zinc center.⁴⁰

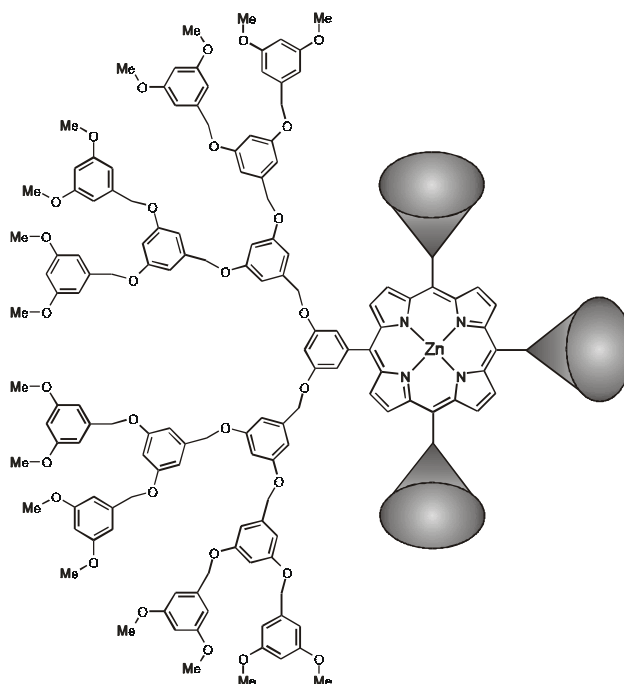


Figure 2.4. Dendritic zinc porphyrin used for the interaction with imidazole-functionalized dendrons.

The singlet excited state of the zinc porphyrin is not affected by the encapsulation within the dendritic framework. This was evidenced by ^1H NMR pulse relaxation time (T_1) measurements, which indicated that the conformational flexibility of the porphyrin skeleton is retained upon increasing the dendrimer generations. Spectrophotometric titration of dendritic imidazoles (G1, G2, and G4) to the porphyrin dendrimers (a one-to-one complexation in all cases) showed a decrease in binding constant upon increasing the size of either the dendritic imidazole or porphyrin, especially in going from the third to the fourth generation dendritic porphyrin. It is noteworthy that the G4-imidazole binds to the G5-porphyrin at all ($K_a = 2.4 \times 10^2 \text{ M}^{-1}$ in CH_2Cl_2 at 20°C), suggesting significant flexibility of the aryl ether dendritic parts.

Coordination of pyridyl-functionalized porphyrins to ruthenium(II) porphyrins was exploited recently by Sanders *et al.* in the construction of dendritic multiporphyrin arrays.⁴¹ These are of considerable interest^{42,43} due to their excellent photophysical and redox properties, which make them suitable candidates for light-harvesting devices, molecular wires, photosensitizers, and (semiconducting) liquid crystalline materials. Sanders and coworkers synthesized a porphyrin trimer dendritic wedge containing a pyridyl group at the focal point. Two of these dendrons were subsequently attached to a Ru^{II} porphyrin by sequential axial displacement of the solvent and CO ligands coordinated to Ru^{II} in the starting porphyrin, to give the heptamer shown in Figure 2.5. The multiporphyrin arrays were characterized by NMR and UV spectroscopy.

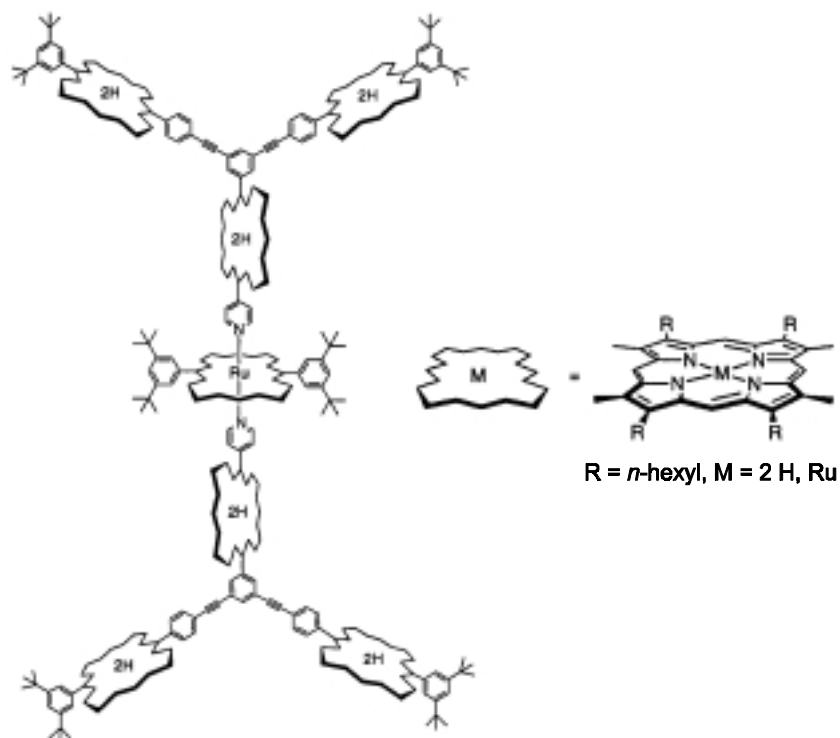


Figure 2.5. Dendritic porphyrin heptamer synthesized by Sanders and coworkers.⁴¹

2.2.6 Other “metals as cores” dendrimers

Recently, Aida *et al.* have attached three aryl ether dendrons (G2-G4) to 1,4,7-triazacyclononane and studied the oxygen-induced dimerization of the corresponding Cu^I complexes, as a non-heme metalloprotein mimic.⁴⁴ Both the rate of formation of the bis(μ -oxo)dicopper(III) moiety and its stability towards oxidative self-decomposition are affected by the size of the attached dendrons (a “dendritic effect”).

The binding of organic dendritic wedges to core (transition) metals has been undertaken in order to change the properties of the metal or to impart new functions on the resulting dendrimer-metal combination. An example of the latter has been reported by Catalano and Parodi.^{45,46} Dendritic Fréchet wedges (G1-G2) were functionalized with focal phosphines and these dendrons were coordinated to Ir^I to produce the dendritic analogs of Vaska’s compound. IR and ³¹P NMR spectroscopy showed that C₆₀ reacted reversibly with the Ir^I dendrimers *via* an oxidative addition. The reversible binding was probed by examining the ³¹P NMR line widths as a function of temperature. This gave the thermodynamic data and equilibrium constants ($K = 388 \text{ M}^{-1}$ at 257 K and 5 M^{-1} at 293 K in chlorobenzene for the G2 Ir^I-C₆₀ complex). The dendritic arms do not play a major role in fullerene binding.

Fréchet and Kawa coordinated three aryl ether dendritic wedges functionalized at the focal point with carboxylates around trivalent lanthanide ions (Er, Eu, and Tb, Figure 2.6) in order to shield the lanthanides from one another for possible use in fiber optics amplification.⁴⁷

Site isolation is important in photoluminescence as it decreases the rate of self-quenching between metal atoms.

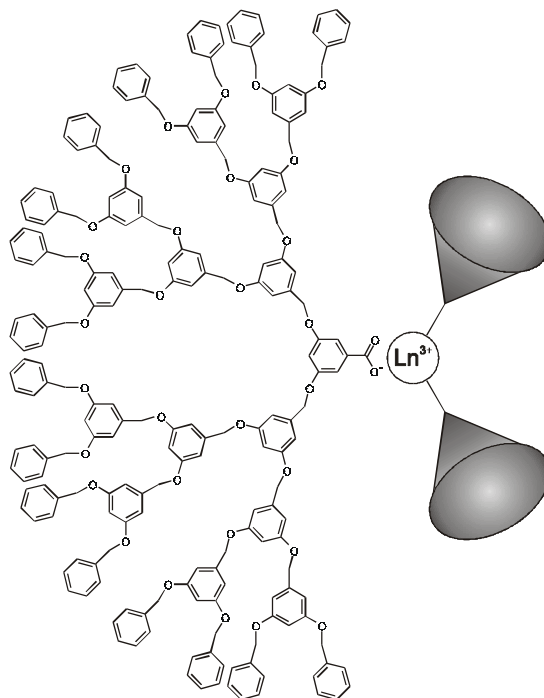


Figure 2.6. Fourth generation dendrimer containing lanthanide ions in the core.

Higher generation dendrimers indeed exhibited enhanced luminescence. The authors observed a non-conjugated “antenna effect” with energy transfer from the dendritic ligands to the lanthanide core.

2.2.7 Concluding remarks

From this section, it can be concluded that positioning metals at the core of dendrimers can significantly alter their properties. More specifically, metals can be shielded from each other and from the environment by incorporation into a dendritic framework. These features might be exploited in applications such as protein mimics, catalysis, immunoassays, and energy-harvesting devices.

2.3 Metals as dendrimer branching units

2.3.1 Introduction

A second alternative for metallodendrimer synthesis involves the coordination of more than one ligand to a (transition) metal that serves to introduce the necessary branching into the dendritic framework. Here, branching occurs at the metal and not in the dendritic building

blocks. The majority of metallodendrimers of this class originates from the combined efforts of the groups of Balzani, Campagna, and Denti (see also ref. 48).

2.3.2 Metallodendrimers based on Ru(II)- and Os(II)-polypyridine complexes

Dendrimers containing Ru^{II}- and Os^{II}-polypyridine complexes arose from precursors such as the hetero-tetrametallic complex reported in 1989 by Balzani and coworkers (Figure 2.7).⁴⁹

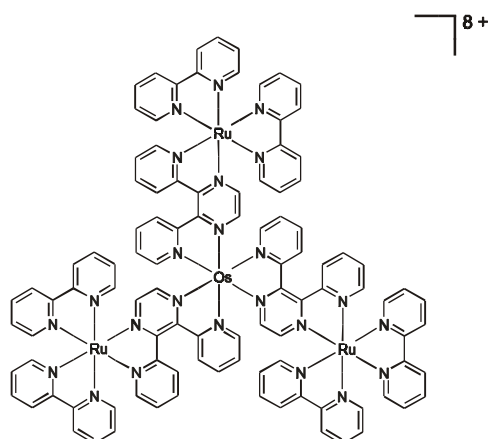
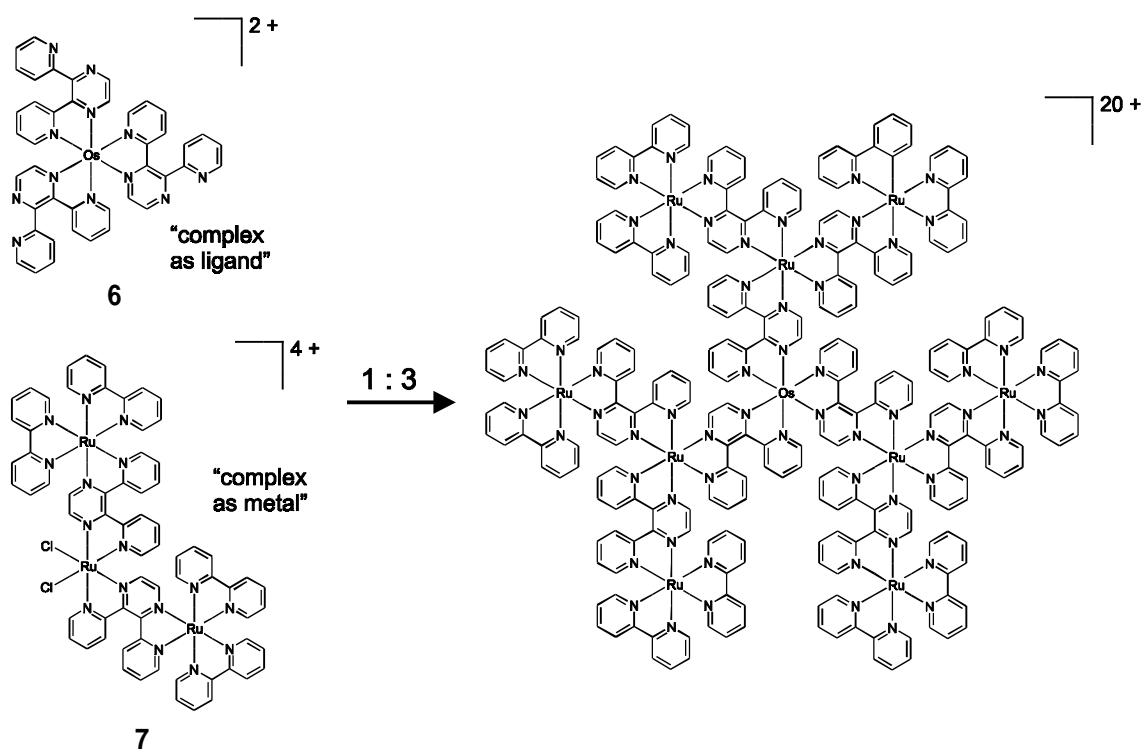


Figure 2.7. Heterometallic tetrameric complex reported by Balzani and coworkers.⁴⁹

Due to their outstanding photophysical and electrochemical properties, such Ru^{II}- and Os^{II}-complexes have been used extensively as luminescent species and as reactants or mediators in light-induced and light-generating electron transfer processes.²⁸ Replacing the peripheral bipyridine units (Figure 2.7) with 2,3-bis(2-pyridyl)pyrazine ligands (2,3-dpp, which in Figure 2.7 are coordinated to the Os^{II} core) opened the way to higher, luminescent oligomers. The synthesis, photophysical, and electrochemical properties of decanuclear homo- and heterometallic polypyridine complexes were reported in 1992.⁵⁰ A “complexes as metals” and “complexes as ligands” strategy was followed in the assembly of the dendritic structures. This strategy relies on a protection/deprotection procedure in which one metal complex is used as a ligand equivalent (**6** in Scheme 2.2) and another as a metal equivalent (**7** in Scheme 2.2).



Scheme 2.2. The “complexes as metal” / “complexes as ligand” strategy in the assembly of Ru(II)- and Os(II)-containing metallodendrimers.

After deprotection of the chlorides with six equivalents of Ag^+ , three equivalents of the “complex metal” species were added to the “complex ligand” core to produce the decanuclear dendrimer in good yields. With this procedure, equivalent sites can only be occupied by the same type of metal ion. As reported later, protection of one of the chelating sites in the bridging ligands (2,3-dpp) allows the coordination of different metals to the same bridging ligand, leading to less symmetric dendrimers (*vide infra*). In principle, each decanuclear compound can exist as different geometrical isomers depending on the arrangement of the ligands around the metal ions. Each complex can also be a mixture of several diastereomeric species, owing to the chiral nature of each metal center. This renders structural characterization of these systems difficult. However, the chirality of similar decanuclear Ru^{II} dendrimers can be controlled using substitutionally inert Ru^{II} trisdiimine complexes as chiral synthons (*vide infra*).⁵¹ The decanuclear complexes exhibit extraordinary large molar absorption coefficients in the UV and visible spectral region. Furthermore, the excitation energy could be channeled in the desired direction by a tailored choice of the components (schematically depicted in Figure 2.8).

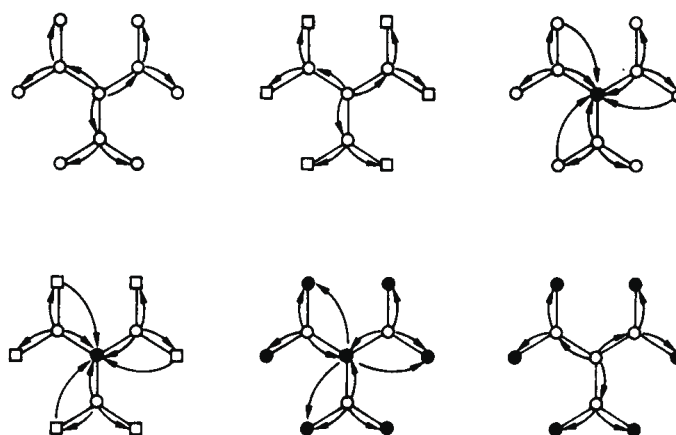


Figure 2.8. Directional energy transfer (represented by the arrows) in Ru(II)- and Os(II)-containing metal dendrimers. Empty and full circles indicate Ru(II) and Os(II), respectively. In the peripheral positions, circles and squares indicate $M(\text{bpy})_2$ and $M(\text{biq})_2$ ($\text{biq} = \text{biquinoline}$) components, respectively.

The electrochemical data of the decanuclear complexes revealed a selectivity in the metal oxidation behavior based on its nature and location in the array, offering a fingerprint of the topological structure of the complexes. The near-infrared luminescence of several polynuclear Os^{II} and Ru^{II} complexes, including two decanuclear dendrimers of the type described above, was reported by Juris *et al.*⁵² Furthermore, light scattering and conductivity experiments showed that the decanuclear complexes aggregate at room temperature in solution at very low concentrations. This was attributed to attractive forces between the hydrophobic assemblies.⁵³

While the above discussed construction of decanuclear complexes could be regarded as *convergent* dendritic growth (although no dendritic growth was required in the preparation of the “wedges”), iterative *divergent* dendritic growth can only be performed using potentially bifunctional building blocks, where one of the two functional groups is temporarily blocked or present as a masked functionality. Such a bifunctional complex was exploited by Serroni *et al.* in the divergent construction of docosanuclear (22 metals) Ru^{II} dendrimers.⁵⁴ Monomethylation of 2,3-dpp followed by complexation of the free chelating sites to Ru^{II} resulted in the dendritic building block **8** (Figure 2.9).

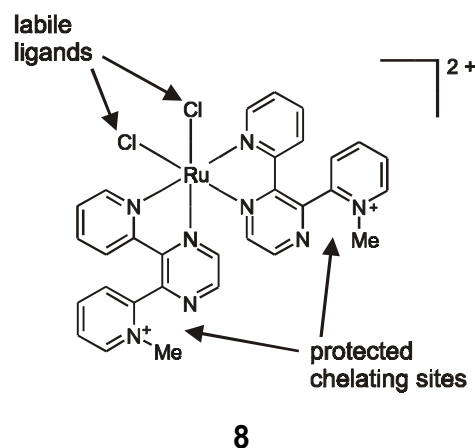


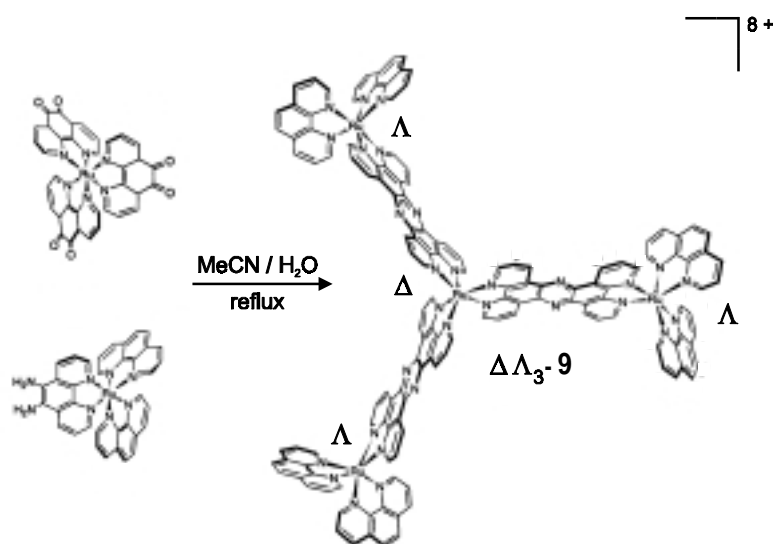
Figure 2.9. Bifunctional Ru(II)-complex used in the divergent construction of metallodendrimers.

After removal of the chloride ligands with AgNO_3 , three of these building blocks were coupled to the core (**6** with Ru^{II} instead of Os^{II} , Scheme 2.2) to produce the corresponding tetranuclear complex in 70% yield. Demethylation of the six chelating sites with DABCO followed by complexation of either the mononuclear building block **8** or the trinuclear capping complex **7** (Scheme 2.2) provided a second generation protected decanuclear complex⁵⁵ or a docosanuclear dendrimer, respectively (both homonuclear complexes). The iterative divergent dendritic growth has so far not been extended beyond the decanuclear second generation complexes. The synthesis, luminescence, and redox properties of a heteronuclear analog of the docosanuclear dendrimer have also been reported.⁵⁶

A number of studies on the properties of similar polynuclear complexes with different metals and/or ligands has been reported.⁵⁷ However, the number of *dendrimers* of the “metals as branching units” type is quite limited. A dendritic heptanuclear Ru^{II} complex containing 1,10-phenanthroline as peripheral ligands and 1,4,5,8,9,12-hexaazatriphenylene (HAT) as bridging ligands was synthesized in a divergent manner by Kirsch-De Mesmaeker and coworkers.⁵⁸ This dendritic coordination complex was characterized by electrospray mass spectrometry (ES-MS). This technique has proven its usefulness in the characterization of metallodendrimers ever since (including in our group, *vide infra*). All peaks observed in the ES spectrum correspond to a single heptametallc Ru^{II} complex associated with different types of counteranions (resulting from the hydrolysis of PF_6^- anions). The excited state of the heptanuclear dendritic Ru^{II} complex was studied by femtosecond transient absorption spectroscopy.⁵⁹ Scanning tunneling microscopy (STM) showed ordered patterns on graphite, indicating packing of the metallodendrimer molecules on the surface.⁶⁰ A distance of $27 \pm 2 \text{ \AA}$ between adjacent lamellae suggests that these are rows of dendritic molecules.

As mentioned before, unequivocal characterization (*e.g.* by NMR) of the dendrimers reported by Balzani and coworkers has been hampered by the presence of numerous diastereoisomers in such polynuclear complexes. This problem originates from the synthetic strategy, in which the complexes are usually assembled *via* ligand displacement reactions with

little or no direct control for the product stereochemistry. Additional stereochemical complications arise when asymmetrically substituted bidentate ligands are being used. An elegant strategy that allows the assembly of enantiomerically pure oligonuclear and dendrimeric Ru^{II} complexes from chiral synthons has been developed by MacDonnell and coworkers.⁶¹⁻⁶³ An irreversible covalent reaction which does not involve ligand displacement at the chiral centers is used to couple the metal centers, thereby avoiding disturbance of the metal-complex stereochemistry. First generation dendritic D_3 -symmetric tetranuclear complexes were described in 1997.^{61,62} A representative example (Scheme 2.3) shows that the condensation reaction between the *o*-dione moiety of the enantiopure Δ -[Ru(1,10-phenanthroline-5,6-dione)₃]²⁺ complex and the *o*-diamine function of enantiopure Λ -[Ru(1,10-phenanthroline)₂(1,10-phenanthroline-5,6-diamine)]²⁺ yields the rigid D_3 -symmetric trigonal-propeller-shaped complex $\Delta\Lambda_3$ -**9** containing tetrapyrido[3,2-*a*:2',3'-*c*:3'',2''-*h*:2'',3''-*j*]phenazine bridges between stereocenters. The three other D_3 isomers were prepared similarly.



Scheme 2.3. Synthesis of enantiomerically pure, first generation dendritic D_3 -symmetric tetranuclear Ru(II)-complexes.

The high symmetry of the complexes greatly facilitated their characterization by ¹H, ¹³C, COSY, and HMQC NMR spectroscopy. MALDI-TOF mass spectrometry, a well-established technique to characterize (metallo)dendrimers nowadays, gave the parent molecular ion signals corresponding to the species [**9** - *n*PF₆]⁺ (*n* = 3-8). Finally, the absolute stereochemistry and optical purity of each of the stereoisomers was established by circular dichroism (CD) spectroscopy. Recently,⁶³ further divergent dendritic growth was achieved from the isomers of **9** by oxidation of the terminal phenanthrolines to quinones (which proceeds with retention of the stereochemistry despite the harsh reaction conditions, H₂SO₄/HNO₃/NaBr at 100 °C), followed by condensation with Λ -[Ru(1,10-phenanthroline)₂(1,10-phenanthroline-5,6-diamine)]²⁺. The decameric Ru^{II} complexes were isolated in \approx 20% yield as robust metallodendrimers (stable

to heat, concentrated acids and bases, and racemization) and were characterized by electrospray mass spectrometry and ^1H and COSY NMR spectroscopy. Interestingly, the two diastereomeric decamers $\Lambda_6\Delta_3\Lambda\text{-Ru}_{10}$ and $\Lambda_6\Lambda_3\Lambda\text{-Ru}_{10}$, which differ in their stereochemistry at three dendritic sites, display remarkably different overall topologies, as suggested by molecular modeling. The *global* stereochemical descriptors *T* (achiral) and *P* (clockwise) were introduced to describe the flat disk-like structure of $\Lambda_6\Delta_3\Lambda\text{-Ru}_{10}$ (Figure 2.10 left) and the right-handed propeller structure of $\Lambda_6\Lambda_3\Lambda\text{-Ru}_{10}$ (Figure 2.10 right), respectively.

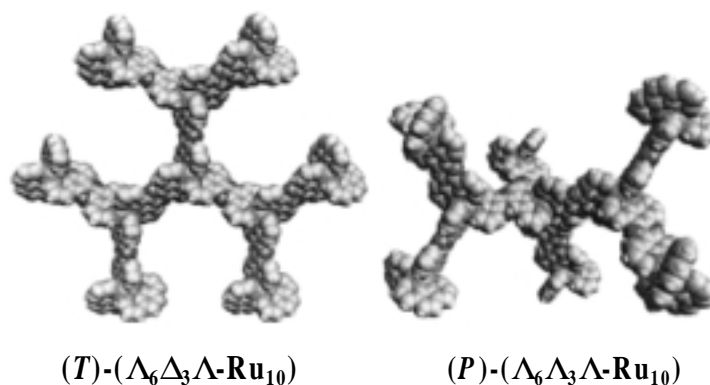


Figure 2.10. Space-filling models of decanuclear $(T)\text{-}(\Lambda_6\Delta_3\Lambda\text{-Ru}_{10})$ (left) and $(P)\text{-}(\Lambda_6\Lambda_3\Lambda\text{-Ru}_{10})$ (right) showing the respective disk-like and propeller structure of these complexes.

Although these differences in the global structure do not influence the CD spectra (which was attributed to weak electronic coupling between the chromophores), the colloidal properties (dynamic light scattering revealed polydisperse aggregation in acetonitrile), as measured by electric birefringence, are significantly different.

2.3.3 Conclusions

Metallodendrimers belonging to the “metals as branching units” class were among the first reported metallodendrimers. Since then, various synthetic strategies have allowed the type of both the incorporated metals and ligands to be varied, thereby tailoring *e.g.* the chiral, electrochemical, and photochemical properties of these metallodendrimers for future applications such as multielectron catalysis, solar energy conversion, and chiral recognition.

2.4 Metals as connectors between dendritic building blocks

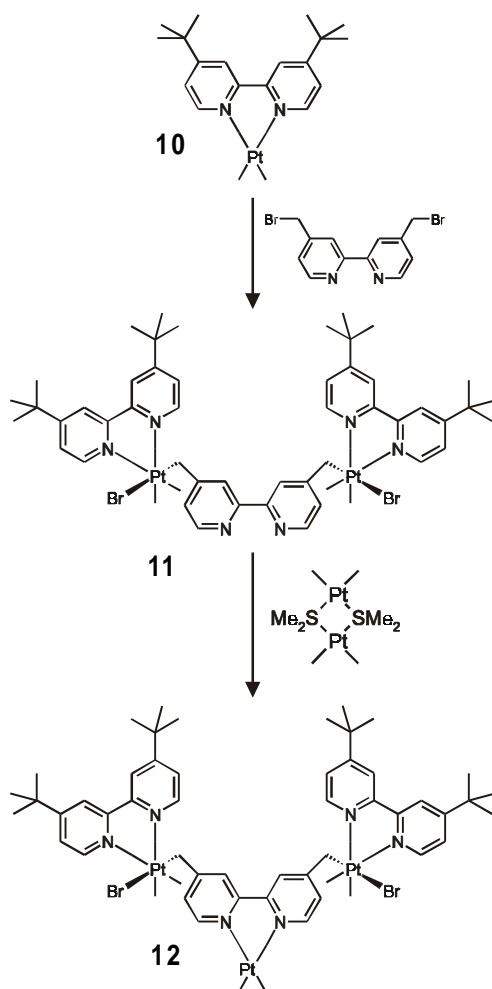
2.4.1 Introduction

In this class of metallodendrimers the necessary branching is incorporated into the dendritic building blocks instead of being located at the metal centers. As a consequence the variation is much larger for this type. The unrestricted freedom in building block design for the

“metals as building block connectors” dendrimers has also led to higher dendritic generations than in the “metals as branching units” type, where a third generation metallodendrimer is yet to be reported (probably due to the compact and rigid structure of these dendrimers).

2.4.2 Organometallic Pt^{II}/Pt^{IV}-containing dendrimers

Puddephatt and Achar were the first to report the synthesis of organometallic dendrimers.⁶⁴ Their synthetic methodology is based on two well-known reactions in organometallic chemistry, namely the displacement of SMe₂ ligands from [Pt₂Me₄(μ-SMe₂)₂] by 2,2'-bipyridines and the oxidative addition of benzylic bromides to [PtMe₂(bipy)]-type complexes. As depicted in Scheme 2.4, a selective *trans* oxidative addition of the C–Br bonds of 4,4'-bis(bromomethyl)-2,2'-bipyridine to [PtMe₂{4,4'-di-*tert*-butyl-2,2'-bipyridine}] **10** gave the binuclear Pt^{IV} complex **11**, which was subsequently reacted with [Pt₂Me₄(μ-SMe₂)₂] to the trinuclear complex **12**. Further convergent dendritic growth occurs from the reactive Pt^{II} center in **12** by a repetition of oxidative addition of 4,4'-bis(bromomethyl)-2,2'-bipyridine and conversion of the resulting bipyridine to the dimethylplatinum(II) complex.



Scheme 2.4. Convergent dendritic growth strategy developed by Puddephatt and Achar.⁶⁴

After the third growth cycle (which yielded a Pt₁₄ dendron), reaction at the focal bipyridine did not proceed well, which was attributed to steric hindrance at the focal point, a common problem in dendritic chemistry. The dendrons were characterized by UV-VIS spectroscopy (useful for distinguishing between Pt^{II} and Pt^{IV}), ¹H and ¹⁹⁵Pt NMR spectroscopy, and gel permeation chromatography (GPC), which provided a rough estimate of the molecular weight.

Fourfold coupling of first and second generation Pt^{II}/Pt^{IV} complexes such as **12** (a first generation dendron) to 1,2,4,5-tetrakis(bromo-methyl)benzene provided large (up to Pt₂₈) dendrimeric organoplatinum complexes, as reported in subsequent papers from the same group.⁶⁵ Moreover, by following the same methodology but employing the monofunctional 4-(bromomethyl)-4'-methyl-2,2'-bipyridine instead of 4,4'-bis(bromomethyl)-2,2'-bipyridine as the reagent in oxidative additions to Pt^{II}, oligomeric linear chains were obtained instead of dendrons, demonstrating the versatility of the synthetic approach.⁶⁶ Starting from bipyridines carrying redox-active ferrocene functions and using the same synthetic methodology, heterometallic dendrimers were synthesized (see the example in Figure 2.11) and electrochemically characterized by Achar, Catalano, and coworkers.⁶⁷

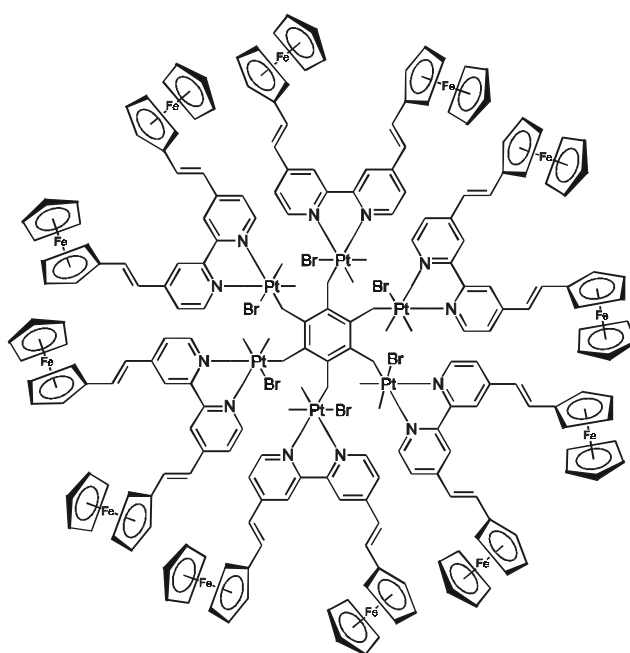
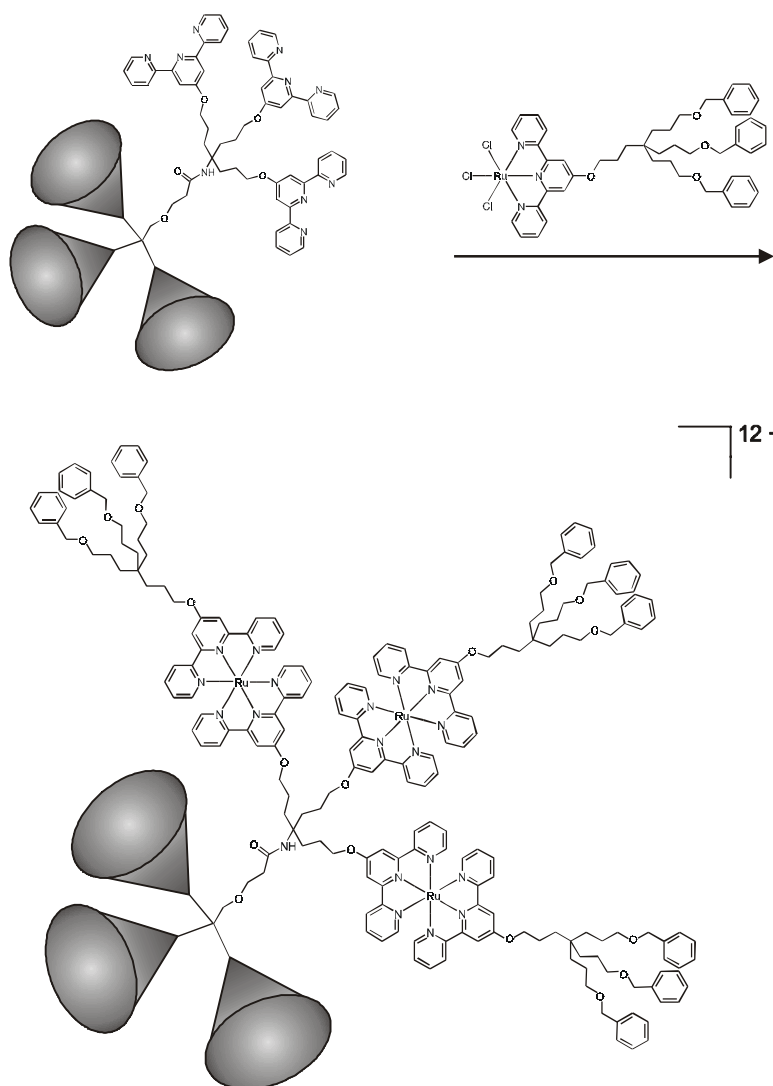


Figure 2.11. Organometallic dendrimers containing peripheral ferrocene units.

Finally, a divergent route to first generation organoplatinum and platinum-palladium dendrimers based on slightly modified building blocks has been reported.⁶⁸ With the bis- and tris(2,2'-bipyridyl) reagents **13** and **14** as the dendritic building block and core, respectively, first generation complexes such as **15** were synthesized (Figure 2.12). Unfortunately, solubility



Scheme 2.5. Dodecaruthenium(II) metallodendrimer reported by Newkome, Constable and coworkers.⁷¹

This strategy of linking dendritic fragments *via* Ru^{II} -terpyridines was later also applied in order to construct the Ru^{II} bis-dendrimers discussed in section 2.2.4. Expanding the stepwise assembly has resulted in double terpyridine- Ru^{II} connectivity in each arm of a tetrahedral metallodendrimer.⁷² The versatility of this synthetic methodology was demonstrated by the synthesis of isomeric metallodendrimers in which different dendrons (G1 and G2), attached to the core and peripheral terpyridine building blocks, were interchanged with respect to each other.⁷³ Recently, Newkome and coworkers also reported dendrimers containing four internal bipyridine units which complex Ru^{II} centers by reaction of the dendritic bipyridines with $[\text{Ru}(\text{bpy})_2\text{Cl}_2]$.⁷⁴ However, here the metals are not essential for the dendritic structure.

Constable and coworkers have predominantly focussed on grafting linear oligonuclear complexes onto cores of different constitution and multiplicity.⁶⁹ Di- and trinuclear linear Ru^{II} -terpyridine arms, incorporating nucleophilic HOTpy ligands on one side as the terminal terpyridine, were coupled to 1,4-bis(bromomethyl)benzene and 1,3,5-tris(bromomethyl)-2,4,6-trimethylbenzene to give the corresponding tetra-, hexa-, and nonanuclear complexes,

respectively.⁷⁵ The nonanuclear complex is depicted in Figure 2.13. All polynuclear complexes could be purified by silica chromatography and were characterized by MALDI-TOF mass spectrometry. Their solubility is dictated by the counterion, the chloride salts are soluble in methanol and even water, and the corresponding PF_6^- salts are soluble in acetonitrile and acetone.

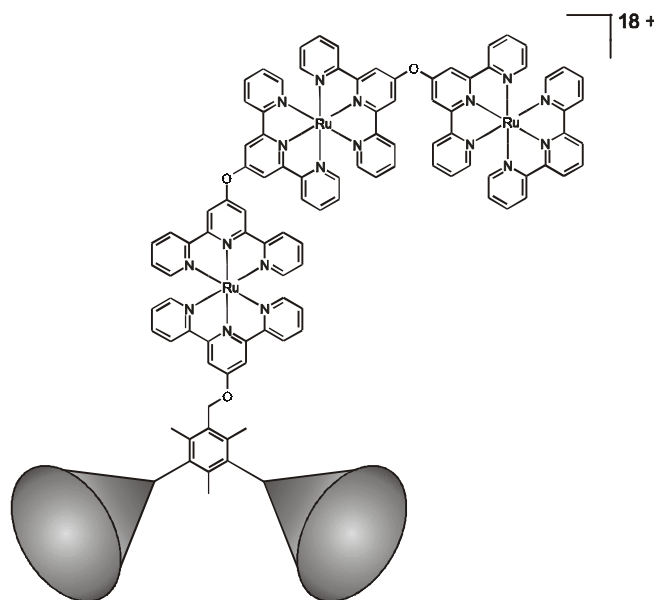
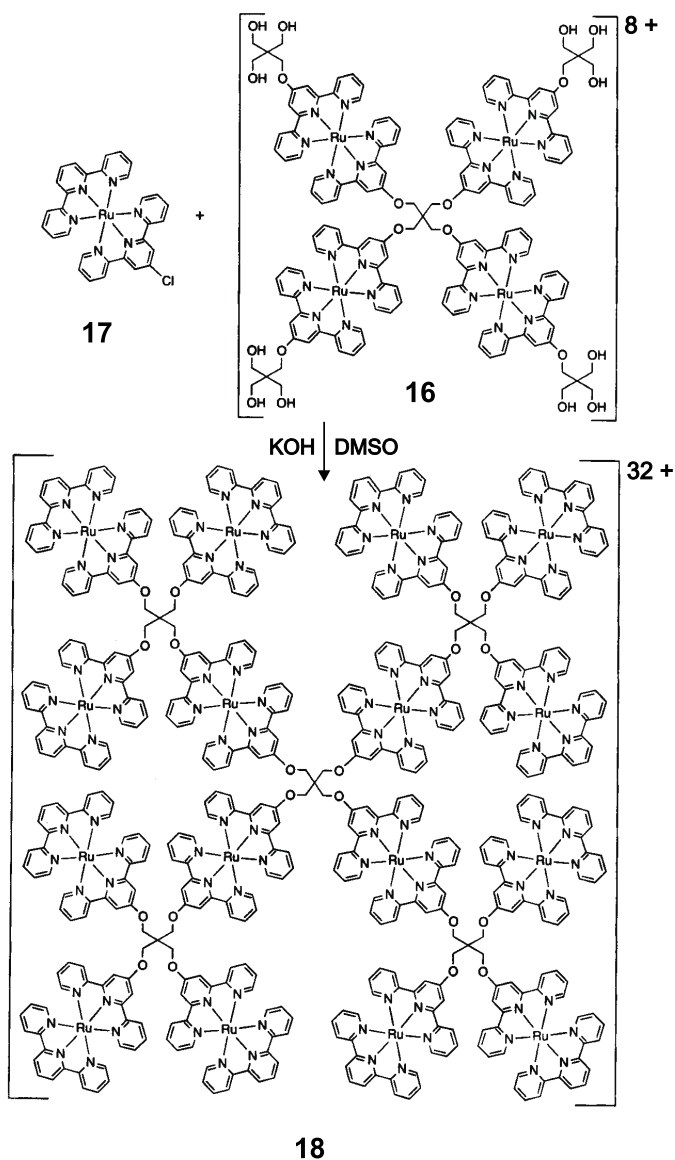


Figure 2.13. Nonanuclear Ru(II)-terpyridine assembly reported by Constable and coworkers.⁷⁵

The trinuclear linear complex was also reacted with hexakis(bromo-methyl)benzene to provide an octadecanuclear species.⁷⁶ These architectures are of the “star” type rather than the dendritic type, since branching only originates from the core. Optical waveguide lightmode spectroscopy showed that the adsorption of the nonanuclear star to silica-titania surfaces heavily depended on the bulk concentration.⁷⁷

Branched Ru^{II} -terpyridine dendrimers (instead of stars) were synthesized by Constable *et al.* by twofold coupling of a Ru^{II} -bisterpyridine complex monofunctionalized with a benzyl bromide to 4,4'-dihydroxy-2,2'-bipyridine, followed by coordination of three of these dendrons to either Fe^{II} or Co^{II} .⁷⁸ Recently, Constable and coworkers have also described pentaerythritol-based Ru^{II} -terpyridine metallodendrimers.⁷⁹ The reaction of pentaerythritol with 4'-chloro-2,2':6',2''-terpyridine could be controlled to provide either a dendritic core containing four terpyridine metal-binding moieties or a building block containing one terpyridine and three pendant CH_2OH groups. These two structures were linked together by Ru^{II} to give the tetranuclear **16** (Scheme 2.6), which remarkably could be completely reacted with $[(\text{tpy})\text{Ru}(\text{Cltpy})]^{2+}$ (**17**) to provide the hexadecanuclear complex **18**. The coordination of 4-halopyridines to transition metals activates the 4-position for nucleophilic attack,⁸⁰ and this is probably the reason why the fully functionalized complex **18** is formed.



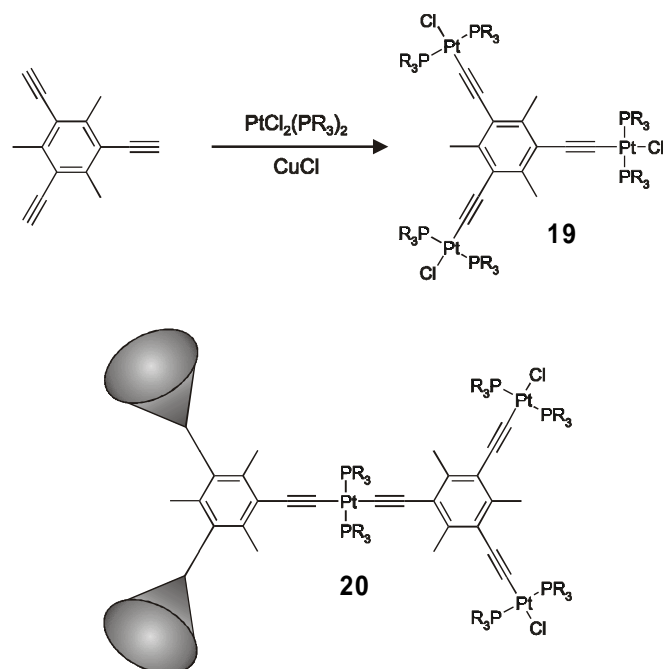
Scheme 2.6. Pentaerythritol-based Ru(II)-terpyridine metallodendrimers.

The fourfold terpyridine-functionalized pentaerythritol unit was earlier described by Constable *et al.* in the synthesis of tetranuclear complexes bearing pendant carborane moieties.⁸¹ Water-soluble boron-rich systems are of interest in the field of boron neutron capture therapy.⁸²

2.4.4 Dendrimers based on metal-acetylide complexes

Novel dendritic architectures based on Pt^{II}-acetylide units have been reported by Takahashi and coworkers. The authors extended their previously developed strategy for transition metal poly-yne polymers⁸³ to the synthesis of metallodendrimers containing triynes as bridging ligands between metal centers. In the first example,⁸⁴ 1,3,5-triethynyl-2,4,6-trimethylbenzene was treated with dichlorobis(tri-*n*-butylphosphine)platinum under CuCl

catalysis to give the trinuclear complex **19** (Scheme 2.7), the molecular structure of which was determined by X-ray crystallography.



Scheme 2.7. Divergently synthesized tri- and nonanuclear Pt(II)-acetylide metallodendrimers.

An excess of this complex was reacted with 1,3,5-triethynyl-2,4,6-trimethylbenzene (under similar conditions, *i.e.* CuCl in Et₂NH) in order to prepare a metallodendrimer of higher generation, *e.g.* the nonanuclear **20**. The terminal chlorides were subsequently substituted by monofunctional phenylacetylene terminal groups. The resulting neutral second generation dendrimer was purified by column chromatography. Stang and coworkers have also reported the divergent synthesis of second generation organoplatinum dendrimers based on 1,3,5-triethynylbenzene building blocks.⁸⁵ Platinum iodide complexes were used instead of chloride complexes, because of the more labile halogen-metal bond in iodide complexes, facilitating their condensation with acetylenic compounds.

A convergent route to third generation Pt^{II}-acetylide dendrimers was recently developed by Takahashi and coworkers.⁸⁶ Their convergent methodology relies on the use of two different trialkylsilyl protecting groups for the acetylene units of triethynylbenzene. Selective desilylation of the trimethylsilyl moiety in **21** (Figure 2.14), followed by conversion of the terminal acetylenes to the corresponding *p*-methoxyphenylethynylplatinum(II) complexes, and final deprotection of the tri(isopropyl)silyl group gave the first generation dendritic wedge **22**. Second and third generation dendrons were similarly synthesized. Coupling of these wedges to the trifunctional complex **19** (Scheme 2.7, R = Et) gave the corresponding metallodendrimers, bearing up to 45 platinum centers (M = ± 26 kDa), in good yields (51% for the third generation).

Due to their symmetry, the dendrimers were characterized by very simple ^1H and ^{31}P NMR spectra.

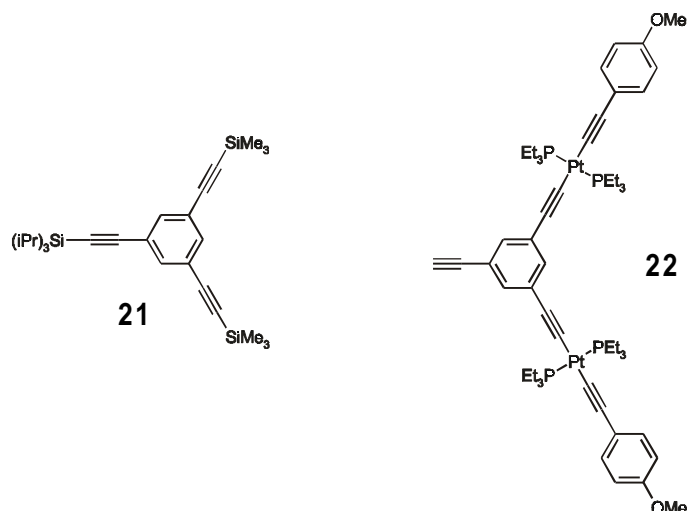


Figure 2.14. Building block (**21**) and dendritic wedge (**22**) used in the convergent construction of Pt(II)-acetylide metallodendrimers.

An alkynylruthenium dendrimer containing a large π -delocalized system was recently synthesized by Humphrey *et al.* as a new organometallic complex for nonlinear optics.⁸⁷ Bisacetylide Ru^{II} units were incorporated into a dendritic wedge bearing a focal acetylene, which was subsequently coupled to a previously reported⁸⁸ trifunctional core to provide a rigid nonanuclear complex (Figure 2.15).

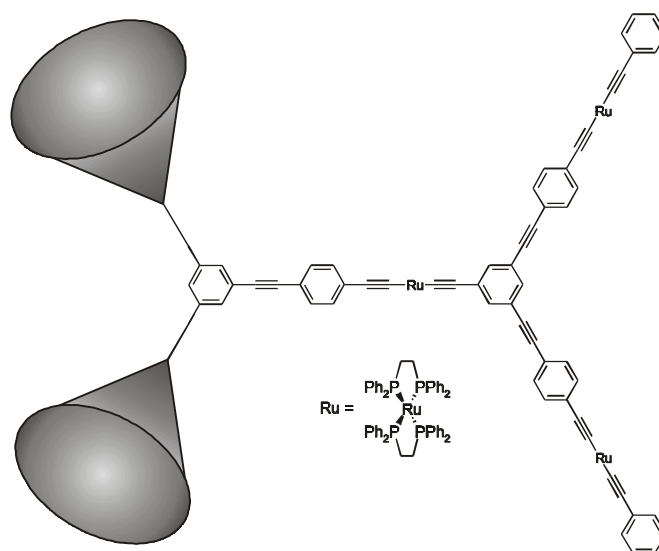


Figure 2.15. Nonanuclear alkynylruthenium metallodendrimer used in nonlinear optics.

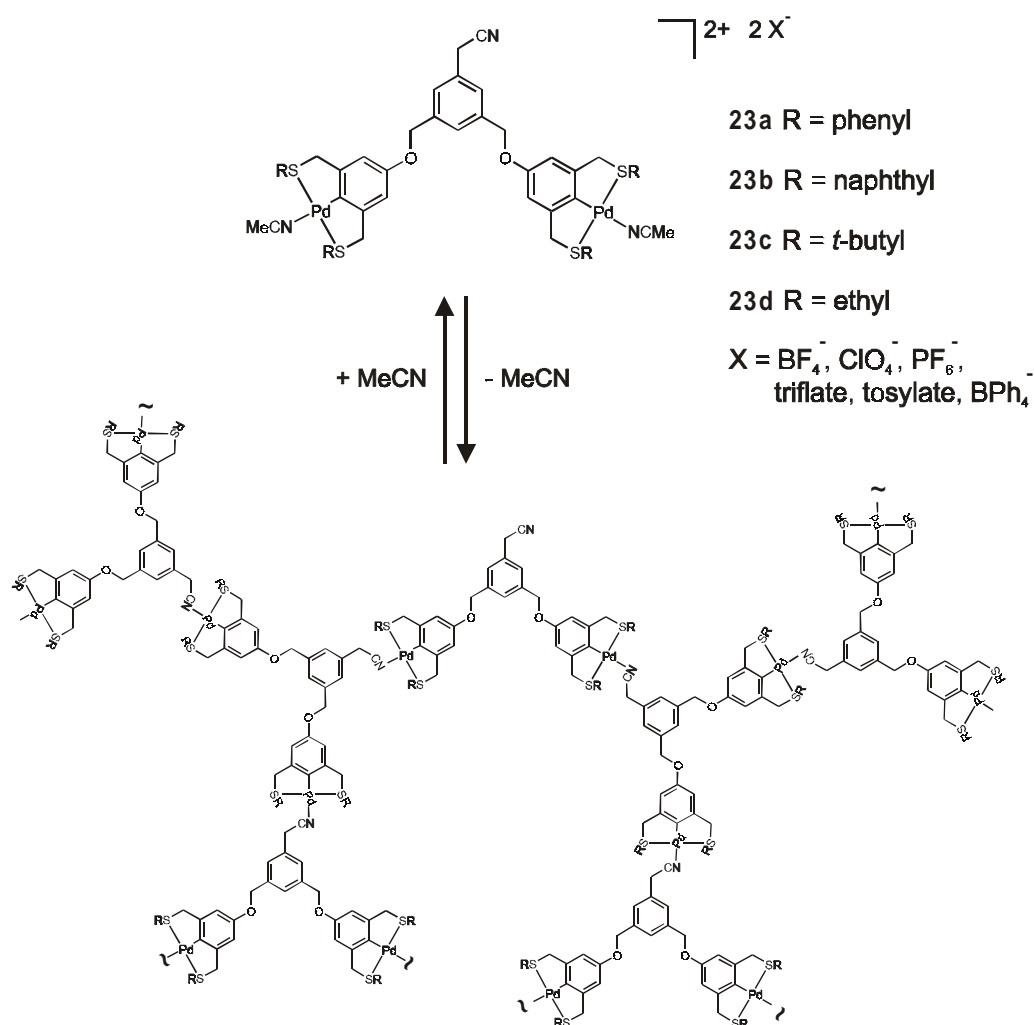
Third-order NLO measurements for this organometallic dendrimer showed a significant enhancement of two-photon absorption (TPA) upon proceeding from the constituent building

blocks to the nonanuclear complex. TPA materials are of interest for applications such as optical data storage and optical limiting.⁸⁹

Rigid dendrimers were synthesized by Osawa and Wakatsuki⁹⁰ by grafting Ru^{II}-terpyridine metallodendrons to a functionalized core Ni^{II}-tris(bipyridine) unit. Metal-terpyridine and -bipyridine connectivities were combined before in the metallodendrimers reported by Constable and coworkers (*vide supra*),⁷⁸ with coordination of the bipyridine dendrons to Ru^{II} as the final step. The final construction step is a covalent palladium-mediated coupling between aryl iodides connected to the core Ni^{II}-tris(bipyridine) moiety and the focal acetylene of the Ru^{II}-terpyridine dendrons. The largest (ca. 90 Å) dendrimer, containing 18 Ru^{II} centers and 1 Ni^{II} center, was characterized by transmission electron microscopy (TEM), which revealed individual molecules of nanosize dimensions.

2.4.5 Metallodendrimers based on SCS Pd^{II} pincer moieties

Our group has been involved in the non-covalent construction of metallodendrimers based on the coordination of suitable ligands to SCS Pd^{II} pincer systems. Cyclopalladated complexes of terdentate, monoanionic SCS pincer ligands, known since 1980,⁹¹ have also been exploited in molecular recognition,⁹² catalysis,⁹³ and self-assembly.⁹⁴ For an overview of metal complexes of different pincer ligands, the reader is referred to chapter 3. Huck *et al.* first studied genuine self-assembly of molecules that have two Pd^{II} pincers and a suitable ligand (*e.g.* RCN) in one building block. Compound **23a** (Scheme 2.8) was synthesized and its self-assembly upon removal of the labile acetonitrile ligands was investigated.⁹⁵



Scheme 2.8. Self-assembled hyperbranched spheres grown from building blocks **23a-d**.

Intermolecular coordination of the nitrile groups to Pd^{II} was evidenced by IR spectroscopy, in which a diagnostic shift of the $\text{C}\equiv\text{N}$ stretch vibration from 2250 cm^{-1} (monomeric building block) to 2290 cm^{-1} was observed upon coordination. Further proof of the self-assembled structure was obtained from quasi-elastic light scattering (QELS), which showed particles having a hydrodynamic diameter of 200 nm, and from both atomic force microscopy (AFM) and TEM, which revealed large globular-shaped assemblies having diameters in the 150-200 nm range. The reversible nature of the self-assembling process was proven by the addition of small amounts of acetonitrile to a nitromethane solution of the assembly, upon which sharp signals appeared in the ^1H NMR spectrum, indicating the presence of monomeric species.

Structural variations in both the building blocks (**23b-23d** in Scheme 2.8) and the non-coordinating anions (X^- in Scheme 2.8) allowed the size of the self-assembled spheres to be controlled.⁹⁶

In contrast to the uncontrolled growth of the self-assembled spheres, a stepwise *controlled* assembly strategy would allow the synthesis of smaller metallodendrimers. Such a

growth scheme requires a suitable dendritic core and a protection/deprotection strategy in order to precisely control the coordination of building blocks at the desired positions. For this purpose the building blocks depicted in Figure 2.16 were developed.⁹⁷

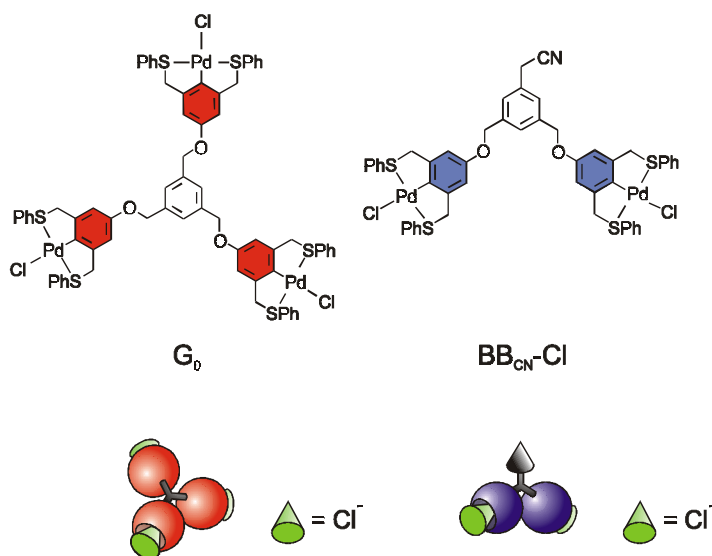
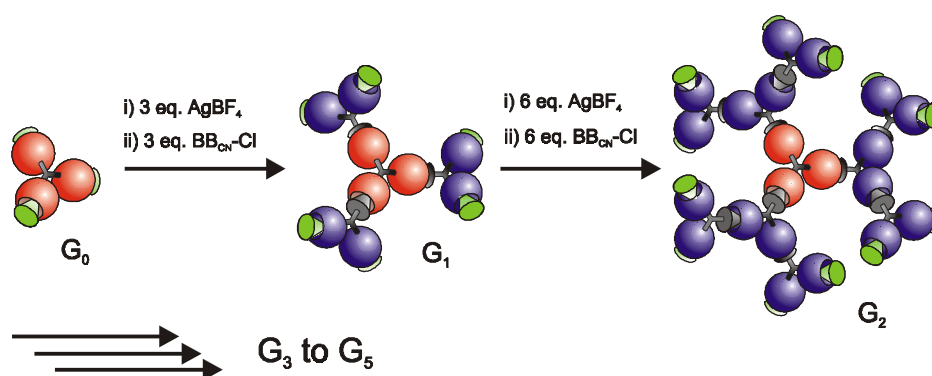


Figure 2.16. Building blocks used in the controlled assembly of Pd(II)-containing metallodendrimers.

In these building blocks, the Pd^{II} centers are protected by strongly coordinating chloride ligands. These chlorides can be removed, however, by precipitation with Ag^I salts, thereby allowing the resulting vacant coordination site to be occupied by other ligands. Therefore, starting from the nucleus **G**₀, the assembly of metallodendrimers can be controlled by the repetitive addition of Ag^I salts and building blocks. At first, the divergent dendritic growth using **G**₀ and **BB**_{CN}-Cl was investigated in our group.⁹⁷ As shown in Scheme 2.9, deprotection of **G**₀ with 3 equiv of AgBF₄ followed by the addition of 3 equiv of **BB**_{CN}-Cl resulted in the first-generation metallodendrimer **G**₁, containing 6 terminal sites for further growth.

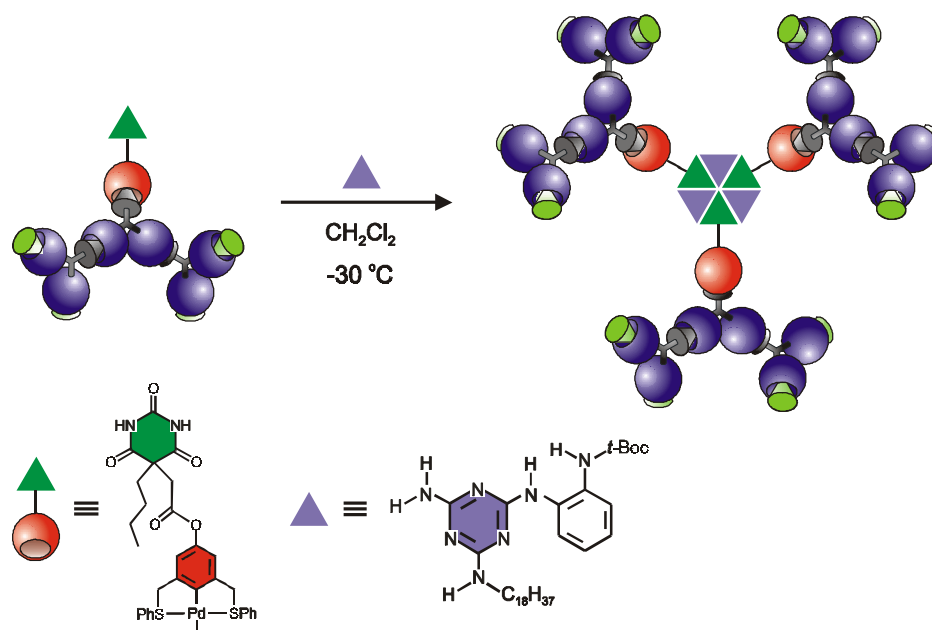


Scheme 2.9. Metallodendrimers of generation one to five assembled via a stepwise divergent growth strategy.

Repetition of the deprotection and building block addition procedure yielded the corresponding higher generation dendrimers (G2-G5). All metallodendrimers were characterized by ^1H NMR and FT-IR spectroscopy, electrospray mass spectrometry (except G5), and tapping mode AFM (TM-AFM) on graphite and mica (G5 only). Molecularly thin films of spincoated G5 dendrimers were studied by TM-AFM measurements.⁹⁸ At low concentrations separate spheres were identified having dimensions of approximately 15 nm in diameter, most likely corresponding to individual metallodendrimers.

Huck *et al.* have also constructed metallodendrimers in a *convergent* fashion by combining building blocks containing cyano ligands with pyridine-based building blocks.⁹⁹ As will be discussed in chapter 3, pyridines are stronger ligands than cyano groups towards SCS Pd^{II} pincers. This difference in coordination strength enables the convergent assembly of metallodendrimers to start from the stronger coordinating pyridine building blocks. This strategy is further discussed in chapter 4. The convergent growth, based on coordination chemistry, allows the introduction of core and/or peripheral functionalities such as redox- or photoactive groups, provided that such moieties can be functionalized with either Pd^{II} pincers or suitable ligands. For example, convergently constructed dendritic assemblies containing up to 12 peripheral porphyrins were prepared starting from 5-pyridyl-10,15,20-triphenylporphyrin.^{43g} Also, metallodendrimers tailored with core *and* peripheral porphyrins have been synthesized, which might provide interesting energy- and electron-transfer behavior.^{43a}

As a final example from our group, the coordination chemistry used to construct metallodendrimers has been combined with hydrogen bonding in the formation of dendritic *rosettes*.¹⁰⁰ The self-assembly of *covalent* dendrons containing focal bis(isophthalic acid) units into hydrogen-bonded hexameric cyclic arrays was reported earlier by Zimmerman and coworkers.¹⁰¹ In our strategy,¹⁰² three metallodendrons, divergently synthesized using **BB_{CN}-Cl** and a barbituric acid-functionalized Pd^{II} pincer, were bound *via* their focal barbituric acid groups to *N*-octadecanyl-*N*-(2-*N*-*tert*-Boc-amino)-phenylmelamine through 18 hydrogen bonds in a cyclic [3 + 3] fashion to form the hexameric rosette (Scheme 2.10), which was characterized using a variety of NMR techniques (low temperature ^1H , 2D-NOESY, and TOCSY). NOE build-up curves were used to determine the rotation correlation times τ_c , and as expected these values increased with increasing size of the rosette dendrimers.



Scheme 2.10. Metallodendrimers held together by a combination of coordination and hydrogen bonds. The core contains the hydrogen-bonded rosette motif.

2.4.6 Conclusions

The class of metallodendrimers belonging to the “metals as building block connectors” type is the most diverse of the three types discussed in this chapter. This is because coordination chemistry has provided this field with a large variety of transition metals and corresponding ligand coordination geometries, thereby hardly posing any restrictions on the design of dendritic building blocks. This allows the resulting metallodendrimers to be tailored with specific functions, arising from the metals themselves (redox or catalytic activity, luminescence, etc.), the organic spacers bridging the metals (*e.g.* conducting acetylenes), or from their interplay.

2.5 Concluding remarks

Metallodendrimers have grown from curiosities one decade ago to common macromolecules nowadays. The exploitation of coordination chemistry has proven to be very useful in the non-covalent synthesis of metallodendrimers. At present, dendritic construction *via* metal-ligand coordination is straightforward in most cases. Moreover, and crucially, the number of techniques being used for (metallo)dendrimer characterization is ever increasing. NMR spectroscopy (from simple ^1H spectra to pulsed field gradient spin-echo measurements), IR, UV-VIS and luminescence spectroscopy, mass spectrometry (in particular ES and MALDI-TOF MS), size exclusion chromatography, cyclic voltammetry, and transmission electron, atomic force and scanning tunneling microscopy are among the most useful characterization methods for these fascinating architectures. With respect to applications, their potential has yet to be fully explored. However, promising applications have already been reported for metallodendrimers in

the fields of catalysis (*e.g.* recyclable homogeneous catalysts)⁷ and medical diagnostics (*e.g.* MRI contrast reagents).¹⁶ No doubt these initial successes will stimulate metallodendrimer research to be intensified in years to come.

2.6 References and notes

- ¹ a) Flory, P. J. *J. Am. Chem. Soc.* **1941**, *63*, 3083; *ibid.* **1941**, *63*, 3091; c) *ibid.* **1941**, *63*, 3096.
- ² Buhleier, E.; Wehner, W.; Vögtle, F. *Synthesis* **1978**, 155.
- ³ Tomalia, D. A.; Baker, H.; Dewald, J. R.; Hall, M.; Kallos, G.; Martin, S.; Roeck, J.; Ryder, J.; Smith, P. *Polym. J.* **1985**, *17*, 117.
- ⁴ Newkome, G. R.; Yao, Z.-Q.; Baker, G. R.; Gupta, K. *J. Org. Chem.* **1985**, *50*, 2003.
- ⁵ For reviews including discussions on dendritic growth strategies, see: a) Matthews, O. A.; Shipway, A. N.; Stoddart, J. F. *Prog. Polym. Sci.* **1998**, *23*, 1; b) Chow, H.-F.; Mong, T. K.-K.; Nongrum, M. F.; Wan, C.-W. *Tetrahedron* **1998**, *54*, 8543.
- ⁶ For an overview, see: Cuadrado, I.; Morán, M.; Casado, C. M.; Alonso, B.; Losada, J. *Coord. Chem. Rev.* **1999**, *193-195*, 395.
- ⁷ For examples, see: a) Knapen, J. W. J.; van der Made, A. W.; de Wilde, J. C.; van Leeuwen, P. W. N. M.; Wijkens, P.; Grove, D. M.; van Koten, G. *Nature* **1994**, *372*, 659; b) Reetz, M. T.; Lohmer, G.; Schwickardi, R. *Angew. Chem. Int. Ed. Engl.* **1997**, *36*, 1526; c) Bourque, S. C.; Maltais, F.; Xiao, W.-J.; Tardif, O.; Alper, H.; Arya, P.; Manzer, L. E. *J. Am. Chem. Soc.* **1999**, *121*, 3035.
- ⁸ a) Newkome, G. R.; Moorefield, C. N. *Polym. Prepr.* **1993**, *34*, 75; b) Newkome, G. R.; Gross, J.; Moorefield, C. N.; Woosley, B. D. *Chem. Commun.* **1997**, 515.
- ⁹ a) Ottaviani, M. F.; Bossmann, S.; Turro, N. J.; Tomalia, D. A. *J. Am. Chem. Soc.* **1994**, *116*, 661; b) Zhao, M.; Sun, L.; Crooks, R. M. *J. Am. Chem. Soc.* **1998**, *120*, 4877; c) Zhao, M.; Crooks, R. M. *Angew. Chem. Int. Ed.* **1999**, *38*, 364; d) Balogh, L.; Tomalia, D. A. *J. Am. Chem. Soc.* **1998**, *120*, 7355.
- ¹⁰ a) Newkome, G. R.; He, E.; Moorefield, C. N. *Chem. Rev.* **1999**, *99*, 1689; b) Bosman, A. W.; Janssen, H. M.; Meijer, E. W. *Chem. Rev.* **1999**, *99*, 1665; c) Fischer, M.; Vögtle, F. *Angew. Chem. Int. Ed.* **1999**, *38*, 884; d) Hearshaw, M. A.; Moss, J. R. *Chem. Commun.* **1999**, 1; e) Gorman, C. B. *Adv. Mater.* **1998**, *10*, 295; f) Zeng, F.; Zimmerman, S. C. *Chem. Rev.* **1997**, *97*, 1681; g) Newkome, G. R.; Moorefield, C. N.; Vögtle, F. *Dendritic Macromolecules: Concepts, Syntheses, Perspectives*; VCH: Weinheim, Germany, 1996.
- ¹¹ Majoral, J.-P.; Caminade, A.-M. *Chem. Rev.* **1999**, *99*, 845.
- ¹² a) Peerlings, H. W. I.; Meijer, E. W. *Chem. Eur. J.* **1997**, *3*, 1563; b) Seebach, D.; Reiner, P. B.; Greiveldinger, G.; Butz, T.; Sellner, H. *Top. Curr. Chem.* **1998**, *197*, 125.
- ¹³ Jayaraman, N.; Nepogodiev, S. A.; Stoddart, J. F. *Chem. Eur. J.* **1997**, *3*, 1193.
- ¹⁴ Adronov, A.; Fréchet, J. M. J. *Chem. Commun.* **2000**, 1701.
- ¹⁵ Schlüter, A. D.; Rabe, J. P. *Angew. Chem. Int. Ed.* **2000**, *39*, 864.
- ¹⁶ Krause, W.; Hackmann-Schlichter, N.; Maier, F. K.; Müller, R. *Top. Curr. Chem.* **2000**, *210*, 261.
- ¹⁷ Hawker, C. J.; Wooley, K. L.; Fréchet, J. M. J. *J. Am. Chem. Soc.* **1993**, *115*, 4375.
- ¹⁸ Hecht, S.; Fréchet, J. M. J. *Angew. Chem. Int. Ed.* **2001**, *40*, 74.

- ¹⁹ a) Bertini, I.; Gray, H. B.; Lippard, S. J.; Valentine, J. S. *Bioinorganic Chemistry*; University Science Books: Mill Valley, USA, 1994; b) Stryer, L. *Biochemistry*, 4th ed.; Freeman: New York, USA, 1995.
- ²⁰ a) Mahler, G.; May, V.; Schreiber, M., Eds. *Molecular Electronics: Properties, Dynamics and Applications*; Marcel Dekker, Inc.: New York, 1996; b) Lazarev, P. I., Ed. *Molecular Electronics: Materials and Methods*; Kluwer Academic: Dordrecht, The Netherlands, 1991.
- ²¹ a) Dandliker, P. J.; Diederich, F.; Gross, M.; Knobler, C. B.; Louati, A.; Sanford, E. M. *Angew. Chem. Int. Ed. Engl.* **1994**, *33*, 1739; b) Dandliker, P. J.; Diederich, F.; Gisselbrecht, J.-P.; Louati, A.; Gross, M. *Angew. Chem. Int. Ed. Engl.* **1995**, *34*, 2725; c) Weyermann, P.; Gisselbrecht, J.-P.; Boudon, C.; Diederich, F.; Gross, M. *Angew. Chem. Int. Ed.* **1999**, *38*, 3215.
- ²² Gorman, C. B.; Parkhurst, B. L.; Su, W. Y.; Chen, K.-Y. *J. Am. Chem. Soc.* **1997**, *119*, 1141.
- ²³ Gorman, C. B.; Hager, M. W.; Parkhurst, B. L.; Smith, J. C. *Macromolecules* **1998**, *31*, 815.
- ²⁴ Gorman, C. B.; Smith, J. C.; Hager, M. W.; Parkhurst, B. L.; Sierzputowska-Gracz, H.; Haney, C. A. *J. Am. Chem. Soc.* **1999**, *121*, 9958.
- ²⁵ Moore, J. S. *Acc. Chem. Res.* **1997**, *30*, 402.
- ²⁶ Gorman, C. B.; Su, W. Y.; Jiang, H.; Watson, C. M.; Boyle, P. *Chem. Commun.* **1999**, 877.
- ²⁷ Wang, R.; Zheng, Z. *J. Am. Chem. Soc.* **1999**, *121*, 3549.
- ²⁸ Juris, A.; Balzani, V.; Barigelletti, F.; Campagna, S.; Belser, P.; von Zelewsky, A. *Coord. Chem. Rev.* **1988**, *84*, 85.
- ²⁹ Issberner, J.; Vögtle, F.; De Cola, L.; Balzani, V. *Chem. Eur. J.* **1997**, *3*, 706.
- ³⁰ a) Newkome, G. R.; Nayak, A.; Behera, R. K.; Moorefield, C. N.; Baker, G. R. *J. Org. Chem.* **1992**, *57*, 358; b) Newkome, G. R.; Moorefield, C. N.; Baker, G. R.; Behera, R. K.; Escamilia, G. H.; Saunders, M. J. *Angew. Chem. Int. Ed. Engl.* **1992**, *31*, 917.
- ³¹ Mattai, S.; Seiler, P.; Diederich, F.; Gramlich, V. *Helv. Chim. Acta* **1995**, *78*, 1904.
- ³² Plevoets, M.; Vögtle, F.; De Cola, L.; Balzani, V. *New J. Chem.* **1999**, 63.
- ³³ Other dendritic antenna systems have been reported. See the work of Balzani and coworkers in the “metals as branching centers” section and also: a) Steward, G. M.; Fox, M. A. *J. Am. Chem. Soc.* **1996**, *118*, 4354; b) Shorttreed, M. R.; Swallen, S. F.; Shi, Z. Y.; Tan, W.; Xu, Z.; Devadoss, C.; Moore, J. S.; Kopelman, R. *J. Phys. Chem. B* **1997**, *101*, 6318.
- ³⁴ Vögtle, F.; Plevoets, M.; Nieger, M.; Azzellini, G. C.; Credi, A.; De Cola, L.; De Marchis, V.; Venturi, M.; Balzani, V. *J. Am. Chem. Soc.* **1999**, *121*, 6290.
- ³⁵ Hoffman, M. Z.; Bolletta, F.; Moggi, L.; Hug, G. L. *J. Phys. Chem. Ref. Data* **1989**, *18*, 219.
- ³⁶ Chow, H.-F.; Chan, I. Y.-K.; Chan, D. T. W.; Kwok, R. W. M. *Chem. Eur. J.* **1996**, *2*, 1085.
- ³⁷ Armstrong, F. A.; Hill, H. A. O.; Walton, N. J. *Acc. Chem. Res.* **1988**, *21*, 407.
- ³⁸ Gray, H. B.; Winkler, J. R. *Ann. Rev. Biochem.* **1996**, *65*, 537.
- ³⁹ Newkome, G. R.; Güther, R.; Moorefield, C. N.; Cardullo, F.; Echegoyen, L.; Pérez-Cordero, E.; Luftmann, H. *Angew. Chem. Int. Ed. Engl.* **1995**, *34*, 2023.
- ⁴⁰ Tomoyoso, Y.; Jiang, D.-L.; Jin, R.-H.; Aida, T.; Yamashita, T.; Horie, K.; Yashima, E.; Okamoto, Y. *Macromolecules* **1996**, *29*, 5236.
- ⁴¹ Darling, S. L.; Mak, C. C.; Bampos, N.; Feeder, N.; Teat, S. J.; Sanders, J. K. M. *New J. Chem.* **1999**, *23*, 359.
- ⁴² There is a vast amount of literature on multiporphyrin systems. For some representative covalent multiporphyrin arrays, see: a) Wagner, R. W.; Johnson, T. E.; Lindsey, J. S. *J. Am. Chem. Soc.* **1996**,

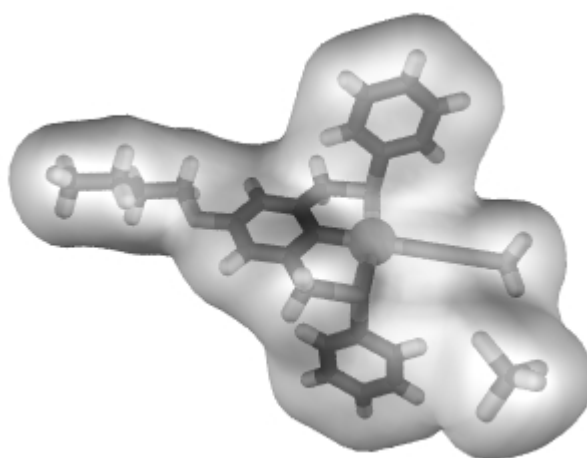
- 118, 11166; b) Officer, D. L.; Burrell, A. K.; Reid, D. C. *Chem. Commun.* **1996**, 1657; c) Mak, C. C.; Bampos, N.; Sanders, J. K. M. *Angew. Chem. Int. Ed. Engl.* **1998**, *37*, 3020; d) Yeow, E. K. L.; Ghiggino, K. P.; Reek, J. N. H.; Crossley, M. J.; Bosman, A. W.; Schenning, A. P. H. J.; Meijer, E. W. *J. Phys. Chem. B* **2000**, *104*, 2596; e) Aratani, N.; Osuka, A.; Kim, Y. H.; Heong, D. H.; Kim, D. *Angew. Chem. Int. Ed.* **2000**, *39*, 1458.
- ⁴³ Non-covalently constructed multiporphyrin arrays: a) Sessler, J. L.; Wang, B.; Springs, S. L.; Brown, C. T. Electron- and Energy-transfer Reactions in Noncovalently Linked Supramolecular Model Systems. In *Comprehensive Supramolecular Chemistry*; Lehn, J.-M., Chair Ed.; Atwood, J. L., Davis, J. E. D., MacNicol, D. D., Vögtle, F., Exec. Eds.; Pergamon: Oxford, UK, 1987-1996; Vol. 4, Chapter 9; b) Harriman, A.; Sauvage, J.-P. *Chem. Soc. Rev.* **1996**, *25*, 41; c) Ward, M. D. *Chem. Soc. Rev.* **1997**, 365; d) Drain, C. M.; Nifiatis, F.; Vasenko, A.; Batteas, J. D. *Angew. Chem. Int. Ed.* **1998**, *37*, 2344; e) Drain, C. M.; Russell, K. C.; Lehn, J.-M. *Chem. Commun.* **1996**, 337; f) Reek, J. N. H.; Schenning, A. P. H. J.; Bosman, A. W.; Meijer, E. W.; Crossley, M. J. *Chem. Commun.* **1998**, 11; g) Huck, W. T. S.; Rohrer, A.; Anilkumar, A. T.; Fokkens, R. H.; Nibbering, N. M. M.; van Veggel, F. C. J. M.; Reinhoudt, D. N. *New J. Chem.* **1998**, *22*, 165.
- ⁴⁴ Enomoto, M.; Aida, T. *J. Am. Chem. Soc.* **1999**, *121*, 874.
- ⁴⁵ Catalano, V. J.; Parodi, N. *Inorg. Chem.* **1997**, *36*, 537.
- ⁴⁶ Balch, A. L.; Catalano, V. J.; Lee, J. W.; Olmstead, M. M.; Parkin, S. R. *J. Am. Chem. Soc.* **1991**, *113*, 8953.
- ⁴⁷ Kawa M.; Fréchet, J. M. J. *Chem. Mater.* **1998**, *10*, 286.
- ⁴⁸ Venturi, M.; Serroni, S.; Juris, A.; Campagna, S.; Balzani, V. *Top. Curr. Chem.* **1998**, *197*, 193.
- ⁴⁹ Campagna, S.; Denti, G.; Sabatino, L.; Serroni, S.; Ciano, M.; Balzani, V. *J. Chem. Soc., Chem. Commun.* **1989**, 1500.
- ⁵⁰ Denti, G.; Campagna, S.; Serroni, S.; Ciano, M.; Balzani, V. *J. Am. Chem. Soc.* **1992**, *114*, 2944.
- ⁵¹ Kim, M.-J.; MacDonnell, F. M.; Gimon-Kinsel, M. E.; du Bois, T.; Asgharian, N.; Griener, J. C. *Angew. Chem. Int. Ed.* **2000**, *39*, 615.
- ⁵² Juris, A.; Balzani, V.; Campagna, S.; Denti, G.; Serroni, S.; Frei, G.; Güdel, H. U. *Inorg. Chem.* **1994**, *33*, 1491.
- ⁵³ Campagna, S.; Giannetto, A.; Serroni, S.; Denti, G.; Trusso, S.; Mallamace, F.; Micali, N. *J. Am. Chem. Soc.* **1995**, *117*, 1754.
- ⁵⁴ Serroni, S.; Denti, G.; Campagna, S.; Juris, A.; Ciano, M.; Balzani, V. *Angew. Chem. Int. Ed. Engl.* **1992**, *31*, 1493.
- ⁵⁵ The protected decanuclear dendrimer and its deprotected analog were reported later in a paper describing generalized versions of the synthetic strategies: Campagna, S.; Denti, G.; Serroni, S.; Juris, A.; Venturi, M.; Ricevuto, V.; Balzani, V. *Chem. Eur. J.* **1995**, *1*, 211.
- ⁵⁶ Serroni, S.; Juris, A.; Venturi, M.; Campagna, S.; Resino, I. R.; Denti, G.; Credi, A.; Balzani, V. *J. Mater. Chem.* **1997**, *7*, 1227.
- ⁵⁷ For an overview of luminescent and redox-active polynuclear transition metal complexes, see: Balzani, V.; Juris, A.; Venturi, M.; Campagna, S.; Serroni, S. *Chem. Rev.* **1996**, *96*, 759.
- ⁵⁸ Moucheron, C.; Kirsch-De Mesmaeker, A.; Dupont-Gervais, A.; Leize, E.; van Dorsselaer, A. *J. Am. Chem. Soc.* **1996**, *118*, 12834.

- ⁵⁹ Latterini, L.; Schweitzer, G.; De Schrijver, F. C.; Moucheron, C.; Kirsch-De Mesmaeker, A. *Chem. Phys. Lett.* **1997**, *281*, 267.
- ⁶⁰ Latterini, L.; Pourtois, G.; Moucheron, C.; Lazzaroni, R.; Brédas, J.-L.; Kirsch-De Mesmaeker, A.; De Schrijver, F. C. *Chem. Eur. J.* **2000**, *6*, 1331.
- ⁶¹ MacDonnell, F. M.; Bodige, S. *Inorg. Chem.* **1996**, *35*, 5758.
- ⁶² Bodige, S.; Torres, A. S.; Maloney, D. J.; Tate, D.; Kinsel, G. R.; Walker, A. K.; MacDonnell, F. M. *J. Am. Chem. Soc.* **1997**, *119*, 10364.
- ⁶³ Kim, M.-J.; MacDonnell, F. M.; Gimon-Kinsel, M. E.; Du Bois, T.; Asgharian, N.; Griener, J. C. *Angew. Chem. Int. Ed.* **2000**, *39*, 615.
- ⁶⁴ Achar, S.; Puddephatt, R. J. *Angew. Chem. Int. Ed. Engl.* **1994**, *33*, 847.
- ⁶⁵ a) Achar, S.; Puddephatt, R. J. *J. Chem. Soc., Chem. Commun.* **1994**, 1895; b) Achar, S.; Vittal, J. J.; Puddephatt, R. J. *Organometallics* **1996**, *15*, 43.
- ⁶⁶ Achar, S.; Puddephatt, R. J. *Organometallics* **1995**, *14*, 1681.
- ⁶⁷ Achar, S.; Immoos, C. E.; Hill, M. G.; Catalano, V. J. *Inorg. Chem.* **1997**, *36*, 2314.
- ⁶⁸ Liu, G.-X.; Puddephatt, R. J. *Organometallics* **1996**, *15*, 5257.
- ⁶⁹ For an overview, see: Constable, E. C. *Chem. Commun.* **1997**, 1073.
- ⁷⁰ Sauvage, J.-P.; Collin, J.-P.; Chambron, J. C.; Guillerez, S.; Coudret, C.; Balzani, V.; Barigelletti, F.; De Cola, L.; Flamigni, L. *Chem. Rev.* **1994**, *94*, 993.
- ⁷¹ Newkome, G. R.; Cardullo, F.; Constable, E. C.; Moorefield, C. N.; Cargill Thompson, A. M. W. *J. Chem. Soc., Chem. Commun.* **1993**, 925.
- ⁷² Newkome, G. R.; He, E. *J. Mater. Chem.* **1997**, *7*, 1237.
- ⁷³ Newkome, G. R.; He, E. *Macromolecules* **1998**, *31*, 4382.
- ⁷⁴ Newkome, G. R.; Patri, A. K.; Godínez, L. A. *Chem. Eur. J.* **1999**, *5*, 1445.
- ⁷⁵ Constable, E. C.; Harverson, P. *Chem. Commun.* **1996**, 33.
- ⁷⁶ Constable, E. C.; Harverson, P. *Inorg. Chim. Acta* **1996**, *252*, 281.
- ⁷⁷ Constable, E. C.; Harverson, P.; Ramsden, J. J. *Chem. Commun.* **1997**, 1683.
- ⁷⁸ Constable, E. C.; Harverson, P.; Oberholzer, M. *Chem. Commun.* **1996**, 1821.
- ⁷⁹ Constable, E. C.; Housecroft, C. E.; Cattalini, M.; Phillips, D. *New J. Chem.* **1998**, *22*, 193.
- ⁸⁰ a) Constable, E. C.; Leese, T. A. *Inorg. Chim. Acta* **1988**, *146*, 55; b) Constable, E. C.; Cargill Thompson, A. M. W.; Harverson, P.; Macko, L.; Zehnder, M. *Chem. Eur. J.* **1995**, *1*, 360.
- ⁸¹ Armspach, D.; Cattalini, M.; Constable, E. C.; Housecroft, C. E.; Philips, D. *Chem. Commun.* **1996**, 1823.
- ⁸² a) Hawthorne, M. F. *Angew. Chem. Int. Ed. Engl.* **1993**, *32*, 950; b) Soloway, A. H.; Tjarks, W.; Barnum, B. A.; Rong, F.-G.; Barth, R. F.; Codogni, I. M.; Wilson, J. G. *Chem. Rev.* **1998**, *98*, 1515.
- ⁸³ Hagihara, N.; Sonogashira, K.; Takahashi, S. *Adv. Polym. Sci.* **1981**, *41*, 149.
- ⁸⁴ Ohshiro, N.; Takei, F.; Onitsuka, K.; Takahashi, S. *Chem. Lett.* **1996**, 871.
- ⁸⁵ Leininger, S.; Stang, P. J.; Huang, S. *Organometallics* **1998**, *17*, 3981.
- ⁸⁶ Onitsuka, K.; Fujimoto, M.; Ohshiro, N.; Takahashi, S. *Angew. Chem. Int. Ed.* **1999**, *38*, 689.
- ⁸⁷ McDonagh, A. M.; Humphrey, M. G.; Samoc, M.; Luther-Davies, B. *Organometallics* **1999**, *18*, 5195.
- ⁸⁸ McDonagh, A. M.; Humphrey, M. G.; Samoc, M.; Luther-Davies, B.; Houbrechts, S.; Wada, T.; Sasabe, H.; Persoons, A. *J. Am. Chem. Soc.* **1999**, *121*, 1405.
- ⁸⁹ Bhawalker, J. D.; He, G. S.; Prasad, P. N. *Rep. Prog. Phys.* **1996**, *59*, 1041.

- ⁹⁰ Osawa, M.; Hoshino, M.; Horiuchi, S.; Wakatsuki, Y. *Organometallics* **1999**, *18*, 112.
- ⁹¹ Errington, J.; McDonald, W. S.; Shaw, B. *J. Chem. Soc., Dalton Trans.* **1980**, 2312.
- ⁹² a) Kickham, J. E.; Loeb, S. J.; Murphy, S. L. *Chem. Eur. J.* **1997**, *3*, 1203; b) Cameron, B. R.; Loeb, S. J.; Yap, G. P. A. *Inorg. Chem.* **1997**, *36*, 5498.
- ⁹³ Bergbreiter, D. E.; Osburn, P. L.; Liu, Y.-S. *J. Am. Chem. Soc.* **1999**, *121*, 9531.
- ⁹⁴ Hall, J.; Loeb, S. J.; Shimizu, G. K. H.; Yap, G. P. A. *Angew. Chem. Int. Ed.* **1998**, *37*, 121.
- ⁹⁵ Huck, W. T. S.; van Veggel, F. C. J. M.; Kropman, B. L.; Blank, D. H. A.; Keim, E. G.; Smithers, M. M. A.; Reinhoudt, D. N. *J. Am. Chem. Soc.* **1995**, *117*, 8293.
- ⁹⁶ a) Huck, W. T. S.; Snellink-Ruël, B. H. M.; Lichtenbelt, J. W. T.; van Veggel, F. C. J. M.; Reinhoudt, D. N. *Chem. Commun.* **1997**, 9; b) Huck, W. T. S.; van Veggel, F. C. J. M.; Reinhoudt, D. N. *J. Mater. Chem.* **1997**, *7*, 1213.
- ⁹⁷ Huck, W. T. S.; van Veggel, F. C. J. M.; Reinhoudt, D. N. *Angew. Chem. Int. Ed. Engl.* **1996**, *35*, 1213.
- ⁹⁸ Huck, W. T. S.; van Veggel, F. C. J. M.; Sheiko, S. S.; Möller, M.; Reinhoudt, D. N. *J. Phys. Org. Chem.* **1998**, *12*, 540.
- ⁹⁹ Huck, W. T. S.; Prins, L. J.; Fokkens, R. H.; Nibbering, N. M. M.; van Veggel, F. C. J. M.; Reinhoudt, D. N. *J. Am. Chem. Soc.* **1998**, *120*, 6240.
- ¹⁰⁰ More information about hydrogen-bonded rosettes can be found in: a) Whitesides, G. M.; Simanek, E. E.; Mathias, J. P.; Seto, C. T.; Chin, D. N.; Mammen, M.; Gordon, D. M. *Acc. Chem. Res.* **1995**, *28*, 37; b) Simanek, E. E.; Li, X.; Choi, I.; Whitesides, G. M. Cyanuric Acid and Melamine: A Platform for the Construction of Soluble Aggregates and Crystalline Materials. In *Comprehensive Supramolecular Chemistry*; Lehn, J.-M., Chair Ed.; Atwood, J. L., Davis, J. E. D., MacNicol, D. D., Vögtle, F., Exec. Eds.; Pergamon: Oxford, UK, 1987-1996; Vol. 9, Chapter 17; c) Timmerman, P.; Vreekamp, R. H.; Hulst, R.; Verboom, W.; Reinhoudt, D. N.; Rissanen, K.; Udachin, K. A.; Ripmeester, J. *Chem. Eur. J.* **1997**, *3*, 1823; d) Prins, L. J.; Timmerman, P.; Reinhoudt, D. N. *Angew. Chem. Int. Ed.* **2001**, *40*, in press.
- ¹⁰¹ Zimmerman, S. C.; Zeng, F.; Reichert, D. E. C.; Kolotuchin, S. V. *Science* **1996**, *271*, 1095.
- ¹⁰² Huck, W. T. S.; Hulst, R.; Timmerman, P.; van Veggel, F. C. J. M.; Reinhoudt, D. N. *Angew. Chem. Int. Ed. Engl.* **1997**, *36*, 1006.

Chapter 3

The coordination chemistry of SCS Pd(II) pincers[#]



X-ray crystal structure of SCS Pd^{II} pincer **7**.

The metallodendrimers studied in our group are held together via non-covalent coordination bonds between SCS Pd(II) pincer moieties and suitable ligands such as nitriles and pyridines. A systematic investigation toward the coordination strengths of a broader ligand range was carried out in order to increase the scope of metallodendrimer synthesis. In this chapter the results of such an investigation are presented. A model SCS Pd(II) pincer compound has been synthesized, and the coordination of nitrogen-, sulfur- and phosphorus-containing ligands to this moiety has been studied. The overall coordination strength of the investigated ligands toward the SCS Pd(II) pincer system is as follows: nitriles < pyridines < thioureas < phosphites < phosphines.

[#] The work described in this chapter has been published: van Manen, H.-J.; Nakashima, K.; Shinkai, S.; Kooijman, H.; Spek, A. L.; van Veggel, F. C. J. M.; Reinhoudt, D. N. *Eur. J. Inorg. Chem.* **2000**, 2533.

3.1 Introduction

As already outlined in chapter 1, the “bottom-up” approach to technological devices is becoming a viable alternative for conventional “top-down” techniques. In particular self-assembly, one of the main themes in supramolecular chemistry, is anticipated to play a vital role in applications of nanotechnology. For example, it has recently been demonstrated by Mirkin and coworkers that self-assembled monolayers on a gold surface¹ combined with scanning probe microscopy leads to a novel lithographic technique called “dip-pen nanolithography”, enabling the creation of patterns on the surface with a resolution of 15 nm.² Initial steps toward molecular electronic devices³ also rely on self-assembly, as a number of recent examples demonstrate. For example, Stoddart and Heath *et al.* have employed redox-active, catenane-based molecular switches and proved them to be reconfigurable (that is, switched on and off) repeatedly on a surface under ambient conditions (Figure 3.1).⁴ The catenane used in this work consists of two mechanically interlinked molecular rings held in specific positions due to non-covalent charge-transfer interactions.

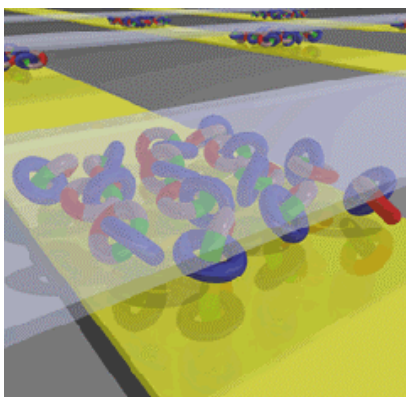


Figure 3.1. Schematic picture of a catenane switch between two wires.

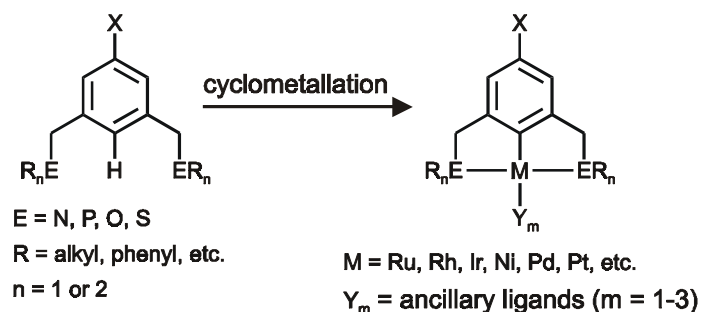
A self-assembled monolayer of rigid oligomeric phenylacetylenes on gold was shown by Tour, Reed and coworkers to exhibit negative differential resistance (a type of switching behavior) and to store information like a memory device.⁵ Finally, an electronic switch consisting of a gold nanocluster bound to a self-assembled film of redox-active viologen ligands was recently developed by Schiffrin, Nichols and their coworkers.⁶

Since this thesis deals with the generation of non-covalent nanosize assemblies formed by the coordination of ligands to SCS Pd^{II} pincers, an overview of transition metal pincer systems in supramolecular chemistry and catalysis will be provided in section 3.2. The role of coordination chemistry in supramolecular chemistry will be further discussed in chapter 4.

3.2 Pincer systems in supramolecular chemistry and transition metal catalysis

Organometallic complexes contain a metal-to-carbon bond, which is often stabilized by chelation, leading to the formation of metallacycles. The first organometallic complexes having terdentate monoanionic ligands were reported in 1976 by Moulton and Shaw.⁷ These “pincer”

ligands are *meta*-xylene derivatives in which the two methylene units carry neutral, two-electron donor moieties such as NR₂, PR₂, OR, or SR. Cyclometallation of pincer ligands with a range of different transition metals occurs with formation of two five-membered metallacycles, where the type of metal that can be inserted is dependent on the type of donor moiety (Scheme 3.1).



Scheme 3.1. Direct cyclometallation of pincer ligands.

Modification of various ligand parameters allows the fine-tuning of both the steric and electronic properties of the complexed metal center. For example, the nature of the donor atoms E, the introduction of functional groups in the benzylic positions, substitution on the aromatic ring, and the type of ancillary ligands all have a profound (electronic) effect on the transition metal.

Most investigations have been carried out with pincer ligands containing phosphorus, nitrogen, or sulfur donor groups.⁸ In this brief overview emphasis is placed on pincer complexes of metals of the nickel triade (Ni, Pd, Pt) based on these donor moieties. Specifically, the versatility of such pincer complexes in supramolecular chemistry and catalysis will be highlighted.

3.2.1 PCP pincer systems

Direct cyclometallation is an attractive method for the formation of a M–C bond, since it does not require prefunctionalization of the pincer ligand in order to achieve selective *ortho*-cyclometallation. In their seminal article, Moulton and Shaw demonstrated the use of PCP ligands (Scheme 3.1, ER_n = P(*t*-Bu)₂, X = H) in direct C–H bond activation and subsequent cyclometallation with Ni, Pd, Pt (Y = Cl, Br, H, CN, C≡CPh), Rh, and Ir.⁷ Since then, a wide variety of other phosphines PR₂ (R = Ph, Me, Et, *i*-Pr, Bn) and metal precursors have been successfully applied in direct cyclometallation.⁹

Metal complexes of PCP pincer ligands have been mainly designed and prepared for their potential in a wide range of catalytic reactions. Dependent on the metal M and donors E (Scheme 3.1), various reactions have been catalyzed, such as alkane dehydrogenation (M = Ir, ER_n = P(*t*-Bu)₂, P(*i*-Pr)₂),¹⁰ hydrogenation (M = Ru, ER_n = PPh₂),¹¹ asymmetric aldol condensation (M = Pt, Pd, ER_n = PPh₂),¹² and the Heck reaction.¹³ A Pd^{II} PCP pincer system in which the methylene

groups had been substituted for oxygens (to produce phosphinites) was recently shown to catalyze even the Heck reaction of aryl chlorides with styrene.¹⁴

In an attempt to construct heteronuclear metallodendrimers containing different metals in each generation, metal complexes (Ni^{II} , Pd^{II} , and Pt^{II}) of PCP pincers were prepared in our group as dendritic building blocks.¹⁵ Both the dendritic core $\mathbf{G}_{0,\text{M}}$ and the branched monomer $\mathbf{BB}_\text{M}-\text{Cl}$ (Chart 3.1) were obtained by cyclometallation of the corresponding free PCP pincer ligands with either $\text{NiCl}_2 \cdot 6\text{H}_2\text{O}/\text{Hünig's base}$, $\text{Pd}[\text{MeCN}]_4(\text{BF}_4)_2$, or $[\text{PtCl}_2(\text{PPh}_3)_2]$, respectively.

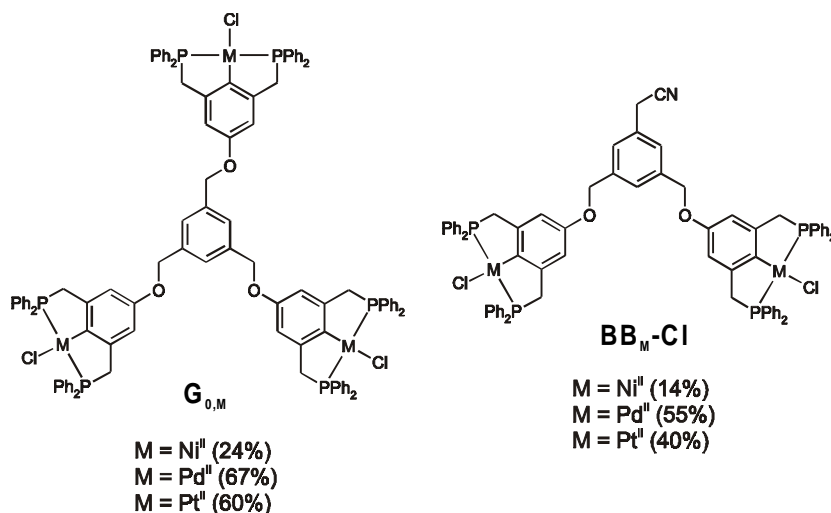


Chart 3.1. Various metal PCP pincer complexes employed as metallodendrimer building blocks (yields of cyclometallation reactions in brackets).

Reaction of the free pincer ligands with $\text{HRh}(\text{PPh}_3)_4$ or $[\text{RhCl}(\text{cod})]_2$ (cod = 1,5-cyclooctadiene) did not give any cyclometallated products, which was attributed to deactivation of the C–H bond toward metal insertion by the electron-donating *para* ether moiety.

Model studies with $\mathbf{G}_{0,\text{M}}$ and $\mathbf{BB}_\text{M}-\text{Cl}$ showed that activation of the M–Cl complexes with AgBF_4 and subsequent coordination of nitrile ligands (MeCN) to the fourth coordination site is fast and quantitative (as determined from ^{31}P NMR spectroscopy). However, assembly experiments aiming at the synthesis of homo- and heteronuclear metallodendrimers from these building blocks showed that the metallodendrimers are not very stable in solution, thereby hampering both their isolation in pure form and their characterization.

Recently, Beletskaya and Van Koten *et al.* reported acetylene-bridged di-,^{16a} tri-^{16b} (very similar to $\mathbf{G}_{0,\text{M}}$ depicted in Chart 3.1) and hexanuclear^{16b} cyclopalladated PCP pincer complexes as potential recyclable catalysts. Due to their rigid structure and nanosize dimensions, these complexes are expected to be isolable from reaction mixtures using nanofiltration membranes. However, no data concerning the use of these pincer complexes as catalysts has been provided yet.

3.2.2 NCN pincer systems

Direct cyclometallation is uncommon in NCN pincer systems, due to the lower bond strength of the amine M–N bond compared to the corresponding M–P bond. Instead of *ortho,ortho* double cyclometallation, bimetallic products from undesired *ortho,para* cyclometallation are often obtained.¹⁷ If the central hydrogen (Scheme 3.1) is replaced by a Me₃Si moiety, this problem can be circumvented and selective C–Si bond activation by a palladium precursor gives the *ortho,ortho* doubly cyclopalladated complex. Another method to provide *ortho,ortho* doubly cyclometallated products from NCN pincer ligands starts from the corresponding aryl bromides or iodides (Scheme 3.1, H replaced by Br or I) and takes place *via* carbon-halogen oxidative addition to Pd,¹⁸ Ni,¹⁹ or Pt²⁰ precursor complexes. Halide-lithium exchange of such aryl halides followed by transmetalation of the aryllithium species with suitable metal complexes is also straightforward.²¹ More than 20 different metals have been complexed with NCN pincer ligands,²² although the binding modes of some metals differ from the meridional η^3 -N,C,N-bonding shown in Scheme 3.1.

Like their PCP counterparts, metal complexes of NCN pincer ligands have been applied in catalysis. In particular, the Kharasch addition of polyhalogenated alkanes to olefinic double bonds catalyzed by Ni^{II} NCN pincer complexes has been studied intensively.²³ Recently, the immobilization of catalytic moieties onto homogeneous supports such as dendrimers and hyperbranched polymers has been under active investigation,²⁴ with the aim of combining homogeneous catalytic applications with heterogeneous separation techniques such as nanofiltration. This strategy was first demonstrated in 1994, when Van Koten and coworkers reported the anchoring of up to twelve Ni^{II} NCN pincers *via* a carbamate linker to the periphery of a carbosilane dendrimer.²⁵ The catalytic activity of the largest dendrimer (in terms of turnovers per Ni^{II} site per hour) was found to be 30% lower than a similar mononuclear pincer catalyst. Direct covalent attachment of the aryldiamine ligands to the dendritic silyl end groups, followed by insertion of catalytically active Ni^{II} centers *via* lithiation/transmetalation procedures, has recently been reported as a viable alternative to the initial carbamate linker strategy (see Figure 3.2 for an example).²⁶



Figure 3.2. Dendrimers having NCN pincer systems directly attached to the peripheral silyl groups.

Dendrimers having up to 36 pincer ligands were synthesized in this manner, however, nickelation of the peripheral ligands beyond 80-90% could not be achieved, probably due to hydrolysis of the intermediate lithiated species. Importantly, increasing the dendrimer generation resulted in a significant decrease in catalytic activity. This negative dendritic effect was attributed to surface congestion effects, since the small intramolecular Ni...Ni distance is likely to promote side reactions. This hypothesis was corroborated by the fact that alternative, less condensed nickelated carbosilane dendrimers displayed significantly improved catalytic activities. The dendrimer depicted in Figure 3.2 was employed in both batch and continuous operating nanofiltration membrane reactor systems. In the second case, a continuous feed of $[\text{Bu}_4\text{N}]\text{Br}$ had to be applied in order to prevent catalyst precipitation, although this resulted in both a lower activity and in part of the addition product containing chlorine and bromine atoms.

In order to circumvent the problem of reduced catalytic activity due to small intramolecular Ni...Ni distances, a third generation Fréchet dendritic wedge has been functionalized with an NCN Ni^{II} pincer moiety at its focal point (Figure 3.3).²⁷

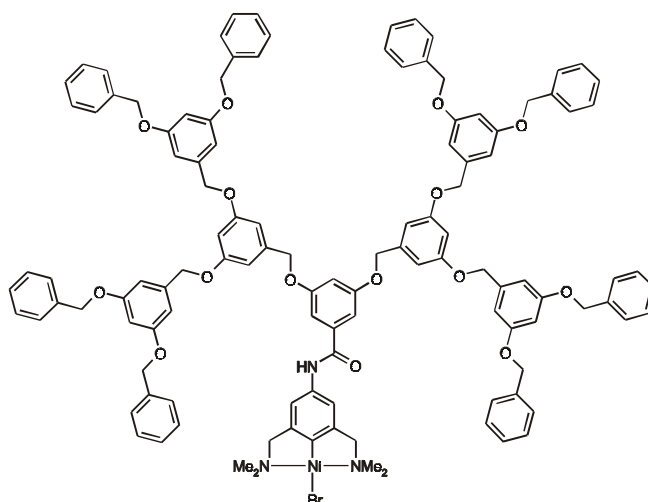


Figure 3.3. Catalytically active Fréchet-type dendritic wedge.

The reaction rate and turnover number of this dendritic wedge in the Kharasch addition of CCl_4 to methyl methacrylate is similar to those of unsupported, mononuclear NCN Ni^{II} pincer catalysts. Moreover, when compartmentalized in a nanofiltration-membrane-capped immersion vial, the catalyst was able to catalyze the reaction between CCl_4 and methyl methacrylate on the other side of the membrane.

Whereas Ni^{II} NCN pincers have mainly been applied as catalytic materials, the corresponding Pt^{II} pincers have been used recently as sensors for the detection of gaseous SO_2 both in solution²⁸ and in the solid state.²⁹ The Pt^{II} centers in square-planar complexes containing the monoanionic NCN pincer ligand display an enhanced nucleophilicity when compared to other d^8 metal centers. As a consequence, they react instantaneously and reversibly with Lewis acids such as SO_2 to form five-coordinate adducts, a process accompanied by a diagnostic color change from colorless to bright orange. Corresponding Ni^{II} adducts are unstable, and similar Pd^{II} adducts do not form at all. Various dendrimers functionalized with sensing NCN Pt^{II} pincer moieties have been constructed. Remarkably, the hexametallc aryl ester dendrimer shown in Figure 3.4 could be synthesized convergently since the organometallic Pt^{II} pincer moiety is stable to both esterification and TBDMS deprotection.

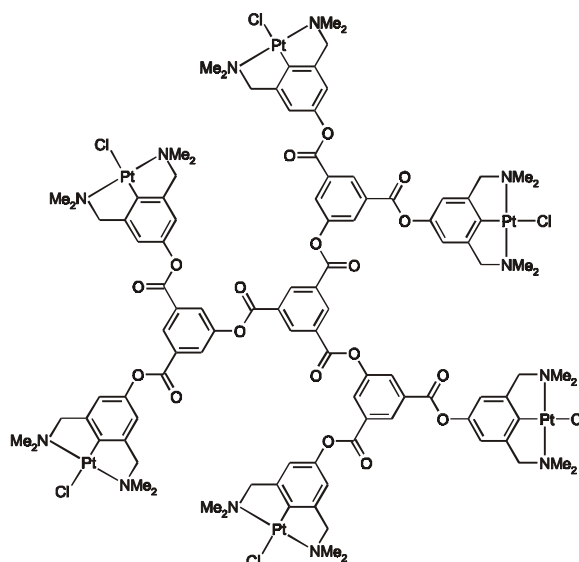


Figure 3.4. Dendrimer containing peripheral Pt(II) NCN pincers for detection of SO₂.

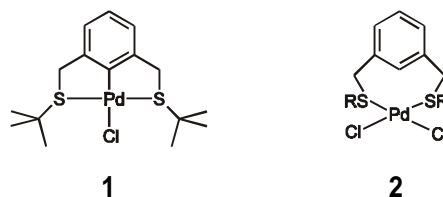
Whereas this metallodendrimer displays a low solubility in common organic solvents, the solubility is greatly enhanced upon binding of SO₂, which is fast and fully reversible. Other characteristics of these sensor devices include facile quantification of the amount of SO₂ present and high selectivities for SO₂ binding (even in the presence of other acids such as HCl, CO₂, or H₂O).

Besides Ni^{II} NCN pincer systems, analogous Pd^{II} pincers have also demonstrated their catalytic potential, albeit to a lesser extent. For example, diaminoaryl Pd^{II} complexes have been grafted onto a hyperbranched polytrialkylsilane support ($M_w = 5500$ g/mol, $M_w/M_n = 5.2$) and their catalytic activity in the aldol condensation of benzaldehyde and methyl isocyanoacetate has been investigated.³⁰ Again, an activity similar to single-site Pd^{II} pincers was found, indicating that the Pd^{II} centers in the macromolecular catalyst function as independent catalytic sites.

3.2.3 SCS pincer systems

The first cyclometallation of an SCS pincer ligand was demonstrated by Errington *et al.* in 1980.³¹ Treatment of 1,3-bis(*tert*-butylthiomethyl)benzene with Na₂PdCl₄ and NaOAc in ethanol gave the cyclopalladated product ([2,6-bis(*tert*-butylthiomethyl)phenyl]chloropalladium(II), **1**) in 53% yield. Since then, various other (often improved) direct cyclopalladation methods have been described, using *e.g.* ligand exchange between a cyclopalladated precursor and the SCS ligand in the presence of acid,³² Pd[MeCN]₄(BF₄)₂ in MeCN,³³ Pd(PhCN)₂Cl₂ in MeCN, and Pd(TFA)₂ in DMF.³⁴ Employing Pd(MeCN)₂Cl as a cyclopalladating reagent, Lucena *et al.* found that the important factors in the promotion of cyclopalladation of SCS pincer ligands are the electronic configuration on the sulfur atoms and the steric hindrance imposed by the substituents on the sulfur donor atoms.³⁵ Moreover, uncyclopalladated compounds such as **2**

could be isolated as intermediates, suggesting that coordination of both sulfur atoms to Pd^{II} is an important first step toward subsequent cyclopalladation.



Remarkably, nearly all studies on cyclometallation of SCS pincer ligands have focussed on Pd^{II} as the inserted transition metal. Only one example of an SCS Pt^{II} complex has been described.³⁶

In contrast to cyclometallated PCP and NCN pincer systems, the catalytic properties of related SCS pincer systems³⁴ have virtually been unexplored so far. Instead, Pd^{II} SCS pincers have recently been applied in molecular recognition^{33,37} and self-assembled coordination architectures ranging from one-dimensional coordination polymers³⁸ to three-dimensional metallodendrimers.³⁹

Metalloreceptors for aromatic amines such as *p*-aminopyridine and the DNA nucleobases adenine and guanine were developed by the group of Loeb.^{37a} In these receptors, binding of guests occurs through simultaneous first- and second-sphere coordination involving three separate interactions: first-sphere σ donation from an aromatic nitrogen to the Pd^{II} center, second-sphere hydrogen bonding between NH₂ groups and polyether oxygens, and π -stacking between the electron-poor aromatic rings of the substrate and the electron-rich aromatic spacing units of the receptor. The structure of a representative metalloreceptor is shown in Figure 3.5a, and the crystal structure of its complex with guanine is depicted in Figure 3.5b.

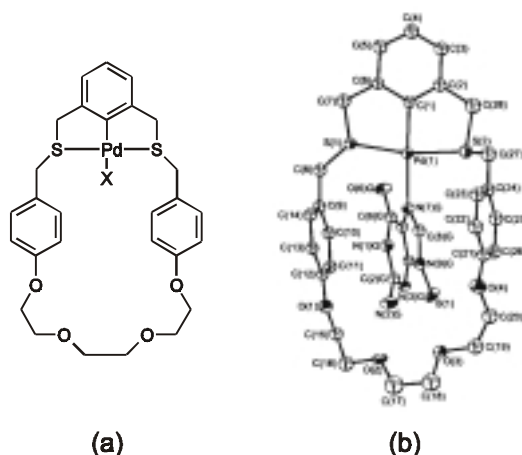
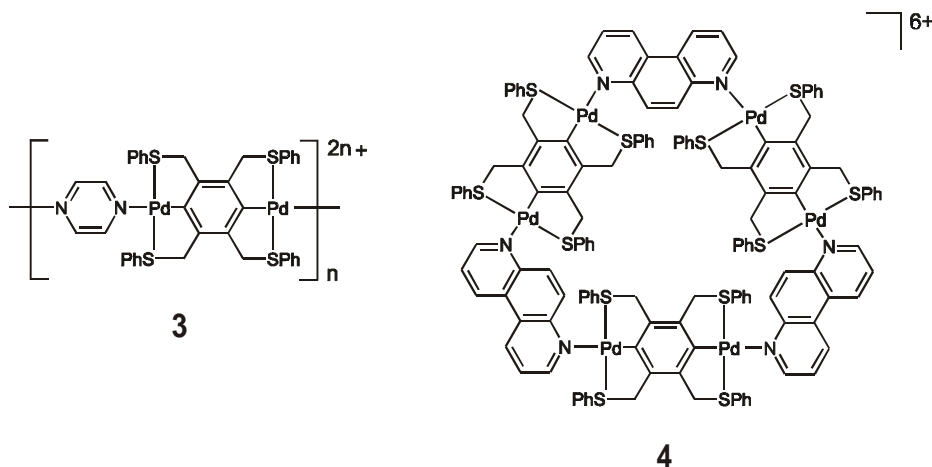


Figure 3.5. a) Structure of a metalloreceptor; b) Crystal structure of its complex with guanine.

Self-assembled structures based on SCS Pd^{II} pincers have been obtained by combining bimetallic synthons with ditopic pyridine-type ligands; this has afforded either polymeric³⁸ structures (such as **3**) or molecular hexagons (**4**).⁴⁰



As stated above, the catalytic properties of SCS Pd^{II} pincer systems have not been investigated in great detail. Bergbreiter *et al.* found that the Heck reaction between various aryl iodides and alkene acceptors was efficiently catalyzed by SCS Pd^{II} pincers appended to 5000 M_n poly(ethylene glycol).³⁴ The PEG-bound Pd^{II} complex could be recycled *via* precipitation three times without deactivation. Recently, six SCS Pd^{II} pincers have been grafted onto a benzene core in order to provide a rigid catalyst of nanosize dimensions, suitable for membrane retention purposes.⁴¹ However, the catalytic properties of this hexametallc system have not been reported so far.

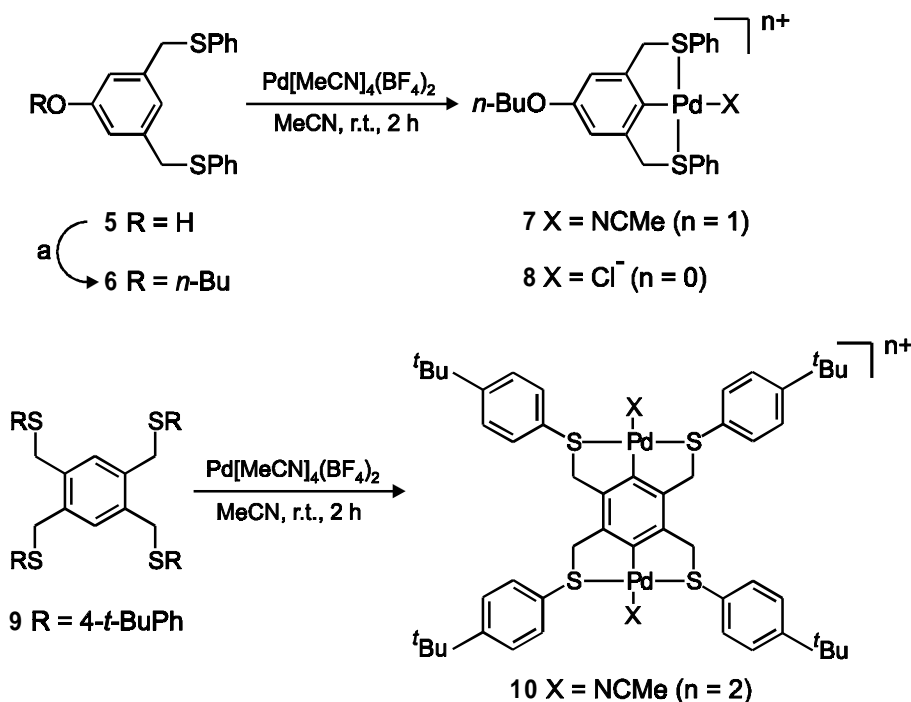
3.3 Aim and scope of this chapter

In our group, the construction of metallodendrimers in which the coordination of nitrile and pyridine groups to SCS Pd^{II} pincers is used as the assembly motif has been investigated.³⁹ In order to increase the scope of metallodendrimer synthesis, a systematic investigation toward the coordination strength of a broader range of ligands is necessary. The results of this investigation are described in this chapter. A model SCS Pd^{II} pincer system has been synthesized and structurally characterized by X-ray crystallography. The coordination of various nitrogen-, sulfur- and phosphorus-containing ligands to this pincer moiety has been studied in detail.

3.4 Results and discussion

3.4.1 Synthesis and characterization of model SCS Pd^{II} pincer complexes

The SCS Pd^{II} pincer complexes **7** and **8** were prepared in two and three steps, respectively (Scheme 3.2). After alkylation of the previously reported⁴² SCS pincer ligand **5** with *n*-butyl bromide (77% yield), cyclopalladation of the resulting ligand **6** was achieved with Pd[CH₃CN]₄(BF₄)₂ in MeCN.



Scheme 3.2. Synthesis of Pd(II) pincer complexes **7**, **8**, and **10**; a) *n*-BuBr, *t*-BuOK, CH₃CN.

The cationic acetonitrile complex **7** (containing the non-coordinating BF₄⁻ counter anion) was obtained in 90% yield, followed by precipitation from CH₃CN solution with Et₂O. The neutral chloride complex **8** was isolated in 94% yield by stirring a solution of **7** in CH₂Cl₂/CH₃CN with saturated NaCl, followed by column chromatography.

Similarly, dipincer system **10** was prepared in two steps from 1,2,4,5-tetrakis(bromomethyl)benzene by first reacting the benzylic bromides with *tert*-butyl thiophenol using K₂CO₃ as a base and 18-crown-6 as a catalyst (81% yield), followed by cyclopalladation of dipincer ligand **9** using Pd[CH₃CN]₄(BF₄)₂ in CH₃CN. The bis(MeCN) complex **10** was purified by precipitation from CH₃CN solution with Et₂O (60% yield). Complexes **7**, **8**, and **10** were isolated as air and moisture stable, yellow solids. All spectroscopic and analytical data are consistent with cyclopalladation. Compared to free ligands **6** and **9**, the ¹H NMR resonances for the diastereotopic CH₂S protons in the palladium complexes are shifted downfield by ≈ 0.5 ppm and they are broad due to slow conformational interconversion of the Pd^{II}-containing five-membered rings. At lower temperatures the coupling of the two diastereotopic CH₂S protons causes the splitting of the broad signal into a pair of doublets (*vide infra*). Also in the ¹H NMR spectra the signal for the *ortho*-protons at δ 6.80 (in **6**) or 6.92 (in **9**) ppm is absent, indicating complete cyclopalladation. In the ¹³C NMR spectra of the acetonitrile complexes **7** and **10**, the signal of the carbon directly linked to Pd^{II} is too weak to be observed (probably due to long relaxation times), whereas in the chloride complex **8** it is present at 150.9 ppm (30 ppm downfield compared to ligand **6**). In the positive FAB mass spectrum of **8**, a signal corresponding to [M - Cl + H]⁺ ($m/z = 499.6$) is present, whereas in the negative FAB mass

spectrum the chloride remains coordinated to Pd^{II}, resulting in a signal at $m/z = 533.7$ ($[M]^-$). The loss of the acetonitrile ligand is observed in both the positive and negative FAB-MS spectra of **7**, resulting in signals corresponding to $[M - \text{MeCN} - \text{BF}_4]^+$ ($m/z = 499.0$) and $[M - \text{MeCN} + \text{BF}_4]^-$ ($m/z = 671.6$), respectively, and both acetonitriles are lost in the positive FAB-MS spectrum of **10** ($m/z = 1001.1$ for $[M - 2\text{MeCN} - 2\text{BF}_4 + \text{H}]^+$).

3.4.2 X-ray structure of **7**

Besides the analytical evidence discussed above, structural proof of the acetonitrile complex **7** was provided by X-ray analysis. A drawing of the acetonitrile complex **7** is shown in Figure 3.6; geometric parameters are provided in the experimental section. The following bond lengths of the atoms bonded to Pd^{II} have been obtained: Pd—S(1) 2.2992(8) Å, Pd—S(2) 2.2961(9) Å, Pd—N 2.110(2) Å, Pd—C(1) 1.975(2) Å.

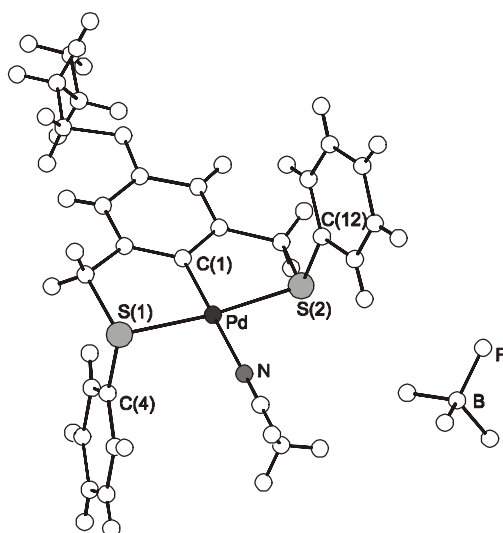


Figure 3.6. X-ray crystal structure of SCS Pd(II) pincer complex **7**.

The Pd atom adopts a slightly distorted square-planar geometry (S(1)—Pd—S(2) 171.11(2)° and N—Pd—C(1) 178.26(11)°) and the two five-membered chelate rings possess somewhat distorted envelope conformations in which the two phenyl rings (oriented anti with respect to the square plane) are in axial positions (Pd—S(1)—C(4) 100.51(9)° and Pd—S(2)—C(12) 103.17(9)°). It should be noted that complex **7** is chiral in the solid state (prepared as a racemate) due to a lack of symmetry elements.

3.4.3 Substitution of the labile MeCN ligand by pyridines

The substitution of the labile acetonitrile ligand of complex **7** by stronger ligands such as pyridines proceeds easily. Upon treatment of **7** with 1.1 equiv of pyridine (in CDCl₃), a fast and quantitative substitution was observed. In the ¹H NMR spectrum of the pyridine adduct (Figure 3.7), the resonance of the pyridine α-protons has shifted *upfield* from 8.70 (free pyridine) to 8.15

ppm (coordinated pyridine). This is different from pyridine complexes of SCS Pd^{II} pincers reported by Loeb and coworkers⁴³ for which upon coordination a *downfield* shift of the pyridine α -protons was observed.

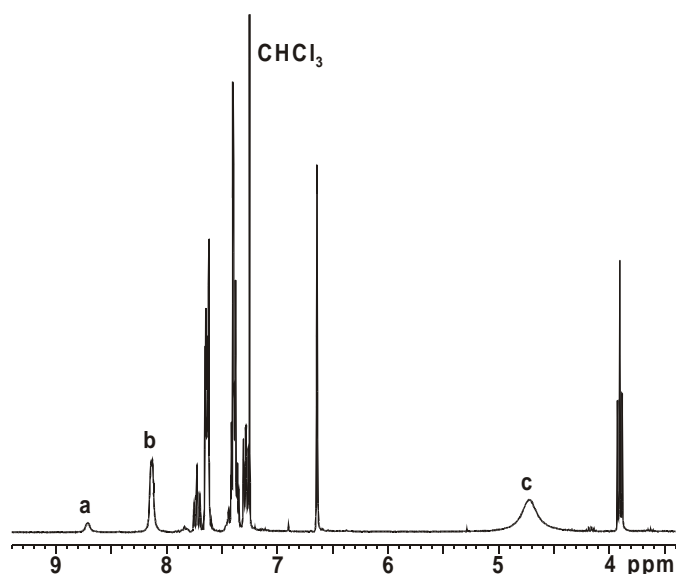


Figure 3.7. Part of the ¹H NMR spectrum (CDCl₃, 298 K) of the pyridine adduct of complex **7**. The designated signals correspond to the pyridine α -protons of free (**a**) and complexed (**b**) pyridine and to the CH₂S protons of the five-membered chelate rings (**c**).

This difference must be due to the presence of the phenyl rings in our system attached to the sulfur atoms. The ring current of these aromatic rings will have a shielding effect on the pyridine protons (mostly the α -protons). The α -proton signal is also considerably broadened, indicating hindered rotation of the pyridine ligands with respect to the plane of coordination. The CH₂S proton signal shifts 0.15 and the aromatic proton signal 0.05 ppm downfield upon substitution of MeCN by pyridine. The increase in coordination strength of the pyridine ligand with respect to acetonitrile is also evident from the positive FAB mass spectrum, in which a small, but significant peak corresponding to the molecular ion [M – BF₄]⁺ is observed at $m/z = 578.4$, in addition to a large signal at $m/z = 499.2$ originating from [M – pyr – BF₄]⁺.

Upon adding excess pyridine, two separate signals for free and complexed pyridine are observed. This observation can be explained by either a slow exchange of pyridine on the NMR timescale or a kinetically stable pyridine complex. Exchange of pyridine was indeed evidenced by treatment of the pyridine complex with an excess (5 equiv) of pyridine-*d*₅. The signal at 8.15 ppm disappeared whereas a new peak appeared at 8.7 ppm, indicating free pyridine. This kinetic lability is consistent with other pyridine–Pd^{II} complexes.⁴⁴

The pyridine exchange rate is dependent on the solvent. In CDCl₃ two separate signals for bound and free pyridine were observed up to 50 °C. However, when acetonitrile complex **7** was treated with 2 equiv of pyridine in DMSO-*d*₆, a coordinating solvent, only one broad signal

for the pyridine α -protons was observed in the ^1H NMR spectrum, indicating a fast exchange on the NMR timescale. When $\text{DMSO-}d_6$ was titrated to a CDCl_3 solution of the pyridine complex containing 1 equiv of excess pyridine (Figure 3.8), the rate of pyridine exchange varied with the concentration of $\text{DMSO-}d_6$.

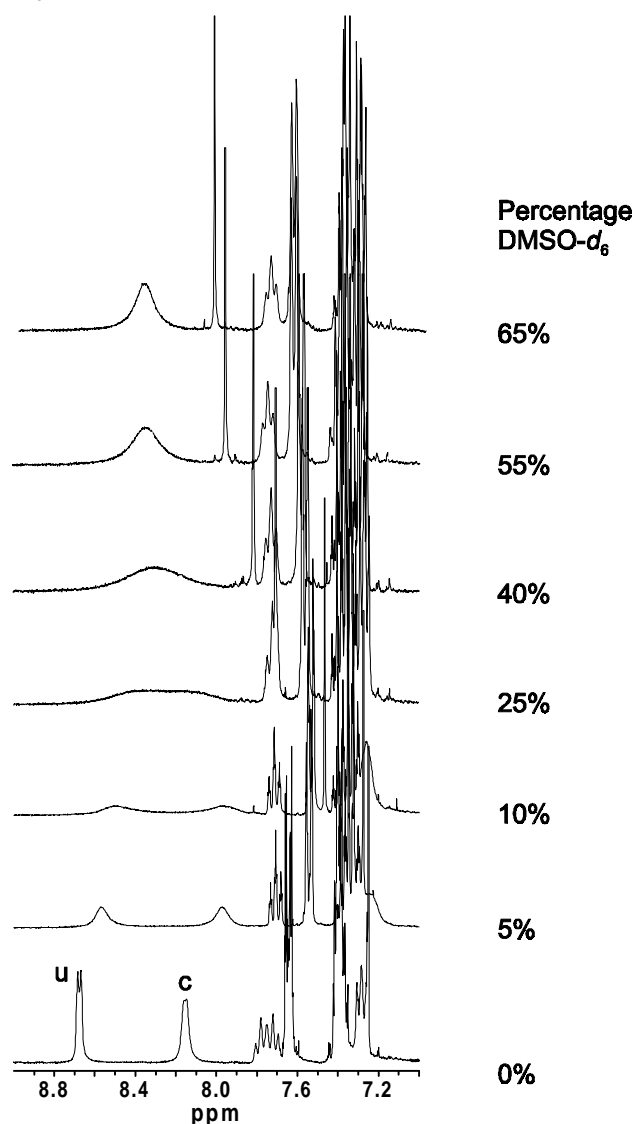
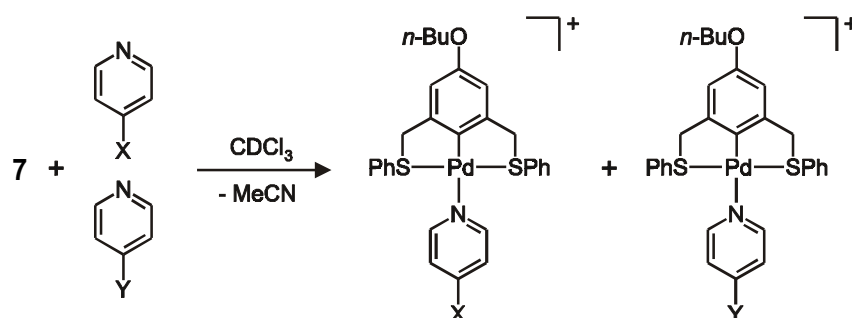


Figure 3.8. ^1H NMR spectra (298 K) of the titration of $\text{DMSO-}d_6$ to a CDCl_3 solution of the pyridine complex of the SCS Pd(II) pincer system containing an excess of 1 equiv of pyridine. The designations *u* and *c* correspond to the pyridine α -proton signals of uncoordinated and coordinated pyridine, respectively.

It is known that the kinetics of substitution in d^8 square-planar complexes depends on two factors, one related to direct ligand attack (associative-dissociative mechanism) and the other to an associative solvolysis pathway, in which the leaving group is first displaced by a solvent molecule, which in turn is subsequently substituted by the incoming ligand (dissociative-associative mechanism).⁴⁵ The observed pyridine exchange rate can be rationalized in this way. With increasing $\text{DMSO-}d_6$ concentration, the pyridine exchange increasingly follows the

solvolysis pathway. In CDCl_3 this pathway is not possible and only slow direct pyridine attack occurs.

Within a series of *para*-substituted pyridines, it is anticipated that subtle differences in nitrogen electron density can control the coordination strength toward the SCS Pd^{II} pincer system.



Scheme 3.3. Competition experiments between *para*-substituted pyridines.

Two different pyridines (each 1 equiv) were mixed with 1 equiv of the acetonitrile complex **7** in CDCl_3 (Scheme 3.3), and the α -proton signals of the two pyridines in the ^1H NMR spectra were used as a probe to determine the extent of coordination of each pyridine (see Figure 3.9 for an example).

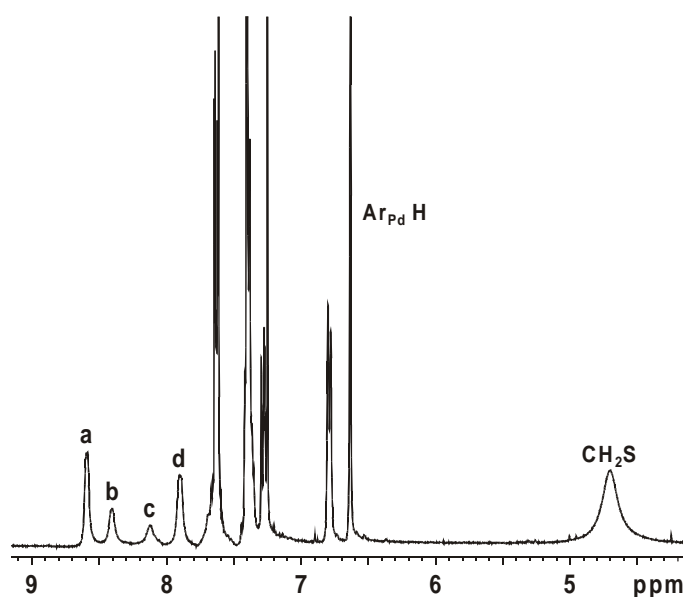


Figure 3.9. Part of the ^1H NMR spectrum (CDCl_3 , 298 K) of a competition experiment between pyridine and 4-methoxypyridine. The designated signals correspond to the pyridine α -proton signals of: free pyridine (**a**), free 4-methoxypyridine (**b**), bound pyridine (**c**), and bound 4-methoxypyridine (**d**).

The degree of coordination of each pyridine in these competition experiments is under thermodynamic, rather than kinetic, control. This was determined by comparing the results of competition experiments using simultaneous versus sequential addition of the two different

pyridines to **7**. For example, upon simultaneous addition of pyridine and 4-methylisonicotinate (each 1 equiv) to **7** (1 equiv) in CDCl_3 , a mixture of 64% complexed pyridine and 36% complexed pyridine ester was obtained (Table 3.1). Within the experimental error, the same distribution resulted upon addition of 1 equiv of the weaker ligand 4-methylisonicotinate to 1 equiv of the *preformed* pyridine complex.

Table 3.1 shows that electron-donating pyridines bind stronger than pyridine, whereas electron-withdrawing pyridines are weaker ligands than pyridine. The stability of these pyridine complexes follows the Hammett equation using the σ^+ constant of Brown and Okamoto.⁴⁶ The use of this modified substituent constant applies to reactions in which a strong acceptor character develops at the aromatic ring, *e.g.* solvolysis of tertiary halides in which ionization is rate-determining.

Table 3.1. Results of coordination competition experiments between substituted pyridines.

X	Y	% bound pyr-X /pyr-Y	Selectivity ^a
4-H	4-NH ₂	17/83	4.88
4-H	4-MeO	32/68	2.13
4-H	4- ^t Bu	40/60	1.50
4-H	4-Me	45/55	1.22
4-H	4-Ph	44/56	1.27
4-H	4-Ac	62/38	0.61
4-H	4-CO ₂ Me	64/36	0.56
2-Me	4-Me	43/57	1.33
2-Me	3-Me	57/43	0.75

^aRatio of bound pyridine-Y over bound pyridine-X.

Using the selectivities as reported in Table 3.1 (only the data of the 4-substituted pyridines are analyzed), a Hammett plot as shown in Figure 3.10 is obtained with a ρ^+ value (*i.e.* the slope of the graph) of -1.0. Usually in systems obeying the Brown-Okamoto equation, the values of ρ^+ are much more negative. However, in those cases a full positive charge develops in the rate-determining step instead of the partial positive charge developing on nitrogen in pyridine-Pd^{II} coordination.

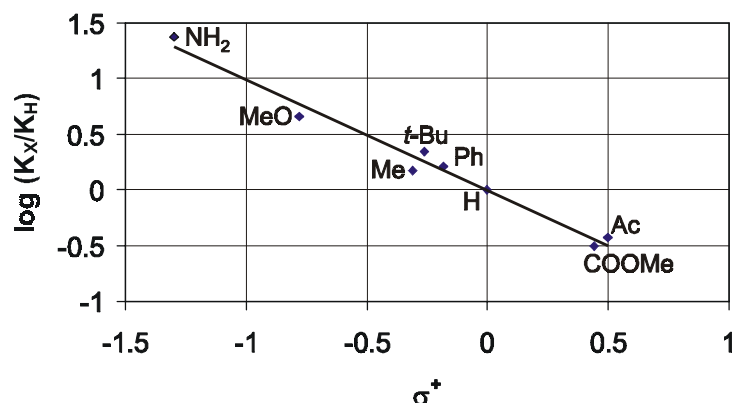


Figure 3.10. Hammett plot of the stability of 4-substituted pyridine complexes with the SCS Pd(II) pincer system against the Brown-Okamoto σ^+ substituent constant.

The effect of steric hindrance was investigated in the picoline series. On the basis of electronic effects alone, it is expected that 2-picoline binds stronger than 3-picoline. However, as the reverse was found experimentally (Table 3.1), it must be concluded that steric hindrance between the 2-methyl group and the aryl groups of the Pd^{II} pincer system overrules electronic effects in this case.

3.4.4 Coordination of triphenylphosphine to SCS Pd^{II} pincers

The coordination of phosphorus-containing ligands to SCS Pd^{II} pincers has, to our knowledge, not been investigated. Only phosphines coordinated to transition metal pincer systems of the PCP⁴⁷ and NCN⁴⁸ type, and a phosphine coordinated to an SCS Pt^{II} pincer³⁶ have been reported. Upon addition of 1 equiv of PPh₃ to **7**, phosphine coordination to Pd^{II} was evidenced by several distinct spectroscopic features. First, in the ¹H NMR spectrum a broad peak corresponding to the CH₂S protons is present. The signal is sharper and is shifted downfield (\pm 0.25 ppm) compared to the MeCN complex. Furthermore, the signal from the aromatic protons is a doublet ($J = 2.9$ Hz) due to proton-phosphorus coupling. In the ³¹P NMR spectrum, the phosphorus signal has shifted from -5.6 ppm (free PPh₃) to 13.6 ppm upon coordination. These combined results strongly indicate the coordination of PPh₃ *trans* to the cyclometallated aryl group. Opening of the S–Pd chelate ring, as suggested by Shaw *et al.*,³¹ did not occur.

3.4.5 X-ray crystal structure of **10**·(PPh₃)₂

Definite proof for the *trans*-coordination of PPh₃ to the SCS Pd^{II} pincer system was obtained by X-ray crystallography. The *dipincer* complex **10**, which is more soluble in organic solvents than reported dipincers³⁸ due to its *tert*-butyl groups, was mixed with 2 equiv of PPh₃. Crystals were grown by vapor diffusion of diethyl ether into a CHCl₃ solution of the bis(PPh₃) complex. Side and top views of the X-ray crystal structure of **10**·(PPh₃)₂ are depicted in Figure 3.11.

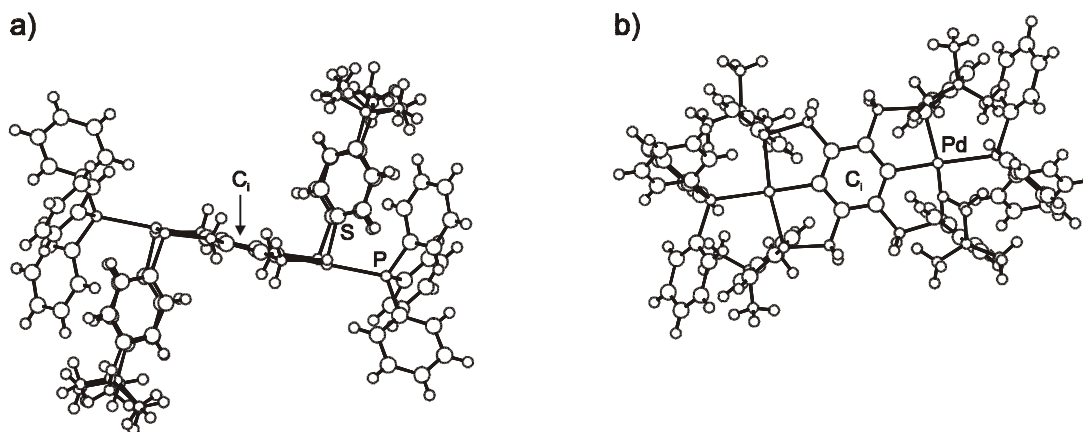


Figure 3.11. X-ray crystal structure of **10**·(PPh₃)₂; a) side view, b) top view.

In the bis(PPh₃) complex, the Pd atoms are in a distorted square-planar environment: S(1)—Pd(1)—S(2) 167.15(3)° and P(1)—Pd(1)—C(1) 178.53(9)°. The following bond lengths of the atoms bonded to Pd^{II} were obtained: Pd—S(1) 2.3075(10) Å, Pd—S(2) 2.3057(9) Å, Pd—P 2.3785(9) Å, Pd—C(1) 2.032(3) Å. The Pd^{II}—C bond is substantially longer than in complex **7** (2.03 vs. 1.98 Å). The complex has C_i symmetry (inversion point at the center of the bispalladated ring) in which the two *tert*-butyl phenyl groups attached to the metal-bound sulfur atoms of the same SCS Pd^{II} pincer moiety are oriented on the same side of the square plane.

3.4.6 Stability of coordinated PPh₃ complexes

In transition metal inorganic complexes, in general PPh₃ is a stronger ligand than pyridine. This is for example expressed in their respective nucleophilicity parameters, which differ substantially ($n_{\text{Pt}}^0 = 3.19$ for pyridine and 8.93 for PPh₃, respectively).⁴⁵ In the ¹H NMR spectrum of a mixture of 1 equiv of PPh₃ and the pyridine complex of compound **7** (Scheme 3.2: X = *pyridine*), the quantitative substitution of pyridine by PPh₃ is shown. The spectrum is a superposition of the spectra of free pyridine and the PPh₃ complex. Refluxing the PPh₃ complex in CHCl₃ with a 10-fold excess of pyridine did not result in any detectable exchange.

As mentioned before, opening of the S—Pd chelate rings by PPh₃ has been suggested.³¹ Upon adding 5 equiv of PPh₃ to *acetonitrile complex 7*, changes were not observed in neither the ¹H nor the ³¹P NMR spectra. The situation was different when PPh₃ was added to the *chloride complex 8*. Increasing amounts (0.25, 0.5, 1.0, 1.5, 2.5 and 5.0 equiv) of PPh₃ were added to **8**. The ¹H and ³¹P NMR spectra showed that an equilibrium is established after each addition. In each case two signals are observed in the ³¹P NMR spectrum, one corresponding to free PPh₃ (-5.6 ppm) and the other indicating coordination of PPh₃ that is different from the above described situation of substitution of acetonitrile, because the signal of coordinated PPh₃ now appears at 21.9 ppm instead of 13.6 ppm. In the ¹H NMR spectrum a signal appears that corresponds to “free” CH₂S protons. This means that *the S—Pd chelate ring opens upon PPh₃ addition*. It also

seems that both chelate rings open together, as only one opening would destroy the symmetry of the system. Substitution of the chloride ligand by PPh₃ is also unlikely, as can be inferred from the ³¹P NMR spectra (*i.e.* no signal observed at 13.6 ppm). Therefore it is concluded that two molecules of PPh₃ displace the sulfur atoms as ligands. This only occurs quantitatively with a large excess (> 4-5 equiv) of PPh₃.

3.4.7 Coalescence temperatures of different SCS Pd^{II} pincer complexes

The two five-membered chelate rings of the cyclopalladated pincer system display a slow conformational interconversion, which is reflected in the ¹H NMR spectrum by a broadening of the CH₂S proton signal of the pincer complexes. Different ligands have a different influence on the conformational interconversion of the chelate rings. This phenomenon is reflected in the coalescence temperature T_c where the two *separate* signals for the CH₂S protons coincide into a broad singlet. As can be seen from Table 3.2, the coalescence temperature decreases in the order acetonitrile > pyridine > chloride > triphenylphosphine.

Table 3.2. Coalescence temperatures and free energies of activation for ring interconversion of SCS Pd(II) pincer complexes **7** (Scheme 3.2, X is varied).

Ligand X	Coalescence temperature T_c (K)	Free energy of activation ΔG_c^\ddagger (kJ/mol) at T_c
MeCN	289 ± 2	57.5 ± 0.3
Pyridine	286 ± 2	56.5 ± 0.3
Cl ⁻	271 ± 2	54.8 ± 0.5
PPh ₃	< 268 ^a	–

^aNo unambiguous coalescence temperature was observed, see also text.

For the neutral ligands this order corresponds to the lone pair electron donation (the nucleophilicity) toward Pd^{II}. In the case of PPh₃, no unambiguous coalescence temperature could be observed. NMR experiments at low temperatures reveal multiple signals for the CH₂S protons for all the complexes mentioned above. On one hand, freezing the ring puckering results in a loss of the apparent C_{2v}-symmetry of the complex that exists at higher temperature in solution. On the other hand, in the PPh₃ complex one very broad signal is observed ranging from 4.3 to 5.2 ppm in going from room temperature to –10 °C. Splitting of the signal into two doublets is not observed, suggesting that besides lowering the rate of ring interconversion the rotation of the bulky PPh₃ ligand around the Pd^{II}–P bond is also restricted, leading to different conformational isomers. Moreover, a long range coupling to ³¹P cannot be excluded *a priori*.

From the coalescence temperature the free energy of activation for ring puckering can be estimated.⁴⁹ The free energies of activation for ring puckering vary between 55 and 58 kJ/mol in the order chloride < pyridine < acetonitrile as a ligand. From Table 3.2 it is evident that higher

coalescence temperatures correspond to higher free energies of activation at T_c for ring puckering in this system.

3.4.8 Coordination of other phosphorus-containing ligands

Besides triphenylphosphine other phosphorus-containing ligands were investigated as ligands for the SCS Pd^{II} pincer system. The coordination of these ligands to Pd^{II} was proven by ¹H and ³¹P NMR spectroscopy and by FAB mass spectrometry (Table 3.3).

Table 3.3. Complexes of phosphorus-containing ligands with the SCS Pd(II) pincer **7**.

Complex 7 with $X =$	¹ H NMR Ar H ^a (ppm) / J (Hz)	³¹ P NMR coord / free ligand (ppm)	FAB-MS: [M] ⁺ found / calcd
P(OMe) ₃	6.72 / 4.8	122.7 / 141.0	623.2 / 623.1
P(OPh) ₃	6.64 / 5.1	114.7 / 127.9	809.1 / 809.1
PCy ₃	6.66 / 2.9	24.0 / 11.5	779.5 / 779.3

^aAromatic protons of cyclopalladated ring.

From Table 3.3 it can be seen that the coupling of phosphites to the aromatic protons of the cyclopalladated ring is larger than the coupling of phosphines to these protons. Phosphites in general exhibit larger couplings to other nuclei than phosphines in metal complexes.⁵⁰ The increase in “s” character of the bonding orbitals in phosphite complexes compared to that in phosphines is responsible for this behavior.

As with the substituted pyridines, competition experiments were employed to establish that the relative coordination strengths of these ligands increase in the order PCy₃ > PPh₃ > P(OMe)₃ > P(OPh)₃. The relative differences in coordination strengths are quite high, as in all cases (PCy₃ vs. PPh₃, PPh₃ vs. P(OMe)₃ and P(OMe)₃ vs. P(OPh)₃) the selectivity exceeds a 4:1 ratio. Further competition experiments revealed that all phosphorus-containing ligands coordinate much more strongly than pyridine. Only a minor amount of pyridine complex was found in competition experiments with the weakest phosphite ligand (P(OPh)₃).

In the case of PCy₃ and P(OPh)₃, the addition of excess ligand to their respective phosphine or phosphite complex had no effect on the complex stability, as was the case for PPh₃ (*vide supra*). However, upon addition of excess P(OMe)₃ to complex **7** ($X = P(OMe)_3$), the SPh ligands were substituted by P(OMe)₃ to form a complex containing three phosphite ligands. This was evidenced by ¹H (the CH₂S protons give a sharp signal at 4.2 ppm) and ³¹P NMR spectroscopy (the two *trans* phosphites couple to the *cis* phosphite and vice versa to give one triplet and one doublet, $J = 73$ Hz). In the other cases the presence of one bulky ligand apparently prevents the coordination of additional ligands.

The observed order of phosphorus ligand strengths matches the order in the χ_i values ($\chi_i = 0.1$ (Cy), 4.3 (Ph), 7.7 (OMe) and 9.7 (OPh)), which is regarded as a parameter of the substituent contribution to the σ electron donor and π acceptor ability of phosphorus-containing ligands.⁵¹ On the other hand, the cone angle θ (the ligand bulkiness) increases in the order $P(\text{OMe})_3$ (107°) < $P(\text{OPh})_3$ (128°) < $P\text{Ph}_3$ (145°) < PCy_3 (170°).⁵¹ Obviously, in our case steric effects can be ignored, as the ligand strength order follows the order in the electronic parameter χ_i and not in the steric parameter θ .

3.4.9 Coordination of sulfur-containing ligands

Finally, we have investigated the coordination of sulfur-containing ligands to the SCS Pd^{II} pincer. First, isothiocyanates were found to be too weak ligands to displace the acetonitrile from complex **7**. In the ¹H NMR spectrum (CDCl_3), the diagnostic signal shift from 2.08 (coordinated MeCN) to 1.99 (uncoordinated MeCN) ppm was not observed upon addition of butyl isothiocyanate to the acetonitrile complex **7**. Moreover, FT-IR spectroscopy failed to demonstrate the coordination of the isothiocyanate to Pd^{II}. Thioureas, having high nucleophilicity values ($n_{\text{Pt}}^0 = 7.17$ for unsubstituted thiourea⁴⁵), were subsequently investigated as ligands. *N*-Benzyl-*N'*-butyl thiourea was prepared from butyl isothiocyanate and benzyl amine. Upon addition of this thiourea to the acetonitrile complex **7**, the ¹H NMR spectrum indicated thiourea coordination. First, the acetonitrile signal was present at 1.99 ppm, indicating the decomplexation of acetonitrile (coordinated MeCN gives rise to a signal at 2.08 ppm). Second, significant changes in the chemical shifts of the thiourea NH protons and the adjacent CH₂ protons were observed. Finally, broad signals of the SPh protons of the pincer and essentially all protons of the thiourea indicated restricted thiourea rotation. Moreover, the FAB-MS spectrum displayed an intense signal at $m/z = 721.2$ corresponding to the thiourea complex.

From their n_{Pt}^0 value we can expect that thioureas are stronger ligands than pyridine but weaker ligands than phosphines. This was confirmed experimentally by competition experiments. The ¹H NMR spectra show that the ratio of coordinated thiourea to coordinated pyridine is higher than 95:5. In the presence of PPh_3 the thiourea did not coordinate significantly, as was inferred from ¹H and ³¹P NMR spectroscopy. FAB mass spectrometry only showed the PPh_3 complex of the SCS Pd^{II} pincer system in such mixtures. This means that the order of ligand strength is $\text{PPh}_3 > \text{thiourea} > \text{pyridine}$.

3.5 Conclusions

In this chapter, a study of the coordination strengths of various ligands toward an SCS Pd^{II} pincer system has been described. After the synthesis and characterization of the model SCS Pd^{II} pincer **7**, several *para*-substituted pyridines have been coordinated to this pincer moiety. The differences in coordination strengths arise from electronic and steric effects. The effect of *para*-substituents was quantitatively analyzed by correlation with Brown-Okamoto σ^+ substituent

constants. Moreover, it was demonstrated that phosphorus- and sulfur-containing ligands are stronger ligands for the SCS Pd^{II} pincer than pyridines. Together, these results allow the *convergent* metallodendrimer assembly to be extended. Results concerning this topic will be described in chapter 4.

3.6 Experimental Section

General comments. Melting points were determined with a Reichert melting point apparatus and are uncorrected. CH₂Cl₂ and hexane were freshly distilled from CaCl₂. CH₃CN (p.a. from Merck) was stored over molecular sieves (4 Å). Other solvents (EtOH, CHCl₃, acetone) were used as received (p.a. from Merck). All reagents were purchased from Aldrich and used without further purification. Solutions containing phosphines or phosphites were degassed prior to use. ¹H, ¹³C, and ³¹P NMR spectra were recorded in CDCl₃ (unless stated otherwise) at 298 K on a Varian Unity 300 locked to the deuterated solvent. Chemical shifts are given relative to tetramethylsilane (TMS). FAB mass spectra were recorded on a Finnigan MAT 90 mass spectrometer with *m*-nitrobenzyl alcohol (NBA) as the matrix. Elemental analyses were performed using a Carlo Erba EA1106. The presence of solvents in the analytical samples was confirmed by ¹H NMR spectroscopy. Column chromatography was performed using silica gel (SiO₂, E. Merck, 0.040-0.063 mm, 230-240 mesh). Pincer ligand **5** was synthesized according to a literature procedure.⁴²

3,5-Bis(phenylthiamethyl)-*n*-butoxybenzene (6). To a solution of 3,5-bis(phenylthiamethyl)phenol (**5**) (1.40 g, 4.1 mmol) in CH₃CN (200 mL) was added *t*-BuOK (0.93 g, 8.3 mmol) and the resulting mixture was stirred at room temperature for 1 h. A solution of *n*-butyl bromide (0.44 mL, 4.1 mmol) in CH₃CN (20 mL) was added dropwise, and the mixture was stirred overnight at 40 °C. After evaporation of the solvent *in vacuo*, the residue was taken up in CH₂Cl₂ (100 mL), washed with 1 M HCl (100 mL), saturated NaHCO₃ (100 mL), and brine (100 mL). The dried (MgSO₄) organic layer was evaporated to dryness and the crude product was purified by column chromatography (SiO₂; eluent: CH₂Cl₂/hexane 1:1 v/v) to afford a colorless oil. Yield 1.26 g (77%). ¹H NMR: δ (ppm) 7.29-7.12 (m, 10 H, SPh), 6.80 (s, 1 H, Ar H), 6.68 (s, 2 H, Ar H), 4.01 (s, 4 H, CH₂S), 3.83 (t, *J* = 6.6 Hz, 2 H, OCH₂), 1.74-1.63 (m, 2 H, OCH₂CH₂), 1.51-1.36 (m, 2 H, CH₂CH₃), 0.94 (t, *J* = 7.3 Hz, 3 H, CH₃). ¹³C NMR: δ (ppm) 158.8, 138.5, 135.8, 129.4, 128.3, 125.8, 121.1, 113.4, 67.1, 38.5, 30.7, 18.7, 13.3. FAB-MS *m/z* 395.1 ([M + H]⁺, calcd for C₂₄H₂₆OS₂: 395.1).

Acetonitrile complex 7. Ligand **6** (233 mg, 0.6 mmol) was dissolved in CH₃CN (50 mL) and the solution was placed under an argon atmosphere. Pd[MeCN]₄(BF₄)₂ (262 mg, 0.6 mmol) was added in one portion, and the mixture was stirred at room temperature for 2 h. After evaporation of the solvent *in vacuo*, the yellow paste was taken up in CH₃CN (3 mL) and the product was precipitated by dropwise addition of diethyl ether. Yield 334 mg (90%). M.p. 68-70 °C. ¹H NMR: δ (ppm) 7.81-7.77 (m, 4 H, SPh), 7.50-7.48 (m, 6 H, SPh), 6.59 (s, 2 H, Ar H), 4.57 (br s, 4 H, CH₂S), 3.88 (t, *J* = 6.4 Hz, 2 H, OCH₂), 2.08 (s, 3 H, CH₃CN), 1.76-1.67 (m, 2 H, OCH₂CH₂), 1.52-1.37 (m, 2 H, CH₂CH₃), 0.95 (t, *J* = 7.3 Hz, 3 H, CH₃). ¹³C NMR (CD₃CN): δ (ppm) 158.2, 151.8, 132.1, 131.5, 131.3, 130.6, 110.2, 68.2, 50.3, 31.4, 19.4, 13.6.

FAB-MS m/z 499.0 ($[M - BF_4 - CH_3CN]^+$, calcd 499.0). Anal. calcd for $C_{26}H_{28}BF_4NOPdS_2 \cdot H_2O$: C, 48.35; H, 4.68; N, 2.17; S, 9.93. Found: C, 48.18; H, 4.50; N, 2.25; S, 9.92.

Chloride complex 8. Acetonitrile complex **7** (0.75 g, 1.2 mmol) was dissolved in a mixture of CH_2Cl_2 (75 mL) and CH_3CN (25 mL). After the addition of brine (100 mL), the mixture was stirred vigorously overnight. After separation of the layers, the organic phase was evaporated *in vacuo* and the residue was purified by column chromatography (SiO_2 ; eluent: CH_2Cl_2/Et_2O 95:5 v/v) to afford a yellow solid. Yield 0.60 g (94%). M.p. 63-64 °C. 1H NMR: δ (ppm) 7.83-7.78 (m, 4 H, SPh), 7.37-7.32 (m, 6 H, SPh), 6.56 (s, 2 H, Ar H), 4.53 (br s, 4 H, CH_2S), 3.85 (t, $J = 6.4$ Hz, 2 H, OCH_2), 1.75-1.66 (m, 2 H, OCH_2CH_2), 1.48-1.40 (m, 2 H, CH_2CH_3), 0.94 (t, $J = 7.3$ Hz, 3 H, CH_3). ^{13}C NMR: δ (ppm) 156.5, 150.9, 149.6, 131.9, 130.9, 129.2, 129.1, 108.3, 67.3, 51.2, 30.8, 18.7, 13.3. FAB-MS m/z 499.6 ($[M - Cl + H]^+$, calcd 500.0). Anal. calcd for $C_{24}H_{25}ClOPdS_2$: C, 53.83; H, 4.71; S, 11.98. Found: C, 53.90; H, 4.70; S, 11.88.

Dipincer ligand 9. A mixture of 1,2,4,5-tetrakis(bromomethyl)benzene (3.00 g, 6.7 mmol), 4-*tert*-butylthiophenol (5.00 g, 30.1 mmol), K_2CO_3 (9.20 g, 66.6 mmol), and 18-crown-6 (1.80 g, 6.8 mmol) in acetone (150 mL) was refluxed overnight under an argon atmosphere. After evaporation of the solvent, the residue was taken up in CH_2Cl_2 (250 mL) and washed with brine (250 mL). After drying the organic layer over $MgSO_4$ and evaporation of the solvent *in vacuo*, the crude product was recrystallized from $EtOH/CHCl_3$ to afford a white solid. Yield 4.30 g (81%). M.p. 185-186 °C. 1H NMR: δ (ppm) 7.27 (d, $J = 8.6$ Hz, 8 H, SAr), 7.19 (d, $J = 8.6$ Hz, 8 H, SAr), 6.92 (s, 2 H, Ar H), 4.04 (s, 8 H, CH_2S), 1.29 (s, 36 H, $C(CH_3)_3$). ^{13}C NMR: δ (ppm) 150.1, 134.9, 132.8, 132.4, 130.8, 36.7, 34.5, 31.3. FAB-MS m/z 625.2 ($[M - SAr]^+$, calcd 625.3). Anal. calcd for $C_{50}H_{62}S_4 \cdot 0.5H_2O$: C, 75.04; H, 7.93; S, 16.03. Found: C, 75.01; H, 7.86; S, 15.90.

Bis(MeCN) complex 10. Dipincer ligand **9** (213 mg, 0.3 mmol) was dissolved in CH_3CN (40 mL) and the solution was placed under argon. $Pd[MeCN]_4(BF_4)_2$ (240 mg, 0.6 mmol) was added in one portion, and the mixture was refluxed overnight. After evaporation of the solvent, the crude product was taken up in CH_3CN (5 mL) and precipitated by dropwise addition of Et_2O . Yield 203 mg (60%). M.p. > 280 °C (dec.). 1H NMR (CD_3CN): δ (ppm) 7.74 (d, $J = 8.8$ Hz, 8 H, SAr H), 7.56 (d, $J = 8.8$ Hz, 8 H, SAr H), 4.61 (br s, 8 H, CH_2S), 1.33 (s, 36 H, $C(CH_3)_3$). ^{13}C NMR (CD_3CN): δ (ppm) 155.2, 145.8, 132.0, 127.9, 127.8, 50.0, 35.2, 30.8. FAB-MS m/z 1001.1 ($[M - 2MeCN - 2BF_4 + H]^+$, calcd 1001.2). Anal. calcd for $C_{52}H_{65}B_2F_8NOPd_2S_4 \cdot 2H_2O$: C, 49.15; H, 5.47; N, 1.10; S, 10.09. Found: C, 48.86; H, 5.14; N, 1.25; S, 10.00 (the found values for the elemental composition correspond to the substitution of one acetonitrile ligand by water, which probably occurs upon prolonged standing).

Crystal structure determinations of **7 and **10**·(PPh_3)₂.** Crystals suitable for X-ray structure determination were mounted on a Lindemann-glass capillary and transferred into the cold nitrogen stream of the diffractometer. Data were collected on a Nonius KappaCCD diffractometer on rotating anode (Mo $K\alpha$ radiation, graphite monochromator, $\lambda = 0.71073$ Å, $T = 150$ K, ϕ and ω scans). Pertinent data for the structure determinations are collected in Table 3.4. Structures were solved with automated Patterson and subsequent difference Fourier methods for structure **7** and direct methods for structure **10**·(PPh_3)₂, using SHELXS86⁵² for both structures. Full-matrix refinement on F^2 was performed with SHELXL-97-2.⁵³ The

hydrogen atoms of structure **7** were located on a difference Fourier map and their coordinates were included as parameters in the refinement; the hydrogen atoms of **10**·(PPh₃)₂ were included in the refinement on calculated positions riding on their carrier atoms. The non-hydrogen atoms were refined with anisotropic displacement parameters. The hydrogen atoms were refined with a fixed isotropic displacement parameter related to the value of the equivalent isotropic displacement parameter of their carrier atoms. The *tert*-butyl groups of **10**·(PPh₃)₂ were refined with a disorder model involving two sites. The BF₄ counter anions and the chloroform solvent molecules of this compound were also disordered. Since no satisfactory disorder model could be obtained the contribution of the disordered region to the structure factors was taken into account using the SQUEEZE procedure as incorporated in PLATON.⁵⁴ A total of 219 e were found in a cavity of 537 Å³, located at the inversion center on (0,0,0). Neutral atom scattering factors and anomalous dispersion corrections were taken from the International Tables for Crystallography.⁵⁵ Geometrical calculations were performed with PLATON.⁵⁴

Table 3.4. Crystallographic data for **7** and **10**·(PPh₃)₂.

	7	10 ·(PPh ₃) ₂
<i>Crystal data</i>		
Formula	C ₂₆ H ₂₈ NOPdS ₂ ·BF ₄	C ₈₆ H ₉₀ P ₂ Pd ₂ S ₄ ·2BF ₄ ·2CHCl ₃
Molecular weight	627.86	1939.07
Crystal system	Monoclinic	Triclinic
Space group	<i>P</i> ₂ / <i>c</i> (No. 14)	<i>P</i> 1bar (No. 2)
<i>a</i> , Å	17.9797(16)	10.2613(12)
<i>b</i> , Å	8.7315(12)	11.807(2)
<i>c</i> , Å	20.390(5)	19.428(3)
α , deg	—	97.598(8)
β , deg	122.084(12)	94.227(10)
γ , deg	—	103.319(10)
<i>V</i> , Å ³	2712.1(9)	2257.1(6)
<i>D</i> _{calc} , g cm ⁻³	1.538	1.426
<i>Z</i>	4	1
<i>F</i> (000)	1272	990
μ , mm ⁻¹ [Mo K α]	0.9	0.8
Crystal color	Yellow	Pale yellow
Crystal size, mm	0.15 × 0.25 × 0.40	0.05 × 0.15 × 0.15
<i>Data collection</i>		
θ_{min} , θ_{max} , deg	1.6, 27.5	0.9, 25.4
X-ray exposure, h	1.5	4
Data set (h, k, l)	-23:23, -11:9, -23:26	-12:12, -14:13, -18:23
Total data	21995	15846
Total unique data	6192	8259
<i>R</i> _{int}	0.0396	0.0601
<i>R</i> _{σ}	0.0370	0.0757
Absorption corr. range	0.953, 1.027 [MULTI-SCAN] ^a	—

	<i>Refinement</i>	
No. of refined params	409	415
Final $R1^b$	0.0291 [$5013 I > 2\sigma(I)$]	0.0442 [$6653 I > 2\sigma(I)$]
Final $wR2^c$	0.0823	0.1171
Goodness of fit	1.075	1.021
w^{-1d}	$\sigma^2(F^2) + (0.0327P)^2 + 1.81P$	$\sigma^2(F^2) + (0.0589P)^2$
$(\Delta/\sigma)_{av}$, $(\Delta/\sigma)_{max}$	<0.001, 0.001	<0.001, 0.001
Min. and max. residual density, $e \text{ \AA}^{-3}$	-0.50, 0.64	-0.52, 0.83

^a incorporated in PLATON;⁵⁴

^b $R1 = \Sigma | |F_o| - |F_c| | / \Sigma |F_o|$;

^c $wR2 = [\Sigma[w(F_o^2 - F_c^2)^2] / \Sigma[w(F_o^2)^2]]^{1/2}$;

^d $P = (\text{Max}(F_o^2, 0) + 2F_c^2) / 3$.

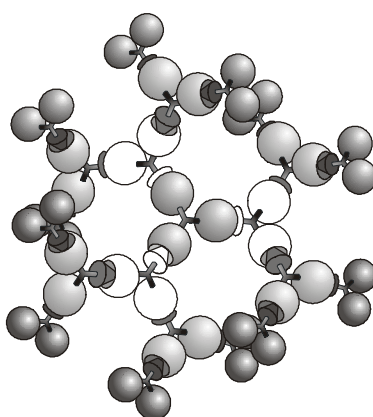
3.7 References and notes

- ¹ See chapter 7 for more information about self-assembled monolayers on gold.
- ² Piner, R. D.; Zhu, J.; Xu, F.; Hong, S.; Mirkin, C. A. *Science* **1999**, *283*, 661.
- ³ a) *Introduction to Molecular Electronic Devices*; Petty, M. C.; Bryce, M. R.; Bloor, D., Eds.; Oxford University Press: New York, 1995; b) *Molecular Electronics*; Jortner, J.; Ratner, M., Eds.; Blackwell Science: Oxford, 1997; c) *Molecular Electronics: Science and Technology*; Aviram, A.; Ratner, M., Eds.; New York Academy of Sciences: New York, 1998.
- ⁴ Collier, C. P.; Mattersteig, G.; Wong, E. W.; Luo, Y.; Beverly, K.; Sampaio, J.; Raymo, F. M.; Stoddart, J. F.; Heath, J. R. *Science* **2000**, *289*, 1172.
- ⁵ Chen, J.; Reed, M. A.; Rawlett, A. M.; Tour, J. M. *Science* **1999**, *286*, 1550.
- ⁶ Gittins, D. I.; Bethell, D.; Schiffrin, D. J.; Nichols, R. J. *Nature* **2000**, *408*, 67.
- ⁷ Moulton, C.; Shaw, B. L. *J. Chem. Soc., Dalton Trans.* **1976**, 1020.
- ⁸ For a short overview, see: Steenwinkel, P.; Gossage, R. A.; van Koten, G. *Chem. Eur. J.* **1998**, *4*, 759.
- ⁹ a) Rimml, H.; Venanzi, L. M. *J. Organomet. Chem.* **1983**, *259*, C6; b) Bennett, M. A.; Jin, H.; Willis, A. C. *ibid.* **1993**, *451*, 249; c) Gorla, F.; Venanzi, L. M.; Albinati, A. *Organometallics* **1994**, *13*, 43; d) Cross, R. J.; Kennedy, A. R.; Muir, K. W. *J. Organomet. Chem.* **1995**, *487*, 227; e) van der Boom, M. E.; Kraatz, H.-B.; Hassner, L.; Ben-David, Y.; Milstein, D. *Organometallics* **1999**, *18*, 3873.
- ¹⁰ a) Gupta, M.; Hagen, C.; Flesher, R. J.; Kaska, W. C.; Jensen, C. M. *Chem. Commun.* **1996**, 2083; b) Gupta, M.; Hagen, C.; Kaska, W. C.; Cramer, R. E.; Jensen, C. M. *J. Am. Chem. Soc.* **1997**, *119*, 840; c) Jensen, C. M. *Chem. Commun.* **1999**, 2443.
- ¹¹ Dani, P.; Karlen, T.; Gossage, R. A.; Gladiali, S.; van Koten, G. *Angew. Chem. Int. Ed.* **2000**, *39*, 743.
- ¹² a) Gorla, F.; Togni, A.; Venanzi, L. M. *Organometallics* **1994**, *13*, 1607; b) Longmire, J. M.; Zhang, X.; Shang, M. *Organometallics* **1998**, *17*, 4374.
- ¹³ Ohff, M.; Ohff, A.; van der Boom, M. E.; Milstein, D. *J. Am. Chem. Soc.* **1997**, *119*, 11687.
- ¹⁴ Morales-Morales, D.; Redón, R.; Yung, C.; Jensen, C. M. *Chem. Commun.* **2000**, 1619.
- ¹⁵ Huck, W. T. S.; Snellink-Ruël, B. H. M.; van Veggel, F. C. J. M.; Reinhoudt, D. N. *Organometallics* **1997**, *16*, 4287.

- ¹⁶ a) Beletskaya, I. P.; Chuchurjukin, A. V.; Dijkstra, H. P.; van Klink, G. P. M.; van Koten, G. *Tetrahedron Lett.* **2000**, *41*, 1075; b) Beletskaya, I. P.; Chuchurjukin, A. V.; Dijkstra, H. P.; van Klink, G. P. M.; van Koten, G. *ibid.* **2000**, *41*, 1081.
- ¹⁷ a) Trofimenko, S. *Inorg. Chem.* **1973**, *12*, 1215; b) Steenwinkel, P.; Gossage, R. A.; Maunula, T.; Grove, D. M.; van Koten, G. *Chem. Eur. J.* **1998**, *4*, 763.
- ¹⁸ Rodríguez, G.; Lutz, M.; Spek, A. L.; van Koten, G. manuscript in preparation (Dec. 2000)
- ¹⁹ a) Grove, D. M.; van Koten, G.; Ubbels, H. J. C.; Zoet, R.; Spek, A. L. *Organometallics* **1984**, *3*, 1003; b) van Beek, J. A. M.; van Koten, G.; Ramp, M. J.; Coenjaarts, N. C.; Grove, D. M.; Goubnitz, K.; Zoutberg, M. C.; Stam, C. H.; Smeets, W. J. J.; Spek, A. L. *Inorg. Chem.* **1991**, *30*, 3059.
- ²⁰ Canty, A. J.; Patel, J.; Skelton, B. W.; White, A. H. *J. Organomet. Chem.* **2000**, *599*, 195.
- ²¹ a) Grove, D. M.; van Koten, G.; Louwen, J. N.; Noltes, J. G.; Spek, A. L.; Ubbels, H. J. C. *J. Am. Chem. Soc.* **1982**, *104*, 6609; b) Terheijden, J.; van Koten, G.; Muller, F.; Grove, D. M.; Vrieze, K.; Nielsen, E.; Stam, C. H. *J. Organomet. Chem.* **1986**, *315*, 401.
- ²² Rietveld, M. H. P.; Grove, D. M.; van Koten, G. *New J. Chem.* **1997**, *21*, 751.
- ²³ Gossage, R. A.; van de Kuil, L. A.; van Koten, G. *Acc. Chem. Res.* **1998**, *31*, 423.
- ²⁴ The literature abounds with examples of the use of metal-containing dendrimers in homogeneous catalysis. For a recent review, see: Oosterom, G. E.; Reek, J. N. H.; Kamer, P. C. J.; van Leeuwen, P. W. N. M. *Angew. Chem. Int. Ed.* **2001**, *40*, 1828.
- ²⁵ Knapen, J. W. J.; van der Made, A. W.; de Wilde, J. C.; van Leeuwen, P. W. N. M.; Wijkens, P.; Grove, D. M.; van Koten, G. *Nature* **1994**, *372*, 659.
- ²⁶ a) Kleij, A. W.; Gossage, R. A.; Jastrzebski, J. T. B. H.; Lutz, M.; Spek, A. L.; van Koten, G. *Angew. Chem. Int. Ed.* **2000**, *39*, 176; b) Kleij, A. W.; Gossage, R. A.; Klein-Gebbink, R. J. M.; Brinkmann, N.; Reijerse, E. J.; Kragl, U.; Lutz, M.; Spek, A. L.; van Koten, G. *J. Am. Chem. Soc.* **2000**, *122*, 12114.
- ²⁷ Albrecht, M.; Hovestad, N. J.; Boersma, J.; van Koten, G. *Chem. Eur. J.* **2001**, *7*, 1289.
- ²⁸ a) Albrecht, M.; van Koten, G. *Adv. Mater.* **1999**, *11*, 171; b) Albrecht, M.; Gossage, R. A.; Lutz, M.; Spek, A. L.; van Koten, G. *Chem. Eur. J.* **2000**, *6*, 1431.
- ²⁹ Albrecht, M.; Lutz, M.; Spek, A. L.; van Koten, G. *Nature* **2000**, *406*, 970.
- ³⁰ Schlenk, C.; Kleij, A. W.; Frey, H.; van Koten, G. *Angew. Chem. Int. Ed.* **2000**, *39*, 3445.
- ³¹ Errington, J.; McDonald, W. S.; Shaw, B. L. *J. Chem. Soc., Dalton Trans.* **1980**, 2312.
- ³² Dupont, J.; Beydoun, N.; Pfeffer, M. *J. Chem. Soc., Dalton Trans.* **1989**, 1715.
- ³³ Kickham, J. E.; Loeb, S. J.; Murphy, S. L. *J. Am. Chem. Soc.* **1993**, *115*, 7031.
- ³⁴ Bergbreiter, D. E.; Osburn, P. L.; Liu, Y.-S. *J. Am. Chem. Soc.* **1999**, *121*, 9531.
- ³⁵ Lucena, N.; Casabó, J.; Escriche, L.; Sánchez-Castelló, G.; Teixidor, F.; Kivekäs, R.; Sillanpää, R. *Polyhedron* **1996**, *15*, 3009.
- ³⁶ Hanan, G. S.; Kickham, J. E.; Loeb, S. J. *J. Chem. Soc., Chem. Commun.* **1991**, 893.
- ³⁷ a) Kickham, J. E.; Loeb, S. J.; Murphy, S. L. *Chem. Eur. J.* **1997**, *3*, 1203; b) Cameron, B. R.; Loeb, S. J.; Yap, G. P. A. *Inorg. Chem.* **1997**, *36*, 5498; c) Kickham, J. E.; Loeb, S. J. *Inorg. Chem.* **1995**, *34*, 5656.
- ³⁸ Loeb, S. J.; Shimizu, G. K. H. *J. Chem. Soc., Chem. Commun.* **1993**, 1395.
- ³⁹ See chapter 2 for representative examples of metallodendrimers from our group based on SCS Pd^{II} pincers.

- ⁴⁰ Hall, J. R.; Loeb, S. J.; Shimizu, G. K. H.; Yap, G. P. A. *Angew. Chem. Int. Ed.* **1998**, *37*, 121.
- ⁴¹ Dijkstra, H. P.; Steenwinkel, P.; Grove, D. M.; Lutz, M.; Spek, A. L.; van Koten, G. *Angew. Chem. Int. Ed.* **1999**, *38*, 2186.
- ⁴² Huck, W. T. S.; van Veggel, F. C. J. M.; Reinhoudt, D. N. *J. Mater. Chem.* **1997**, *7*, 1213.
- ⁴³ Kickham, J. E.; Loeb, S. J. *Inorg. Chem.* **1994**, *33*, 4351.
- ⁴⁴ For example, see: Fujita, M.; Ibukuro, F.; Hagihara, H.; Ogura, K. *Nature* **1994**, *367*, 720.
- ⁴⁵ Tobe, M. L.; Burgess, J. *Inorganic Reaction Mechanisms*, Longman: Essex, 1999.
- ⁴⁶ Brown, H. C.; Okamoto, Y. *J. Am. Chem. Soc.* **1958**, *80*, 4979.
- ⁴⁷ Gozin, M.; Weisman, A.; Ben-David, Y.; Milstein, D. *Nature* **1993**, *364*, 699.
- ⁴⁸ Abbenhuis, R. A. T. M.; Del Río, I.; Bergshoef, M. M.; Boersma, J.; Veldman, N.; Spek, A. L.; van Koten, G. *Inorg. Chem.* **1998**, *37*, 1749.
- ⁴⁹ Oki, M. *Applications of Dynamic NMR Spectroscopy to Organic Chemistry*, Methods in Stereochemical Analysis Vol. 4, VCH: Weinheim, 1985.
- ⁵⁰ a) Mathew, N.; Jagirdar, B. R.; Gopalan, R. S.; Kulkarni, G. U. *Organometallics* **2000**, *19*, 4506; b) George, T. A.; Sterner, C. D. *Inorg. Chem.* **1976**, *15*, 165.
- ⁵¹ Tolman, C. A. *Chem. Rev.* **1977**, *77*, 313.
- ⁵² *SHELXS86 Program for crystal structure determination*; Sheldrick, G. M.; University of Göttingen, Germany, 1986.
- ⁵³ *SHELXL-97-2 Program for crystal structure refinement*; Sheldrick, G. M.; University of Göttingen, Germany, 1997.
- ⁵⁴ *PLATON, A multi-purpose crystallographic tool*; Spek, A. L.; Utrecht University, The Netherlands, 2000. Internet: <http://www.cryst.chem.uu.nl/platon/>
- ⁵⁵ *International Tables for Crystallography, Volume C*; Wilson, A. J. C., Ed.; Kluwer Academic Publishers: Dordrecht, The Netherlands, 1992.

Convergent synthesis of nanosize, layer-block metallodendrimers[#]



Schematic picture of metallodendrimer $G_1^{\text{phos}}-G_{3,\text{conv}}$.

In the previous chapter it was reported that the coordination strength of ligands toward the SCS Pd(II) pincer system is as follows: nitriles < pyridines < thioureas < phosphites < phosphines. This finding has been exploited in the non-covalent, convergent synthesis of layer-block metallodendrimers. The synthesis of hydrophobic dendritic Fréchet wedges containing focal phosphine moieties is first described. Coordination of these wedges to the SCS Pd(II) pincer groups of metallodendritic building blocks is the first step in the convergent assembly of metallodendrimers, which is subsequently discussed in detail. Due to the peripheral hydrophobic shell of Fréchet dendrons, the metallodendrimers display a significantly higher solubility in organic solvents than the metallodendrimers previously synthesized in our group. All dendrons and dendrimers have been characterized by ^1H and ^{31}P NMR spectroscopy and MALDI-TOF mass spectrometry. Proton T_1 relaxation time constants have been measured in order to probe the mobility of methyl groups located in the metallodendrimer core, showing that upon increasing the dendrimer size, the mobility of these methyl protons increases accordingly.

[#] The work described in this chapter has been published: van Manen, H.-J.; Fokkens, R. H.; Nibbering, N. M. M.; van Veggel, F. C. J. M.; Reinhoudt, D. N. *J. Org. Chem.* **2001**, 66, 4643.

4.1 Introduction

One of the most versatile types of non-covalent interactions applied in self-assembly is the coordination bond of ligands to transition metals. Since these bonds are weaker than covalent bonds but much stronger than hydrogen bonds, the resulting assemblies are relatively stable yet often reversible, allowing reorganizations to produce the thermodynamically most favorable structure. Moreover, coordination chemistry enables a wide variety of geometries to be obtained, ranging from square planar to octahedral, depending on the transition metal employed.

The coordination of cyano and pyridine groups to SCS Pd^{II} pincer systems has been exploited in our group in the controlled assembly of both divergently and convergently constructed metallodendrimers (see section 2.4.5). In order to extend the convergent growth methodology to larger, more complex, and functionalized dendritic assemblies, additional ligands for the SCS Pd^{II} pincer system are needed that are stronger than pyridines. In chapter 3 it has been described that, among others, phosphines are such ligands. In this chapter the successful incorporation of phosphine dendritic wedges into our convergent metallodendrimer assembly process is discussed. The resulting assemblies are the first examples of a covalent-noncovalent “layer-block”¹ dendritic architecture, *i.e.* a non-covalently assembled metallodendritic interior surrounded by covalently synthesized dendrimer wedges. The literature overview in section 4.2 will demonstrate the important role of coordination chemistry in the synthesis of discrete, self-assembled architectures.

4.2 Coordination chemistry in self-assembly

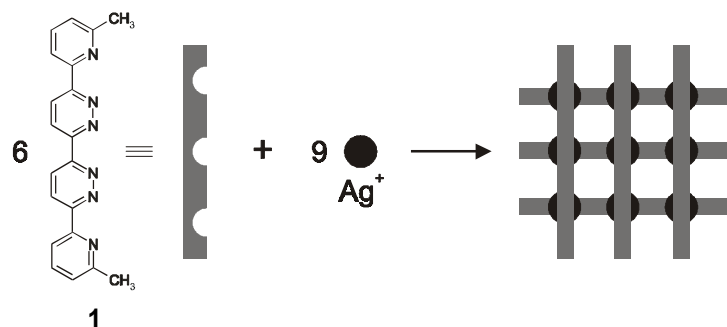
In this section a concise overview is presented concerning the application of coordination chemistry in the fabrication of self-assembled nanosize structures. Only finite assemblies will be covered here, excluding the rather large field of coordination polymers. A distinction can be made according to the motifs that the coordination assemblies exhibit:²

- Latticed motifs;
- Cyclic motifs;
- Filamentous motifs;
- Interlaced motifs.

4.2.1 Latticed motifs

A characteristic feature of latticed motifs, represented by *grid*, *rack*, and *ladder* structures, is the formation of coordination bonds at alternating (right) angles. In grids, this is generally achieved by the combination of tetrahedrally or octahedrally disposed metal ions with rigidly linear ligands containing multiple chelating sites, whereas racks and ladders involve the presence of an additional ligand-containing binding sites at one or both ends.

Oligomeric nitrogen-containing heterocycles and tetrahedral metal ions (such as Cu^{I} and Ag^{I}) have by far been the most studied ligands and metals employed in the formation of latticed coordination motifs. For example, when ligand **1** was mixed with Ag^{I} ions in a 2:3 stoichiometry a so-called $[3 \times 3]$ grid was formed in 99% yield by thermodynamic self-assembly (Scheme 4.1).³



Scheme 4.1. $[3 \times 3]$ grid of $\text{Ag}(\text{I})$ with a rigidly linear hexadentate ligand.

Most reported grids have been of the $[2 \times 2]$ or $[3 \times 3]$ type, however, a $[4 \times 4]$ grid based on octahedral Pb^{II} ions was recently reported by Lehn, Fenske and coworkers (Figure 4.1a).⁴ Other octahedral ions employed in grid formation include Co^{II} , Cu^{II} , Ni^{II} , Cd^{II} , and Zn^{II} .

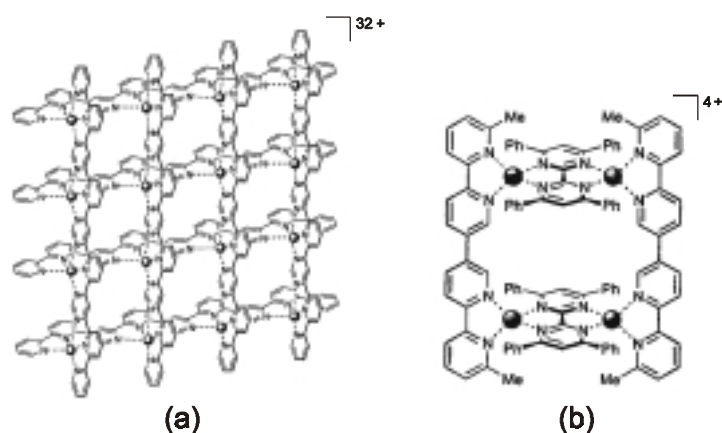


Figure 4.1. a) $[4 \times 4]$ grid based on $\text{Pb}(\text{II})$ ions; b) $[2 \times 2]$ ladder based on $\text{Cu}(\text{I})$ ions.

Ordered thin films of various $[3 \times 3]$ grids (such as the grid shown in Scheme 4.1) have been prepared at the air-water interface.⁵ Recently, Co^{II} $[2 \times 2]$ grids were shown by scanning tunneling microscopy (STM) to form highly ordered monolayers on a graphite surface.⁶ A single grid could be extracted from the surface by a short negative voltage pulse of the STM tip.

Racks and ladders differ from grids in that additional mono- or bidentate ligands are present at one (ladder) or both ends (racks) of the rigid linear polydentate ligand. Nearly all reported examples originate from Lehn and coworkers. A $[2 \times 2]$ ladder synthesized by this group is shown in Figure 4.1b.⁷

4.2.2 Cyclic motifs

Complexes displaying closed 2-D or 3-D structures incorporating metal ions are collectively known as metallocycles. The “molecular library” approach systematized by Stang allows a rational design of geometrically shaped metallocycles.⁸ Construction of almost any type of macrocyclic assembly containing transition metals can be achieved by assessing the appropriate angles between the binding sites of the donor and acceptor subunits. For example, Fujita *et al.* combined a square planar Pd^{II} metal ion having two vacant *cis*-coordination sites with a rigidly linear ditopic 4,4'-bipyridine ligand in water. This led to the formation of a molecular square (Figure 4.2a) in more than 90% yield by precipitation with ethanol.⁹

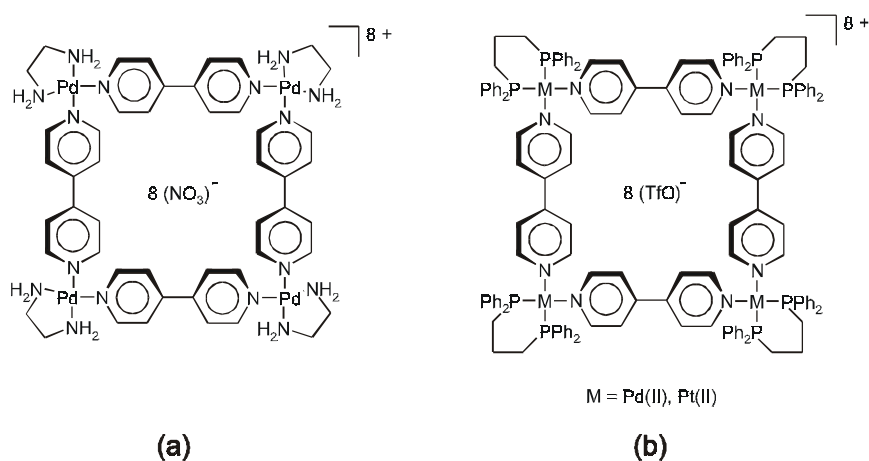


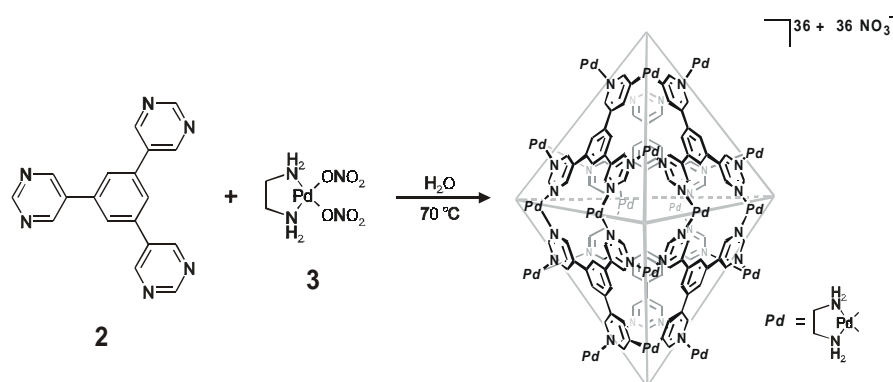
Figure 4.2. a) Fujita's water-soluble molecular square;⁹ b) Stang's molecular square soluble in organic solvents.¹⁰

The corresponding Pt^{II} molecular square was obtained in a different manner from that of the Pd^{II} system. Since the Pt^{II}-py (py = pyridine) coordination bond is inert, kinetically distributed oligomeric products were initially obtained upon mixing the required building blocks. Heating the mixture at 100 °C gradually transformed the oligomers into the thermodynamically most stable product, the molecular square, which was isolated in 81% yield after a few weeks. This example illustrates the significant difference between the labile Pd^{II}-py and the inert Pt^{II}-py bond.

Whereas Fujita's metallocycles are water-soluble due to the hydrophilic bidentate ligands and anions (ethylenediamine and nitrate, respectively, in Figure 4.2a), Stang *et al.* have focussed on similar metallocycles that are soluble in organic solvents. With more lipophilic bis- or monophosphines as ligands and employing triflates instead of nitrates, molecular squares soluble in a variety of organic solvents were obtained in high yields (Figure 4.2b). Structural variations in both the ligands representing the walls and the corners of the squares, the metals, and the anions have permitted a wide variety of molecular squares to be assembled. Comprehensive reviews provide detailed descriptions of these variations, as well as discussing other metallocyclic polygons.^{8,11} Examples of functional ligands incorporated into two-dimensional

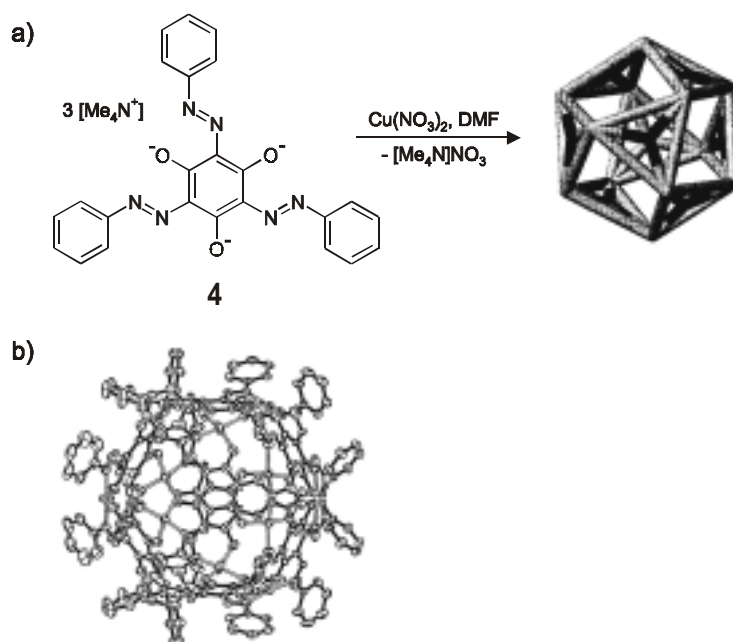
metallocycles include ferrocenes,¹² uracils,¹³ crown ethers and calixarenes,¹⁴ porphyrins,¹⁵ and fullerenes.¹⁶

The design of three-dimensional metal-based cage compounds and polyhedra generally involves building blocks more sophisticated than two-dimensional polygons. As a prerequisite, at least one of the building blocks must possess three or more binding sites in order to extend the assembly into the third dimension. Nanoscopic cages and polyhedra have also been reviewed extensively,^{8,11,17} and only two recent examples will be discussed. Fujita *et al.* designed the hexatopic ligand 1,3,5-tris(3,5-pyrimidyl)benzene (**2**) and attempted to construct either a tetrahedron or an octahedron by coordinating it to the *cis*-Pd^{II} complex **3**.¹⁸ However, the ¹H NMR spectrum of the obtained product suggested a trigonal-bipyramidal structure. X-ray crystallographic analysis provided evidence for the proposed structure, the hexahedron shown in Scheme 4.2.



Scheme 4.2. Fujita's hexahedron displaying a trigonal-bipyramidal structure.

Although artificial non-covalent assemblies of *I* and *O* symmetry are rare, several cuboctahedra of *O* symmetry have been constructed *via* coordination-driven, face-directed self-assembly. The only cuboctahedron that has been characterized structurally is the one shown in Scheme 4.3, reported by Robson and coworkers.¹⁹ Coordination of the deprotonated trianion **4** to Cu(NO₃)₂ in DMF gave crystals of a cuboctahedron in which each of the eight organic ligands is attached to three Cu^{II} centers *via* a bidentate *N,O*-chelating system.



Scheme 4.3. a) Cuboctahedron synthesized by Robson and coworkers;¹⁹ b) Crystal structure.

The inclusion properties and host-guest behavior of metallocycles have been reviewed extensively.²⁰ For example, Fujita's water-soluble molecular square (Figure 4.2a) offers a hydrophobic cavity in which electron-rich neutral molecules such as 1,3,5-trimethoxybenzene ($K_a = 750 \text{ M}^{-1}$) can be complexed.

4.2.3 Filamentous motifs

Rods and metallodendrimers are two of the most common coordination oligomers that belong to the class of the filamentous motifs, *i.e.* 1-D, 2-D, or 3-D linear coordination oligomers. Since metallodendrimers have been discussed extensively in chapter 2, this section only describes molecular rods. A substantial number of such rods has been reported, primarily with the aim of studying the photophysical or redox properties of these “molecular wires”.²¹ Divergent synthetic strategies have generally been employed in their preparation. In this approach, a bidentate initiator ligand containing a rigid spacer to separate the binding moieties is progressively elongated into a linear complex by the attachment of further bi- or monodentate ligands *via* metal-ligand coordination. Among the most versatile ligands employed in molecular rod formation are polypyridine-type ligands, in particular bisterpyridines. An example of a trinuclear rod based on metal-bisterpyridine coordination is shown in Figure 4.3.²²

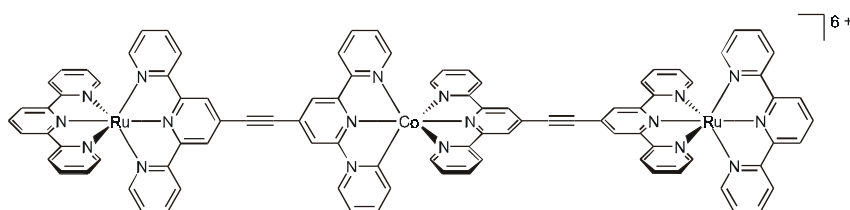


Figure 4.3. Trinuclear rod based on metal-bisterpyridine coordination.

Other ligand types employed in the formation of rods include bipyridyl-,²³ phenanthroline-,²³ and pincer-type²⁴ (see chapter 3) ligands. Moreover, numerous different spacers have been incorporated in rods in order to tune the electronic communication between the ligand and metal components. Among them are phenylene, polyene, poly(ethyne), adamantane, and bicyclo[2.2.2]octane groups.

4.2.4 Interlaced motifs

Coordination complexes having interlaced motifs are characterized by a metal ion-directed threading of one ligand through or about itself or another ligand. Representative examples include rotaxanes, catenanes, and knots. This large field has amply been reviewed,²⁵ and this section serves to highlight some recent achievements.

Rotaxanes are interlaced moieties in which a filamentous species, stoppered at each end, is threaded through a cyclic moiety, while pseudorotaxanes lack bulky stoppers and are therefore physically able to dethread to their separate components. Sauvage and coworkers have pioneered the field of rotaxanes and pseudorotaxanes based on transition metal complexes.^{25a,b} The combination of phenanthrolines and tetrahedrally disposed Cu^{I} ions has been exploited most in the formation of these interlaced architectures. The incorporation of porphyrins²⁶ or fullerenes²⁷ into rotaxanes has allowed the photoinduced electron transfer between *chemically nonconnected* chromophores to be studied as a model of the electronic processes in photosynthesis.²⁸

The ability to induce controlled molecular motion in rotaxanes and pseudorotaxanes enables them to function as artificial molecular machines. Controlled motion in transition metal-based rotaxanes has mainly been achieved *via* electrochemical stimuli, *e.g.* oxidation and reduction of Cu^{I} . Back and forth translation of a rotaxane ring along its linear rod, *i.e.* *gliding*, has been achieved by incorporating different coordinating units in the thread, as schematically shown in Figure 4.4.²⁹

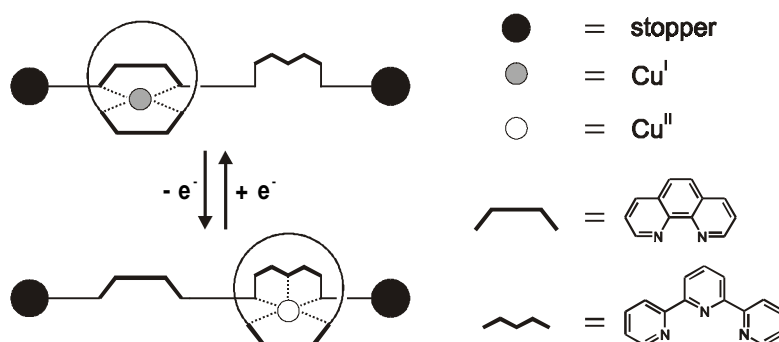


Figure 4.4. Electrochemically induced, reversible gliding of a rotaxane ring along its thread.

In the Cu^{I} state, two bidentate phenanthroline units (one of the ring, one of the string) coordinate to the metal ion in a tetrahedral geometry, whereas in the Cu^{II} state, the ring phenanthroline and the terdentate terpyridine of the string afford a five-coordinate geometry. The gliding of the ring

could also be carried by an oxidative photochemical process using *p*-nitrobenzyl bromide as an electron acceptor. Rotation of a rotaxane ring around its thread has been demonstrated in a similar fashion by incorporating both the phenanthroline and the terpyridine moiety in the ring.³⁰

Cu^I-directed formation of a *doubly* threaded assembly was recently reported by Sauvage and coworkers.³¹ Attaching a rotaxane ring to a string (both containing phenanthroline ligands) led to a self-complementary hermaphrodite molecule able to dimerize both in solution and in the solid state (Figure 4.5).

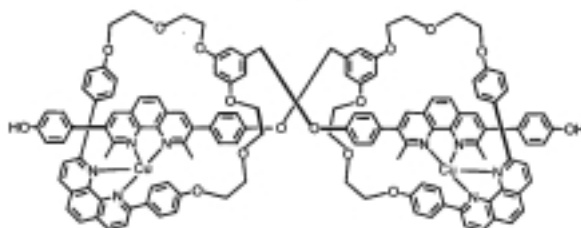


Figure 4.5. Doubly threaded rotaxane formed by dimerization of a hermaphrodite molecule.

Extending the linear part of this hermaphrodite molecule with a terpyridine ligand system allowed the contraction and stretching of the linear rotaxane dimer, representing a synthetic molecular muscle.³² This system contains four-coordinate Cu^I as the assembling and templating metal, however, the movement is induced by a metal exchange with five-coordinate Zn^{II}. The stretched and contracted situations are depicted in Figures 4.6a and 4.6b, respectively.

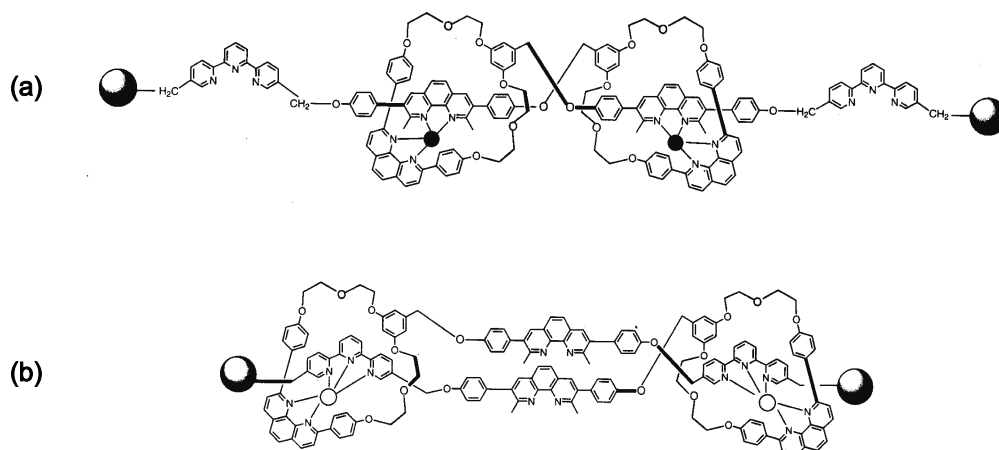


Figure 4.6. Stretched (a) and contracted (b) situation of a synthetic molecular muscle. Black and white circles represent Cu(I) and Zn(II) ions, respectively.

Ring closure of self-assembled, metal-templated pseudorotaxanes to yield catenanes has been achieved using both conventional organic reactions (such as etherification (already in 1984!))³³ or ring-closing metathesis³⁴) and the coordination of suitable ligands to transition metals.³⁵ Like in rotaxanes, the controlled molecular motion of transition metal-based catenanes

has been studied extensively.³⁶ Recently, the attachment of a Cu^I catenane incorporating a disulfide bridge onto gold nanoparticles was reported as a first step toward surface-confined molecular machines.³⁷

An alternative route to [2]metallocatenanes, mainly pursued by Fujita and coworkers, does not rely on postmodification of self-assembled pseudorotaxanes but on strict self-assembly from (en)Pd^{II} or (en)Pt^{II} units (en = ethylene diamine) and pyridine-containing ligands. For example, the self-assembly of **3** (Scheme 4.2) and pyridine-based bridging ligand **5** (Figure 4.7) in aqueous solution leads to an equilibrium mixture of catenane **6** and monomer ring **7**.³⁸

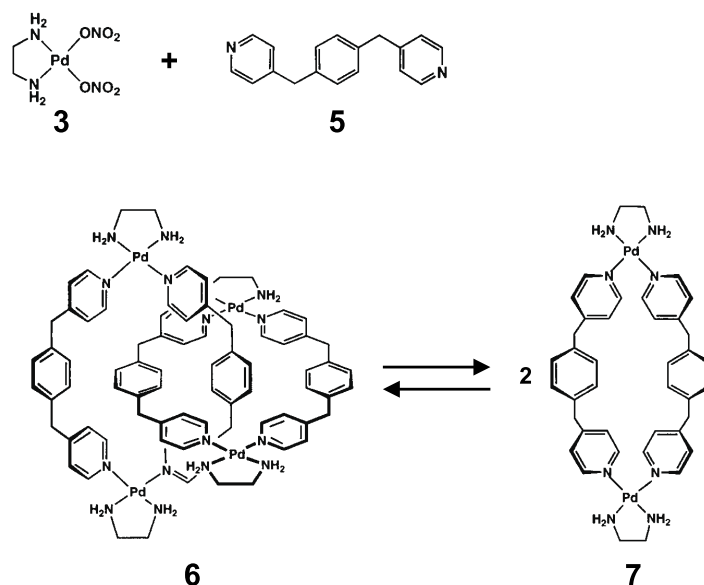


Figure 4.7. Self-assembled catenane **6** and monomer metallocycle **7**.

The ratio between the catenane and the monomer ring could be controlled by adjusting the concentration, the solvent mixture, and by using specific guests (*e.g.* **7** can be selectively stabilized by addition of sodium (*p*-methoxyphenyl)acetate). The driving force for the self-assembly of the catenane is the efficient aromatic contact between two monomer rings. By employing a slightly different ligand (*i.e.* removing one methylene part from **5**), the formation of only the catenane structure was observed.³⁹ From its crystal structure, very efficient stacking of four aromatic rings was observed, with a van der Waals interplane separation of ca. 3.5 Å. Since then, a series of pyridine-based bridging ligands have been examined for their ability to form catenanes, and even mixtures of ligands have been found to produce catenanes.⁴⁰ Since neither covalent nor coordinate bonds exist between component rings, the assembly of the catenane lies on a delicate thermodynamic balance. When the component rings have a cavity with an appropriate interplane distance, catenanes are obtained efficiently.

Both the strategies for catenane formation outlined above (“template” and “self-assembly”) have been combined recently by Fujita, Sauvage *et al.* in the quantitative formation of a doubly interlocking, 4-crossing [2]catenane using Cu^I and Pd^{II} as the templating and assembling centers, respectively.⁴¹

Knots are species in which a single strand alternately passes over and under itself several times in a continuous loop. In coordination chemistry, they are typically obtained by connecting opposite ends of the two ligands in a double-stranded helicate. Only the trefoil knot, which has three crossing points, will briefly be discussed here. It was first synthesized by Dietrich-Buchecker and Sauvage in low yield by cyclization of a binuclear double-stranded helicate based on tetrahedral Cu^{I} -terpyridine coordination, as schematically depicted in Figure 4.8.⁴² Improved yields have been obtained by optimization of both the spacer⁴³ between the phenanthroline ligands and the ring-closing reaction.⁴⁴

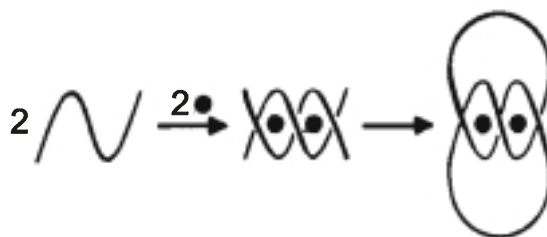
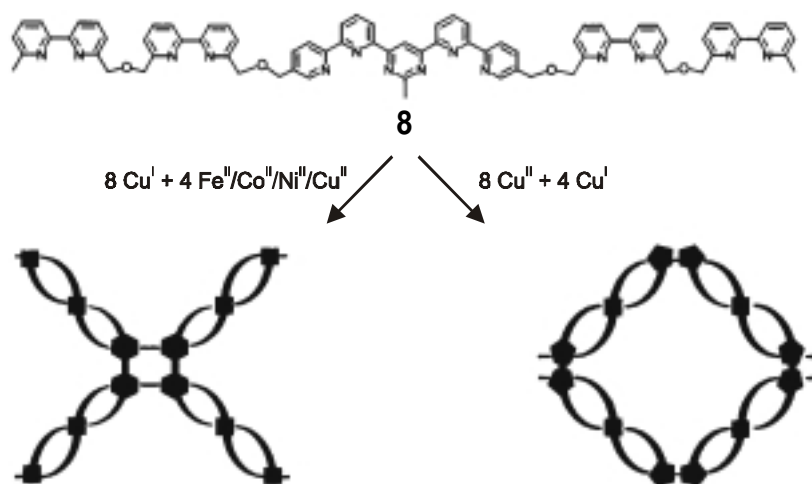


Figure 4.8. Strategy for formation of a trefoil knot from a binuclear helicate.

Since helicates are chiral and may possess *M*- or *P*-helicity, the trefoil knots which are prepared from them are usually obtained as a racemic mixture of topological enantiomers. Separation of knot enantiomers has been achieved by diastereoselective crystallization using a chiral counteranion⁴³ and by HPLC on a chiral stationary phase.⁴⁵

4.2.5 Mixed-motif complexes

A number of coordination complexes is known in which two or more different motifs can be distinguished. The most interesting example has been described by Lehn and coworkers (Scheme 4.4).⁴⁶ The self-assembly of linear ligand **8** with a number of transition metal ions having different coordination geometries leads to a so-called linear combination architecture (Scheme 4.4 left) or a crossover architecture (Scheme 4.4 right), both of which display a combination of grid and helicate motifs.



Scheme 4.4. Self-assembly modes of ligand 8 and metal ions with different coordination geometries, represented by a hexagon (octahedral hexacoordination), a pentagon (trigonal bipyramidal pentacoordination), and a square (tetrahedral tetracoordination).

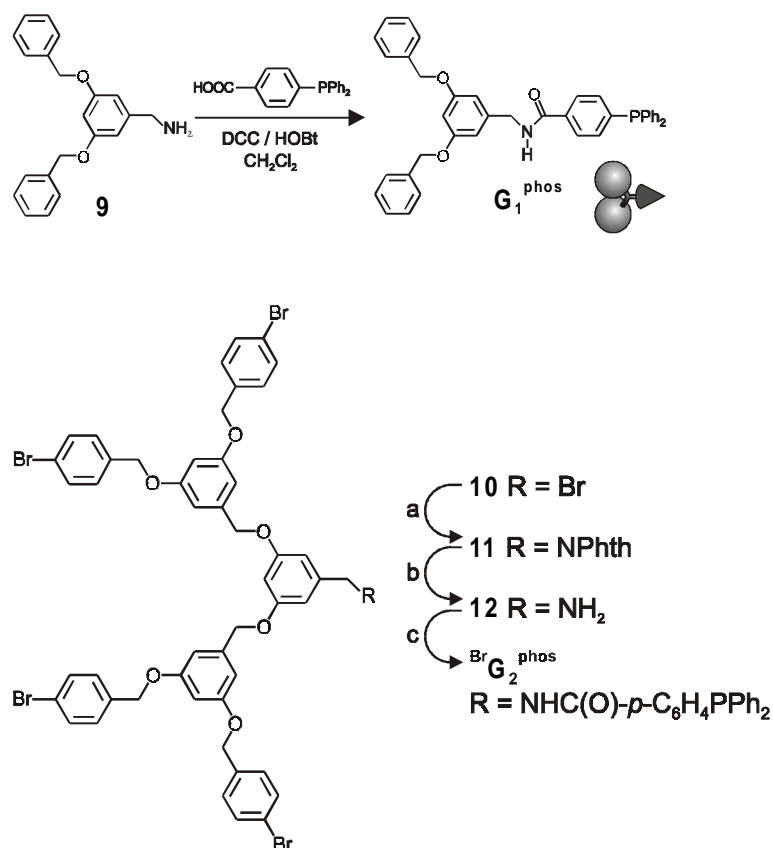
4.3 Aim and scope of this chapter

This chapter describes the convergent synthesis and characterization of hybrid covalent-noncovalent metallodendrimers in which the coordination of three different ligand types to SCS Pd^{II} pincer moieties is employed. Starting from first and second generation dendritic wedges having focal phosphines, metallodendrimers are constructed in a stepwise manner by coordination of these dendritic ligands to building blocks containing ligands of decreasing coordination strengths. The final step consists of coordination of the resulting dendritic wedges to a trifunctional core. In order to characterize the dendritic structures, various analytic techniques such as ¹H and ³¹P NMR spectroscopy, MALDI-TOF mass spectrometry, and elemental analysis have been employed.

4.4 Results and discussion

4.4.1 Synthesis of covalent phosphine-functionalized dendritic wedges

In order to place hydrophobic layers of covalent dendritic wedges around previously constructed metallodendrimers, Fréchet-type⁴⁷ dendritic wedges functionalized at their focal point with phosphines were synthesized.⁴⁸ Thus, 3,5-(benzyloxy)benzyl amine⁴⁹ **9** was coupled to 4-(diphenylphosphino)benzoic acid in the presence of 1,3-dicyclohexylcarbodiimide (DCC) and 1-hydroxybenzotriazole (HOBt) to afford the first generation phosphine wedge **G₁^{phos}** in near quantitative yield after column chromatography (Scheme 4.5).



Scheme 4.5. Synthesis of dendritic wedges containing focal phosphine groups; a) KNPhth, MeCN, reflux, 2 h, 85%; b) $\text{H}_2\text{NNH}_2 \cdot \text{H}_2\text{O}$, EtOH, THF, reflux, 2 h, 90%; c) 4-(diphenylphosphino)benzoic acid, DCC, HOBt, CH_2Cl_2 , r.t., 2 h, 85%.

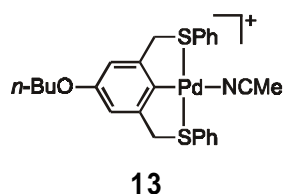
Similarly, second generation phosphine wedge $\text{BrG}_2^{\text{phos}}$ (Scheme 4.5) was prepared in 79% yield from the corresponding wedge **12** containing a benzylic amine at the focal point, which in turn was prepared from the known bromide **10**⁵⁰ by a Gabriel reaction. Both wedges G_1^{phos} and $\text{BrG}_2^{\text{phos}}$ were fully characterized by ^1H , ^{13}C , and ^{31}P NMR spectroscopy, FAB mass spectrometry, and elemental analysis. They display a signal at -5.6 ppm in the ^{31}P NMR spectrum, which is very close to triphenylphosphine (-5.5 ppm). In the positive FAB mass spectra, signals corresponding to $[\text{M} + \text{H}]^+$ were found at m/z values of 608.6 and 1348.2 for G_1^{phos} and $\text{BrG}_2^{\text{phos}}$, respectively, and in addition small signals were observed corresponding to the oxidized molecules. Oxidation most likely occurred inside the spectrometer since phosphine oxidation was not evident from both ^1H and ^{31}P NMR spectroscopy.

4.4.2 Coordination of phosphine wedges to SCS Pd^{II} pincer systems

The requirements for convergent metallodendrimer growth starting from the dendritic phosphine wedges are that the phosphines should be able to coordinate to the Pd^{II} of the SCS pincer systems incorporated in our building blocks, and the coordination should be much stronger than pyridine coordination (otherwise ligand scrambling will result when both pyridine and phosphine building blocks are used simultaneously). Therefore systematic studies including

competition experiments with model compounds between pyridines and phosphines were undertaken, and the results have been reported in chapter 3. For example, it has been shown that triphenylphosphine completely suppresses the coordination of pyridines, thus enabling the uncoordinated pyridine ligand to bind to other SCS Pd^{II} pincers.

Coordination of wedges G_1^{phos} and BrG_2^{phos} to model SCS Pd^{II} pincer **13** (see chapter 3 for its synthesis) was investigated by exchange experiments.



Upon addition of 1 equiv of dendritic phosphine wedge G_1^{phos} or BrG_2^{phos} to **13**, the coordinated acetonitrile ligand was quantitatively replaced by the phosphine, as shown by ¹H NMR spectroscopy; the signal of the acetonitrile methyl protons shifted upfield from 2.08 (coordinated) to 1.99 (uncoordinated) ppm. Furthermore, in the ¹H NMR spectrum a characteristic doublet was observed for the aromatic protons of the cyclopalladated aromatic ring (6.77 ppm), which arises from ¹H–³¹P coupling ($J = 2.9$ Hz, see Figure 4.9).

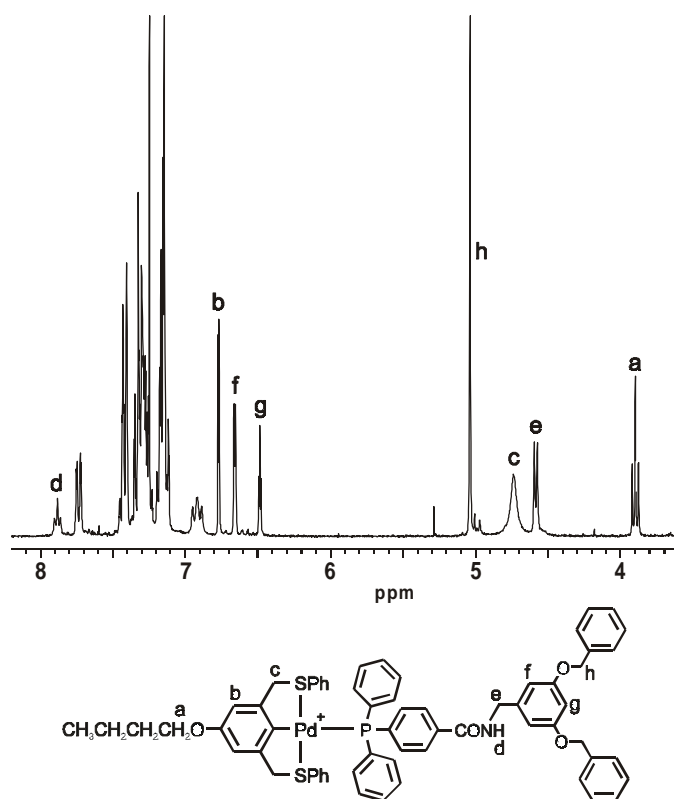


Figure 4.9. Part of the ¹H NMR spectrum (CDCl₃, 298 K) of the complex **13**· G_1^{phos} .

The coordination of the phosphine to Pd^{II} was also evident from the ³¹P NMR spectra, in which a diagnostic shift from -5.6 to 13.7 ppm was observed upon coordination (see also chapter 3).

4.4.3 Convergent metallodendrimer growth starting from phosphine wedge G₁^{phos}

The building blocks required for convergent synthesis of a full metallodendrimer, besides the phosphine wedges, and their schematic representations are depicted in Chart 4.1.

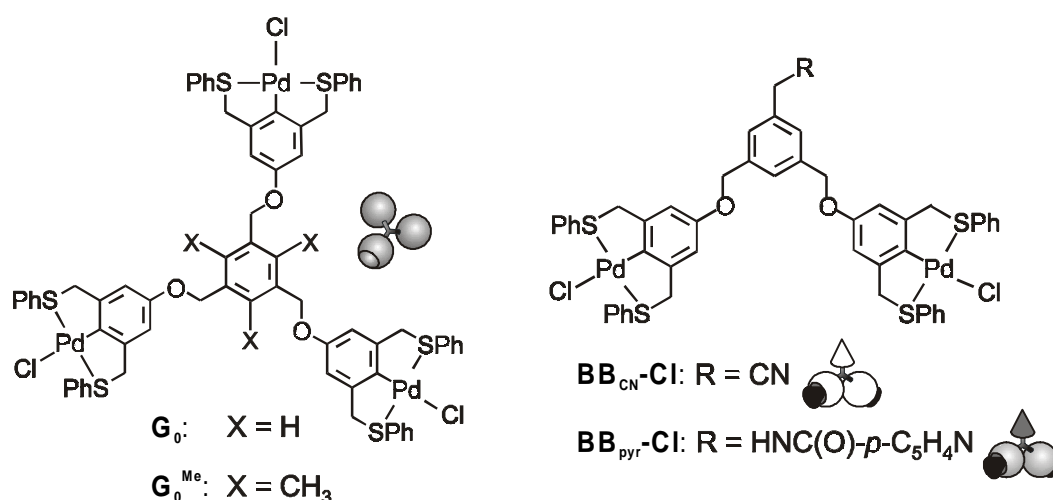
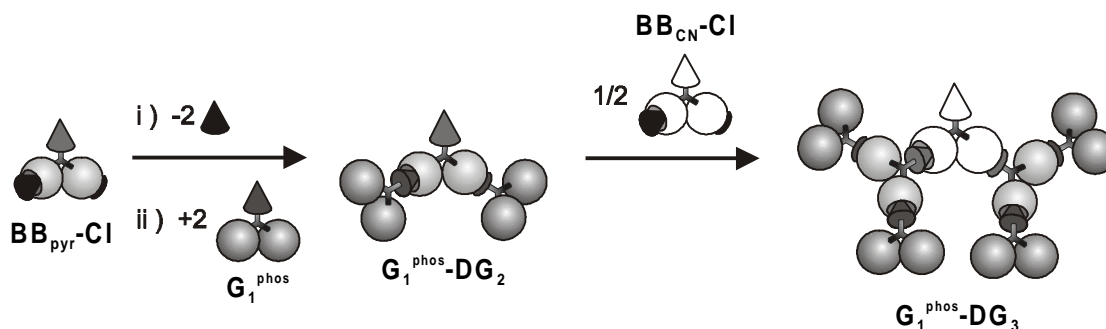


Chart 4.1. Metallodendritic building blocks and their schematic representations.

First, **BB_{pyr}-Cl** was reacted in CH₂Cl₂ with 2 equiv of AgBF₄ to remove the two chlorides coordinated to the Pd^{II} centers (which precipitated as AgCl), and subsequently 2 equiv of **G₁^{phos}** were added (Scheme 4.6).



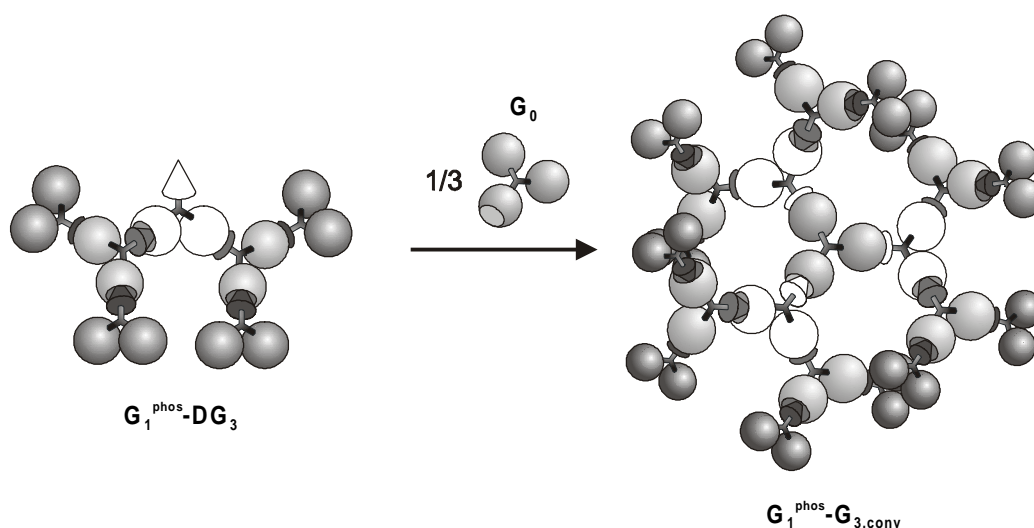
Scheme 4.6. Schematic representation of the convergent synthesis of metallodendritic wedge **G₁^{phos}-DG₃**.

After the reaction mixture was stirred for 10 min and filtered over Hyflo, **G₁^{phos}-DG₂** was obtained as a yellow solid in 89% yield. As stated above, the stronger coordination strength of phosphine over pyridine suppresses the coordination of the pyridine moiety to Pd^{II}. This is indeed observed experimentally in the ¹H NMR spectrum, which unequivocally shows the absence of a broadening and upfield shift of the signal for the pyridine α-protons, features that have previously been shown to be due to coordination to Pd^{II}.⁵¹ Interestingly, the ¹H NMR

spectrum displays *three* doublets between 4.2 and 4.6 ppm, which originate from CH₂N protons in both **BB**_{pyr} and **G**₁^{phos}. However, only two doublets are expected (in a 1:2 ratio) based on the (alleged) symmetry of **G**₁^{phos}-**DG**₂. The combined integrals of the three doublets correspond to the expected six protons. Moreover, the relative intensities of the doublets vary as a function of solvent (in CD₂Cl₂ three doublets of almost equal intensity are observed, whereas in CDCl₃/CD₃NO₂ 4:1 one large and two small doublets are found). Also heating the sample (up to 50 °C) resulted in different intensities of the doublets. These data suggest hindered rotation of the phosphine wedges around the Pd^{II}-P bond, resulting in different rotational isomers with different symmetries. In subsequent generations, the three doublets could not be separately observed due to overlapping and broad signals, but similar behavior is expected.

In the ³¹P NMR spectrum only one signal was observed at 13.6 ppm, indicating complete phosphine coordination. The pyridine moiety of **G**₁^{phos}-**DG**₂ was next used for coordination to two Pd^{II} centers in **BB**_{CN}-**Cl**. In the same manner as described above, the two chlorides of **BB**_{CN}-**Cl** were removed by AgBF₄ and two **G**₁^{phos}-**DG**₂ were added to produce the third generation metallodendrimer wedge **G**₁^{phos}-**DG**₃ (Scheme 4.6). Coordination of the pyridine moieties was confirmed by ¹H NMR spectroscopy, as very broad signals were observed in the region around 8.0 ppm.⁵¹ Furthermore, the successful formation of this wedge was proven by MALDI-TOF mass spectrometry (*vide infra*).

Finally, three of the dendritic wedges **G**₁^{phos}-**DG**₃ were coordinated around deprotected **G**₀ in the usual manner to produce the full hybrid covalent-noncovalent metallodendrimer **G**₁^{phos}-**G**_{3,conv} (Scheme 4.7).



Scheme 4.7. Schematic representation of the coupling of dendrons **G**₁^{phos}-**DG**₃ to the core **G**₀ to produce the hybrid covalent-noncovalent metallodendrimer **G**₁^{phos}-**G**_{3,conv}.

The ^1H NMR spectrum (Figure 4.10a, CD_2Cl_2 , 298 K) of this dendrimer revealed broad signals, most likely due to slow tumbling times and restricted mobility of the nanosize metallodendrimer (estimated size 5-10 nm) in solution.

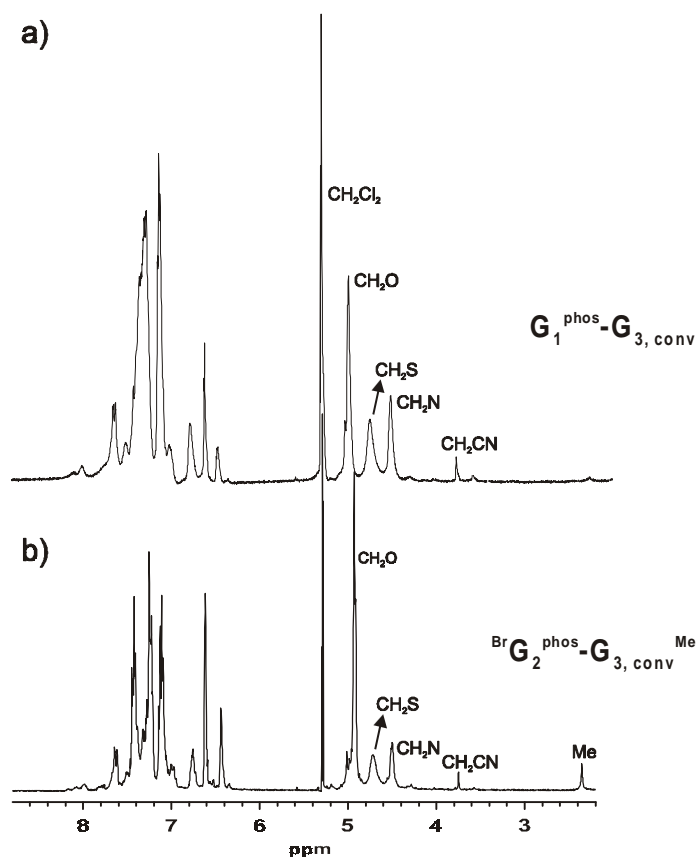


Figure 4.10. ^1H NMR spectra (CD_2Cl_2 , 298 K) of metallodendrimers $\text{G}_1^{\text{phos}}\text{-G}_{3,\text{conv}}$ (a) and $\text{BrG}_2^{\text{phos}}\text{-G}_{3,\text{conv}}^{\text{Me}}$ (b).

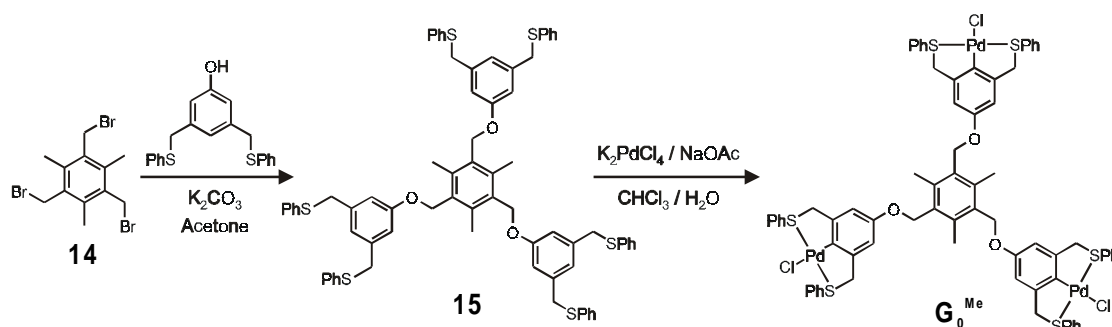
Similar signal broadening has been observed for other metallodendrimers.⁵¹ Evidence for the dendritic structure was obtained from other analytical techniques. First, in the ^{31}P NMR spectrum the signal at 13.6 ppm was still present as the only peak, excluding decomplexation of the phosphine. Furthermore, in the MALDI-TOF mass spectrum a signal at 20.27 kDa (corresponding to $[\text{M} - \text{BF}_4]^+$) was observed as the only signal in the region 5-45 kDa, indicating the presence of a monodisperse metallodendrimer (*vide infra*). Finally, the correct molecular composition was determined by elemental analysis of $\text{G}_1^{\text{phos}}\text{-G}_{3,\text{conv}}$. Remarkably, in going from the wedge $\text{G}_1^{\text{phos}}\text{-DG}_2$ to the dendrimer $\text{G}_1^{\text{phos}}\text{-G}_{3,\text{conv}}$ the products become increasingly soluble in apolar solvents such as dichloromethane and chloroform, and $\text{G}_1^{\text{phos}}\text{-G}_{3,\text{conv}}$ displays a very high solubility at room temperature in these solvents. This is in sharp contrast to some of our metallodendrimers reported before, which displayed limited solubility in nitromethane or mixtures thereof with chlorinated solvents, even when heated.⁵¹ This difference must be due to the increasing number of hydrophobic phosphine wedges at the periphery of the dendrimers.

Controlling the solubility properties of dendrimers by judicious choice of the peripheral groups is very common in dendrimer chemistry.^{52,53}

4.4.4 Convergent metallodendrimer growth starting from phosphine wedge $\text{BrG}_2^{\text{phos}}$

A metallodendrimer with an even thicker hydrophobic shell was obtained by the convergent growth starting from the second generation phosphine wedge $\text{BrG}_2^{\text{phos}}$. Therefore, a full metallodendrimer was constructed in the same manner as described in the previous section. First, $\text{BB}_{\text{pyr}}\text{-Cl}$ was deprived of its chlorides by AgBF_4 and 2 equiv of $\text{BrG}_2^{\text{phos}}$ were subsequently coordinated to Pd^{II} . The resulting wedge $\text{BrG}_2^{\text{phos}}\text{-DG}_2$ was characterized by ^1H and ^{31}P NMR spectroscopy, MALDI-TOF mass spectrometry (*vide infra*) and elemental analysis. Next, two of these wedges were coordinated to deprotected $\text{BB}_{\text{CN}}\text{-Cl}$ to produce the dendritic wedge $\text{BrG}_2^{\text{phos}}\text{-DG}_3$. This wedge was characterized by the same analytical techniques as $\text{BrG}_2^{\text{phos}}\text{-DG}_2$. Finally, coordination of three of these wedges around G_0 was performed in order to assemble the full covalent-noncovalent metallodendrimer $\text{BrG}_2^{\text{phos}}\text{-G}_{3,\text{conv}}$. However, this dendrimer gave no signal in the expected region in the MALDI-TOF mass spectrum. This result might indicate that the large size of the wedge $\text{BrG}_2^{\text{phos}}\text{-DG}_3$ prevents the nitriles at the focal points from coordination to the Pd^{II} centers in G_0 . Coupling of large dendritic wedges to a rather small core is one of the main problems in convergent dendrimer synthesis.^{47,54} Nevertheless, a slightly modified dendritic core was employed in the convergent synthesis of the desired metallodendrimer. This core (termed G_0^{Me} , Chart 4.1) contains three methyl groups instead of protons at its central benzene unit. These methyl groups display a signal around 2.4 ppm in the ^1H NMR spectrum, a region devoid of other metallodendrimer proton signals. This makes it an ideal diagnostic probe for the dendrimer conformation by measuring its T_1 relaxation time constant. It has been shown that proton T_1 relaxation rates of methyl protons in substituted aromatic molecules are sensitive to the steric environment.⁵⁵ Concerning dendrimers, Hecht and Fréchet⁵⁶ found that the T_1 relaxation time constants of methylene protons near the dendrimer core increase with increasing dendrimer generation. This was attributed to a more extended conformation of the core as the steric bulk of the dendrimer wedges increases, which leads to more conformational freedom of the methylene protons and thereby an increasing T_1 value.

G_0^{Me} was synthesized starting from 1,3,5-tris(bromomethyl)-2,4,6-trimethylbenzene⁵⁷ (**14**) by triple alkylation with 3,5-bis(phenylthiamethyl)phenol,⁵⁸ followed by cyclopalladation of the three pincer ligands of **15** with $\text{K}_2\text{PdCl}_4/\text{NaOAc}$ in a refluxing two-phase mixture of chloroform and water (Scheme 4.8). Conventional cyclopalladation using $\text{Pd}[\text{MeCN}]_4(\text{BF}_4)_2$ as the palladium source was found to cleave the benzylic ether bonds, a phenomenon which does not occur in G_0 . Obviously, the three methyl moieties render the benzylic ethers more labile toward the HBF_4 that is released upon cyclopalladation with $\text{Pd}[\text{MeCN}]_4(\text{BF}_4)_2$.



Scheme 4.8. Synthesis of modified dendritic core G_0^{Me} .

4.4.5 Characterization of $\text{Br}G_2^{\text{phos}}\text{-}G_{3,\text{conv}}^{\text{Me}}$ and measurements of methyl proton relaxation rate constants

Using the modified core G_0^{Me} , the influence of several ligands on the T_1 relaxation rate constant of the core methyl groups was investigated by ^1H NMR spectroscopy. The core G_0^{Me} was deprotected using 3 equiv of AgBF_4 and subsequently 3 equiv of either PPh_3 , $\text{Br}G_2^{\text{phos}}\text{-DG}_2$, or $\text{Br}G_2^{\text{phos}}\text{-DG}_3$ were added in order to produce assemblies of varying size. Measurements of methyl proton relaxation rate constants were performed on these assemblies at low concentration (e.g. 0.4 mM for $\text{Br}G_2^{\text{phos}}\text{-}G_{3,\text{conv}}^{\text{Me}}$) in CD_2Cl_2 . The T_1 values were found to increase in the ligand series Cl (0.70 ± 0.01 s) < PPh_3 (0.83 ± 0.01 s) < $\text{Br}G_2^{\text{phos}}\text{-DG}_2$ (1.03 ± 0.01 s) < $\text{Br}G_2^{\text{phos}}\text{-DG}_3$ (1.10 ± 0.01 s), reflecting the increase in steric bulk in this series. These results imply that a similar phenomenon is occurring in the metallodendrimers as in the covalent dendrimers studied by Fréchet, namely the formation of more extended core conformations with increasing dendrimer generations. Moreover, the T_1 values show that the largest metallodendrimer $\text{Br}G_2^{\text{phos}}\text{-}G_{3,\text{conv}}^{\text{Me}}$ has indeed been assembled successfully. Its ^1H NMR spectrum (CD_2Cl_2 , 298 K) is shown in Figure 4.10b. In contrast to $\text{Br}G_2^{\text{phos}}\text{-}G_{3,\text{conv}}$, for which a signal in the expected region of the MALDI-TOF mass spectrum was not observed, MALDI-TOF mass spectrometry of metallodendrimer $\text{Br}G_2^{\text{phos}}\text{-}G_{3,\text{conv}}^{\text{Me}}$ revealed the presence of a small but significant signal at m/z 29.3 kDa, which is in the expected range for $\text{Br}G_2^{\text{phos}}\text{-}G_{3,\text{conv}}^{\text{Me}}$.⁵⁹ Finally, the correct molecular composition was determined by elemental analysis. It is noteworthy that nearly all metallodendrons and metallodendrimers reported in this chapter lack the presence of solvent in the analytical samples, in contrast to previously reported metallodendrimers which were found to include substantial amounts of nitromethane in the solid samples.^{51,60} The growth strategy reported here avoids the use of nitromethane.

In view of the similarity between the cores G_0 and G_0^{Me} , it can also be concluded from these results that the convergent assembly using the original core G_0 has been successful as well.

4.4.6 MALDI-TOF mass spectrometry of metallodendrimers

The determination of the molecular masses of dendrimers has become one of the most powerful techniques in their characterization. This is in part due to the symmetrical nature of

dendrimers, which might hamper complete structure assignment by NMR spectroscopy. Particularly, ESI (electrospray ionization) and MALDI (matrix-assisted laser desorption ionization) mass spectrometry have recently been applied extensively to dendritic systems.⁶¹ Previously, we have also characterized metallodendrimers by either one of these techniques.^{51,60} The dendritic structures reported here were all characterized by MALDI-TOF mass spectrometry. Table 4.1 displays the results of these measurements, and the spectrum of $G_1^{\text{phos}}-G_{3,\text{conv}}$ is depicted in Figure 4.11.

Table 4.1. Characterization of metallodendrimers by MALDI-TOF mass spectrometry.

Compound	Fragment	Obsd mass (Da)	Calcd mass (Da)
$G_1^{\text{phos}}-DG_2$	$[M - BF_4]^+$	2426.3	2426.3
$G_1^{\text{phos}}-DG_3$	$[M - BF_4]^+$	6140.6	6142.0
$G_1^{\text{phos}}-G_{3,\text{conv}}$	$[M - BF_4]^+$	20271.5	20283.1
$BrG_2^{\text{phos}}-DG_2$	$[M - BF_4]^+$	3908.7	3908.5
$BrG_2^{\text{phos}}-DG_3$	$[M - BF_4]^+$	9107.2	9102.3
$BrG_2^{\text{phos}}-G_{3,\text{conv}}^{\text{Me}}$	$[M]^+$	29332.4	29315.6

From Table 4.1 it is evident that all found m/z values of the metallodendrimers except $BrG_2^{\text{phos}}-G_{3,\text{conv}}^{\text{Me}}$ correspond to the loss of only one BF_4 anion, a characteristic feature which we have also observed in previously reported metallodendrimers.⁵¹

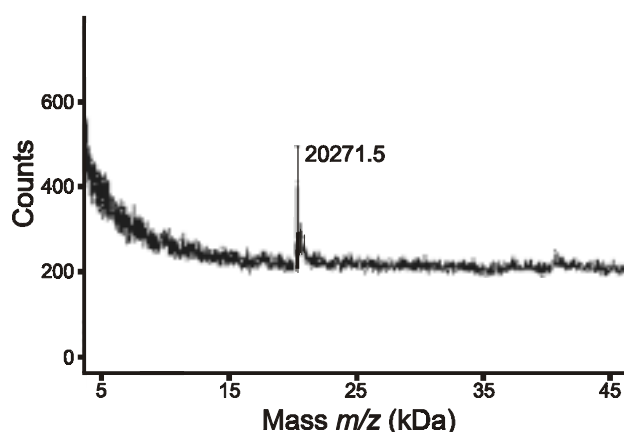


Figure 4.11. MALDI-TOF mass spectrum of $G_1^{\text{phos}}-G_{3,\text{conv}}$.

This is in contrast to ES-MS spectra of similar metallodendrimers, which display a preferential loss of a number of anions (up to 39 BF_4 anions for a fourth generation metallodendrimer).⁶⁰ In the case of $BrG_2^{\text{phos}}-G_{3,\text{conv}}^{\text{Me}}$, the broad signal in the MALDI-TOF spectrum centers around 29.33 kDa, which corresponds to $[M]^+$ instead of $[M - BF_4]^+$.

4.5 Conclusions

Both covalent and non-covalent syntheses of dendritic structures have been combined in the assembly of “layer-block” metallodendrimers containing hydrophobic dendrons at their periphery. First and second generation Fréchet wedges functionalized at their focal point with phosphines coordinate to SCS Pd^{II} pincers, and their coordination was combined with the coordination of nitriles and pyridines to convergently assemble non-covalent metallodendrimers. All metallodendrimers were fully characterized by ¹H and ³¹P NMR spectroscopy, elemental analysis, and MALDI-TOF mass spectrometry. The introduction of hydrophobic dendrons at the periphery of metallodendrimers significantly increases their solubility in apolar organic solvents, compared to metallodendrimers lacking these dendrons. The mobility of methyl protons at the metallodendrimer core was probed by proton *T*₁ relaxation time measurements, and it was found that upon increasing the dendrimer size, the mobility of these methyl protons increases accordingly.

Using the convergent metallodendrimer assembly described in this chapter, the introduction of functional groups at either the periphery or the core of the metallodendrimer becomes feasible. The next chapter in this thesis deals with the introduction of a fluorescent rhodamine B at the dendritic core, whereas in chapter 6 the introduction of water-solubilizing groups at the periphery of metallodendrimers is discussed.

4.6 Experimental Section

General comments. For general information on instruments, procedures, and chemicals, see chapter 3.

Matrix Assisted Laser Desorption Ionisation (MALDI) Time-of-Flight (TOF) mass spectra⁶² were recorded using a Perkin Elmer/PerSeptive Biosystems Voyager-DE-RP MALDI-TOF mass spectrometer (PerSeptive Biosystems, Inc., Framingham, MA, USA) equipped with delayed extraction.⁶³ A 337 nm UV nitrogen laser producing 3 ns pulses was used and the mass spectra were obtained in the linear and reflectron mode. Samples were prepared by mixing 10 μL of chloroform solution of the sample with 30 μL of a solution of 0.5 mg/L hydroxybenzylidene malononitrile (HBM) and 0.5 mg/L dithranol (DIT) in chloroform/liquid poly(ethylene glycol). One μL of the solution was loaded on a gold-sample plate, the solvent was removed in warm air and the sample transferred to the vacuum of the mass spectrometer for analysis.

Materials. 3,5-Bis(benzyloxy)benzyl amine **9**,⁴⁹ **BrG₂Br** (**10**),⁵⁰ 1,3,5-tris(bromomethyl)-2,4,6-trimethylbenzene,⁵⁷ **G₀**,⁶⁰ **BB_{CN}-Cl**,⁵⁸ **BB_{pyr}-Cl**,⁵¹ and 3,5-bis(phenylthiomethyl)phenol⁵⁸ were prepared according to literature procedures.

Phosphine-functionalized first generation dendrimer wedge (G₁^{phos}). To a mixture of 3,5-bis(benzyloxy)benzyl amine **9** (0.24 g, 0.75 mmol), 4-(diphenylphosphino)benzoic acid (0.21 g, 0.69 mmol) and 1-hydroxybenzotriazole hydrate (HOBt, 0.09 g, 0.67 mmol) in CHCl₃ (50 mL) was added 1,3-dicyclohexylcarbodiimide (DCC, 0.16 g, 0.78 mmol) and the resulting solution was stirred at room

temperature under an argon atmosphere for 3.5 h. The solution was subsequently washed with saturated aqueous solutions of NaHCO₃ and NaCl and dried over MgSO₄. After evaporation of the solvent the crude product was purified by column chromatography (SiO₂; eluent: CH₂Cl₂) to afford pure dendritic wedge **G₁^{phos}** as a white solid. Yield 0.50 g (quant). M.p. 164-166 °C. ¹H NMR: δ (ppm) 7.74 (d, *J* = 7.0 Hz, 2 H, Ar H), 7.47-7.33 (m, 22 H, Ar H), 6.63 (d, *J* = 2.2 Hz, 2 H, Ar H), 6.60 (t, *J* = 2.2 Hz, 1 H, Ar H), 6.35 (t, *J* = 5.5 Hz, 1 H, NH), 5.36 (s, 4 H, CH₂O), 4.63 (d, *J* = 5.5 Hz, 2 H, CH₂N). ¹³C NMR: δ (ppm) 166.5, 159.7, 141.7, 139.9, 136.2, 135.8, 133.7, 133.5, 133.2, 132.9, 128.6, 128.2, 128.1, 127.5, 127.0, 126.4, 126.3, 106.4, 100.7, 69.6, 43.6. ³¹P NMR: δ (ppm) -5.6. FAB-MS: *m/z* 608.6 ([M + H]⁺, calcd 608.7). Anal. calcd for C₄₀H₃₄NO₃P·H₂O: C, 76.78; H, 5.80; N, 2.24. Found: C, 76.68; H, 5.55; N, 2.44.

BrG₂^{NPh} (11). A mixture of **BrG₂^{Br} (10)**, 0.40 g, 0.36 mmol), potassium phthalimide (0.08 g, 0.43 mmol) and K₂CO₃ (0.08 g, 0.58 mmol) in MeCN (50 mL) was refluxed under an argon atmosphere for 3 h. After evaporation of the solvent, the resulting paste was taken up in CH₂Cl₂ (100 mL) and the solution was washed with brine and dried over Na₂SO₄. After removal of the solvent, the crude product was purified by column chromatography (SiO₂; eluent; CH₂Cl₂/hexane 80/20) to afford a white solid. Yield 0.41 g (96%). M.p. 140-142 °C. ¹H NMR: δ (ppm) 7.83-7.80 (m, 2 H, Phth), 7.70-7.67 (m, 2 H, Phth), 7.48 (d, *J* = 8.1 Hz, 8 H, Ar H), 7.26 (d, *J* = 8.1 Hz, 8 H, Ar H), 6.64 (d, *J* = 2.2 Hz, 2 H, Ar H), 6.61 (d, *J* = 2.2 Hz, 4 H, Ar H), 6.47 (t, *J* = 2.2 Hz, 2 H, Ar H), 6.44 (t, *J* = 2.2 Hz, 1 H, Ar H), 4.96 (s, 8 H, CH₂O), 4.92 (s, 4 H, CH₂O), 4.76 (s, 2 H, CH₂N). ¹³C NMR: δ (ppm) 167.4, 159.4, 159.3, 138.8, 138.1, 135.3, 133.5, 131.5, 131.2, 128.6, 122.9, 121.4, 107.1, 105.9, 101.2, 100.9, 69.3, 68.8, 41.1. FAB-MS: *m/z* 1190.1 ([M + H]⁺, calcd 1190.6). Anal. calcd for C₅₇H₄₃Br₄NO₈: C, 57.55; H, 3.64; N, 1.18. Found: C, 57.59; H, 3.42; N, 0.91.

BrG₂^{amine} (12). A solution of dendritic phthalimide **11** (0.14 g, 0.12 mmol) in EtOH (30 mL) and THF (10 mL) was heated to reflux, and hydrazine monohydrate (0.5 mL) was added. After refluxing for 2 h, the solution was cooled to room temperature and evaporated until 20 mL of solution. HCl (1 M, 50 mL) was added, and the solution was extracted with CH₂Cl₂ (2×50 mL). The organic layer was washed with NaHCO₃ (aq), brine, and dried over Na₂SO₄. After evaporation of the solvent, the dendritic amine **12** was obtained as a colorless oil. Yield 0.12 g (96%). For characterization, the amine was further purified by column chromatography (SiO₂; eluent: CH₂Cl₂/MeOH 95:5). ¹H NMR: δ (ppm) 7.48 (d, *J* = 7.7 Hz, 8 H, Ar H), 7.26 (d, *J* = 7.7 Hz, 8 H, Ar H), 6.63 (d, *J* = 2.2 Hz, 4 H, Ar H), 6.54 (d, *J* = 2.2 Hz, 2 H, Ar H), 6.49 (t, *J* = 2.2 Hz, 2 H, Ar H), 6.44 (t, *J* = 2.2 Hz, 1 H, Ar H), 4.97 (s, 8 H, CH₂O), 4.96 (s, 4 H, CH₂O), 3.79 (s, 2 H, CH₂N). ¹³C NMR: δ (ppm) 159.5, 159.4, 145.2, 139.0, 135.2, 131.2, 128.6, 121.4, 105.9, 105.6, 101.1, 100.0, 69.3, 68.8, 46.0. FAB-MS: *m/z* 1060.0 ([M + H]⁺, calcd for C₄₉H₄₁Br₄NO₆: 1060.5).

Phosphine-functionalized second generation dendrimer wedge (BrG₂^{phos}). To a solution of dendritic amine **12** (0.18 g, 0.17 mmol), 4-(diphenylphosphino)benzoic acid (48 mg, 0.16 mmol) and 1-hydroxybenzotriazole hydrate (HOBt, 21 mg, 0.16 mmol) in CHCl₃ (50 mL) was added 1,3-dicyclohexylcarbodiimide (DCC, 35 mg, 0.17 mmol) and the resulting solution was stirred at room temperature under an argon atmosphere for 3 h. The solution was subsequently washed with saturated aqueous solutions of NaHCO₃ and NaCl, and dried over Na₂SO₄. After evaporation of the solvent the

crude product was purified by column chromatography (SiO₂; eluent: CH₂Cl₂) to afford dendritic wedge **BrG₂^{phos}** as an off-white solid. Yield 0.18 g (79%). M.p. 108-110 °C. ¹H NMR: δ (ppm) 7.65 (d, *J* = 8.0 Hz, 2 H, Ar H), 7.47 (d, *J* = 8.4 Hz, 8 H, Ar H), 7.36-7.28 (m, 12 H, Ar H), 7.24 (d, *J* = 8.4 Hz, 8 H, Ar H), 6.61 (d, *J* = 2.2 Hz, 4 H, Ar H), 6.53 (d, *J* = 2.2 Hz, 2 H, Ar H), 6.48-6.46 (m, 3 H, Ar H), 6.41 (t, *J* = 5.5 Hz, NH), 4.93 (s, 12 H, CH₂O), 4.53 (d, *J* = 5.5 Hz, 2 H, CH₂N). ¹³C NMR: δ (ppm) 166.5, 159.5, 159.4, 141.8, 140.1, 138.8, 135.7, 135.2, 133.5, 133.22, 133.16, 132.9, 131.2, 128.6, 128.2, 126.3, 121.4, 106.4, 105.8, 101.1, 100.7, 69.3, 68.8, 43.6. ³¹P NMR: δ (ppm) -5.6. FAB-MS: *m/z* 1348.2 ([M]⁺, calcd 1347.8). Anal. calcd for C₆₈H₅₄Br₄NO₇P·1.1CH₂Cl₂: C, 56.96; H, 3.89; N, 0.96. Found: C, 56.78; H, 3.74; N, 0.96.

G₀^{Me} precursor (14). A mixture of 1,3,5-tris(bromomethyl)-2,4,6-trimethylbenzene (0.25 g, 0.63 mmol), 3,5-bis(phenylthiamethyl)phenol (0.63 g, 1.86 mmol), K₂CO₃ (0.51 g, 3.69 mmol), and 18-crown-6 (0.05 g, 0.19 mmol) in acetone (60 mL) was refluxed overnight under an argon atmosphere. After evaporation of the solvent *in vacuo*, the resulting paste was taken up in CH₂Cl₂ (100 mL) and washed with brine. The organic phase was dried over Na₂SO₄ and the solvent was removed under reduced pressure. The crude product was purified by column chromatography (using CH₂Cl₂/hexane 65:35 (v/v) as the eluent), affording a white solid. Yield 0.52 g (71%). M.p. 77-79 °C. ¹H NMR: δ (ppm) 7.32-7.17 (m, 30 H, SPh H), 6.88 (s, 3 H, Ar H), 6.76 (s, 6 H, Ar H), 4.92 (s, 6 H, CH₂O), 4.05 (s, 12 H, CH₂S), 2.33 (s, 9 H, CH₃). ¹³C NMR: δ (ppm) 158.7, 138.7, 135.6, 131.1, 129.7, 128.3, 126.0, 121.5, 113.4, 64.4, 38.6, 15.4. FAB-MS: *m/z* 1170.5 ([M]⁺, calcd 1170.3). Anal. calcd for C₇₂H₆₆O₃S₆·0.2H₂O: C, 73.58; H, 5.69; S, 16.37. Found: C, 73.36; H, 5.59; S, 16.25.

G₀^{Me}. A solution of K₂PdCl₄ (0.29 g, 0.89 mmol) and NaOAc (73 mg, 0.89 mmol) in water (100 ml) was added to a solution of **14** (0.29 g, 0.25 mmol) in CHCl₃ (100 ml). The two-phase mixture was refluxed for 2 h and subsequently cooled to r.t. After filtration of the mixture over Hyflo, the organic phase was washed with brine and dried over anhydrous Na₂SO₄. As TLC and ¹H NMR indicated incomplete cyclopalladation, the crude product was subjected to the same reaction conditions once more. After work-up, the crude product was purified by column chromatography (using CH₂Cl₂/MeOH 97:3 (v/v) as the eluent), which afforded a yellow solid. Yield 85 mg (22%). M.p. 191-193 °C. ¹H NMR: δ (ppm) 7.86-7.83 (m, 12 H, SPh H), 7.39-7.35 (m, 18 H, SPh H), 6.66 (s, 6 H, Ar H), 4.97 (s, 6 H, CH₂O), 4.57 (br s, 12 H, CH₂S), 2.38 (s, 9 H, CH₃). ¹³C NMR: δ (ppm) 156.4, 151.5, 149.7, 138.8, 131.8, 131.0, 129.4, 129.1, 108.3, 64.5, 51.4, 15.4. FAB-MS: *m/z* 1555.2 ([M - Cl]⁺, calcd 1555.0). Anal. calcd for C₇₂H₆₃Cl₃O₃Pd₃S₆: C, 54.24; H, 3.98; S, 12.07. Found: C, 54.32; H, 3.84; S, 12.15.

General procedure for the convergent growth of metallodendritic wedges and dendrimers. Building block, wedge or core (1 – 6 μmol), was dissolved in CH₂Cl₂ and the required amount of AgBF₄ was added as a concentrated solution (0.10 – 0.20 M) in water. After the mixture was stirred for 5 min, the required amount of other building block or wedge was added in one portion. The mixture was vigorously stirred for 15 min, and subsequently CH₂Cl₂ and H₂O were removed under reduced pressure. The crude product was again dissolved in CH₂Cl₂, and AgCl was removed by filtration over Hyflo. After evaporation of the solvent, the product was obtained as a yellow solid.

G₁^{phos}-DG₂. Building block **BB_{pyr}-Cl** (3.6 mg, 3.0 μmol) was deprotected with AgBF₄ (6.0 μmol, 35 μL of a 0.1699 M solution), and subsequently phosphine wedge **G₁^{phos}** (3.7 mg, 6.0 μmol) was added. Yield 6.8 mg (89%). ¹H NMR (CD₂Cl₂): δ (ppm) 8.60 (d, *J* = 6.0 Hz, 2 H, pyr α H), 7.75 (d, *J* = 6.0 Hz, 2 H, pyr β H), 7.63 (d, *J* = 7.0 Hz, 4 H, Ar H), 7.47-7.22 (m, 43 H, Ar H), 7.16-7.00 (m, 24 H, Ar H), 6.83 (t, *J* = 5.5 Hz, 1 H, NH), 6.79-6.47 (10 H, Ar H), 5.01 (s, 8 H, CH₂O), 4.97 (s, 4 H, CH₂O), 4.73 (br s, 8 H, CH₂S), 4.57 (d, *J* = 5.5 Hz, 1.5 H, CH₂N), 4.53 (d, *J* = 5.5 Hz, 2.5 H, CH₂N), 4.47 (d, *J* = 5.5 Hz, 2 H, CH₂N). ³¹P NMR (CD₂Cl₂): δ (ppm) 13.6. MALDI-TOF MS *m/z* 2426.3 ([M – BF₄]⁺, calcd 2426.3). Anal. calcd for C₁₃₅H₁₁₄B₂F₈N₄O₉P₂Pd₂S₄: C, 64.52; H, 4.57; N, 2.23; S, 5.10. Found: C, 64.41; H, 4.27; N, 2.09; S, 5.10.

G₁^{phos}-DG₃. Building block **BB_{CN}-Cl** (2.1 mg, 1.9 μmol) was deprotected with AgBF₄ (3.8 μmol, 33 μL of a 0.1145 M solution), and subsequently dendritic wedge **G₁^{phos}-DG₂** (9.2 mg, 3.8 μmol) was added. Yield 10.6 mg (92%). ¹H NMR (CD₂Cl₂): δ (ppm) 7.99 (very br s, 4 H, pyr α H), 7.61 (d, *J* = 7.0 Hz, 8 H, Ar H), 7.49 (br s, 4 H, pyr β), 7.42-6.94 (m, 157 H, Ar H), 6.79-6.45 (3 × m, 24 H, Ar H), 5.01 (s, 4 H, CH₂O), 4.97 (s, 8 H, CH₂O), 4.96 (s, 16 H, CH₂O), 4.73 (br s, 24 H, CH₂S), 4.50 (br d, 12 H, CH₂N), 3.74 (s, 2 H, CH₂CN). ³¹P NMR (CD₂Cl₂): δ (ppm) 13.6. MALDI-TOF MS *m/z* 6140.6 ([M – BF₄]⁺, calcd 6142.0). Anal. calcd for C₃₂₀H₂₆₉B₆F₂₄N₉O₂₀P₄Pd₆S₁₂: C, 61.71; H, 4.35; N, 2.02; S, 6.18. Found: C, 61.46; H, 4.52; N, 1.75; S, 6.27.

G₁^{phos}-G_{3,conv}. Dendrimer core **G₀** (2.1 mg, 1.4 μmol) was deprotected with AgBF₄ (4.3 μmol, 40 μL of a 0.1077 M solution), and subsequently dendritic wedge **G₁^{phos}-DG₃** (25.9 mg, 4.2 μmol) was added. Yield 24.0 mg (85%). ¹H NMR (CD₂Cl₂): δ (ppm) 8.0 (very br s, 12 H, pyr α H), 7.6 (d, *J* = 7.0 Hz, 24 H, Ar H), 7.5-6.9 (m, 516 H, Ar H + pyr β H), 6.75 (br d, 42 H, Ar H), 6.6 (br s, 24 H), 6.4 (br s, 12 H, Ar H), 4.95 (br s, 90 H, CH₂O), 4.65 (br s, 84 H, CH₂S), 4.45 (br s, 36 H, CH₂N), 3.7 (s, 6 H, CH₂CN). ³¹P NMR (CD₂Cl₂): δ (ppm) 13.6. MALDI-TOF MS *m/z* 20271.5 ([M – BF₄]⁺, calcd 20283.1). Anal. calcd for C₁₀₂₉H₈₆₄B₂₁F₈₄N₂₇O₆₃P₁₂Pd₂₁S₄₂·CH₂Cl₂: C, 60.42; H, 4.26; N, 1.85; S, 6.58. Found: C, 60.10; H, 4.21; N, 1.85; S, 6.26.

BrG₂^{phos}-DG₂. Building block **BB_{pyr}-Cl** (4.7 mg, 3.9 μmol) was deprotected with AgBF₄ (7.9 μmol, 35 μL of a 0.2255 M solution), and subsequently phosphine wedge **BrG₂^{phos}** (10.6 mg, 7.9 μmol) was added. Yield 14.5 mg (92%). ¹H NMR (CD₂Cl₂): δ (ppm) 8.56 (d, *J* = 6.0 Hz, 2 H, pyr α H), 7.73 (d, *J* = 6.0 Hz, 2 H, pyr β H), 7.62 (d, *J* = 7.0 Hz, 4 H, Ar H), 7.46-6.97 (m, 79 H, Ar H), 6.73-6.40 (22 H, Ar H), 4.98 (s, 4 H, CH₂O), 4.92 (s, 16 H, CH₂O), 4.85 (s, 8 H, CH₂O), 4.67 (br s, 8 H, CH₂S), 4.55 (d, *J* = 5.5 Hz, 1.8 H, CH₂N), 4.50 (d, *J* = 5.5 Hz, 2.9 H, CH₂N), 4.43 (d, *J* = 5.5 Hz, 1.3 H, CH₂N). ³¹P NMR (CD₂Cl₂): δ (ppm) 13.6. MALDI-TOF MS *m/z* 3908.7 ([M – BF₄]⁺, calcd 3908.5). Anal. calcd for C₁₉₁H₁₅₆B₂Br₈F₈N₄O₁₇P₂Pd₂S₄: C, 57.45; H, 3.89; N, 1.40; S, 3.21. Found: C, 57.60; H, 4.24; N, 1.68; S, 2.86.

BrG₂^{phos}-DG₃. Building block **BB_{CN}-Cl** (1.2 mg, 1.1 μmol) was deprotected with AgBF₄ (2.2 μmol, 19 μL of a 0.1145 M solution), and subsequently dendritic wedge **BrG₂^{phos}-DG₂** (8.8 mg, 2.2 μmol) was added. Yield 8.3 mg (82%). ¹H NMR (CD₂Cl₂): δ (ppm) 7.70 (br s, 4 H, pyr β), 7.60 (d, *J* = 7.0 Hz, 8 H, Ar H),

7.4-6.9 (m, 181 H, Ar H), 6.75-6.35 (3 × br s, 48 H, Ar H), 4.9 (br s, 60 H, CH₂O), 4.65 (br s, 24 H, CH₂S), 4.5-4.4 (br d, 12 H, CH₂N), 3.7 (s, 2 H, CH₂CN). ³¹P NMR (CD₂Cl₂): δ (ppm) 13.6. MALDI-TOF MS *m/z* 9107.2 ([M – BF₄]⁺, calcd 9102.3). Anal. calcd for C₄₃₂H₃₄₉B₆Br₁₆F₂₄N₉O₃₆P₄Pd₆S₁₂: C, 56.44; H, 3.87; N, 1.37; S, 4.19. Found: C, 56.63; H, 4.12; N, 1.25; S, 3.88.

BrG₂^{phos}-G_{3,conv}^{Me}. Dendrimer core G₀^{Me} (1.4 mg, 0.9 μmol) was deprotected with AgBF₄ (2.7 μmol, 24 μL of a 0.1128 M solution), and subsequently dendritic wedge BrG₂^{phos}-DG₃ (23.9 mg, 2.7 μmol) was added. Yield 22.1 mg (87%). ¹H NMR (CD₂Cl₂): δ (ppm) 8.0 (very br s, 12 H, pyr α H), 7.6 (d, *J* = 7.0 Hz, 24 H, Ar H), 7.5-6.9 (m, 603 H, Ar H + pyr β H + NH), 6.75 (br s, 42 H, Ar H), 6.6 (br s, 72 H), 6.4 (br s, 36 H, Ar H), 4.90 (br s, 186 H, CH₂O), 4.65 (br s, 84 H, CH₂S), 4.5 (br s, 36 H, CH₂N), 3.7 (s, 6 H, CH₂CN), 2.4 (s, 9 H, CH₃). ³¹P NMR (CD₂Cl₂): δ (ppm) 14.1. MALDI-TOF MS *m/z* 29332.4 ([M]⁺, calcd 29315.6). Anal. calcd for C₁₃₆₈H₁₁₁₀B₂₁Br₄₈F₈₄N₂₇O₁₁₁P₁₂Pd₂₁S₄₂: C, 56.05; H, 3.82; N, 1.29; S, 4.59. Found: C, 56.04; H, 4.15; N, 1.20; S, 4.33.

4.7 References and notes

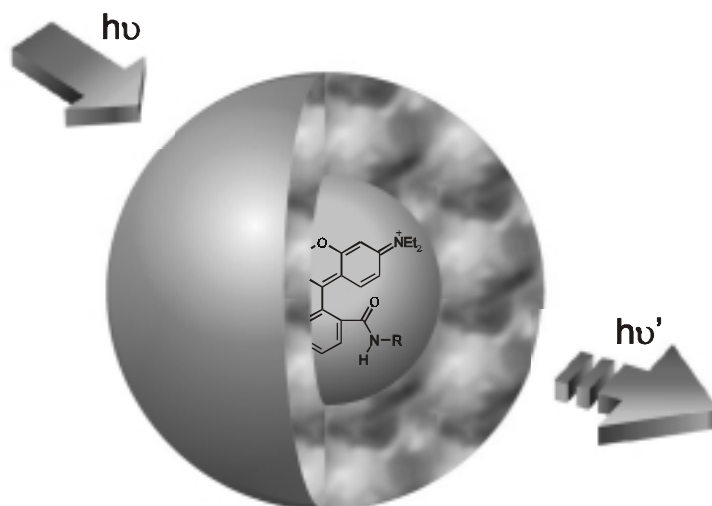
- ¹ Hawker, C. J.; Wooley, K. L.; Fréchet, J. M. J. *Macromol. Symp.* **1994**, *77*, 11.
- ² This distinction was taken from a review titled “New Self-Assembled Structural Motifs in Coordination Chemistry”, Swiegers, G. F.; Malefetse, T. J. *Chem. Rev.* **2000**, *100*, 3483.
- ³ Baxter, P. N. W.; Lehn, J.-M.; Fischer, J.; Youinou, M.-T. *Angew. Chem., Int. Ed. Engl.* **1994**, *33*, 2284.
- ⁴ Garcia, A. M.; Romero-Salguero, F. J.; Bassani, D. M.; Lehn, J.-M.; Baum, G.; Fenske, D. *Chem. Eur. J.* **1999**, *5*, 1803.
- ⁵ Weisbuch, I.; Baxter, P. N. W.; Cohen, S.; Cohen, H.; Kjaer, K.; Howes, P. B.; Als-Nielsen, J.; Hanan, G. S.; Schubert, U. S.; Lehn, J.-M.; Leiserowitz, L.; Lahav, M. *J. Am. Chem. Soc.* **1998**, *120*, 4850.
- ⁶ Semenov, A.; Spatz, J. P.; Möller, M.; Lehn, J.-M.; Sell, B.; Schubert, D.; Weidl, C. H.; Schubert, U. S. *Angew. Chem. Int. Ed.* **1999**, *38*, 2547.
- ⁷ Baxter, P. N. W.; Hanan, G. S.; Lehn, J.-M. *Chem. Commun.* **1996**, 2019.
- ⁸ Stang, P. J.; Olenyuk, B. *Acc. Chem. Res.* **1997**, *30*, 502.
- ⁹ Fujita, M.; Yazaki, J.; Ogura, K. *J. Am. Chem. Soc.* **1990**, *112*, 5645.
- ¹⁰ Stang, P. J.; Cao, D. H. *J. Am. Chem. Soc.* **1994**, *116*, 4981.
- ¹¹ a) Fujita, M.; Ogura, K. *Bull. Chem. Soc. Jpn.* **1996**, *69*, 1471; b) Olenyuk, B.; Fechtenkötter, A.; Stang, P. J. *J. Chem. Soc., Dalton Trans.* **1998**, 1707; c) Stang, P. J. *Chem. Eur. J.* **1998**, *4*, 19; d) Jones, C. J. *Chem. Soc. Rev.* **1998**, *27*, 289; e) Leininger, S.; Olenyuk, B.; Stang, P. J. *Chem. Rev.* **2000**, *100*, 853.
- ¹² Stang, P. J.; Olenyuk, B.; Fan, J.; Arif, A. M. *Organometallics* **1996**, *15*, 904.
- ¹³ Rauter, H.; Hillgeris, E. C.; Erxleben, A.; Lippert, B. *J. Am. Chem. Soc.* **1994**, *116*, 616.
- ¹⁴ Stang, P. J.; Cao, D. H.; Chen, K.; Gray, G. M.; Muddiman, D. C.; Smith, R. D. *J. Am. Chem. Soc.* **1997**, *119*, 5163.
- ¹⁵ a) Anderson, S.; Anderson, H. L.; Sanders, J. K. M. *J. Chem. Soc., Perkin Trans. 1* **1995**, 2255; b) Drain, C. M.; Lehn, J.-M. *J. Chem. Soc., Chem. Commun.* **1994**, 2313; c) Chi, X.; Guerin, A. J.; Haycock, R. A.; Hunter, C. A.; Sarson, L. D. *J. Chem. Soc., Chem. Commun.* **1995**, 2567; d) Alessio,

- E.; Macchi, M.; Heath, S. L.; Marzilli, L. G. *Inorg. Chem.* **1997**, *36*, 5614; e) Fan, J.; Whiteford, J. A.; Olenyuk, B.; Levin, M. D.; Stang, P. J.; Fleischer, E. B. *J. Am. Chem. Soc.* **1999**, *121*, 2741.
- ¹⁶ Habicher, T.; Nierengarten, J.-F.; Gramlich, V.; Diederich, F. *Angew. Chem. Int. Ed.* **1999**, *37*, 1916.
- ¹⁷ Fujita, M.; Umemoto, K.; Yoshizawa, M.; Fujita, N.; Kusukawa, T.; Biradha, K. *Chem. Commun.* **2001**, 509.
- ¹⁸ Takeda, N.; Umemoto, K.; Yamaguchi, K.; Fujita, M. *Nature* **1999**, *398*, 794.
- ¹⁹ Abrahams, B. F.; Egan, S. J.; Robson, R. *J. Am. Chem. Soc.* **1999**, *121*, 3535.
- ²⁰ a) Fujita, M. *Chem. Soc. Rev.* **1998**, 417; b) Linton, B.; Hamilton, A. D. *Chem. Rev.* **1997**, *97*, 1669.
- ²¹ For reviews, see: a) Sauvage, J.-P.; Collin, J.-P.; Chambron, J.-C.; Guillerez, S.; Coudret, C.; Balzani, V.; Barigelletti, F.; De Cola, L.; Flamigni, L. *Chem. Rev.* **1994**, *94*, 993; b) Harriman, A.; Ziessel, R. *Chem. Commun.* **1996**, 1707; c) Collin, J.-P.; Gaviña, P.; Heitz, V.; Sauvage, J.-P. *Eur. J. Inorg. Chem.* **1998**, 1.
- ²² Grosshenny, V.; Harriman, A.; Ziessel, R. *Angew. Chem. Int. Ed. Engl.* **1995**, *34*, 2705.
- ²³ Wärnmark, K.; Thomas, J. A.; Heyke, O.; Lehn, J.-M. *Chem. Commun.* **1996**, 701.
- ²⁴ Sutter, J.-P.; Grove, D. M.; Beley, M.; Collin, J.-P.; Veldman, N.; Spek, A. L.; Sauvage, J.-P.; van Koten, G. *Angew. Chem. Int. Ed. Engl.* **1994**, *33*, 1282.
- ²⁵ a) *Molecular Catenanes, Rotaxanes, and Knots*; Sauvage, J.-P.; Dietrich-Buchecker, C., Eds.; Wiley-VCH: Weinheim, 1999; b) Chambron, J.-C.; Dietrich-Buchecker, C.; Sauvage, J.-P. *Transition Metals as Assembling and Templating Species: Synthesis of Catenanes and Molecular Knots*. In *Comprehensive Supramolecular Chemistry*; Lehn, J.-M., Chair Ed.; Atwood, J. L., Davis, J. E. D., MacNicol, D. D., Vögtle, F., Exec. Eds.; Pergamon: Oxford, UK, 1987-1996; Vol. 9, Chapter 2; c) Fujita, M. *Acc. Chem. Res.* **1999**, *32*, 53.
- ²⁶ a) Solladié, N.; Chambron, J.-C.; Dietrich-Buchecker, C.; Sauvage, J.-P. *Angew. Chem., Int. Ed. Engl.* **1996**, *35*, 906; b) Linke, M.; Chambron, J.-C.; Heitz, V.; Sauvage, J.-P. *J. Am. Chem. Soc.* **1997**, *119*, 11329.
- ²⁷ Armaroli, N.; Diederich, F.; Dietrich-Buchecker, C.; Flamigni, L.; Marconi, G.; Nierengarten, J.-F.; Sauvage, J.-P. *Chem. Eur. J.* **1998**, *4*, 406.
- ²⁸ a) Harriman, A.; Sauvage, J.-P. *Chem. Soc. Rev.* **1996**, *25*, 41; b) Flamigni, L.; Barigelletti, F.; Armaroli, N.; Collin, J.-P.; Sauvage, J.-P. *Chem. Eur. J.* **1998**, *4*, 1744.
- ²⁹ Armaroli, N.; Balzani, V.; Collin, J.-P.; Gaviña, P.; Sauvage, J.-P.; Ventura, B. *J. Am. Chem. Soc.* **1999**, *121*, 4397.
- ³⁰ Raehm, L.; Kern, J.-M.; Sauvage, J.-P. *Chem. Eur. J.* **1999**, *5*, 3310.
- ³¹ Jiménez, M. C.; Dietrich-Buchecker, C.; Sauvage, J.-P.; De Cian, A. *Angew. Chem. Int. Ed.* **2000**, *39*, 1295.
- ³² Jiménez, M. C.; Dietrich-Buchecker, C.; Sauvage, J.-P. *Angew. Chem. Int. Ed.* **2000**, *39*, 3284.
- ³³ Dietrich-Buchecker, C.; Sauvage, J.-P.; Kern, J.-M. *J. Am. Chem. Soc.* **1984**, *106*, 3043.
- ³⁴ Mohr, B.; Weck, M.; Sauvage, J.-P.; Grubbs, R. H. *Angew. Chem. Int. Ed. Engl.* **1997**, *36*, 1308.
- ³⁵ Cárdenas, D. J.; Gaviña, P.; Sauvage, J.-P. *J. Am. Chem. Soc.* **1997**, *119*, 2656.
- ³⁶ Sauvage, J.-P. *Acc. Chem. Res.* **1998**, *31*, 611.
- ³⁷ Raehm, L.; Hamann, C.; Kern, J.-M.; Sauvage, J.-P. *Org. Lett.* **2000**, *2*, 1991.
- ³⁸ Fujita, M.; Ibukuro, F.; Hagihara, H.; Ogura, K. *Nature* **1994**, *367*, 720.
- ³⁹ Fujita, M.; Ibukuro, F.; Yamaguchi, K.; Ogura, K. *J. Am. Chem. Soc.* **1995**, *117*, 4175.

- ⁴⁰ Fujita, M.; Aoyagi, M.; Ibukuro, F.; Ogura, K.; Yamaguchi, K. *J. Am. Chem. Soc.* **1998**, *120*, 611.
- ⁴¹ Ibukuro, F.; Fujita, M.; Yamaguchi, K.; Sauvage, J.-P. *J. Am. Chem. Soc.* **1999**, *121*, 11014.
- ⁴² Dietrich-Buchecker, C.; Sauvage, J.-P. *Angew. Chem., Int. Ed. Engl.* **1989**, *28*, 189.
- ⁴³ Dietrich-Buchecker, C.; Rapenne, G.; Sauvage, J.-P.; De Cian, A., Fischer, J. *Chem. Eur. J.* **1999**, *5*, 1432.
- ⁴⁴ Rapenne, G.; Dietrich-Buchecker, C.; Sauvage, J.-P. *J. Am. Chem. Soc.* **1999**, *121*, 994.
- ⁴⁵ Rapenne, G.; Dietrich-Buchecker, C.; Sauvage, J.-P. *J. Am. Chem. Soc.* **1998**, *120*, 10932.
- ⁴⁶ Funeriu, D. P.; Lehn, J.-M.; Fromm, K. M.; Fenske, D. *Chem. Eur. J.* **2000**, *6*, 2103.
- ⁴⁷ Hawker, C. J.; Fréchet, J. M. J. *J. Am. Chem. Soc.* **1990**, *112*, 7638.
- ⁴⁸ Other phosphine-functionalized wedges have been reported before: Catalano, V. J.; Parodi, N. *Inorg. Chem.* **1997**, *36*, 537.
- ⁴⁹ Vögtle, F.; Plevoets, M.; Nachtsheim, G.; Wörsdörfer, U. *J. Prakt. Chem.* **1998**, *340*, 112.
- ⁵⁰ Wooley, K. L.; Hawker, C. J.; Fréchet, J. M. J. *J. Chem. Soc., Perkin Trans. 1* **1991**, 1059.
- ⁵¹ Huck, W. T. S.; Prins, L. J.; Fokkens, R. H.; Nibbering, N. M. M.; van Veggel, F. C. J. M.; Reinhoudt, D. N. *J. Am. Chem. Soc.* **1998**, *120*, 6240.
- ⁵² A hydrocarbon dendrimer terminated with carboxylates acts as a unimolecular anionic micelle: Newkome, G. R.; Moorefield, C. N.; Baker, G. R.; Saunders, M. J.; Grossman, S. H. *Angew. Chem. Int. Ed. Engl.* **1991**, *30*, 1178.
- ⁵³ Amphiphilic dendrimers, which assemble in stable monolayers at the air-water interface, have been made by functionalization of hydrophilic poly(propylene imine) dendrimers with hydrophobic palmitoyl chains: Schenning, A. P. H. J.; Elissen-Román, C.; Weener, J.-W.; Baars, M. W. P. L.; van der Gaast, S. J.; Meijer, E. W. *J. Am. Chem. Soc.* **1998**, *120*, 8199.
- ⁵⁴ For examples, see: a) Morikawa, A.; Kakimoto, M.; Imai, Y. *Macromolecules* **1992**, *25*, 3247; b) Xu, Z.; Kahr, M.; Walker, K. L.; Wilkins, C. L.; Moore, J. S. *J. Am. Chem. Soc.* **1994**, *116*, 4537; c) Pollak, K. W.; Leon, J. W.; Fréchet, J. M. J.; Maskus, M.; Abruña, H. D. *Chem. Mater.* **1998**, *10*, 30.
- ⁵⁵ Chazin, W. J.; Colebrook, L. D. *Magn. Reson. Chem.* **1985**, *23*, 597.
- ⁵⁶ Hecht, S.; Fréchet, J. M. J. *J. Am. Chem. Soc.* **1999**, *121*, 4084.
- ⁵⁷ Van der Made, A. W.; Van der Made, R. H. *J. Org. Chem.* **1993**, *58*, 1262.
- ⁵⁸ Huck, W. T. S.; van Veggel, F. C. J. M.; Reinhoudt, D. N. *J. Mater. Chem.* **1997**, *7*, 1213.
- ⁵⁹ In addition to the signal at 29.33 kDa, larger signals are present at m/z 14.61, 10.11, 7.35, and 4.97 kDa, corresponding to various substructures of $^{Br}G_2^{phos}-G_{3,conv}^{Me}$ formed by fragmentation in the mass spectrometer.
- ⁶⁰ Huck, W. T. S.; van Veggel, F. C. J. M.; Reinhoudt, D. N. *Angew. Chem. Int. Ed. Engl.* **1996**, *35*, 1213.
- ⁶¹ Bosman, A. W.; Janssen, H. M.; Meijer, E. W. *Chem. Rev.* **1999**, *99*, 1665.
- ⁶² Karas, M.; Bachmann, D.; Bahr, U.; Hillenkamp, F. *Int. J. Mass Spectrom. Ion Process.* **1987**, *78*, 53.
- ⁶³ Vestal, M. L.; Juhasz, P.; Martin, S. A. *Rapid Commun. Mass Spectrom.* **1995**, *9*, 1044.

Chapter 5

Fluorescent metallodendrimers: Toward switchable single molecules



Schematic picture of a dendrimer containing a fluorescent rhodamine B core.

In this chapter the synthesis and spectroscopic properties of metallodendrimers incorporating a chemically switchable rhodamine B core are described. The acid-induced ring opening of the non-fluorescent spirolactam form to the fluorescent amide form has been investigated by UV-Vis and fluorescence spectroscopy for a series of four rhodamine B derivatives. The rate of ring opening was found to decrease with increasing dendritic generation, with first order rate constants ranging from 10.9×10^{-4} to $1.8 \times 10^{-4} \text{ s}^{-1}$. The base-induced ring closure was much faster for all derivatives. Evaporation of dilute solutions of the dendritic assemblies on a silicon oxide surface resulted in the spatial isolation of single nanosize dendrimers, as shown by tapping mode AFM experiments.

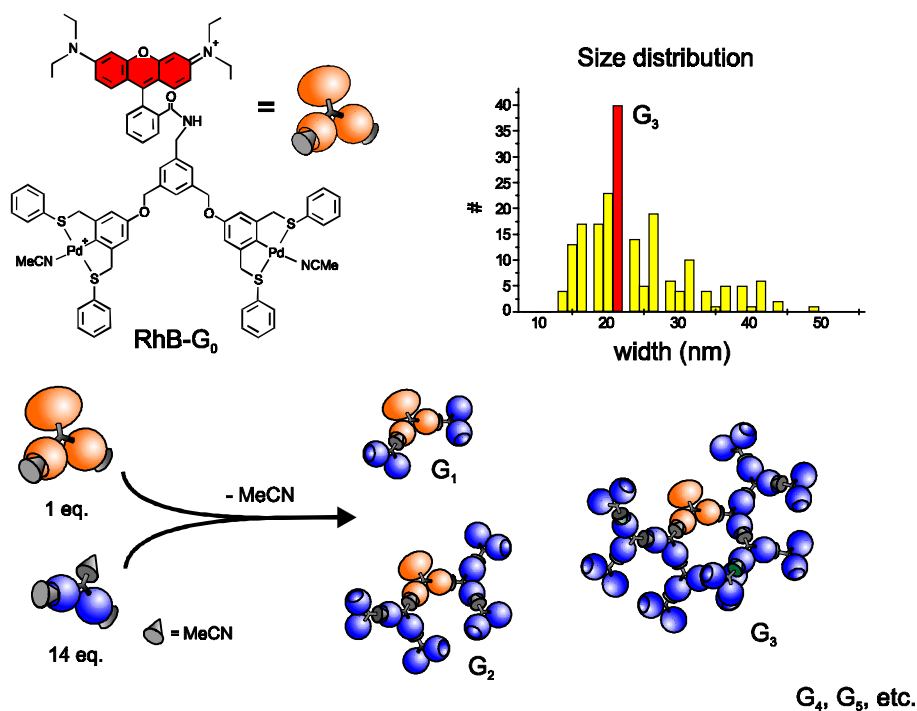
5.1 Introduction

In the previous chapter the non-covalent synthesis of metallodendrimers starting from dendritic phosphine wedges was discussed in detail. The convergent growth strategy, in which building blocks incorporating different ligands for coordination to the SCS Pd^{II} pincer moiety are employed, allows the construction of *functional* metallodendrimers with great tailorability. For example, functional molecules containing Pd^{II} pincers might act as metallodendrimer cores, whereas molecules having suitable ligands (*e.g.* pyridines, phosphines) can serve as functional peripheral groups. An example of the latter case is the incorporation of pyridyl porphyrins as peripheral groups in metallodendrimers (see also chapter 2).¹ This chapter will focus on the use of functional molecules acting as metallodendrimer cores.

The dendritic encapsulation of functional moieties is an expanding topic in dendrimer research, as it has been realized that photo- and/or redoxactive molecules surrounded by dendritic shells may find use as *e.g.* artificial enzymes, (recyclable) catalysts, and light-harvesting systems.² In the first reported example, provided by Fréchet and coworkers,³ *p*-nitroaniline was used as solvatochromic dye to probe the polarity of the local environment near the chromophore core. At high generation a polarity similar to DMF was found for the core environment. Since then, a variety of other functionalities have been employed as dendrimer cores, among them photoactive groups such as porphyrins (groups of Aida,⁴ Diederich,⁵ and Fréchet⁶), perylene,⁷ anthracenes,⁸ and coumarins,⁹ and redoxactive moieties such as transition metal-polypyridine complexes, ferrocenes,¹⁰ fullerenes,¹¹ and iron-sulfur clusters (see also chapter 2).

In contrast to dendrimers containing cores with a specific property, *switching* of a dendritic nucleus by external means (photons, electrons, chemicals) has hardly been investigated. Molecular switches represent important members of the family of molecular machines,¹² since they are molecular analogs of the digital “0” and “1” states. It is even anticipated that, ultimately, molecular computers can be fabricated from them.¹³ In order to generate switchable dendrimers, the incorporation of *azobenzenes* into the dendritic framework has been most popular. The azobenzene *E* to *Z* photoisomerization has been studied intensively, and many photoswitchable devices have been constructed from azobenzene derivatives.¹⁴ Whereas several groups have focussed on dendrimer having peripheral azobenzenes,¹⁵ the switching of azobenzene dendritic cores has been reported by Aida and coworkers,¹⁶ Junge and McGrath,¹⁷ and Ghosh and Banthia.¹⁸

Xanthene dyes occupy a very important position among different dye families because of their widespread use as dyeing agents for paper, leather, woods, food, ink, drugs, cosmetics, etc.¹⁹ They contain the xanthylium **1** or dibenzo- γ -pyran nucleus **2** as the chromophore, with hydroxy or amino groups *meta* to the oxygen as usual auxochromes. The resulting dyes are known as *fluoresceins* and *rhodamines*, respectively.



Scheme 5.2. Mixture of metallodendrimers containing a rhodamine B core.

The fluorescence of individual dendritic molecules was investigated by NSOM. This technique has recently proven to be very useful in the visualization of single molecules.²⁶ Height and optical images of individual metallodendrimer molecules were obtained simultaneously, allowing co-localization of single-molecule fluorescence with dendritic molecules. No differences were found in the height distribution of the dendrimers obtained with dynamic mode AFM and shear-force NSOM, emphasizing the non-destructiveness of both techniques. Moreover, the three-dimensional orientation of the individual fluorescent cores within the dendritic matrix could be determined, and these measurements indicated orientational mobility of the core.

To the best of our knowledge, there has only been one other reported example of a dendrimer encapsulating a rhodamine derivative. Otomo and coworkers used aryl ether Fréchet dendrimers functionalized at the core with a rhodamine B moiety (such as the dendrimer shown in Figure 5.1) in poly(methylmethacrylate) waveguides in order to avoid concentration quenching of the rhodamine group.²⁸ In contrast to amides at the 2'-position of the rhodamine B moiety, esters at this position cannot convert to a closed form. Therefore the dendrimer shown below cannot serve as a chemical switch.

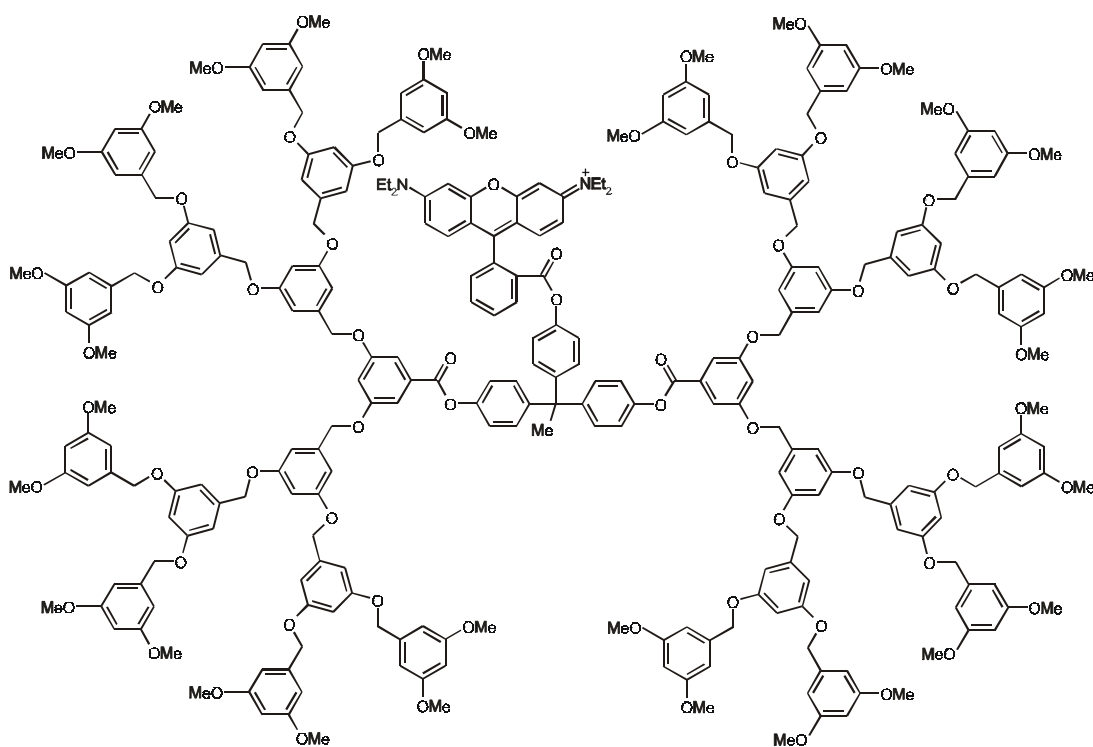


Figure 5.1. Structure of a rhodamine B-cored Fréchet aryl ether dendrimer.

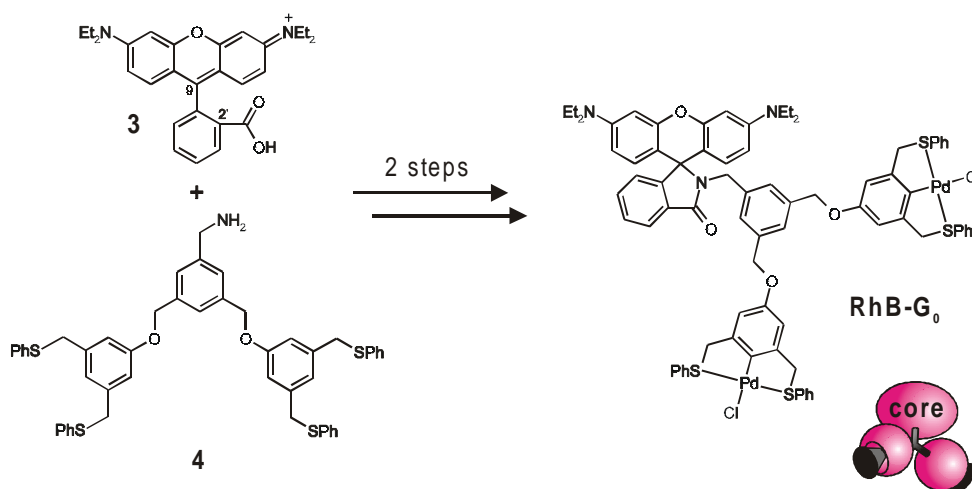
5.2 Aim and scope of this chapter

The *controlled* synthesis of nanosize metallodendrimers having a chemically switchable rhodamine B core is described in this chapter. In solution, the switching of these non-covalent dendritic assemblies has been studied by NMR, UV-Vis and fluorescence spectroscopy, and the results will be described herein. AFM investigations on the metallodendrimers will briefly be summarized.

5.3 Results and discussion

5.3.1 Synthesis of rhodamine B-cored metallodendrimers

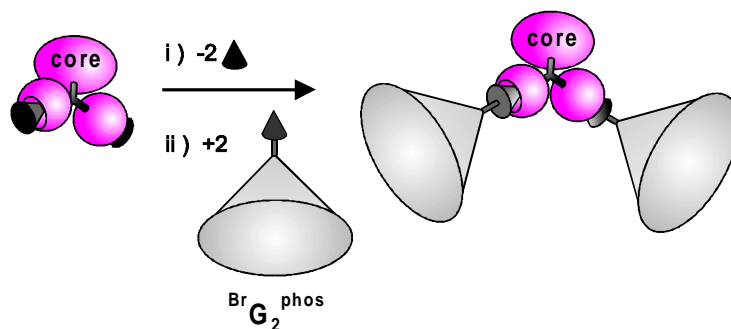
Metallodendritic core **RhB-G₀** containing two SCS Pd^{II} pincer moieties was prepared in 2 steps as shown in Scheme 5.3.²⁹ First, the 2'-carboxylic acid of rhodamine B (**3**) was amidated with benzylic amine **4**³⁰ functionalized with two pincer ligands (Scheme 5.3). In the literature, amidation at the 2'-position of rhodamine B^{25b,31} is rare compared to esterification at this position³² or esterification/amidation of corresponding rhodamines functionalized at the 4'- or 5'-position with (activated) carboxylic acids.³³



Scheme 5.3. Synthesis of **RhB-G₀** from rhodamine B **3**.

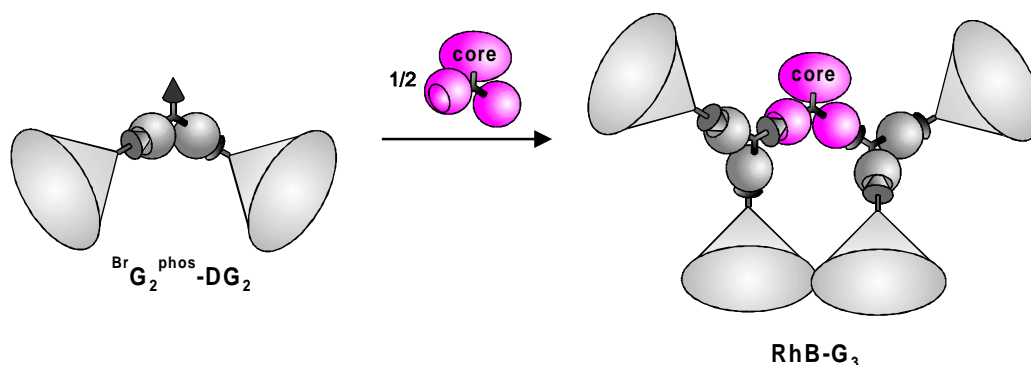
Second, cyclopalladation with $\text{Pd}[\text{MeCN}]_4(\text{BF}_4)_2$, followed by conversion of the intermediate labile bisacetonitrile complex to the inert bischloride complex, gave the neutral **RhB-G₀**. Rhodamine B **3** was also amidated with benzylamine to produce the non-functional rhodamine B *N*-benzyl lactam, which serves as a model system in spectroscopic studies (*vide infra*).

Starting from **RhB-G₀**, divergent dendritic growth was achieved employing the second generation phosphine-functionalized Fréchet wedge $\text{BrG}_2^{\text{phos}}$ reported in chapter 4 (see Scheme 4.5 for its structure). After removal of the two chloride ligands in **RhB-G₀** with 2 equiv of AgBF_4 , addition of 2 equiv of $\text{BrG}_2^{\text{phos}}$ gave second generation rhodamine B dendrimer **RhB-G₂** in 89% yield (Scheme 5.4).



Scheme 5.4. Schematic representation of the synthesis of **RhB-G₂**.

The largest rhodamine B cored metallodendrimer was synthesized in a convergent manner starting from $\text{BrG}_2^{\text{phos}}$. As already discussed in chapter 4, coordination of 2 equiv of $\text{BrG}_2^{\text{phos}}$ to the Pd^{II} pincers of pyridine-functionalized building block $\text{BB}_{\text{pyr}}\text{-Cl}$ furnishes a third generation metallodendritic wedge containing a focal pyridine moiety suitable for further growth *via* coordination ($\text{BrG}_2^{\text{phos}}\text{-DG}_2$, see section 4.4.4). Two of these wedges were added to freshly deprotected **RhB-G₀** to give third generation rhodamine B metallodendrimer **RhB-G₃** in 79% yield (Scheme 5.5).



Scheme 5.5. Schematic representation of the synthesis of **RhB-G₃** by coupling of **BrG₂^{phos}-DG₂** to deprotected **RhB-G₀**.

5.3.2 Characterization by NMR spectroscopy and mass spectrometry

Evidence for the formation of the dendritic structures discussed in the previous section was obtained from a combination of ¹H and ³¹P NMR spectroscopy and MALDI-TOF mass spectrometry.

Protons from the rhodamine B system display diagnostic resonances in ¹H NMR spectra, as exemplified by the model compound rhodamine B *N*-benzyl lactam, the ¹H NMR spectrum of which is displayed in Figure 5.2, along with the assignment of all rhodamine B protons (based on integral ratios and ¹H-¹H COSY NMR experiments).³⁴

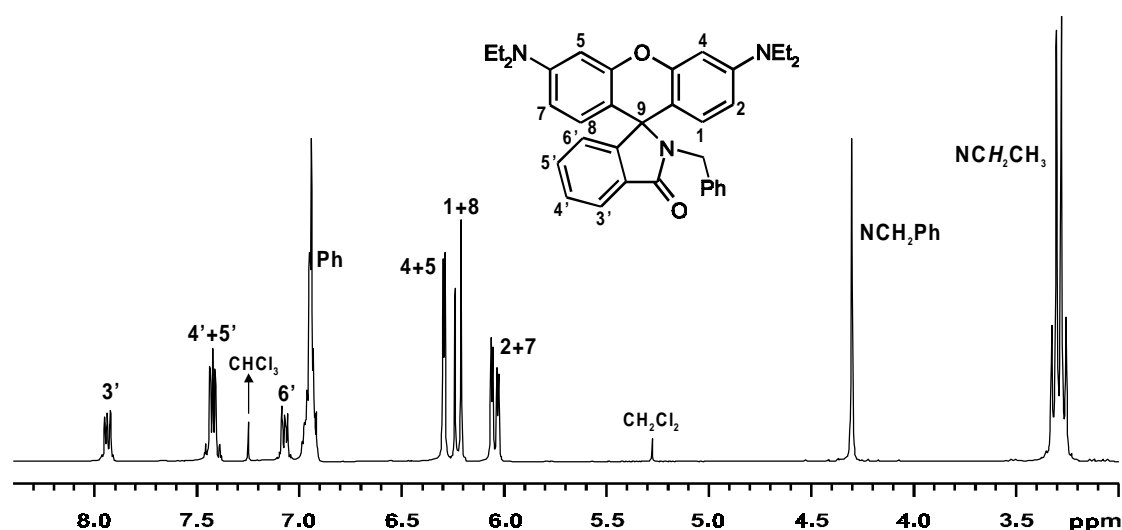


Figure 5.2. ¹H NMR spectrum and signal assignment of rhodamine B *N*-benzyl lactam (CDCl₃, 298 K).

The symmetric nature of the xantheno ring is expressed by the fact that protons H1 and H8 (d, $\delta = 6.23$), H2 and H7 (dd, $\delta = 6.05$), and H4 and H5 (d, $\delta = 6.29$) are indistinguishable. Moreover, their chemical shifts (between 6.0 and 6.3 ppm) are characteristic for the non-fluorescent, closed spiro lactam form. The signal at 64.8 ppm in the ¹³C NMR spectrum of rhodamine B *N*-benzyl

lactam is also indicative of the spiro lactam form, since the chemical shift of this signal is consistent with an sp^3 -hybridized 9-carbon bound to a nitrogen atom.^{25b}

The rhodamine B moiety in **RhB-G₀** displays almost identical signals in the ¹H NMR spectrum (CDCl₃) as the above discussed rhodamine B *N*-benzyl lactam, the largest differences being observed for H1 and H8 (d, $\Delta\delta = 0.08$ ppm upfield) and H2 and H7 (dd, $\Delta\delta = 0.14$ ppm upfield), which must be due to the influence (electronically and/or sterically) of the bispincer part on these xanthene protons. Therefore, it can be concluded that this compound is also obtained in the non-fluorescent form after purification.³⁵ Furthermore, the signals at 6.56 (s, Ar_{Pd} H) and 4.49 (br s, CH₂S) ppm are consistent with SCS Pd^{II} pincers having chloride ligands (see also chapter 3).

All signals in the ¹H NMR spectrum of **RhB-G₂** could be assigned unambiguously by considering chemical shifts, integral ratios, and data obtained from ¹H-¹H COSY NMR experiments. The signals at 6.75 (d, $J = 2.1$ Hz, Ar_{Pd} H) and 4.67 (br s, CH₂S) ppm, both significantly shifted downfield compared to the chloride complex, indicate the coordination of the phosphine groups from **BrG₂^{phos}** to the Pd^{II} centers in deprotected **RhB-G₀**. This was corroborated by the signal at 13.6 ppm in the ³¹P NMR spectrum of **RhB-G₂**, which is diagnostic for phosphine coordination to Pd^{II}. The chemical shifts of the proton signals from the rhodamine B core are very similar to those in rhodamine B *N*-benzyl lactam and **RhB-G₀**, demonstrating that **RhB-G₂** has also been obtained in the closed spiro lactam form.

In contrast to the three rhodamine B derivatives discussed above, the signals in the ¹H NMR spectrum of **RhB-G₃** are very broad and therefore difficult to assign. This is due to the increased size of the molecule, causing the dendrimer to tumble slowly on the NMR time scale. Despite this difficulty, the coordination of the pyridine and phosphine groups to Pd^{II} could be proven by ¹H and ³¹P NMR spectroscopy, respectively. The upfield shift (from 8.56 ppm in **BrG₂^{phos}-DG₂** to 8.20 ppm in **RhB-G₃**) and broadening of the α -pyridyl proton signal in the ¹H NMR spectrum is a clear indication of the coordination of the pyridine groups to the Pd^{II} pincers of the rhodamine B core. In the ³¹P NMR spectrum of **RhB-G₃** a signal at 13.7 ppm was observed, indicating phosphine coordination to Pd^{II}.

Whereas both rhodamine B *N*-benzyl lactam and **RhB-G₀** were characterized by FAB mass spectrometry, the less stable nature of the non-covalent metallodendrimers **RhB-G₂** and **RhB-G₃** necessitated their characterization by MALDI-TOF mass spectrometry. The most intense signal (at m/z 4262.2) in the MALDI-TOF mass spectrum of **RhB-G₂** could be assigned to $[M - BF_4]^+$. The loss of one BF₄ anion in MALDI-TOF mass spectra of metallodendrimers from our group is commonly observed (see also chapters 4 and 6). Furthermore, in the MALDI-TOF mass spectrum of **RhB-G₃** only one signal (at m/z 9555, corresponding to $[M - BF_4]^+$) is observed between 5 and 20 kDa, indicating the monodispersity of the metallodendrimer.

5.3.3 Switching of rhodamine B-cored metallodendrimers

The switching behavior of all four rhodamine derivatives described in the previous section was investigated by UV-VIS and fluorescence spectroscopy. It was anticipated that the spectroscopic properties of the rhodamine core would be influenced by the size or structure of the dendritic shell around it, similar to previously reported photo- or redoxactive cores encapsulated by dendrimers.²

In their isolated state, all four rhodamine B derivatives hardly display any fluorescence in CH_2Cl_2 solution, confirming that they are present in the non-fluorescent spirolactam form in this solvent (which was also proven by NMR spectroscopy). The ring opening of the lactam by trifluoroacetic acid (TFA) and the subsequent ring closure by triethylamine was investigated for all derivatives.

5.3.3.1 UV-Vis spectroscopic studies

The smallest member, rhodamine B *N*-benzyl lactam, displays almost the same absorption characteristics in CH_2Cl_2 as the known^{25a} rhodamine B *N*-phenyl lactam in CH_3CN .³⁶ After the addition of TFA (300 equiv) to a 4 μM solution in CH_2Cl_2 , the ring opening of the spirolactam was followed in time by UV-Vis spectroscopy. In Figure 5.3 the UV-Vis spectra taken between $t = 0$ (just before addition of TFA) and $t = 1.5$ h are displayed. The rise in the absorption at 558 nm is indicative for the formation of the fluorescent xanthene part of the rhodamine B 2'-amide.

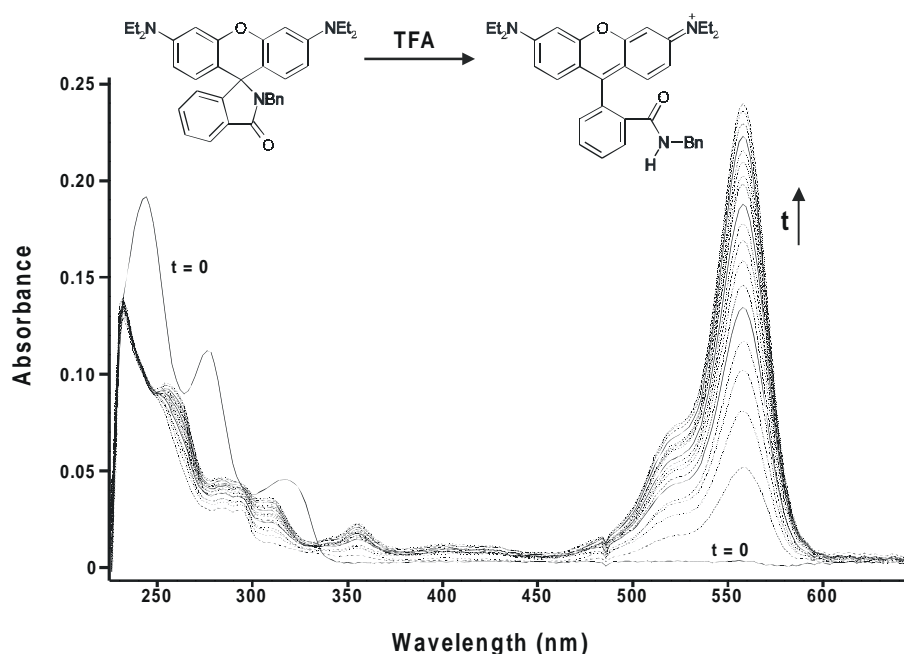


Figure 5.3. UV-Vis spectra of the ring opening of rhodamine B *N*-benzyl lactam by TFA in CH_2Cl_2 . Intervals between spectra: 5 min; $c = 4 \mu\text{M}$, 300 equiv TFA added.

The increase in absorbance at 558 nm (monitored for a period of 10 h) is displayed in Figure 5.4, along with the curve obtained by fitting the data to a first order reaction kinetics model.

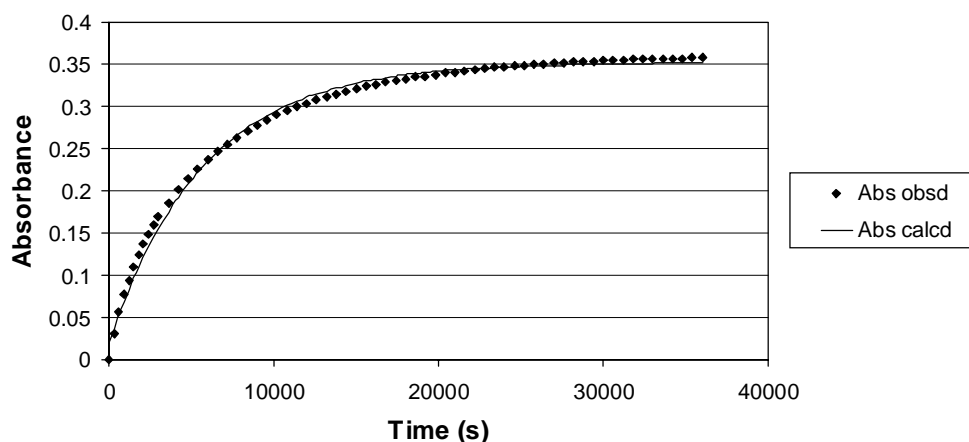


Figure 5.4. UV-Vis absorbance at 558 nm followed in time for rhodamine B N-benzyl lactam ($4 \mu\text{M}$ in CH_2Cl_2) treated with TFA (300 equiv).

The experimental absorbance data (at 558 nm) were fitted using both the first order rate constant k (in s^{-1}) and the molar absorption coefficient ϵ_{fit} (in $\text{L}\cdot\text{mol}^{-1}\cdot\text{cm}^{-1}$) as parameters. The ring opening of the other rhodamine B derivatives was investigated in an identical manner ($4 \mu\text{M}$ in CH_2Cl_2 , 300 equiv TFA added) by UV-Vis spectroscopy. The obtained values for k and $\log \epsilon_{\text{fit}}$ are displayed in Table 5.1, along with values for $\log \epsilon_{\text{obsd}}$ and $t_{1/2}$. Values for ϵ_{obsd} were calculated from the absorbance at full ring opening (at 558 nm) and the concentration by applying the law of Lambert-Beer. From Table 5.1 it can be seen that the values of $\log \epsilon_{\text{fit}}$ and $\log \epsilon_{\text{obsd}}$ correspond very well.

Table 5.1. Absorption characteristics (at 558 nm), first order rate constants, and $t_{1/2}$ values for the TFA-induced ring opening (in CH_2Cl_2) of metallodendrimers containing a rhodamine B core.

Compound	$\log \epsilon_{\text{fit}}$	$\log \epsilon_{\text{obsd}}$	k (10^{-5} s^{-1})	$t_{1/2}$ (h) ^a
RhB N-benzyl lactam ^b	4.77 ± 0.03	4.86 ± 0.02	10.9 ± 0.1	1.8 ± 0.1
RhB-G₀	4.66	4.68	6.7	2.9
RhB-G₂	4.64	4.58	2.6	7.3
RhB-G₃	4.76	4.75	1.8	10.9

^a $t_{1/2} = \ln 2 / k$ for first order reactions.

^bError margins were estimated for RhB N-benzyl lactam from 3 independent measurements. Margins for other rhodamine B derivatives are expected to be similar.

The assumption of first order kinetics for the ring opening was validated by performing the ring opening at different starting concentrations (1-4 μM) of rhodamine B derivative (while maintaining a constant concentration of TFA). For a first order ring opening, this should have no effect on the obtained value for k . By taking three different concentrations of rhodamine B derivative, no change in k within the experimental error was observed.

Remarkably, large differences in rate constants were found for the ring opening of the spirolactam moieties (Table 5.1), the rate decreasing substantially with increasing dendritic size. On one hand, access of TFA to the rhodamine B dendritic core might be impeded by the increasing steric bulk of the dendritic shell, causing the ring opening to slow down with increasing dendrimer generation. Limited access to a dendritic core by external molecules has been shown for a variety of dendritic systems.^{2a} On the other hand, the generation of an open, cationic amide form from the initially neutral spirolactam form might become increasingly unfavorable with increasing size of the hydrophobic dendritic shell. This reasoning was supported by the fact that the ring opening of rhodamine B *N*-benzyl lactam by TFA was found to proceed much faster in MeOH than in CH_2Cl_2 . Polar solvents are better able to stabilize the developing cationic charge on the rhodamine B system than apolar solvents.

After complete ring opening of all four rhodamine B derivatives, excess NEt_3 (600 equiv) was added to the solutions used for the ring opening experiments. In this way, the initial fast TFA neutralization (absorbing 300 equiv of NEt_3) was followed by ring closure of the fluorescent rhodamine B amide form by the remaining NEt_3 . The decrease in absorbance at 558 nm (see Figure 5.5) was again followed by UV-Vis spectroscopy.

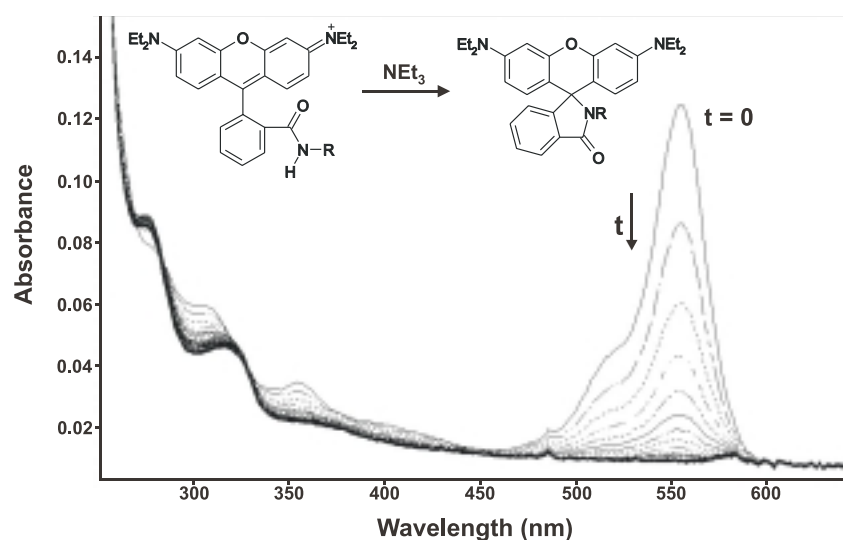


Figure 5.5. UV-Vis spectra of the ring closing of rhodamine B *N*-benzyl amide by NEt_3 in CH_2Cl_2 . Intervals between spectra: 2 min; $c = 4 \mu\text{M}$, 600 equiv NEt_3 added (300 equiv used for TFA neutralization).

The curves obtained in this manner (see Figure 5.6 for **RhB-G₂**) were again fitted to a first order reaction kinetics model, and the results of these studies are compiled in Table 5.2.

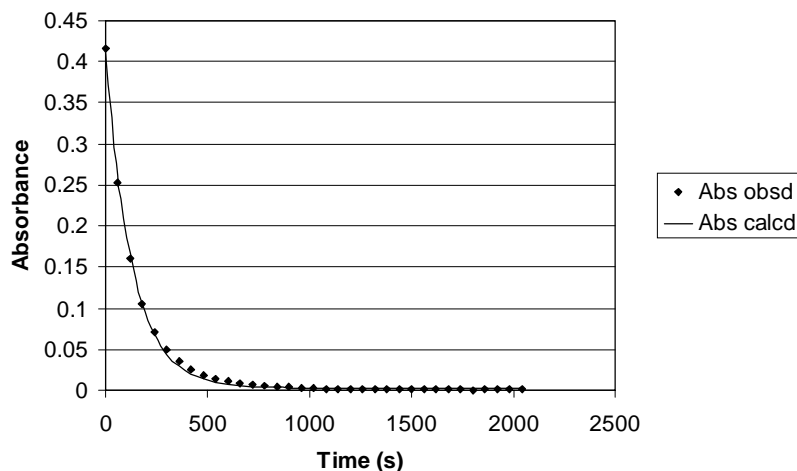


Figure 5.6. UV-Vis absorbance at 558 nm followed in time for ring closure of **RhB-G₂** (4 μM in CH_2Cl_2) by treatment with NEt_3 (600 equiv).

Table 5.2. First order rate constants and $t_{1/2}$ values for the NEt_3 -induced ring closure of metallodendrimers containing a rhodamine B core.

Compound	k (10^{-2} s^{-1})	$t_{1/2}$ (s) ^a
RhB <i>N</i> -benzyl lactam ^b	1.3 ± 0.1	53 ± 5
RhB-G₀	1.2	58
RhB-G₂	0.8	87
RhB-G₃	0.9	77

^a $t_{1/2} = \ln 2 / k$ for first order reactions.

^bError margins were estimated for RhB *N*-benzyl lactam from 3 independent measurements. Margins for other rhodamine B derivatives are expected to be similar.

It is clear from this table that the k values for ring closure are significantly higher (approximately 100-1000 times) for all rhodamine B derivatives than the corresponding ring opening, and that they are similar for all derivatives. This implies that restricted access to the rhodamine B core is probably the wrong explanation for the experimentally observed decrease in TFA-induced ring opening with increasing dendritic size. The hypothesis that the generation of cationic charge is unfavorable with increasing size of the hydrophobic shell is more plausible.

5.3.3.2 Fluorescence spectroscopic studies

Ring opening of the rhodamine B spirolactam derivatives by TFA causes them to become highly fluorescent. Upon excitation at 558 nm, all four rhodamine derivatives were found to

fluoresce with an emission maximum at 575 nm. The dendritic shell around the rhodamine B core has no influence on the Stokes shift. Figure 5.6 shows the excitation and emission spectra of **RhB-G₂** after 0, 3.5, and 62 h following addition of 1000 equiv of TFA. In order to avoid concentration quenching, fluorescence spectroscopy experiments were performed at 1 μM in CH_2Cl_2 . It is clear from Figure 5.6 that the fluorescence at $t = 0$ h is negligible, again demonstrating that the isolated form of **RhB-G₂** is the closed spirolactam form.

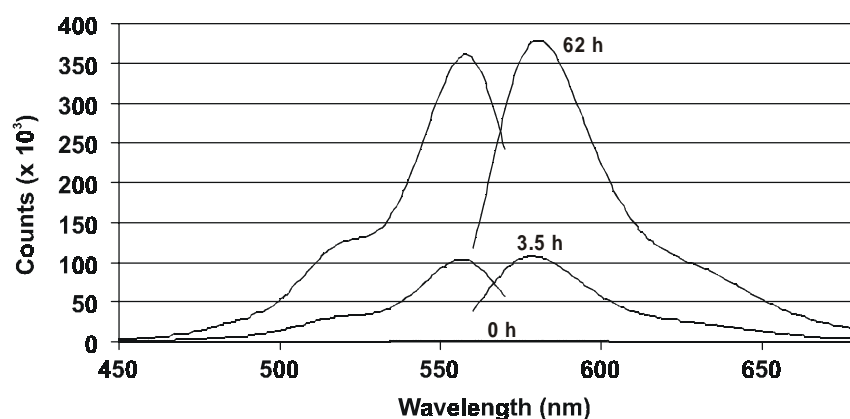


Figure 5.6. Excitation (emission at 575 nm) and emission (excitation at 558 nm) spectra of **RhB-G₂** after 0, 3.5, and 62 h following TFA addition; $c = 1 \mu\text{M}$, 1000 equiv TFA added.

After the addition of excess TFA, the increase in fluorescence at 575 nm was monitored in time for all derivatives. Qualitatively, the same results were obtained as the UV-Vis experiments, as shown in Figure 5.7.

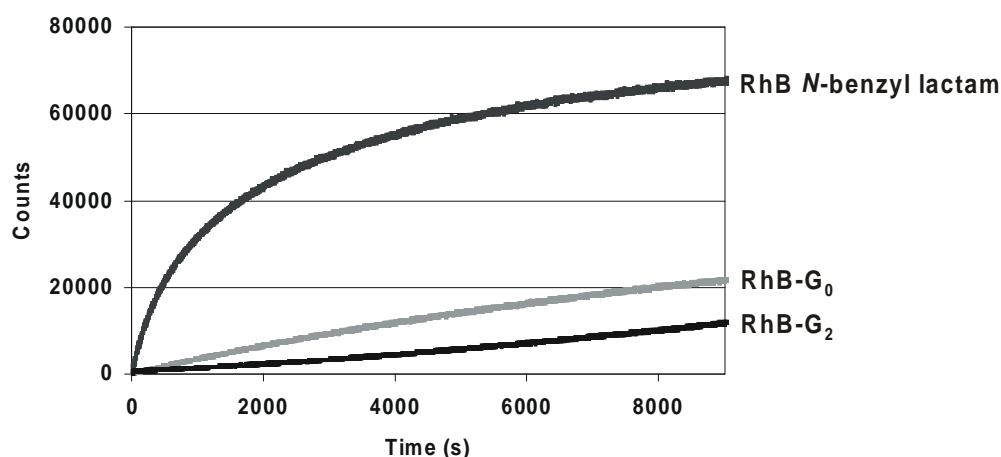


Figure 5.7. Fluorescence increase at 575 nm upon addition of TFA, monitored in time for rhodamine B derivatives. All experiments were performed in CH_2Cl_2 at 1 μM .

For first order reactions, it can be shown that a plot of $-\ln(1-(N/N_{\text{max}}))$ (where N is the number of fluorescence counts at $t = t$ and N_{max} is the maximum number of fluorescence counts) against

time should yield a straight line with slope k . The graph for rhodamine B *N*-benzyl lactam is displayed in Figure 5.8, and a slope of $31.6 \pm 0.4 \times 10^{-5} \text{ s}^{-1}$ was determined.

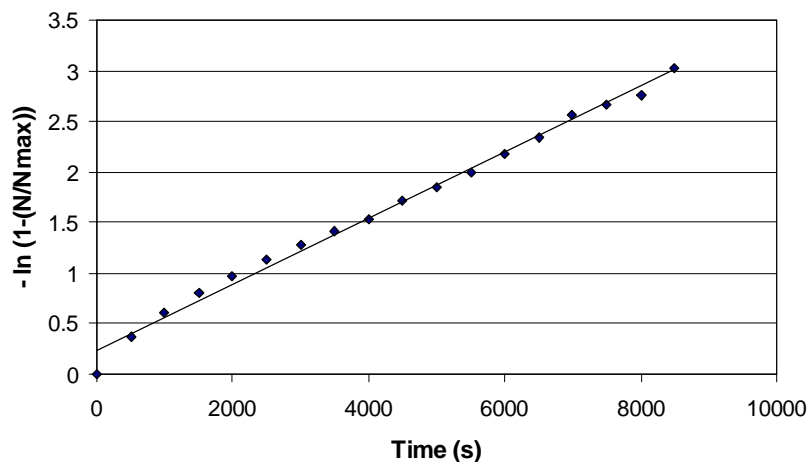


Figure 5.8. Plot of $-\ln(1-(N/N_{\max}))$ against time for the determination of the rate constant of TFA-induced ring opening of rhodamine B *N*-benzyl amine by fluorescence spectroscopy.

The value for the rate constant found by fluorescence spectroscopy is in the same order of magnitude as that determined from UV-Vis spectroscopy for rhodamine B *N*-benzyl lactam ($10.9 \pm 0.1 \times 10^{-5} \text{ s}^{-1}$).

5.3.4 AFM measurements on rhodamine B metallodendrimers

The advent of scanning probe microscopic techniques such as scanning tunneling microscopy (STM) and atomic force microscopy (AFM) has enabled detailed structural investigations of a variety of nanosize dendrimers, as will be discussed more extensively in chapter 7. Fifth generation metallodendrimers based on \mathbf{G}_0 and $\mathbf{BB}_{\text{CN}}\text{-Cl}$ (see section 2.4.5) have previously been characterized in our group by tapping mode (TM) AFM experiments.³⁷ Dilute solutions of \mathbf{G}_5 were found to form monolayers with a granular structure on apolar graphite, the single grains having a diameter of 15-20 nm. In contrast, on hydrophilic mica separate spheres of approximately 15 nm were observed. Closely packed films were not formed on this substrate.

The rhodamine B metallodendrimers described in this chapter were studied by TM-AFM after evaporation of dilute solutions (10^{-6} M in CH_2Cl_2) on a silicon oxide surface. In most cases, spatially isolated features of nanosize dimensions were observed, the feature height increasing in going from $\mathbf{RhB-G}_0$ to $\mathbf{RhB-G}_3$.³⁸ As shown in Figure 5.9, the isolated spheres possess a height of around 8 nm in the case of $\mathbf{RhB-G}_3$. The absolute value of the height depends heavily on the tapping conditions employed, and might therefore deviate from the expected size in solution (the diameter of $\mathbf{RhB-G}_3$ is estimated at 4-5 nm).

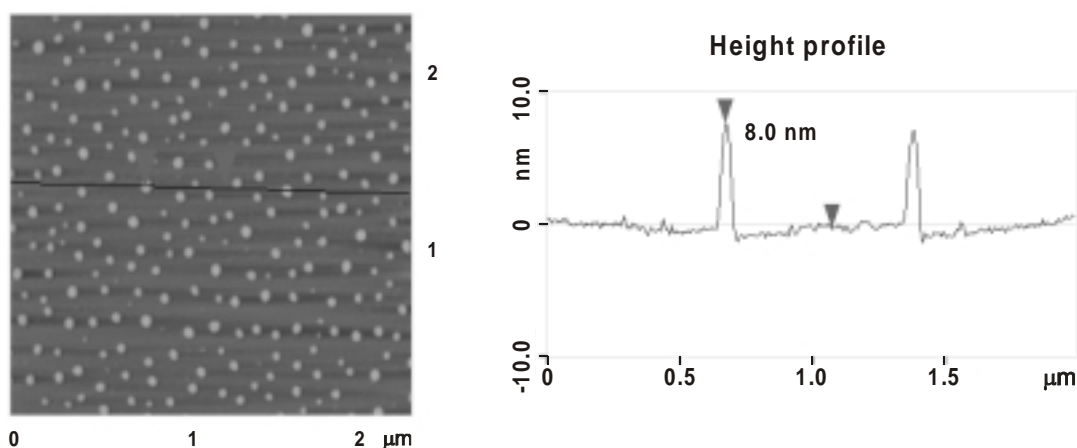


Figure 5.9. TM-AFM image of **RhB-G₃** on a silicon oxide surface. The height profile shown on the right corresponds to the line drawn in the AFM image.

A three-dimensional AFM image of **RhB-G₂** on silicon oxide is shown in Figure 5.10. The height of the pillars in this image is roughly 6 nm. It is very likely that individual pillars correspond to single metallodendrimers.

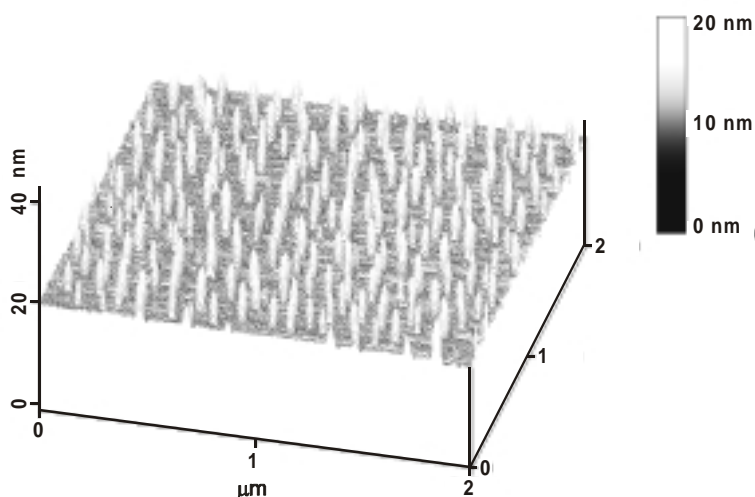


Figure 5.10. Three-dimensional AFM image of **RhB-G₂** on a silicon oxide substrate.

5.4 Conclusions

In this chapter the synthesis and spectroscopic properties of non-covalent metallodendrimers containing fluorescent rhodamine B cores have been discussed. The synthesized rhodamine B derivatives were all isolated in their non-fluorescent, closed spirolactam form. The acid-induced ring opening of the spirolactam form to the fluorescent, cationic amide form has been investigated by UV-Vis and fluorescence spectroscopy in CH₂Cl₂. A decrease in the rate of ring opening with increasing size of the dendritic shell has been observed, and this was rationalized by assuming that generation of the cationic fluorescent form becomes increasingly difficult with increasing size of the hydrophobic dendritic shell. The ring

closure with base was found to be much faster for all rhodamine B derivatives. Finally, spatially isolated metallodendrimers were obtained by evaporation of dilute solutions on a silicon oxide surface. Tapping mode AFM experiments showed individual features with increasing dimensions in going from **RhB-G₀** to **RhB-G₃**.

5.5 Experimental Section

General comments. For general information on instruments, procedures, and chemicals, see chapter 3. For a description of MALDI-TOF experiments, see chapter 4. UV-Vis spectroscopy was performed on a Hewlett Packard 8452A diode array spectrophotometer using quartz sample cells of 10 mm. Fluorescence measurements were performed on an Edinburgh FS900 fluorospectrophotometer. A 450 W xenon arc lamp was used as excitation source. M300 gratings with 1800 l/mm were used on both excitation and emission arms. Signals were detected by a Peltier element cooled, red sensitive, Hamamatsu R928 photomultiplier system. TM-AFM experiments were carried out by S. Levi (University of Twente). Further information regarding the AFM experiments can be found elsewhere.³⁹

Materials. Rhodamine B *N*-benzyl lactam and **RhB-G₀** were synthesized by S. Levi.³⁹ **BB_{pyr}-Cl** was synthesized according to the procedure previously reported.³⁰ The syntheses of **BrG₂^{phos}** and **BrG₂^{phos}-DG₂** were described in chapter 4.

RhB-G₂. To a solution of **RhB-G₀** (5.9 mg, 3.9 μ mol) in degassed CH₂Cl₂ (5 mL) was added 35 μ L of a AgBF₄ solution (0.2255 M in H₂O), and the mixture was stirred vigorously for 5 min, after which **BrG₂^{phos}** (10.5 mg, 7.8 μ mol) was added. After stirring for 15 min at r.t., the mixture was filtered over Hyflo and subsequently evaporated to dryness. The product was obtained as a yellow film. Yield 15 mg (89%). ¹H NMR: δ (ppm) 7.90-7.85 (m, 3 H, H3'+NH), 7.72 (d, J = 8.0 Hz, 4 H, Ar H), 7.47-7.10 (m, 74 H, H4'+H5', Ar H) 7.07 (s, 1 H, Ar H), 7.04-7.01 (m, 1 H, H6'), 6.91 (t, J = 9.6 Hz, 4 H, Ar H), 6.89 (s, 2 H, Ar H), 6.75 (d, J = 2.1 Hz, 4 H, Ar H), 6.66-6.64 (m, 12 H, Ar H+Ar_{Pd} H), 6.46-6.43 (2 t, J = 2.1 Hz, 6 H, Ar H), 6.27 (d, J = 2.4 Hz, 2 H, H4+H5), 6.16 (d, J = 8.7 Hz, H1+H8), 5.96 (dd, J = 2.4 Hz, 8.7 Hz, 2 H, H2+H7), 4.97 (s, 8 H, CH₂O), 4.93 (s, 16 H, CH₂O), 4.76 (s, 4 H, CH₂O), 4.67 (br s, 8 H, CH₂S), 4.56 (d, J = 5.7 Hz, 4 H, CH₂N), 4.28 (s, 2 H, CH₂N), 3.22 (q, J = 6.9 Hz, 8 H, NCH₂CH₃), 1.07 (t, J = 6.9 Hz, 12 H, NCH₂CH₃). ³¹P NMR: δ (ppm) 13.6. MALDI-TOF MS m/z 4262.2 ([M - BF₄]⁺, calcd for C₂₁₃H₁₈₀BClBr₈F₄N₅O₁₈P₂Pd₂S₄: 4262.4)

RhB-G₃. To a solution of **BB_{pyr}-Cl** (5.4 mg, 4.5 μ mol) in degassed CH₂Cl₂ (3 mL) was added 29 μ L of a AgBF₄ solution (0.1576 M in H₂O), and the mixture was stirred vigorously for 5 min, after which **BrG₂^{phos}** (12.2 mg, 9.0 μ mol) was added. After stirring for 15 min at r.t., the mixture was filtered over Hyflo and subsequently evaporated to dryness. The yellow product obtained in this manner was added to a solution of **RhB-G₀** (3.5 mg, 2.3 μ mol) in CH₂Cl₂ (3 mL), previously deprotected with 14 μ L of a AgBF₄ solution (0.1576 M in H₂O). After stirring for 15 min at r.t., the mixture was filtered over Hyflo and subsequently evaporated to dryness. Yield 17 mg (79%). ¹H NMR: δ (ppm) 8.20 (br s, 4 H, pyr α H), 7.88-7.84 (m, 5 H, H3'+NH), 7.74-7.65 (m, 12 H, pyr β H+Ar H), 7.47-7.02 (m, 176, Ar H), 6.97-6.85 (m, 10 H, Ar H),

6.76-6.58 (m, 36 H, Ar H), 6.45-6.39 (m, 12 H, Ar H), 6.32-6.26 (br s, 2 H, H4+H5), 6.22-6.14 (br m, 2 H, H1+H8), 6.04-5.96 (br s, 2 H, H2+H7), 4.94-4.90 (3 s, 56 H, CH₂O), 4.76 (s, 4 H, CH₂O), 4.66 (br s, 24 H, CH₂S), 4.58-4.53 (m, 12 H, CH₂N), 4.30 (br s, 2 H, CH₂N), 3.24 (br s, 8 H, NCH₂CH₃), 1.07 (t, $J = 6.6$ Hz, 12 H, NCH₂CH₃). ³¹P NMR: δ (ppm) 13.6. MALDI-TOF MS m/z 9555 ([M - BF₄]⁺, calcd for C₄₅₉H₃₈₀B₅ClBr₁₆F₂₀N₁₁O₃₈P₄Pd₆S₁₂: 9553.2).

Determination of reaction rate constants by UV-Vis spectroscopy.

Ring opening: For all rhodamine B derivatives, stock solutions of 4 μ M in CH₂Cl₂ (p.a. grade) were prepared. To 2.3 ml of these solutions in a quartz cuvette was added 40 μ L of a TFA solution (75 mM) in CH₂Cl₂. The absorbance at 558 nm was monitored (by the UV-Vis software program) for a certain period of time. First order reaction rate constants were estimated by non-linear least squares fitting of the absorbance data points to Eq. 5.1, using k and ϵ_{fit} as parameters.

$$[\text{Amide}]_t = [\text{Lactam}]_0 \cdot (1 - e^{-k \cdot t}) \quad (\text{Eq. 5.1})$$

[Amide]_t = concentration of the open form at $t = t$;

[Lactam]₀ = concentration of the closed form at $t = 0$ (= 4 μ M);

k = first order rate constant (in s⁻¹).

At low absorbances the law of Lambert-Beer applies, stating that [Amide]_t = A_{amide,t} / ($\epsilon_{\text{fit}} \cdot d$), where A_{amide,t} is the absorbance of the amide at $t = t$, ϵ_{fit} is the molar absorption coefficient (in L·mol⁻¹·cm⁻¹), and d is the solution path length (in cm).

Ring closing: After complete ring opening of the rhodamine B derivatives, 80 μ L of a NEt₃ solution (75 mM) in CH₂Cl₂ was added to the same cuvettes used for the ring opening experiments. The decrease in absorbance at 558 nm was monitored for 2 h, after which all derivatives had returned to their non-fluorescent, closed form. First order reaction rate constants were estimated by non-linear least squares fitting of the absorbance data points to the Eq. 5.2:

$$[\text{Amide}]_t = [\text{Amide}]_0 \cdot e^{-k \cdot t} \quad (\text{Eq. 5.2})$$

[Amide]_t = concentration of the open form at $t = t$;

[Amide]₀ = concentration of the open form at $t = 0$ (= 4 μ M);

k = first order rate constant (in s⁻¹).

5.6 References and notes

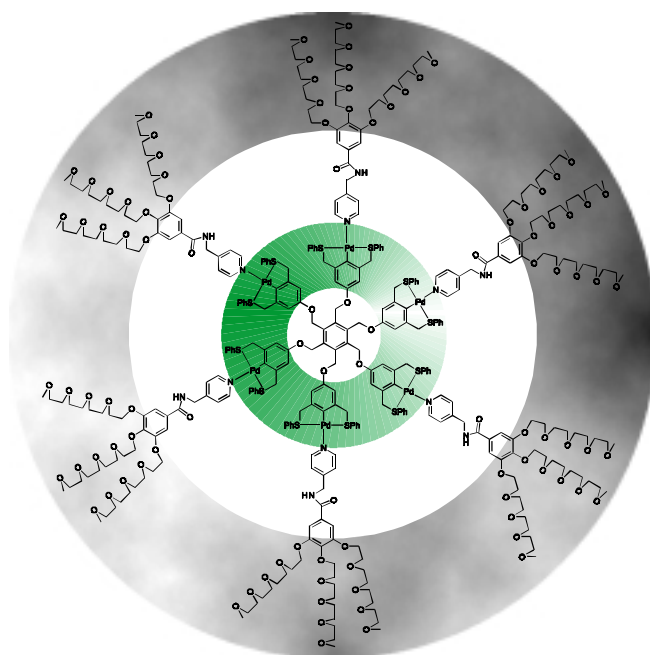
- ¹ Huck, W. T. S.; Rohrer, A.; Anilkumar, A. T.; Fokkens, R. H.; Nibbering, N. M. M.; van Veggel, F. C. J. M.; Reinhoudt, D. N. *New J. Chem.* **1998**, *22*, 165.
- ² For recent reviews, see: a) Hecht, S.; Fréchet, J. M. J. *Angew. Chem. Int. Ed.* **2001**, *40*, 74; b) Cardona, C. M.; Mendoza, S.; Kaifer, A. E. *Chem. Soc. Rev.* **2000**, *29*, 37.
- ³ Hawker, C. J.; Wooley, K. L.; Fréchet, J. M. J. *J. Am. Chem. Soc.* **1993**, *115*, 4375.

- ⁴ a) Tomoyoso, Y.; Jiang, D.-L.; Jin, R.-H.; Aida, T.; Yamashita, T.; Horie, K.; Yashima, E.; Okamoto, Y. *Macromolecules* **1996**, *29*, 5236; b) Sadamoto, R.; Tomioka, N.; Aida, T. *J. Am. Chem. Soc.* **1996**, *118*, 3978; c) Jiang, D.-L.; Aida, T. *J. Am. Chem. Soc.* **1998**, *120*, 10895; d) Tomioka, N.; Takasu, D.; Takahashi, T.; Aida, T. *Angew. Chem. Int. Ed.* **1998**, *37*, 1531.
- ⁵ a) Dandliker, P. J.; Diederich, F.; Gross, M.; Knobler, C. B.; Louati, A.; Sanford, E. M. *Angew. Chem. Int. Ed. Engl.* **1994**, *33*, 1739; b) Dandliker, P. J.; Diederich, F.; Gisselbrecht, J.-P.; Louati, A.; Gross, M. *Angew. Chem. Int. Ed. Engl.* **1995**, *34*, 2725; c) Weyermann, P.; Gisselbrecht, J.-P.; Boudon, C.; Diederich, F.; Gross, M. *Angew. Chem. Int. Ed.* **1999**, *38*, 3215.
- ⁶ Pollak, K. W.; Leon, J. W.; Fréchet, J. M. J.; Maskus, M.; Abruña, H. D. *Chem. Mater.* **1998**, *10*, 30.
- ⁷ Devadoss, C.; Bharathi, P.; Moore, J. S. *J. Am. Chem. Soc.* **1996**, *118*, 9635.
- ⁸ a) Wang, P.-W.; Liu, Y.-J.; Devadoss, C.; Bharathi, P.; Moore, J. S. *Adv. Mater.* **1996**, *8*, 237; b) Cao, D.; Meier, H. *Angew. Chem. Int. Ed.* **2001**, *40*, 186.
- ⁹ a) Gilat, S. L.; Adronov, A.; Fréchet, J. M. J. *Angew. Chem. Int. Ed.* **1999**, *38*, 1422; b) Adronov, A.; Gilat, S. L.; Fréchet, J. M. J.; Ohta, K.; Neuwahl, F. V. R.; Fleming, G. R. *J. Am. Chem. Soc.* **2000**, *122*, 1175.
- ¹⁰ Cardona, C. M.; Kaifer, A. E. *J. Am. Chem. Soc.* **1998**, *120*, 4023; b) Wang, Y.; Cardona, C. M.; Kaifer, A. E. *J. Am. Chem. Soc.* **1999**, *121*, 9756; c) Cardona, C. M.; McCarley, T. D.; Kaifer, A. E. *J. Org. Chem.* **2000**, *65*, 1857; d) Smith, D. K. *J. Chem. Soc., Perkin Trans. 2* **1999**, 1563.
- ¹¹ a) Wooley, K. L.; Hawker, C. J.; Fréchet, J. M. J.; Wudl, F.; Srdanov, G.; Shi, S.; Li, C.; Kao, M. *J. Am. Chem. Soc.* **1993**, *115*, 9836; b) Hawker, C. J.; Wooley, K. L.; Fréchet, J. M. J. *J. Chem. Soc., Chem. Commun.* **1994**, 925; c) Camps, X.; Schönberger, H.; Hirsch, A. *Chem. Eur. J.* **1997**, *3*, 561.
- ¹² For a recent review, see: Balzani, V.; Credi, A.; Raymo, F. M.; Stoddart, J. F. *Angew. Chem. Int. Ed.* **2000**, *39*, 3348.
- ¹³ For a bottom-up approach to molecular computers, see: Dagani, R. *Chem. & Eng. News* **2000**, *78* (42), 27.
- ¹⁴ a) Shinkai, S.; Manabe, O. *Top. Curr. Chem.* **1984**, *121*, 67; b) Kumar, G. S.; Neckers, D. C. *Chem. Rev.* **1989**, *89*, 1915.
- ¹⁵ a) Schenning, A. P. H. J.; Elissen-Román, C.; Weener, J.-W.; Baars, M. W. P. L.; van der Gaast, S. J.; Meijer, E. W. *J. Am. Chem. Soc.* **1998**, *120*, 8199; b) Weener, J.-W.; Meijer, E. W. *Adv. Mater.* **2000**, *12*, 741; c) Tsuda, K.; Dol, G. C.; Gensch, T.; Hofkens, J.; Latterini, L.; Weener, J.-W.; Meijer, E. W.; De Schryver, F. C. *J. Am. Chem. Soc.* **2000**, *122*, 3445; d) Archut, A.; Vögtle, F.; De Cola, L.; Azzellini, G. C.; Balzani, V.; Ramanujam, P. S.; Berg, R. H. *Chem. Eur. J.* **1998**, *4*, 699.
- ¹⁶ Jiang, D.-L.; Aida, T. *Nature* **1997**, *388*, 454.
- ¹⁷ Junge, D. M.; McGrath, D. V. *Chem. Commun.* **1997**, 857.
- ¹⁸ Ghosh, S.; Banthia, A. K. *Tetrahedron Lett.* **2001**, *42*, 501.
- ¹⁹ *Xanthene Dyes*. Kirk-Othmer Encyclopedia of Chemical Technology, 4th ed, Supplement; John Wiley & Sons: New York, 1996.
- ²⁰ *Handbook of Fluorescent Probes and Research Chemicals*; 6th Ed.; Haugland, R. P., Ed.; Molecular Probes: Eugene, 1996.
- ²¹ *Dye Laser Principles*. Duarte, F. J.; Hillmann, L. W. (Eds.); Academic Press: New York, 1990.
- ²² a) Morlière, P.; Santus, R.; Bazin, M.; Kohen, E.; Carillet, V.; Bon, F.; Rainasse, J.; Dubertret, L. *Photochem. Photobiol.* **1990**, *52*, 703; b)

- ²³ Archer, M. D.; Ferreira, M. I. C. *Photochemical Conversion and Storage of Solar Energy*, Connolly, J. S. (Ed.); Academic Press: New York, 1982.
- ²⁴ a) Rigler, R.; Widengren, J.; Mets, Ü. *Fluorescence Spectroscopy*, Wolfbeis (Ed.); Springer: Berlin-Heidelberg, 1992; b) Keller, R. A.; Ambrose, W. P.; Goodwin, P. M.; Jett, J. H.; Martin, J. C.; Wu, M. *Appl. Spectroscopy* **1996**, *50*(7), 12A;
- ²⁵ a) Knauer, K.-H.; Gleiter, R. *Angew. Chem.* **1977**, *89*, 116; b) Adamczyk, M.; Grote, J. *Bioorg. Med. Chem. Lett.* **2000**, *10*, 1539.
- ²⁶ For recent reviews on NSOM, see: a) De Feyter, S.; Hofkens, J.; van der Auweraer, M.; Nolte, R. J. M.; Müllen, K.; De Schryver, F. C. *Chem. Commun.* **2001**, 585; b) Dunn, R. C. *Chem. Rev.* **1999**, *99*, 2891; c) Paesler, M. A.; Moyer, P. J. *Near-Field Optics: Theory, Instrumentation, and Applications*; John Wiley & Sons: New York, 1996.
- ²⁷ Veerman, J. A., Levi, S. A.; van Veggel, F. C. J. M.; Reinhoudt, D. N.; van Hulst, N. F. *J. Phys. Chem. A* **1999**, *103*, 11264.
- ²⁸ Otomo, A.; Yokoyama, S.; Nakahama, T.; Mashiko, S. *Appl. Phys. Lett.* **2000**, *77*, 3881.
- ²⁹ The syntheses of **RhB-G₀** and rhodamine B *N*-benzyl lactam were performed in our group. Levi, S. L., *Ph.D. Thesis*, University of Twente, in progress.
- ³⁰ Huck, W. T. S.; Prins, L. J.; Fokkens, R. H.; Nibbering, N. M. M.; van Veggel, F. C. J. M.; Reinhoudt, D. N. *J. Am. Chem. Soc.* **1998**, *120*, 6240.
- ³¹ Roy, B. C.; Peterson, R.; Mallik, S.; Campiglia, A. D. *J. Org. Chem.* **2000**, *65*, 3644.
- ³² Various rhodamine derivatives esterified at the 2'-carboxylic position are commercially available, see: www.molecularprobes.com.
- ³³ Esterification/amidation at the 4'- or 5'-carboxylic acids of rhodamine B: a) Ramzaeva, N.; Rosemeyer, H.; Leonard, P.; Mühlegger, K.; Bergmann, F.; von der Eitz, H.; Seela, F. *Helv. Chim. Acta* **2000**, *83*, 1108; b) Durroux, T.; Peter, M.; Turcatti, G.; Chollet, A.; Balestre, M.-N.; Barberis, C.; Seyer, R. *J. Med. Chem.* **1999**, *42*, 1312.
- ³⁴ See also: Ilich, P.; Mishra, P. K.; Macura, S.; Burghardt, T. P. *Spectrochim. Acta Part A* **1996**, *52*, 1323.
- ³⁵ Although rhodamine B *N*-benzyl lactam and **RhB-G₀** are purple colored on the acidic silica gel column used for their purification, they lose their color once eluted from the column, indicating the conversion of the fluorescent to the non-fluorescent form.
- ³⁶ For rhodamine *N*-benzyl lactam (CH₂Cl₂): λ_{\max} at 244 (log ϵ = 4.68), 276 (4.44), and 316 (4.03) nm. For rhodamine *N*-phenyl lactam (CH₃CN): λ_{\max} at 239 (4.74), 474 (4.52), and 314 (4.11) nm (Ref.25a).
- ³⁷ Huck, W. T. S.; van Veggel, F. C. J. M.; Sheiko, S. S.; Möller, M.; Reinhoudt, D. N. *J. Phys. Org. Chem.* **1998**, *11*, 540.
- ³⁸ The height of the spheres is a better representation of the feature dimensions than the lateral width due to tip convolution. See also chapter 7.
- ³⁹ Levi, S. L., *Ph.D. Thesis*, University of Twente, in progress.

Chapter 6

Water-soluble, non-covalent Pd^{II} pincer assemblies



Schematic picture of $[\mathbf{H}\cdot\mathbf{5}_6]^{6+}(\text{BF}_4^-)_6$. The inner shell depicts the hexanuclear Pd^{II} pincer core, whereas the outer shell shows the 18 water-solubilizing tetraethyleneglycol chains.

In this chapter the synthesis and characterization of water-soluble, non-covalent coordination assemblies is discussed. Two different water-solubilizing moieties, one based on a linear carbohydrate and the other based on tetraethyleneglycol chains, have been functionalized with pyridine and phosphine ligands. The coordination of the resulting ligands to various SCS Pd(II) pincer systems has been investigated by ¹H and ³¹P NMR spectroscopy, and by MALDI-TOF mass spectrometry, both in water and in organic solvents. It has been found that, in general, the assemblies incorporating tetraethyleneglycol chains display a higher water solubility than the ones containing linear sugar moieties. A hexapincer core decorated with six linear carbohydrates was found to form aqueous gels. Finally, a water-soluble metallodendrimer having 18 peripheral tetraethyleneglycol groups was constructed in a convergent manner.

6.1 Introduction

In the previous chapter the encapsulation of a rhodamine B core by non-covalent metallodendrimers was discussed. It was also pointed out that the convergent growth strategy, in which building blocks incorporating different ligands for coordination to the SCS Pd^{II} pincer moiety are employed, allows the construction of metallodendrimers containing functional *peripheral* groups. For example, the metallodendrimer periphery has been decorated with pyridyl porphyrins by coordination of the pyridyl moieties to SCS Pd^{II} pincers.¹ Core encapsulation and peripheral functionalization are the most popular methods for introducing a particular function in dendrimers. This is a consequence of the fact that two main synthetic strategies are commonly applied in dendrimer preparation, *i.e.* divergent and convergent dendritic growth. With the commercially available, divergently synthesized poly(amidoamine) (PAMAM) and poly(propylene imine) (PPI) dendrimers, functionalization of the peripheral amines has been studied extensively. Amide formation using activated carboxylic acids (*e.g.* acid chlorides, acid anhydrides, pentafluorophenyl esters, *N*-hydroxysuccinimide esters) is most commonly applied. These and other methods have recently been reviewed by Vögtle and coworkers.² On the other hand, dendritic wedges prepared *via* the convergent strategy are well suited for coupling to a functional core in the final step. Dendrons of the Fréchet-type (*i.e.* poly(aryl ether) dendrimers) are usually employed for this purpose.

The introduction of peripheral groups that render dendrimers *water soluble* may prove a prerequisite for a number of (biochemical and pharmaceutical) applications. For example, PAMAM dendrimers and DNA form stable supramolecular complexes at physiological pH (due to charge neutralization between the cationic ammonium groups of the dendrimer and the anionic phosphate groups of DNA).³ Based on this phenomenon, the use of PAMAM dendrimers as efficient gene transfection vectors has been reported.⁴ Short DNA sequences can wrap around dendrimers and allow genetic material to be delivered to mammalian cells. The specific advantage of PAMAM dendrimers is their high solubility in aqueous solution without peripheral modification. A widely used method to confer water solubility on more hydrophobic dendrimers is to introduce multiple carboxylate groups. In pioneering work, Newkome *et al.* demonstrated that hydrocarbon dendrimers having peripheral carboxylates act as unimolecular micelles and can encapsulate hydrophobic guests such as Phenol Blue and naphthalene within their branches.⁵ The convergent synthesis of poly(aryl ether) dendrimers with 32 carboxylate moieties on the periphery was reported by Fréchet and coworkers.⁶ Similar to the work of Newkome *et al.*, the aqueous solubility of polycyclic aromatic compounds such as pyrene and anthracene was found to increase dramatically in the presence of a dendrimer. Diederich and coworkers developed water-soluble dendritic cyclophanes (Figure 6.1) as models for globular proteins.⁷ Water solubility was again obtained by terminating the dendritic poly(ether amide) architecture with carboxylate groups.

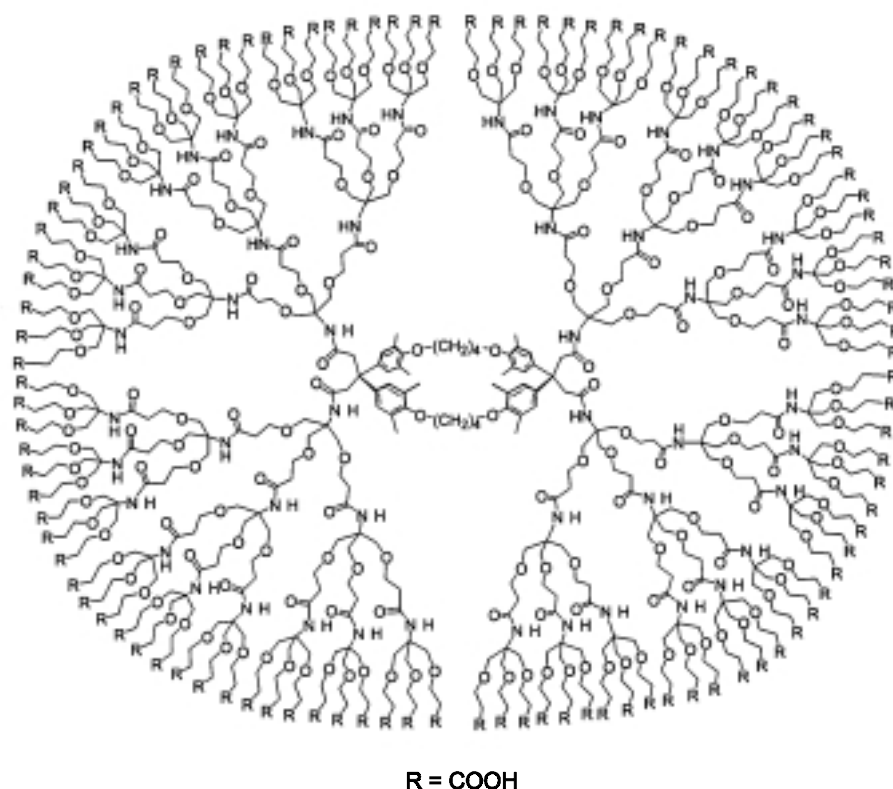


Figure 6.1. Water-soluble dendritic cyclophane as a receptor for hydrophobic guests.

Based on π - π stacking and C-H \cdots π interactions, complexation of aromatic guests such as arenes (by a small cyclophane core) and steroids (by an extended cyclophane core) has been demonstrated, with association constants similar to complexes lacking the dendritic shell. Other examples of water-soluble carboxylate-terminated dendrimers include the poly(phenylenes) reported by Kim and Webster,⁸ and the poly(phenylacetylene) dendrimers synthesized by Moore and Pesak.⁹

Besides anionic carboxylates as water-solubilizing end groups for dendrimers, cationic moieties have also been employed. Krska and Seyferth reported reactions between mercapto-substituted amphiphiles and carbosilane dendrimers bearing peripheral (chloromethyl)silyl groups to produce amphiphilic dendrimers with alcohol, dimethylamino, or sodium sulfonate moieties at the periphery.¹⁰ The anionic sulfonate-terminated dendrimers are soluble in water, as are the cationic poly(ammonium) salts derived from the dimethylamino-terminated derivatives. The well-known phosphorus-containing dendrimers from the group of Majoral were rendered water-soluble by protonation or methylation of the terminal tertiary amines.¹¹ Interestingly, these dendrimers were tested as transfecting agents for the luciferase gene. Both the dendrimer generation and the chemical nature of the end groups were found to influence the efficacy of the transfection.

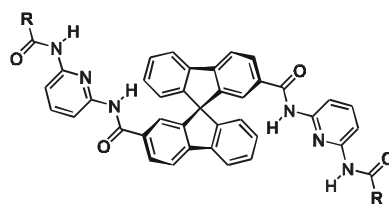
Instead of introducing charged groups, water-soluble dendrimers have also been obtained by functionalization of the periphery with hydrophilic neutral groups. The introduction of peripheral *carbohydrates* has been studied extensively by the groups of Okada, Roy, Lindhorst,

and Stoddart. Multivalent glycoconjugates such as carbohydrate dendrimers (also known as glycodendrimers) can effectively inhibit carbohydrate-protein interactions and are therefore potentially useful therapeutic agents in the prevention of bacterial and viral infections.¹² Among the different strategies for linking carbohydrates to dendritic end groups are the reaction of peripheral amines with sugar lactones,¹³ *N*-carboxyanhydrides,¹⁴ *N*-succinimidyl-activated esters,¹⁵ and isothiocyanates.¹⁶ Glycodendrimers have also been synthesized in a convergent manner starting from glycosyl bromides by glycosylation with amino-protected tris(hydroxymethyl)aminomethane (“tris”).¹⁷

Another method for the preparation of polyhydroxylated dendrimers exploits the transamidation of peripheral methyl ester groups with “tris”. This strategy was already reported in 1985 by Newkome and coworkers,¹⁸ and it has been applied to numerous dendritic systems, including those containing alkyne,¹⁹ tetrathiafulvalene,²⁰ and calix[4]arene²¹ cores. Recently, modification of PAMAM dendrimers with peripheral “tris” groups resulted in highly water-soluble hosts for small acidic hydrophobic molecules such as benzoic acid, salicylic acid, and 2,6-dibromo-4-nitrophenol.²²

Several groups have reported the peripheral functionalization of a variety of dendrimers with oligoethyleneglycol units in order to improve their solubility in polar solvents such as methanol and water, while retaining high solubilities in apolar solvents such as dichloromethane and chloroform. For handling and characterization purposes, a high solubility in both apolar and polar solvents is advantageous. In the first example, reported by Diederich and coworkers,²³ divergent Newkome-type dendrimer construction (see also chapter 2 for this type of dendritic growth) started from a porphyrin core. The final step consisted of esterification of the peripheral carboxylic acids with triethyleneglycol monomethyl ether. When the resulting dendrimer was dissolved in water, the redox potential of the porphyrin metal center was significantly shifted compared to the potential of lower generation iron porphyrins, demonstrating the shielding of the encapsulated redox center by the dendritic architecture. A similar shielding effect is found in natural heme-containing proteins such as cytochrome *c*.²⁴

Other cores encapsulated in a dendritic shell having peripheral oligoethylene glycol chains include the 2,6-di(carboxamido)pyridine-functionalized 9,9'-spirobi[9*H*-fluorene] **1** (used as chiral cleft for the recognition of monosaccharides in CDCl₃, albeit with low association constants),²⁵ and ferrocene.²⁶



Recently, Baars *et al.* reported the modification of poly(propylene imine) dendrimers with 3,4,5-tris(tetraethyleneoxy)benzoyl units.²⁷ The host-guest properties of the resulting dendrimers were studied by UV-Vis spectroscopy in buffered aqueous media using two anionic, water-soluble xanthene dyes. The strong associations found (K_a 's of 3×10^4 and $5 \times 10^5 \text{ M}^{-1}$ for 4,5,6,7-tetrachlorofluorescein and Rose Bengal, respectively) were explained by acid-base interactions between the anionic functionality of the guests and the protonated tertiary amines of the dendritic hosts, which was supported by a strong pH-dependent association behavior. Moreover, small angle X-ray scattering (SAXS) measurements further indicated that the dyes are preferentially located in the core of the dendritic interior.

Whereas the above examples all concern the *covalent* modification of the dendrimer periphery with water-solubilizing groups, a few groups have exploited the *non-covalent* interactions between dendrimer peripheral guests and water-soluble hosts. It is well known that hydrophobic molecules such as arene, ferrocene, and adamantane derivatives form strong complexes in water with *cyclodextrins*,²⁸ cyclic glucose oligomers having a hydrophilic exterior and a hydrophobic interior. Cuadrado, Kaifer and their coworkers prepared dendrimers containing up to 64 peripheral ferrocene²⁹ and 32 cobaltocene³⁰ moieties. These dendrimers (first to fourth generation in case of the ferrocene dendrimers,³¹ and first to third generation in case of the cobaltocene dendrimers³⁰) were solubilized in water upon the addition of β -cyclodextrin, owing to the complexation of the metallocenes in the cyclodextrin cavity. In our group, adamantyl-functionalized poly(propylene imine) dendrimers of generations 1 to 5 were effectively solubilized in water at pH = 2 upon β -cyclodextrin addition.³² At this pH the dendrimers adopt an extended conformation due to protonation of the tertiary amines. For steric reasons the 64 peripheral adamantanes of the fifth generation dendrimer could not all be complexed by cyclodextrins, and this provides the first *supramolecular* example of sterically induced stoichiometry (Figure 6.2).

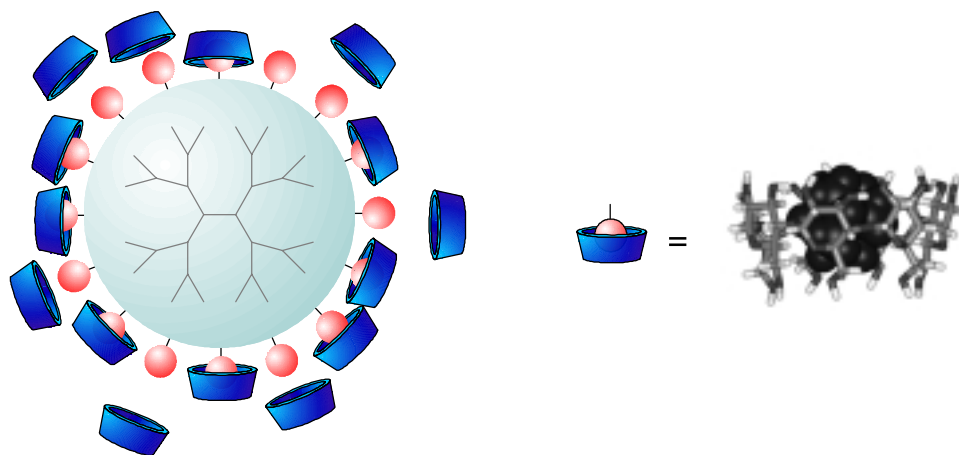


Figure 6.2. Complexation of adamantyl-dendrimers by β -cyclodextrin. Supramolecular sterically induced stoichiometry is schematically shown on the left side (not all adamantanes can be complexed by β -cyclodextrin). The adamantane-cyclodextrin complexation is displayed on the right.

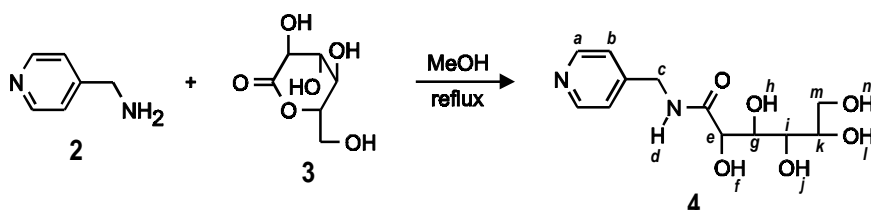
6.2 Aim and scope of this chapter

Conferring water solubility on intrinsically hydrophobic dendrimers is possible using a number of different strategies, as shown in the introduction of this chapter. The non-covalent metallodendrimers reported in this thesis might be rendered water soluble by employing water-solubilizing ligands suitable for coordination to SCS Pd^{II} pincers. A prerequisite for these ligands is that their coordination to Pd^{II} must be stable to aqueous media. In this chapter the synthesis of such ligands is described, and their coordination to a number a different pincer systems will be discussed. Due to their large size, the multinuclear assemblies might be useful as recyclable catalysts for catalytic reactions in water. They should be recoverable from reaction mixtures by nanofiltration methods (see also the work of Van Koten *et al.* discussed in chapter 3).

6.3 Results and discussion

6.3.1 Synthesis of water-solubilizing ligands

From the work of Fujita's group (see chapter 4) it is known that the Pd^{II}–pyridine bond is not hydrolyzed by water. Therefore it was anticipated that water-solubilizing ligands based on pyridines and phosphines would be suitable for preparing water-soluble metallodendrimers. A pyridine having a polyhydroxylated tail (**4**) was synthesized by ring-opening of gluconolactone (**3**) with 4-aminomethylpyridine (**2**) (Scheme 6.1), a reaction based on similar chemistry developed by Aoyama *et al.* for the ring-opening of lactonolactone by a calix[4]resorcinarene octaamine.³³



Scheme 6.1. Ring-opening of gluconolactone by 4-aminomethylpyridine.

Product **4** was found to precipitate from the reaction mixture upon refluxing stoichiometric amounts of **2** and **3** in methanol. It was characterized by ¹H and ¹³C NMR spectroscopy, and FAB mass spectrometry. The CH framework of the linear carbohydrate chain could be assigned with the aid of ¹H-¹H COSY NMR spectroscopy in D₂O, whereas the COSY spectrum of **4** in DMSO-*d*₆ is more complex due to additional couplings with OH protons (Figure 6.3).

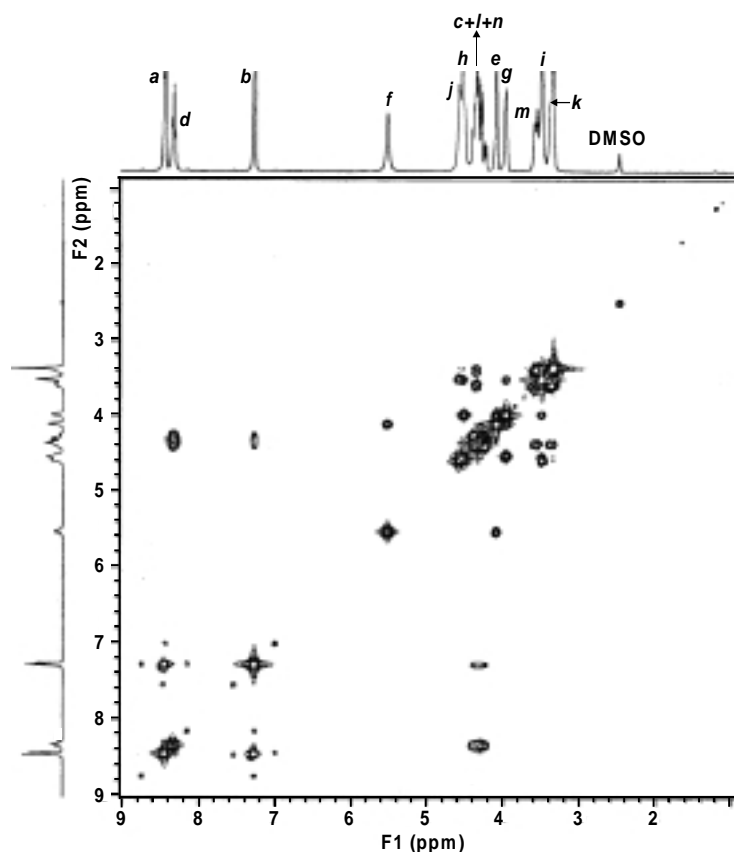
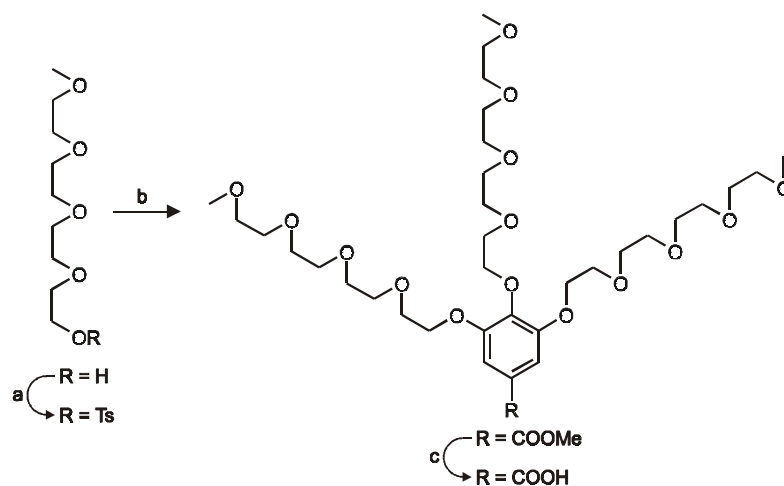


Figure 6.3. ^1H - ^1H COSY NMR spectrum of pyridine ligand **4** in DMSO-d_6 . See Scheme 6.1 for signal assignment.

Furthermore, the four CH carbons of the carbohydrate chain display diagnostic signals between 70 and 66 ppm in the ^{13}C NMR spectrum. The hydroxyl groups of pyridine **4** provide a high solubility in water and DMSO, whereas the solubility in apolar solvents such as chloroform was found to be negligible.

As another type of water-solubilizing ligand, the 3,4,5-tris(tetraethyleneoxy)benzoyl moiety, also used by Baars *et al.*, was chosen.³⁴ Starting from commercially available tetraethyleneglycol monomethyl ether, 3,4,5-tris(tetraethyleneoxy)benzoic acid was synthesized in three steps in 58% overall yield (Scheme 6.2).



Scheme 6.2. Synthesis of 3,4,5- tris(tetraethyleneoxy)benzoic acid: a) TsCl , NaOH , $\text{THF}/\text{H}_2\text{O}$, $0\text{ }^\circ\text{C}$, 2 h, 75%; b) methyl gallate, K_2CO_3 , 18-crown-6, acetone, reflux, 8 h, 82%; c) KOH , MeOH , $60\text{ }^\circ\text{C}$, 8 h, 94%.

Tetraethyleneglycol monomethyl ether was tosylated with tosyl chloride using NaOH in a $\text{THF}/\text{H}_2\text{O}$ mixture,³⁵ and the tosylate was subsequently employed in the threefold alkylation of methyl gallate using standard alkylation conditions (K_2CO_3 and 18-crown-6 in refluxing acetone). Finally, the methyl benzoate was converted to the benzoic acid by saponification with KOH in MeOH . Subsequently, 3,4,5-tris(tetraethyleneoxy)benzoic acid was reacted with 4-aminomethylpyridine or 2-(diphenylphosphino)ethylamine using $\text{EDC}/\text{HOBt}/\text{DIPEA}$ as the coupling reagents to produce the water-solubilizing ligands **5** and **6**, both in 78% yield (Chart 6.1).

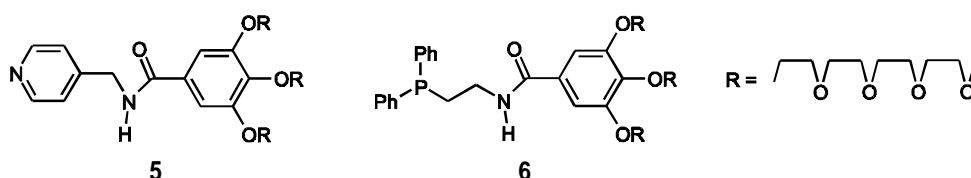


Chart 6.1.

They were obtained as colorless, transparent oils and characterized by ^1H , ^{13}C , and ^{31}P (ligand **6** only) NMR spectroscopy and FAB mass spectrometry. The ^1H NMR spectrum of **5** in CD_3CN is displayed in Figure 6.4 (top). From the region between 3 and 4 ppm it is clear that the tetraethyleneglycol chain attached to the 4-position is different from those attached to the 3- and 5-position, since signals in a 1:2 ratio are observed, e.g. for the methyl protons at 3.3 ppm. Besides the signal at -20.4 ppm in the ^{31}P NMR spectrum of **6** (corresponding to the diphenylethylphosphino moiety), a small signal at 31.8 ppm was also observed, indicating the oxidation of the phosphine group. This could not be avoided even though the synthesis and purification of **6** were carried out in degassed solvents. However, it is likely that phosphine oxidation occurs in the solvent used for NMR analysis, as the signal at 31.8 ppm was found to

increase with time in CD₃CN solution. Both **5** and **6** display a high solubility in both water and apolar solvents such as chloroform and dichloromethane, which is an advantage compared to polyhydroxylated ligand **4** with respect to handling, characterization, and dendrimer construction (see section 6.3.3).

6.3.2 Coordination of water-solubilizing ligands to SCS Pd^{II} pincers

Having available water-solubilizing ligands **4**, **5**, and **6**, their coordination to a variety of SCS Pd^{II} pincer systems was investigated: monopincer **M**⁺, dipincer **D**²⁺, tripincer **T**³⁺, and hexapincer **H**⁶⁺ (Chart 6.2).

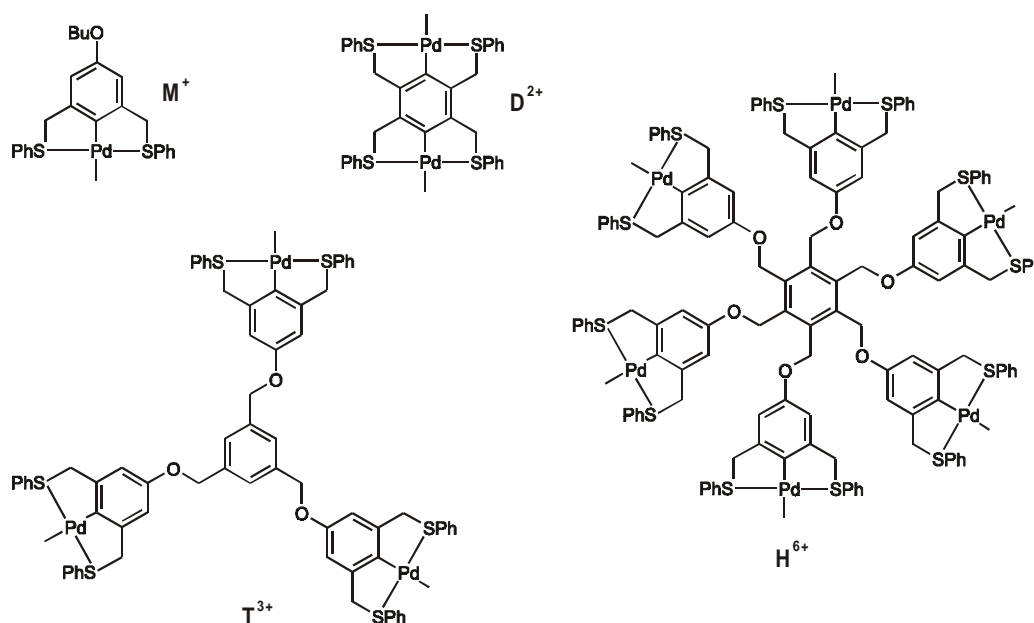


Chart 6.2.

Monopincer **M**⁺ was already discussed in chapter 3, dipincer **D**²⁺ was synthesized according to a literature procedure,³⁶ and tripincer **T**³⁺ is the core normally employed in metallodendrimer synthesis (see chapter 4). Hexapincer **H**⁶⁺ was synthesized by sixfold alkylation of hexakis(bromomethyl)benzene with 3,5-bis(phenylthiamethyl)phenol, followed by cyclopalladation of the resulting hexapincer ligand with Pd[MeCN]₄(BF₄)₂. All cationic pincer systems were isolated as the corresponding tetrafluoroborate salts, which might affect their water-solubility after coordination of **4**, **5**, or **6**. It has been reported that the nature of the anions is a determining factor in the solubility of metallodendrimers.³⁷

6.3.2.1 Complexes with ligand **4**

The coordination of polyhydroxylated pyridine ligand **4** to SCS Pd^{II} pincers was investigated with **T**³⁺ and **H**⁶⁺. The three chloride ligands of **G**₀ were removed in CH₂Cl₂/CH₃CN with 3 equiv of AgBF₄. After filtration over Hyflo and evaporation of the solvent, activated [T·MeCN]₃³⁺(BF₄)₃ was dissolved in CH₃CN and mixed with 3 equiv of **4** in H₂O. After

evaporation of the solvents, the resulting assembly was found to be insoluble in D₂O, and its ¹H NMR spectrum was therefore taken in DMSO-*d*₆. The signal from the α-pyridyl protons of **4** was broad and had shifted upfield compared to uncoordinated **4**, and the broad signal of the CH₂S protons had shifted downfield with respect to [T·MeCN₃]³⁺(BF₄⁻)₃. These features both prove the coordination of pyridine ligand **4** to the pincer moieties of **T**. Changing the deprotecting agent from AgBF₄ to AgNO₃, thereby introducing hydrophilic nitrate anions instead of hydrophobic tetrafluoroborate anions (which are both non-coordinating), resulted in a better water solubility of the trinuclear assembly. However, the ¹H NMR spectrum of this complex in D₂O revealed very broad signals which could not be assigned.

Hexanuclear [H·MeCN₆]⁶⁺(BF₄⁻)₆ was mixed in CD₃CN (0.3 mL) with 6 equiv of **4** dissolved in hot MeOH-*d*₄ (0.8 mL). The clear solution thus obtained was analyzed by ¹H NMR spectroscopy. Coordination of **4** was evident from the broadening and upfield shift of the signal from the α-pyridyl protons. After evaporation of the solvents, the assembly could be dissolved in hot D₂O. Upon cooling of this solution a gel was formed, and the ¹H NMR spectrum of the very viscous D₂O solution only showed signals that could be assigned to protons of ligand **4**. Gel formation from other polyhydroxylated dendrimers, *e.g.* the arborols having peripheral “tris” moieties reported by Newkome³⁸ and others,²⁰ is a well known phenomenon. The addition of DMSO-*d*₆ to the aqueous gel resulted in the appearance of signals that could be ascribed to the hexanuclear pincer moiety, although at 50% DMSO these signals were still very broad. In order to verify that H⁶⁺ was indeed present in the aqueous gel, an excess of pyridine-*d*₅ was added, which resulted in the precipitation of a yellow solid. This material was extracted with CH₂Cl₂, and subsequently identified as [H·(pyr-*d*₅)₆]⁶⁺(BF₄⁻)₆ by ¹H NMR spectroscopy.

6.3.2.2 Complexes with ligand **5**

Since M⁺, D²⁺, and H⁶⁺ were all synthesized as acetonitrile complexes, they are all highly soluble in acetonitrile. Therefore they were mixed with 1, 2, and 6 equiv of pyridine ligand **5** in CD₃CN, respectively, and the resulting clear solutions were analyzed by ¹H NMR spectroscopy. The following features are shared by the NMR spectra of [M·**5**]⁺(BF₄⁻), [D·**5**]²⁺(BF₄⁻)₂, and [H·**5**]⁶⁺(BF₄⁻)₆ in CD₃CN:

- An upfield shift from 8.50 (in free **5**) to 8.25-8.15 ppm of the α-pyridyl protons of ligand **5** upon coordination, as exemplified by the ¹H NMR spectra of **5** and [M·**5**]⁺(BF₄⁻) displayed in Figure 6.4. Moreover, a significant broadening of the α-pyridyl proton signal (signal *e* in Figure 6.4) occurs upon coordination. This may be caused by slow rotation of the pyridine ligands with respect to the plane of coordination and/or a ligand exchange rate that is comparable to the NMR time scale. Upon adding an excess of **5** (1.4 equiv) the α-pyridyl proton signal remains broad and shifts downfield. No α-pyridyl proton doublet from uncoordinated **5** at 8.5 ppm is observed (as in the top spectrum of Figure 6.4), indicating that the signals are averaged due to ligand exchange in this solvent, however, the exchange

is not fast enough to produce a sharp signal. In order to further probe which of the two above effects is dominant, the NMR spectrum of $[\mathbf{M}\cdot\mathbf{5}]^+(\text{BF}_4^-)$ was also recorded in CDCl_3 . The sharp doublet for the coordinated α -pyridyl protons at 7.73 ppm (shifted 0.77 ppm upfield compared to uncoordinated $\mathbf{5}$ in CDCl_3) indicates fast rotation of the pyridine ligand with respect to the plane of coordination. Moreover, the coordination shift of the α -pyridyl protons is much larger than in CD_3CN . Upon the addition of CD_3CN to the CDCl_3 solution the doublet at 7.73 ppm becomes broad and shifts downfield. In another experiment, the addition of excess pyridine ligand $\mathbf{5}$ to $[\mathbf{M}\cdot\mathbf{5}]^+(\text{BF}_4^-)$ in CDCl_3 resulted in two separate signals for free and coordinated ligand, indicating slow ligand exchange on the NMR time scale.

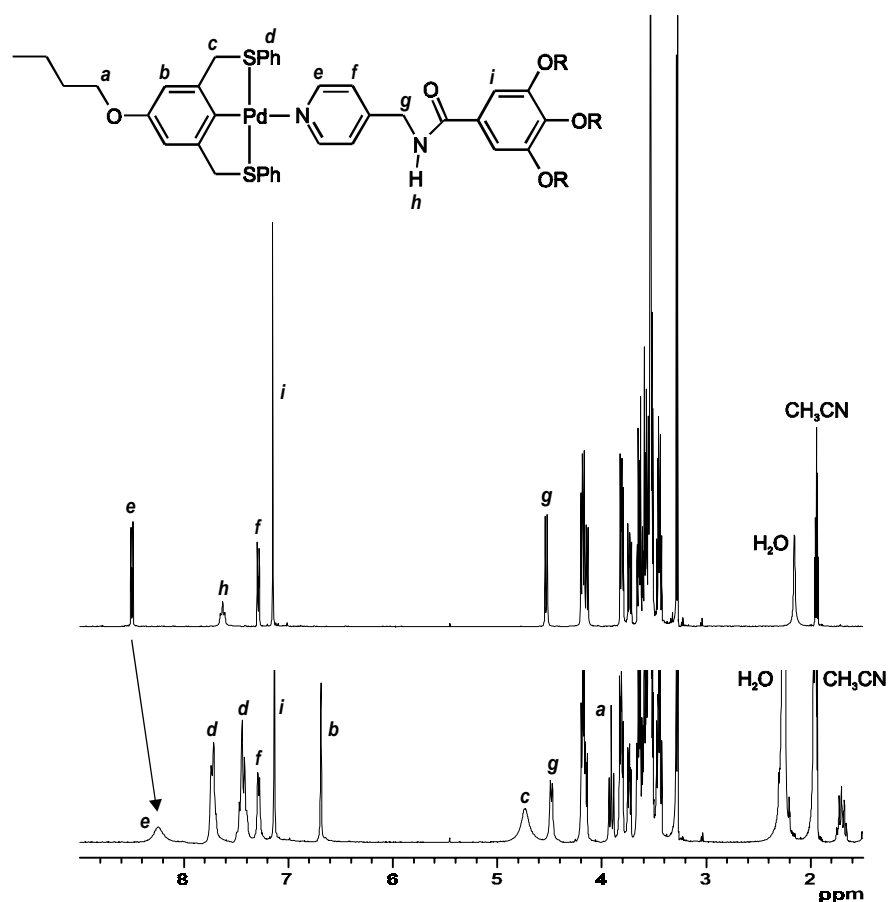


Figure 6.4. ^1H NMR spectra (CD_3CN , 298 K) of ligand **5** (top) and complex $[\mathbf{M}\cdot\mathbf{5}]^+(\text{BF}_4^-)$.

In chapter 3 the influence of $\text{DMSO-}d_6$ on the pyridine exchange rate in CDCl_3 was discussed, and the increase in the rate upon adding $\text{DMSO-}d_6$ was rationalized by assuming that DMSO facilitates an associative solvolysis pathway. Figure 3.8 shows that the signals for uncoordinated and coordinated pyridine merge into one broad signal upon increasing the percentage of DMSO. A similar experiment with CD_3CN instead of $\text{DMSO-}d_6$ indicates that acetonitrile also increases the rate of ligand exchange. However, acetonitrile differs from DMSO in the sense that it also competes with **5** for ligation to the fourth coordination site of the pincer. Upon increasing the concentration of CD_3CN , the amount

of ligand **5** that is expelled from the pincer by acetonitrile also increases. The fast ligand exchange then results in a downfield shift of the broad α -pyridyl proton signal toward the position of uncoordinated **5**. For $[\mathbf{M}\cdot\mathbf{5}]^+(\text{BF}_4^-)$ in $\text{CDCl}_3/\text{CD}_3\text{CN}$ 90:10 (v/v), the α -pyridyl proton signal is found at 7.78 ppm (close to 7.73 ppm for neat CDCl_3), whereas in neat CD_3CN this signal is observed at 8.23 ppm (Figure 6.4 bottom). In summary, the above NMR observations indicate the following:

1. Slow exchange of pyridine ligand **5** in CDCl_3 , and no competition from the solvent for coordination to the SCS Pd^{II} pincer;
 2. A ligand exchange rate that is comparable to the NMR time scale in CD_3CN , and competition from the solvent for coordination;
- A broad signal at 4.62-4.74 ppm from the CH_2S protons of the pincer moiety. This also indicates coordination of **5** to Pd^{II} , since the CH_2S protons give a signal at 4.5-4.6 ppm in the acetonitrile complexes.
 - Sharp signals of other resonances.

After evaporation of CD_3CN , enough material of complexes $[\mathbf{D}\cdot\mathbf{5}_2]^{2+}(\text{BF}_4^-)_2$ and $[\mathbf{H}\cdot\mathbf{5}_6]^{6+}(\text{BF}_4^-)_6$ could be taken up in D_2O in order to obtain meaningful ^1H NMR spectra. Complex $[\mathbf{M}\cdot\mathbf{5}]^+(\text{BF}_4^-)$ was less soluble in D_2O , and a satisfactory ^1H NMR spectrum could not be obtained. However, $[\mathbf{M}\cdot\mathbf{5}]^+(\text{BF}_4^-)$ was successfully characterized by MALDI-TOF mass spectrometry (*vide infra*). In contrast to CD_3CN , $[\mathbf{D}\cdot\mathbf{5}_2]^{2+}(\text{BF}_4^-)_2$ and $[\mathbf{H}\cdot\mathbf{5}_6]^{6+}(\text{BF}_4^-)_6$ display very broad signals in their ^1H NMR spectra in D_2O . Moreover, the signals from the SCS pincer parts are very hard to distinguish. A representative spectrum of $[\mathbf{H}\cdot\mathbf{5}_6]^{6+}(\text{BF}_4^-)_6$ in D_2O is shown in Figure 6.5.

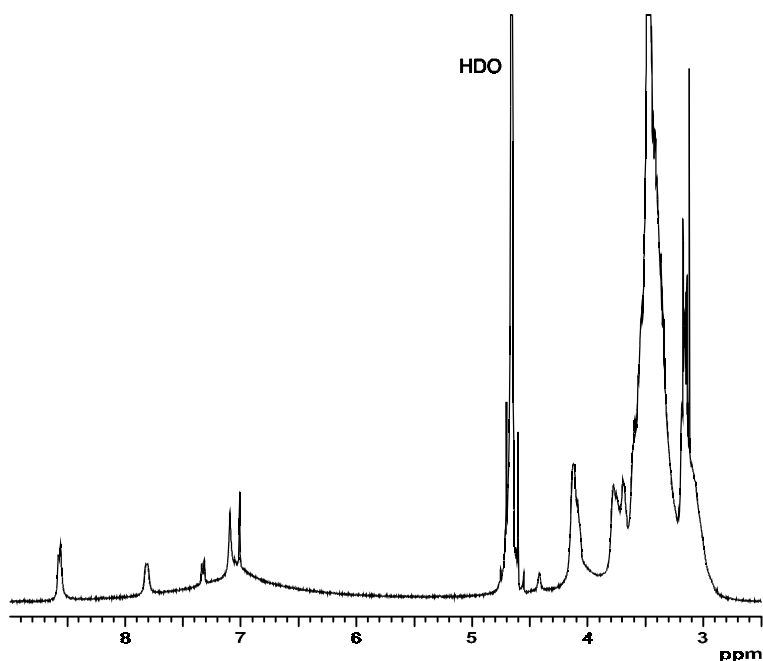


Figure 6.5. ^1H NMR spectrum (D_2O , 298 K) of $[\mathbf{H}\cdot\mathbf{5}_6]^{6+}(\text{BF}_4^-)_6$.

The sharp signals between 6 and 9 ppm in this spectrum originate from coordinated ligand **5**, whereas the very broad signal centered around 7 ppm probably arises from protons of the hexanuclear core. It is probable that the hydrophobic parts of these assemblies are very restricted in their motion because they are shielded from the solvent by the more hydrophilic parts, and that this causes their very broad signals.

Trinuclear complex $[\mathbf{T}\cdot\mathbf{5}_3]^{3+}(\text{NO}_3^-)_3$ was synthesized from **G₀** by deprotection of the chloride ligands with AgNO_3 in CH_2Cl_2 , followed by addition of 3 equiv of pyridine ligand **5**. The resulting assembly was first investigated by ^1H NMR spectroscopy in D_2O . As in the case of the assemblies described in the previous paragraph, signals from the trinuclear core could not be distinguished, and the spectrum is nearly identical to that of **5** alone in D_2O . However, addition of CD_3CN resulted in a significant increase in the intensity of the signals from the core, although the integrals were still too low to fit a 1:3 ratio of **T** to **5**. Unfortunately, MALDI-TOF mass spectrometry of $[\mathbf{T}\cdot\mathbf{5}_3]^{3+}(\text{NO}_3^-)_3$ gave poor results, and signals that could be assigned to $[\text{M} - n(\text{NO}_3)]^+$ ($n = 1-3$) were not found.

6.3.2.3 Complexes with ligand **6**

Hexanuclear complex \mathbf{H}^{6+} was mixed in CD_3CN with 6 equiv of phosphine ligand **6**. Coordination of all phosphine ligand to the pincers was evident from both ^1H and ^{31}P NMR spectroscopy. In the ^1H NMR spectrum of the assembly the doublet at 6.72 ppm indicates the splitting of the Ar_{Pd} protons by $^1\text{H}-^{31}\text{P}$ coupling (see also chapter 3), whereas the ^{31}P NMR spectrum shows a shift from -20.4 (free **6**) to 2.0 ppm upon coordination (Figure 6.6).

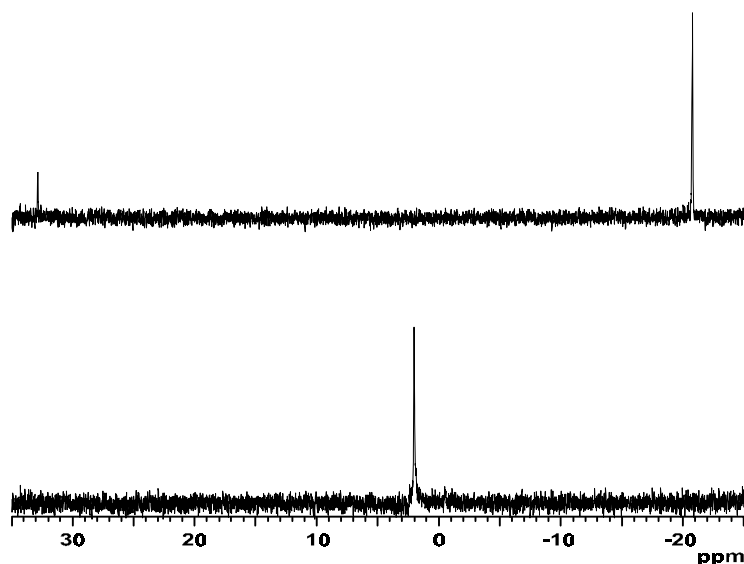


Figure 6.6. ^{31}P NMR spectra of **6** (top) and $[\mathbf{H}\cdot\mathbf{6}_6]^{6+}(\text{BF}_4^-)_6$ (bottom) in CD_3CN . The signal at 31.8 ppm in the top spectrum is due to oxidized phosphine.

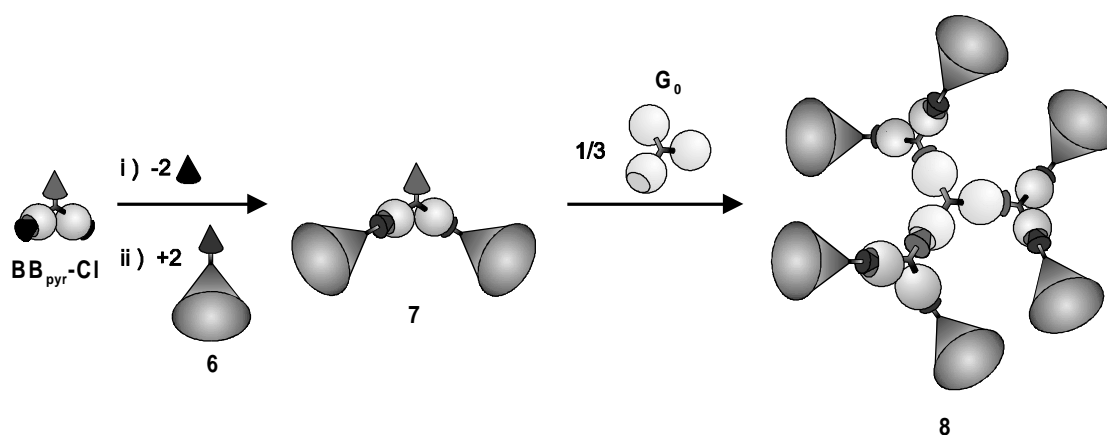
Assembly $[\mathbf{H}\cdot\mathbf{6}_6]^{6+}(\text{BF}_4^-)_6$ is highly water-soluble, however, its ^1H NMR spectrum in D_2O again reveals very broad, unassignable signals. Moreover, the signal at 2.0 ppm in the ^{31}P NMR

spectrum has almost disappeared in D₂O. Again this is assigned to the restricted mobility of the hexanuclear core. The assembly of $[\mathbf{H}\cdot\mathbf{6}_6]^{6+}(\text{BF}_4^-)_6$ was further evidenced by a very intense signal at m/z 8959.2 in its MALDI-TOF mass spectrum, corresponding to $[\text{M} - \text{BF}_4]^+$ (calcd 8960.2).

6.3.3 Convergent metallodendrimer synthesis starting from ligand **6**

The convergent synthesis of metallodendrimers starting from phosphine dendritic wedges was discussed in chapter 4. It was anticipated that replacing the phosphine dendrons by phosphine ligand **6** in this growth scheme would lead to water-soluble metallodendrimers. There are three advantages of using phosphine **6** for this purpose over pyridine **4**. First, ligand **6** is a better water-solubilizing ligand than **4**, due to its three tetraethyleneglycol chains compared to one polyhydroxylated chain in **4**. Second, convergent growth starting from phosphines enables higher dendritic generations to be constructed than growth commencing from pyridines. Third, both ligand **6** and assemblies built from it are also soluble in apolar solvents such as CH₂Cl₂ and CHCl₃, which is advantageous in both synthesis and characterization.

Two phosphine ligands **6** were coordinated to the SCS Pd^{II} pincer moieties of deprotected **BB**_{pyr}-Cl (Scheme 6.3) to give dendritic wedge **7** containing a focal pyridine moiety, which was immediately used for further coordination. Three equivalents of **7** were complexed around deprotected **G**₀ to produce metallodendrimer **8** in 89% overall yield.



Scheme 6.3. Synthesis of water-soluble metallodendrimer **8**.

The structural integrity of the dendritic structure in CDCl₃ was confirmed by ¹H and ³¹P NMR spectroscopy, and MALDI-TOF mass spectrometry. The coordination of the phosphine moieties to Pd^{II} was evident from the ³¹P NMR spectrum of **8**, in which a diagnostic signal at 2.2 ppm was observed. The very broad signal around 8.2 ppm in the ¹H NMR spectrum of **8** indicated the coordination of the pyridine groups of **7** to the Pd^{II} centers of deprotected **G**₀. As for other metallodendrimers (see chapters 4 and 5) and due to its size, broad signals for nearly all protons were observed in the ¹H NMR spectrum of metallodendrimer **8**. The intense signal at m/z 11.2 kDa in the MALDI-TOF mass spectrum of **8**, originating from the $[\text{M} - \text{BF}_4]^+$ ion, confirms its successful assembly.

6.3.4 MALDI-TOF mass spectrometry of water-soluble assemblies

MALDI-TOF and ES mass spectrometry have emerged as powerful analytical techniques in supramolecular chemistry,³⁹ notably in the characterization of assemblies based on non-covalent metal-ligand coordination, and recently even in the mass determination of hydrogen-bonded assemblies.^{39,40} Both ES-MS and MALDI-TOF MS have been employed in the characterization of metallodendrimers constructed in our group.^{41,42} Most of the water-soluble coordination assemblies reported in this chapter were also characterized by MALDI-TOF mass spectrometry, and the results are compiled in Table 6.1. The spectrum of $[\mathbf{H}\cdot\mathbf{6}_6]^{6+}(\text{BF}_4^-)_6$ shown in Figure 6.7 is representative.

Table 6.1. Characterization of coordination assemblies by MALDI-TOF mass spectrometry.

Compound	Solvent	Fragment	Obs. mass (Da)	Calcd mass (Da)
$[\mathbf{M}\cdot\mathbf{5}]^+(\text{BF}_4^-)$	CH ₃ CN	$[\mathbf{M} - \text{BF}_4]^+$	1329.3	1329.5
$[\mathbf{D}\cdot\mathbf{5}_2]^{2+}(\text{BF}_4^-)_2$	CD ₃ CN	$[\mathbf{M} - \text{BF}_4]^+$	2534.6 ^a	2526.4
$[\mathbf{D}\cdot\mathbf{5}_2]^{2+}(\text{BF}_4^-)_2$	D ₂ O	$[\mathbf{M} - \text{BF}_4]^+$	2530.1 ^a	2526.4
$[\mathbf{H}\cdot\mathbf{5}_6]^{6+}(\text{BF}_4^-)_6$	CH ₃ CN	$[\mathbf{M} - \text{BF}_4]^+$	8224.7	8225.6
$[\mathbf{H}\cdot\mathbf{5}_6]^{6+}(\text{BF}_4^-)_6$	H ₂ O	$[\mathbf{M} - \text{BF}_4]^+$	8224.7	8225.6
$[\mathbf{H}\cdot\mathbf{6}_6]^{6+}(\text{BF}_4^-)_6$	CH ₃ CN	$[\mathbf{M} - \text{BF}_4]^+$	8959.2	8960.2
8	CDCl ₃	$[\mathbf{M} - \text{BF}_4]^+$	11227	11225.1

^aDifference between observed and calculated mass is enhanced by deuterium exchange.

Millimolar solutions of the assemblies in water or acetonitrile were covered on the MALDI-TOF sample plate with a thin poly(ethyleneglycol) film. In this way the original constitution of the sample solutions is preserved, and evaporation is kept to a minimum. Using this method, the $[\mathbf{M} - \text{BF}_4]^+$ signals in the MALDI-TOF spectra confirm the stability of the assemblies in the original solutions. It can therefore be concluded from Table 6.1 that the non-covalent coordination assemblies based on pyridine and phosphine coordination are stable enough both in acetonitrile and in water in order to be characterized successfully by MALDI-TOF mass spectrometry, even though there is competition from acetonitrile for coordination to the pincer in the case of pyridine ligand **5**, as discussed in section 6.3.2.2. The presence of $[\mathbf{M}\cdot\text{MeCN}]^+(\text{BF}_4^-)$ in the acetonitrile solution of $[\mathbf{M}\cdot\mathbf{5}]^+(\text{BF}_4^-)$ (the first entry in Table 6.1) was indicated by a signal at m/z 500.8 in the MALDI-TOF spectrum of $[\mathbf{M}\cdot\mathbf{5}]^+(\text{BF}_4^-)$, corresponding to $[\mathbf{M} - \text{MeCN} - \text{BF}_4]^+$. However, this signal might also originate from fragmentation of $[\mathbf{M}\cdot\mathbf{5}]^+(\text{BF}_4^-)$ inside the mass spectrometer.

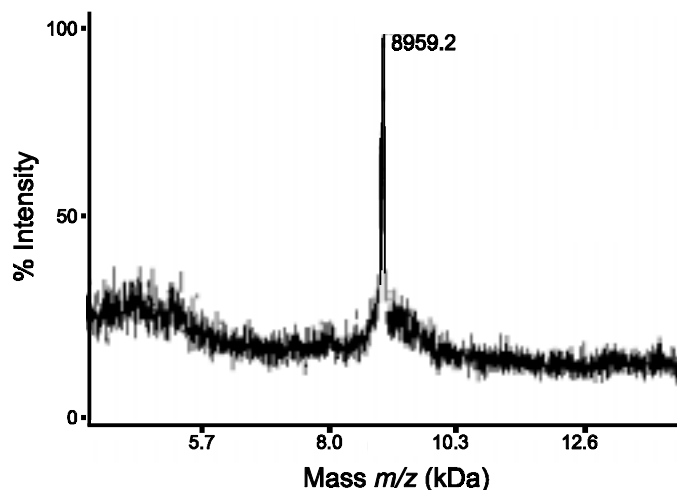


Figure 6.7. MALDI-TOF mass spectrum of $[\mathbf{H}\cdot\mathbf{6}_6]^{6+}(\mathbf{BF}_4^-)_6$.

6.4 Conclusions

In this chapter the synthesis and characterization of water-soluble assemblies based on metal-ligand coordination have been described. Carbohydrate and oligoethyleneglycol moieties have been functionalized with pyridine and phosphine groups, and the resulting molecules have been employed as water-solubilizing ligands for mono-, di-, tri-, and hexanuclear SCS Pd^{II} pincer systems. The majority of these assemblies are soluble in water, and most complexes have been characterized by NMR spectroscopy and MALDI-TOF mass spectrometry. An aqueous gel has been obtained for a hexanuclear SCS Pd^{II} pincer system decorated with six linear carbohydrate ligands. Finally, water-soluble metallodendrimers have been obtained by convergent dendritic growth starting from a phosphine ligand containing three tetraethyleneglycol chains.

Since SCS Pd^{II} pincers have recently been shown to be catalytically active for a number of reactions, the water-soluble multinuclear Pd^{II} pincers reported in this chapter might be useful as recyclable catalysts in aqueous systems. Because of their size, the assemblies should be separable from reaction mixtures *via* nanofiltration methods.

6.5 Experimental Section

General comments. For general information on instruments, procedures, and chemicals, see chapter 3. For a description of MALDI-TOF experiments, see chapter 4.

Materials. \mathbf{G}_0 ,⁴³ $\mathbf{BB}_{\text{pyr}}\text{-Cl}$,⁴⁴ $[\mathbf{D}\cdot\text{MeCN}_2]^{2+}(\text{BF}_4^-)_2$,³⁶ and 3,5-bis(phenylthiamethyl)phenol⁴⁵ were synthesized according to literature procedures. The synthesis of $[\mathbf{M}\cdot\text{MeCN}]^+(\text{BF}_4^-)$ was reported in chapter 3. 3,4,5-Tris(tetraethyleneoxy)benzoic acid was synthesized using a similar procedure as

described by Baars *et al.*^{27,34} Hexa(bromomethyl)benzene, 4-aminomethylpyridine and 2-(diphenylphosphino)ethylamine were obtained from Aldrich.

Pyridine ligand 4. To a solution of gluconolactone (2.55 g, 14.3 mmol) in MeOH (50 mL) was slowly added 4-aminomethylpyridine (1.5 mL, 14.8 mmol). The mixture was refluxed overnight under an argon atmosphere, and subsequently the white precipitate was filtered and thoroughly dried. Pure product was obtained in this manner, as determined by TLC ($R_f = 0.22$ in 2-propanol/EtOAc/H₂O 3:6:2 (v/v/v)). Yield 2.98 g (73%). M.p. 169-171 °C. ¹H NMR (DMSO-*d*₆): δ (ppm) 8.44 (d, $J = 5.9$ Hz, 2 H, α -pyr H), 8.33 (t, $J = 5.9$ Hz, 1 H, NH), 7.27 (d, $J = 5.9$ Hz, 2 H, β -pyr H), 5.53 (s, 1 H, OH), 4.59 (s, 1 H, OH), 4.54 (s, 1 H, OH), 4.41-4.29 (m, 4 H, CH₂N + OH), 4.10 (s, 1 H, CH), 3.98 (s, 1 H, CH), 3.59 (d, $J = 9.9$ Hz, CH₂OH), 3.51 (s, 1 H, CH), 3.40 (s, 1 H, CH). ¹³C NMR (DMSO-*d*₆): δ (ppm) 169.0, 145.2, 144.7, 118.0, 69.9, 68.5, 67.5, 66.1, 59.3, 36.8. FAB-MS m/z 287.1 ([M + H]⁺, calcd for C₁₂H₁₈N₂O₆: 287.1). A satisfactory elemental composition could not be obtained.

Pyridine ligand 5. To a solution of 3,4,5-tris(tetraethyleneoxy)benzoic acid (1.08 g, 1.46 mmol), 1-hydroxybenzotriazole hydrate (0.22 g, 1.63 mmol), 1-(3-dimethylaminopropyl)-3-ethyl-carbodiimide hydrochloride (0.31 g, 1.62 mmol), and *N,N*-diisopropylethylamine (0.63 mL, 3.62 mmol) in CH₂Cl₂ (100 mL) was added dropwise a solution of 4-aminomethylpyridine (0.16 g, 1.48 mmol) in CH₂Cl₂ (20 mL). After the reaction mixture was stirred at r.t. overnight, the solution was washed with NaHCO₃ (sat) and brine. After drying over Na₂SO₄, the organic phase was evaporated under reduced pressure. The crude product was purified by column chromatography using CH₂Cl₂/CH₃OH/NH₃ (25% aq) 95:5:1 (v/v/v) as the eluent, affording a transparent viscous oil. Yield 0.95 g (78%). ¹H NMR: δ (ppm) 8.52 (d, $J = 5.9$ Hz, 2 H, α -pyr H), 7.37 (t, $J = 6.2$ Hz, 1 H, NH), 7.26 (d, $J = 5.9$ Hz, 2 H, β -pyr H), 7.20 (s, 2 H, Ar H), 4.60 (d, $J = 6.2$ Hz, 2 H, CH₂N), 4.21-4.17 (m, 6 H, CH₂), 3.81-3.75 (m, 6 H, CH₂), 3.68-3.65 (m, 6 H, CH₂), 3.62-3.57 (m, 24 H, CH₂), 3.52-3.47 (m, 6 H, CH₂), 3.34 (s, 3 H, CH₃), 3.31 (s, 6 H, CH₃). ¹³C NMR: δ (ppm) 166.6, 152.0, 149.0, 148.0, 141.4, 128.4, 122.0, 107.4, 71.8, 71.4, 70.0-69.8, 69.2, 68.7, 58.4, 42.3. FAB-MS m/z 831.5 ([M + H]⁺, calcd for C₄₀H₆₇N₂O₁₆: 831.4), 853.5 ([M + Na]⁺), 869.5 ([M + K]⁺).

Phosphine ligand 6. To a solution of 3,4,5-tris(tetraethyleneoxy)benzoic acid (0.55 g, 0.74 mmol), 1-hydroxybenzotriazole hydrate (0.11 g, 0.81 mmol), 1-(3-dimethylaminopropyl)-3-ethyl-carbodiimide hydrochloride (0.16 g, 0.83 mmol), and *N,N*-diisopropylethylamine (0.26 mL, 1.49 mmol) in CH₂Cl₂ (50 mL) was added dropwise a solution of 2-(diphenylphosphino)ethylamine (0.17 g, 0.74 mmol) in CH₂Cl₂ (10 mL). After the reaction mixture was stirred at r.t. overnight under an argon atmosphere, the solution was washed with NaHCO₃ (sat) and brine. After drying over Na₂SO₄, the organic phase was evaporated under reduced pressure. The crude product was purified by column chromatography using CH₂Cl₂/CH₃OH 96:4 (v/v) as the eluent, affording a transparent viscous oil. Yield 0.55 g (78%). ¹H NMR: δ (ppm) 7.48-7.42 (m, 4 H, Ar H), 7.35-7.30 (m, 6 H, Ar H), 6.99 (s, 2 H, Ar H), 6.55 (t, $J = 5.7$ Hz, 1 H, NH), 4.18-4.15 (m, 6 H, CH₂), 3.83-3.75 (m, 6 H, CH₂), 3.70-3.59 (m, 30 H, CH₂), 3.56-3.48 (m, 8 H, CH₂), 3.35 (s, 3 H, CH₃), 3.33 (s, 6 H, CH₃), 2.43-2.38 (m, 2 H, PCH₂). ¹³C NMR: δ (ppm) 166.3, 151.9, 137.2, 132.2, 130.1, 128.4, 128.3, 128.0, 106.8, 71.8, 71.4, 70.1-70.0, 69.2, 68.6, 58.5, 37.0 (d, $J = 20.8$ Hz, PCH₂), 27.9 (d, $J = 13.1$ Hz, PCH₂CH₂). FAB-MS m/z 952.6 ([M + H]⁺, calcd for C₄₈H₇₅NO₁₆P: 952.5), 968.6 ([MO + H]⁺).

Hexapincer ligand. A mixture of hexakis(bromomethyl)benzene (0.16 g, 0.25 mmol), 3,5-bis(phenylthiamethyl)phenol (0.60 g, 1.77 mol), K_2CO_3 (0.49 g, 3.55 mmol), and 18-crown-6 (0.07 g, 0.26 mmol) in acetone (100 mL) was refluxed overnight under an argon atmosphere. After evaporation of the solvent under reduced pressure, the resulting paste was taken up in CH_2Cl_2 (100 mL) and washed with brine. The organic phase was dried over Na_2SO_4 , and subsequently evaporated to dryness. The crude product was purified by column chromatography using CH_2Cl_2 /hexane 60:40 (v/v) as the eluent, affording a colorless viscous oil. Yield 0.45 g (82%). 1H NMR: δ (ppm) 7.22-7.07 (m, 30 H, SPh H), 6.82 (s, 6 H, Ar H), 6.63 (s, 12 H, Ar H), 4.97 (s, 12 H, CH_2O), 3.91 (s, 24 H, CH_2S). ^{13}C NMR: δ (ppm) 158.1, 138.8, 137.2, 135.7, 129.3, 128.3, 125.9, 122.0, 113.6, 63.2, 38.3. FAB-MS m/z 2179.6 ($[M + H]^+$, calcd for $C_{132}H_{115}O_6S_{12}$: 2179.5).

$[H \cdot MeCN_6]^{6+}(BF_4^-)_6$. To a solution of the hexapincer ligand (60 mg, 0.028 mmol) in a mixture of CH_3CN (40 mL) and CH_2Cl_2 (10 mL) was added $Pd[MeCN]_4(BF_4)_2$ (77 mg, 0.173 mmol) in one portion. The solution was stirred at r.t. under an argon atmosphere for 1 h, followed by evaporation of the solvents *in vacuo*. The crude product was purified by size exclusion chromatography using Sephadex LH-20 as the column material and CH_3CN as the eluent, affording a yellow/brown solid. Yield 53 mg (54%). 1H NMR (CD_3CN): δ (ppm) 7.80-7.77 (m, 12 H, SPh H), 7.53-7.47 (m, 18 H, SPh H), 6.56 (s, 12 H, Ar_{Pd} H), 5.14 (s, 12 H, CH_2O), 4.51 (br s, 24 H, CH_2S).

Metalloendrimer 8. To a solution of BB_{pyr-Cl} (5.6 mg, 4.7 μ mol) in CH_2Cl_2 (2 mL) was added $AgBF_4$ (92 μ L of a 0.1019 M solution, 9.4 μ mol), and the mixture was stirred vigorously for 10 min, followed by addition of phosphine ligand **6** (8.9 mg, 9.4 μ mol) in CH_2Cl_2 (1 mL). After stirring at r.t. for 10 min, the mixture was filtered over Hyflo and evaporated to dryness. The resulting dendritic wedge **7** was dissolved in CH_2Cl_2 (1 mL) and added to G_0 (2.4 mg, 1.6 μ mol) which had been deprotected with $AgBF_4$ (46 μ mol of a 0.1019 M solution, 4.7 μ mol). After stirring for 10 min, the mixture was filtered over Hyflo and evaporated to dryness, affording a yellow film. Yield 15.6 mg (89%). 1H NMR: δ (ppm) 8.2 (br s, 6 H, α -pyr H), 7.58 (d, $J = 5.7$ Hz, 6 H, β -pyr H), 7.50-7.40 (m, 24 H, PPh_2 H), 7.35-7.28 (m, 72 H, SPh H + PPh_2 H), 7.22-7.05 (m, 66 H, SPh H + Ar H), 7.00 (s, 12 H, Ar H), 6.79-6.67 (m, 18 H, Ar_{Pd} H), 5.05-4.96 (m, 18 H, CH_2O), 4.69 (br s, 24 H, CH_2S), 4.59 (m, 18 H, $CH_2S + CH_2N$), 4.18 (br s, 36 H, CH_2), 3.87-3.74 (m, 36 H, CH_2), 3.70-3.55 (m, 180 H, CH_2), 3.54-3.50 (m, 48 H, CH_2), 3.36-3.30 (m, 54 H, OCH_3), 2.65-2.55 (m, 12 H, CH_2). ^{31}P NMR: δ (ppm) 2.2. MALDI-TOF MS m/z 11227 ($[M - BF_4]^+$, calcd for $C_{522}H_{639}B_8F_{32}N_{12}O_{108}P_6Pd_9S_{18}$: 11225.1).

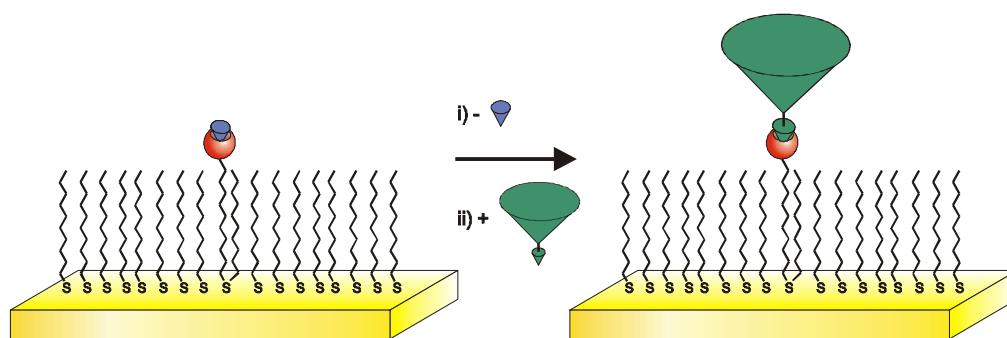
6.6 References and notes

- ¹ Huck, W. T. S.; Rohrer, A.; Anilkumar, A. T.; Fokkens, R. H.; Nibbering, N. M. M.; van Veggel, F. C. J. M.; Reinhoudt, D. N. *New J. Chem.* **1998**, 22, 165.
- ² Vögtle, F.; Gestermann, S.; Hesse, R.; Schwierz, H.; Windisch, B. *Prog. Polym. Sci.* **2000**, 25, 987.
- ³ Ottaviani, M. F.; Furini, F.; Casini, A.; Turro, N. J.; Jockusch, S.; Tomalia, D. A.; Messori, L. *Macromolecules* **2000**, 33, 7842.

- ⁴ a) Bielinska, A. U.; Kukowska-Latallo, J. F.; Johnson, J.; Tomalia, D. A.; Baker, J. R. *Nucleic Acids Res.* **1996**, *24*, 2176; b) Kukowska-Latallo, J. F.; Bielinska, A. U.; Johnson, J.; Spindler, R.; Tomalia, D. A.; Baker, J. R. *Proc. Natl. Acad. Sci. USA* **1996**, *93*, 4897.
- ⁵ Newkome, G. R.; Moorefield, C. N.; Baker, G. R.; Saunders, M. J.; Grossman, S. H. *Angew. Chem. Int. Ed. Engl.* **1991**, *30*, 1178.
- ⁶ Hawker, C. J.; Wooley, K. L.; Fréchet, J. M. J. *J. Chem. Soc., Perkin Trans. 1* **1993**, 1287.
- ⁷ Mattei, S.; Wallimann, P.; Kenda, B.; Amrein, W.; Diederich, F. *Helv. Chim. Acta* **1997**, *80*, 2391.
- ⁸ Kim, Y. H.; Webster, O. W. *J. Am. Chem. Soc.* **1990**, *112*, 4592.
- ⁹ Pesak, D. J.; Moore, J. S. *Tetrahedron* **1997**, *53*, 15331.
- ¹⁰ Krska, S. W.; Seyferth, D. *J. Am. Chem. Soc.* **1998**, *120*, 3604.
- ¹¹ Loup, C.; Zanta, M.-A.; Caminade, A.-M.; Majoral, J.-P.; Meunier, B. *Chem. Eur. J.* **1999**, *5*, 3644.
- ¹² a) Roy, R. *Top. Curr. Chem.* **1997**, *187*, 241; b) Zanini, D.; Roy, R. *J. Am. Chem. Soc.* **1997**, *119*, 2088.
- ¹³ a) Aoi, K.; Itoh, K.; Okada, M. *Macromolecules* **1995**, *28*, 5391; b) Schmitzer, A.; Perez, E.; Rico-Lattes, I.; Lattes, A.; Rosca, S. *Langmuir* **1999**, *15*, 4397.
- ¹⁴ Aoi, K.; Tsutsumiuchi, K.; Yamamoto, A.; Okada, M. *Macromol. Rapid Commun.* **1998**, *19*, 5.
- ¹⁵ a) Ashton, P. R.; Boyd, S. E.; Brown, C. L.; Nepogodiev, S. A.; Meijer, E. W.; Peerling, H. W. I.; Stoddart, J. F. *Chem. Eur. J.* **1997**, *3*, 974; b) Peerlings, H. W. I.; Nepogodiev, S. A.; Stoddart, J. F.; Meijer, E. W. *Eur. J. Org. Chem.* **1998**, 1879.
- ¹⁶ a) Pagé, D.; Roy, R. *Bioconjugate Chem.* **1997**, *8*, 714; b) Lindhorst, T. K.; Kieburg, C. *Angew. Chem. Int. Ed. Engl.* **1996**, *35*, 1953;
- ¹⁷ a) Ashton, P. R.; Boyd, S. E.; Brown, C. L.; Jayaraman, N.; Nepogodiev, S. A.; Stoddart, J. F. *Chem. Eur. J.* **1996**, *2*, 1115; b) Ashton, P. R.; Boyd, S. E.; Brown, C. L.; Jayaraman, N.; Stoddart, J. F. *Angew. Chem. Int. Ed. Engl.* **1997**, *36*, 732; c) Ashton, P. R.; Hounsell, E. F.; Jayaraman, N.; Nilsen, T. M.; Spencer, N.; Stoddart, J. F.; Young, M. *J. Org. Chem.* **1998**, *63*, 3429.
- ¹⁸ Newkome, G. R.; Yao, Z.-Q.; Baker, G. R.; Gupta, V. K. *J. Org. Chem.* **1985**, *50*, 2003.
- ¹⁹ Newkome, G. R.; Moorefield, C. N.; Baker, G. R.; Behera, R.K.; Escamillia, G. H.; Saunders, M. J. *Angew. Chem. Int. Ed. Engl.* **1992**, *31*, 917.
- ²⁰ Jorgensen, M.; Bechgaard, K.; Bjornholm, T.; Sommer-Larsen, P.; Hansen, L. G.; Schaumburg, K. *J. Org. Chem.* **1994**, *59*, 5877.
- ²¹ Newkome, G. R.; Hu, Y.; Saunders, M. J.; Fronczek, F. R. *Tetrahedron Lett.* **1991**, *32*, 1133.
- ²² Twyman, L. J.; Beezer, A. E.; Esfand, R.; Hardy, M. J.; Mitchell, J. C. *Tetrahedron Lett.* **1999**, *40*, 1743.
- ²³ Dandliker, P. J.; Diederich, F.; Gisselbrecht, J.-P.; Louati, A.; Gross, M. *Angew. Chem. Int. Ed. Engl.* **1995**, *34*, 2725.
- ²⁴ Moore, G. R.; Pettigrew, G. W. *Cytochromes c: Evolutionary, Structural, and Physicochemical Aspects*, Springer: Berlin, 1990, pp. 309-362.
- ²⁵ Smith, D. K.; Diederich, F. *Chem. Commun.* **1998**, 2501.
- ²⁶ Smith, D. K. *J. Chem. Soc., Perkin Trans. 2* **1999**, 1563.
- ²⁷ Baars, M. W. P. L.; Kleppinger, R.; Koch, M. H. J.; Yeu, S.-L.; Meijer, E. W. *Angew. Chem. Int. Ed.* **2000**, *39*, 1285.

- ²⁸ a) Cyclodextrins. In *Comprehensive Supramolecular Chemistry*; Lehn, J.-M., Chair Ed.; Atwood, J. L., Davis, J. E. D., MacNicol, D. D., Vögtle, F., Exec. Eds.; Pergamon: Oxford, UK, 1987-1996; Vol. 3; b) *Chem. Rev.* **1998**, 98, Issue no. 5.
- ²⁹ Takada, K.; Díaz, D. J.; Abruña, H. D.; Cuadrado, I.; Casado, C.; Alonso, B.; Morán, M.; Losada, J. J. *Am. Chem. Soc.* **1997**, 119, 10763.
- ³⁰ González, B.; Casado, C. M.; Alonso, B.; Cuadrado, I.; Morán, M.; Wang, Y.; Kaifer, A. E. *Chem. Commun.* **1998**, 2569.
- ³¹ Castro, R.; Cuadrado, I.; Alonso, B.; Casado, C. M.; Morán, C. M.; Kaifer, A. E. *J. Am. Chem. Soc.* **1997**, 119, 5760.
- ³² Michels, J. J.; Baars, M. W. P. L.; Meijer, E. W.; Huskens, J.; Reinhoudt, D. N. *J. Chem. Soc., Perkin Trans. 2* **2000**, 1914.
- ³³ Fujimoto, T.; Shimizu, C.; Hayashida, O.; Aoyama, Y. *J. Am. Chem. Soc.* **1997**, 119, 6676.
- ³⁴ The article by Baars *et al.* (ref. 27) appeared while the work described in this chapter was in progress.
- ³⁵ Ouchi, M.; Inoue, Y.; Liu, Y.; Nagamune, S.; Nakamura, S.; Wada, K.; Hakushi, T. *Bull. Chem. Soc. Jpn.* **1990**, 63, 1260.
- ³⁶ Loeb, S. J.; Shimizu, G. K. H. *J. Chem. Soc., Chem. Commun.* **1993**, 1395.
- ³⁷ Constable, E. C.; Harverson, P. *Chem. Commun.* **1996**, 33.
- ³⁸ Newkome, G. R.; Baker, G. R.; Arai, S.; Saunders, M. J.; Russo, P. S.; Theriot, K. J.; Moorefield, C. N.; Rogers, L. E.; Miller, J. E.; Lieux, T. R.; Murray, M. E.; Phillips, B.; Pascal, L. *J. Am. Chem. Soc.* **1990**, 112, 8458.
- ³⁹ For a recent overview, see: Schalley, C. A. *Int. J. Mass Spectrom.* **2000**, 194, 11.
- ⁴⁰ Timmerman, P.; Jolliffe, K. A.; Crego Calama, M.; Weidmann, J.-L.; Prins, L. J.; Cardullo, F.; Snellink-Ruël, B. H. M.; Fokkens, R. H.; Nibbering, N. M. M.; Shinkai, S.; Reinhoudt, D. N. *Chem. Eur. J.* **2000**, 6, 4104.
- ⁴¹ Characterization of metallodendrimers by ES-MS: Ref. 44.
- ⁴² Characterization of metallodendrimers by MALDI-TOF MS: a) Ref. 43; b) This thesis.
- ⁴³ Huck, W. T. S.; Prins, L. J.; Fokkens, R. H.; Nibbering, N. M. M.; van Veggel, F. C. J. M.; Reinhoudt, D. N. *J. Am. Chem. Soc.* **1998**, 120, 6240.
- ⁴⁴ Huck, W. T. S.; van Veggel, F. C. J. M.; Reinhoudt, D. N. *Angew. Chem. Int. Ed. Engl.* **1996**, 35, 1213.
- ⁴⁵ Huck, W. T. S.; van Veggel, F. C. J. M.; Reinhoudt, D. N. *J. Mater. Chem.* **1997**, 7, 1213.

Single molecules on a gold surface: Isolation, visualization, and coordination chemistry[#]



Schematic representation of coordination chemistry on individual SCS Pd^{II} pincer moieties embedded into alkanethiol self-assembled monolayers on a gold surface.

In this chapter it is shown that both non-covalent metallodendrimers and covalent Fréchet-type dendrimers can be inserted into preformed self-assembled monolayers (SAMs) of alkanethiols on gold, provided that they are functionalized with a dialkylsulfide chain suitable for binding to gold. Atomic force microscopy (AFM) experiments have established that this procedure leads to isolated, individual dendrimers of nanosize dimensions bound to the gold surface. Furthermore, the suitability of SCS Pd(II) pincers for performing coordination chemistry on individual molecules on gold is demonstrated herein. Besides in solution, ligand exchange on pincers has been shown to occur in SAMs as well, as exemplified by the substitution of coordinated pyridine by dendritic wedges and monolayer-protected gold nanoclusters, appropriately functionalized with phosphine ligands.

[#] The work described in this chapter has been published: a) Huisman, B.-H.; Schönherr, H.; Huck, W. T. S.; Friggeri, A.; van Manen, H.-J.; Menozzi, E.; Vancso, G. J.; van Veggel, F. C. J. M.; Reinhoudt, D. N. *Angew. Chem. Int. Ed.* **1999**, *38*, 2248; b) Friggeri, A.; Schönherr, H.; van Manen, H.-J.; Huisman, B.-H.; Vancso, G. J.; Huskens, J.; van Veggel, F. C. J. M.; Reinhoudt, D. N. *Langmuir* **2000**, *16*, 7757; c) Friggeri, A.; van Manen, H.-J.; Auletta, T.; Li, X.-M.; Zapotoczny, S.; Schönherr, H.; Vancso, G. J.; Huskens, J.; van Veggel, F. C. J. M.; Reinhoudt, D. N. *J. Am. Chem. Soc.* **2001**, *123*, 6388.

7.1 Introduction

The development of ever more powerful microprocessors, driven by consumer demands for speed and computational power, depends heavily on continued progress in miniaturization their components (*via* “top down” methods). The enormous increase in integration density of silicon chips has been sustained in large part by advances in optical lithography. However, if the current rate of device miniaturization is to be maintained, a point will be reached where optical lithography can no longer attain the required feature sizes. Therefore scientific attention has been shifted toward X-ray, electron beam, and extreme ultraviolet lithography as successors to optical lithography in order to overcome the current resolution limits.¹ Even when these alternatives will prove to be successful, conventional silicon-based microelectronics are not expected to continue following Moore’s law due to other technological (*e.g.* heat dissipation, current leakage) and economical obstacles.

The “bottom up” strategy² is rapidly gaining importance in nanotechnology,³ as it has been realized that computation carried out by individual molecules might offer the information industry a possibility to continue the exponential increase in performance for an additional two to five decades.⁴ Already in 1974 it was proposed that a molecule with a conjugated electronic structure could act as a molecular rectifier.⁵ Since then, advances in synthetic supramolecular chemistry (in particular self-assembly⁶), coupled with developments in device fabrication and scanning probe methods,⁷ have brought the field of molecular electronics⁸ to a level where single molecules have been imaged,⁹ manipulated,¹⁰ and investigated for their electronic properties.¹¹ Recently reported molecular electronic devices, all incorporating self-assembled monolayers (*vide infra*), have demonstrated their potential as electronic switches (see also section 3.1).¹²

Self-assembled monolayers (SAMs) on surfaces are useful starting platforms for the development of nanometer-scale devices since they are highly ordered and have uniform film thicknesses.¹³ In general, SAMs are defined as monomolecular films of a surfactant formed spontaneously on a substrate upon exposure to a surfactant solution. The principal driving force for formation of these films is specific interactions between the surfactant head group and the substrate surface. Other weaker interactions, such as hydrogen bonding, π - π stacking, and Van der Waals interactions contribute to the overall order and stability of the monolayers. Virtually any functional group can be introduced into these monolayers as a tail group (either by incorporating them in the surfactant or by surface modification reactions¹⁴), and this ability to precisely control surface composition makes the monolayers invaluable tools for studying interfacial properties such as wettability, adhesion, lubrication, corrosion resistance, and electrical resistance.¹³

Besides SAM formation by organosilanes on oxidized silicon or glass substrates,¹⁵ the adsorption of organosulfur compounds on gold has probably received most attention in SAM research. Since the first sulfur-based monolayers on gold were reported in 1983 by Nuzzo and Allara,¹⁶ a plethora of sulfur-containing adsorbates has been employed in SAM formation, the most important being dialkyldisulfides (RS-SR),^{16,17} alkylthiols (RSH),¹⁸ and dialkylsulfides

(RSR)¹⁹. There are several advantages of using gold in combination with organosulfur adsorbates over other substrate-surfactant combinations. Gold, as a substrate, can be handled in ambient conditions because it does not form a stable oxide at room temperature. Moreover, the sulfur-containing adsorbates mentioned above form very stable SAMs due to strong S-Au interactions (S-Au bond strength for chemisorbed thiolates: 126 ± 2 kJ/mol,²⁰ S-Au interaction in physisorbed dibutylsulfide: 86 kJ/mol²⁰). Adsorption and desorption kinetics and thermodynamics of organosulfur adsorbate binding to gold have been studied intensively.^{13a} It is generally accepted that alkylthiols and disulfides adsorb on gold as the corresponding thiolates,^{18a,21} whereas the interaction between sulfides and gold is of a coordinative, and consequently weaker, nature. Monolayers formed from physisorption of dialkylsulfides are relatively disordered compared to thiol and disulfide SAMs.^{19a,d} In our group, SAMs formed from receptor molecules (*e.g.* resorcin[4]arenes,²² carceplexes,²³ and cyclodextrins²⁴) that contain multiple dialkylsulfide chains have been studied in great detail. The potential of such receptor adsorbate SAMs as sensing devices for a variety of analytes has been shown.²⁵

An important topic regarding application of SAMs in *e.g.* microelectronics is the ability to form *patterned* architectures on a nanometer level. Seminal advances in this direction have been made through the use of *e.g.*:

- Coadsorption of different types of adsorbates (leading to mixed monolayers);²⁶
- Microcontact printing using elastomeric stamps;²⁷
- Scanning probe lithographies such as nanoshaving/nanografting²⁸ and “dip-pen” nanolithography;²⁹
- Advanced lithographic methods such as UV,³⁰ deep UV,³¹ extreme UV,³² X-ray,^{32,33} electron beam,³⁴ and ion beam³⁵ etching.

Most of these techniques were recently reviewed.³⁶ While they have created patterns with resolutions below 10 nm, patterning SAMs with the ultimate resolution of a single molecule has remained unattainable so far.

Atomic and (sub)molecular resolution are readily obtained nowadays with scanning tunneling microscopy (STM),³⁷ whereas atomic force microscopy (AFM) requires ultrahigh vacuum to achieve true atomic and molecular, subnanometer resolution.⁷ Unlike STM, however, AFM does not require conducting samples. Moreover, shear forces between sample and tip can be minimized in AFM through the use of *tapping mode* (TM) conditions.³⁸ These features, and the fact that measurements on nanometer-sized objects can be performed even under physiological conditions in liquids, make AFM the microscopic tool of choice when studying “soft” samples such as biological materials.³⁹

Due to their nanosize dimensions, single *dendritic* molecules (see chapter 2) are amenable to investigation by AFM techniques under ambient conditions. For example, Crooks and coworkers⁴⁰ have measured the height of G4 and G8 polyamidoamine (PAMAM)

dendrimers on gold using TM-AFM. Similarly, Tomalia and coworkers⁴¹ have measured the molecular diameter and height of individual G5-G10 PAMAM dendrimers on mica, using TM-AFM. However, AFM images of individual dendrimers smaller than G5 could not easily be obtained. De Schryver and coworkers⁴² have used TM-AFM to measure the height of G4 polyphenylene dendrimer molecules spincoated on mica. Good agreement was found between the observed height and values calculated from molecular dynamics simulations.

Spatial isolation of individual molecules embedded into SAMs on gold has only been reported incidentally. Weiss *et al.* studied single, conducting molecules of 4,4'-bis(phenylene-ethynylene)-benzothioacetate incorporated into *n*-dodecanethiol SAMs by STM.⁴³ However, large clusters of molecules were also observed, probably due to fast exchange of adsorbed thiolates for solution thiols, especially at gold step edges that contain an increased number of defect sites. Similar adsorbates composed of linear phenyl oligomers were inserted into *n*-nonanethiol SAMs by Ishida *et al.*⁴⁴ Using STM experiments, the insertion process was found to depend on the organic solvent and the length of the conjugated molecule.

The insertion of a second, different adsorbate into a pre-assembled monolayer of a first adsorbate (usually an alkylthiol) is a versatile technique for creating SAMs incorporating spatially isolated molecules, which can subsequently be studied using scanning probe microscopic methods. This strategy, which makes use of the fact that surface-bound thiols can be exchanged with solution thiols or disulfides,⁴⁵ has the advantage that the ratio of the two components can be controlled, in general, by varying the insertion time or the concentration of the second adsorbate.

7.2 Aim and scope of this chapter

In our group, the incorporation of nanosize dendritic adsorbates into preformed alkylthiol SAMs has been performed using the above described insertion process. Focussing on synthetic aspects, this chapter will describe the results of these studies. Detailed monolayer⁴⁶ and AFM^{46,47} aspects of our investigations have been described elsewhere.

In the first part of this chapter, the synthesis of both non-covalent and covalent dendritic molecules functionalized with a dialkylsulfide chain suitable for binding to gold is described. Monolayer experiments that lead to spatial isolation of individual dendritic molecules on a gold surface (as demonstrated by AFM experiments) will be discussed briefly.

Having established the conditions necessary for the successful visualization of single dendritic molecules on a gold surface, the coordination chemistry of isolated SCS Pd^{II} pincer molecules, embedded into SAMs on gold, will be described in the second part of this chapter. A strategy for exchanging small, "AFM silent" ligands coordinated to Pd^{II} on the gold surface by nanosize dendritic wedges, easily identifiable by AFM, will be presented.

adsorbate **3a** to gold is mainly due to sulfide-gold interactions and not to physisorption or Van der Waals interactions between hydrocarbon chains.

Removal of the chloride ligand in pincer complexes **1a-1c** by 1 equiv of AgBF_4 , followed by addition of 1 equiv of building block **BB_{pyr}-Cl**, gave first generation dendrimers **2a-2c**. Subsequently, the two peripheral chlorides of **2a-2c** were removed with 2 equiv of AgBF_4 and 2 equiv of **BB_{pyr}-Cl** were coordinated to the vacant Pd^{II} sites to produce second generation adsorbates **3a-3c** in moderate yields. They were characterized by ^1H NMR spectroscopy and MALDI-TOF mass spectrometry (Table 7.1).

Table 7.1. ^1H NMR and MALDI-TOF MS data for metallodendritic adsorbates **3a-3c** and building blocks **BB_{pyr}-Cl** and **1a**.

Entry	Pyr α H ^a	Ar _{Pd} H ^a	ArCH ₂ S + CH ₂ N ^a	CH ₂ SCH ₂ ^a	MALDI-TOF MS Obsd/calcd (Da)
BB_{pyr}-Cl ^b	8.69	6.72	4.65	–	–
1a ^c	–	6.51	4.48 ^e	2.50	–
3a ^d	8.25	6.70	4.85-4.40	2.40	4461.3/4458.2 ^g
3b ^d	8.22	6.65	4.75-4.35	–	4437.9/4440.2 ^g
3c ^d	8.17	6.52, 6.58 ^f	4.70-4.35	–	4270.0/4271.9 ^g

^aChemical shifts in ppm relative to tetramethylsilane; ^bIn $\text{CD}_2\text{Cl}_2/\text{CD}_3\text{NO}_2$;

^cIn CDCl_3 ; ^dIn $\text{CDCl}_3/\text{CD}_3\text{NO}_2$; ^eOnly ArCH₂S protons; ^fTwo signals resolved;

^gCorresponding to $[\text{M} - \text{BF}_4]^+$.

The coordination of the pyridine ligands in **3a-3c** to the Pd^{II} pincer moieties was confirmed by the upfield shift of the α -pyridyl protons from 8.69 (in **BB_{pyr}-Cl**) to 8.25-8.17 ppm in the ^1H NMR spectra (Table 7.1), similar to previously reported metallodendrimers based on Pd^{II} -pyridine coordination.⁴⁸ Moreover, strong signals corresponding to the $[\text{M} - \text{BF}_4]^+$ species were observed for **3a-3c** in the MALDI-TOF mass spectra, and this is also in accordance with other metallodendrimers synthesized in our group (see *e.g.* chapter 4). Finally, the fact that the dendritic assemblies are only soluble in mixtures of nitromethane and chlorinated solvents (whereas building blocks **1a** and **BB_{pyr}-Cl** are highly soluble in CH_2Cl_2 and CHCl_3), is also a clear indication that the dendritic assembly has been successful. This solubility behavior of the metallodendrimers has important consequences for their insertion into preformed alkylthiol SAMs (*vide infra*).

7.3.1.2 Isolation of metallodendrimers in SAMs on gold

The insertion of dendritic adsorbate **3a** into preformed SAMs is shown schematically in Figure 7.1, together with TM-AFM images of the decanethiol monolayer before and after

exposure to the solution of **3a**. Whereas Figure 7.1a is a typical AFM image of an alkylthiol SAM on gold,⁵¹ isolated features can be observed in Figure 7.1b.

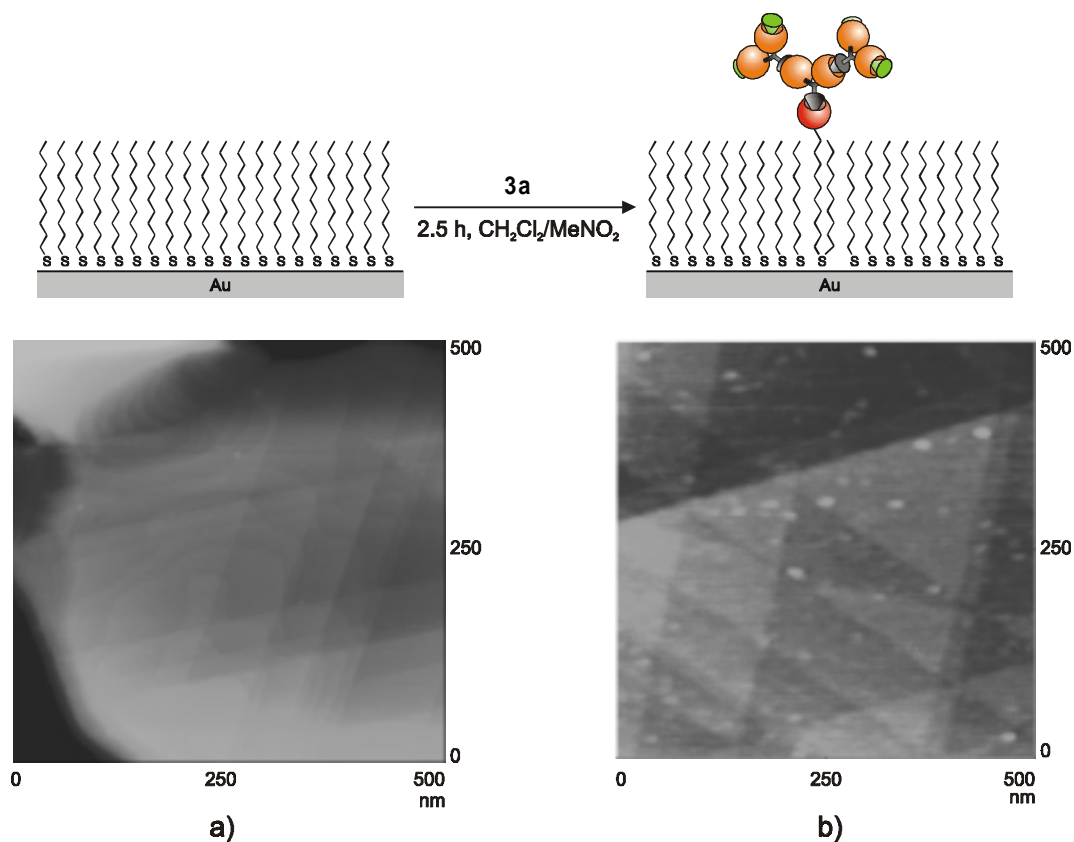
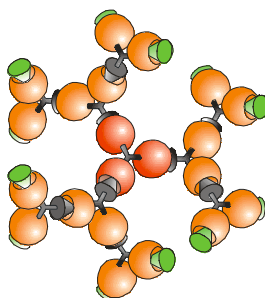


Figure 7.1. Schematic representation of the insertion of adsorbate **3a** into a decanethiol SAM, and TM-AFM images (acquired in air) before (a) and after (b) treatment of the SAM with a solution of **3a** ($44 \mu\text{M}$ in $\text{CH}_2\text{Cl}_2 / \text{CH}_3\text{NO}_2$ 1:2) for 2.5 h.

These features, having a height⁵² of 0.9 ± 0.2 nm and a width⁵³ of 23 ± 4 nm, do not change position upon repeated scanning in either tapping or contact mode, and therefore are chemisorbed on the gold surface *via* the sulfide moiety. This was confirmed by control experiments employing both adsorbates **3b-3c** and a previously reported⁴⁸ metallodendrimer **4** (which lacks both the sulfide and the alkyl chain).

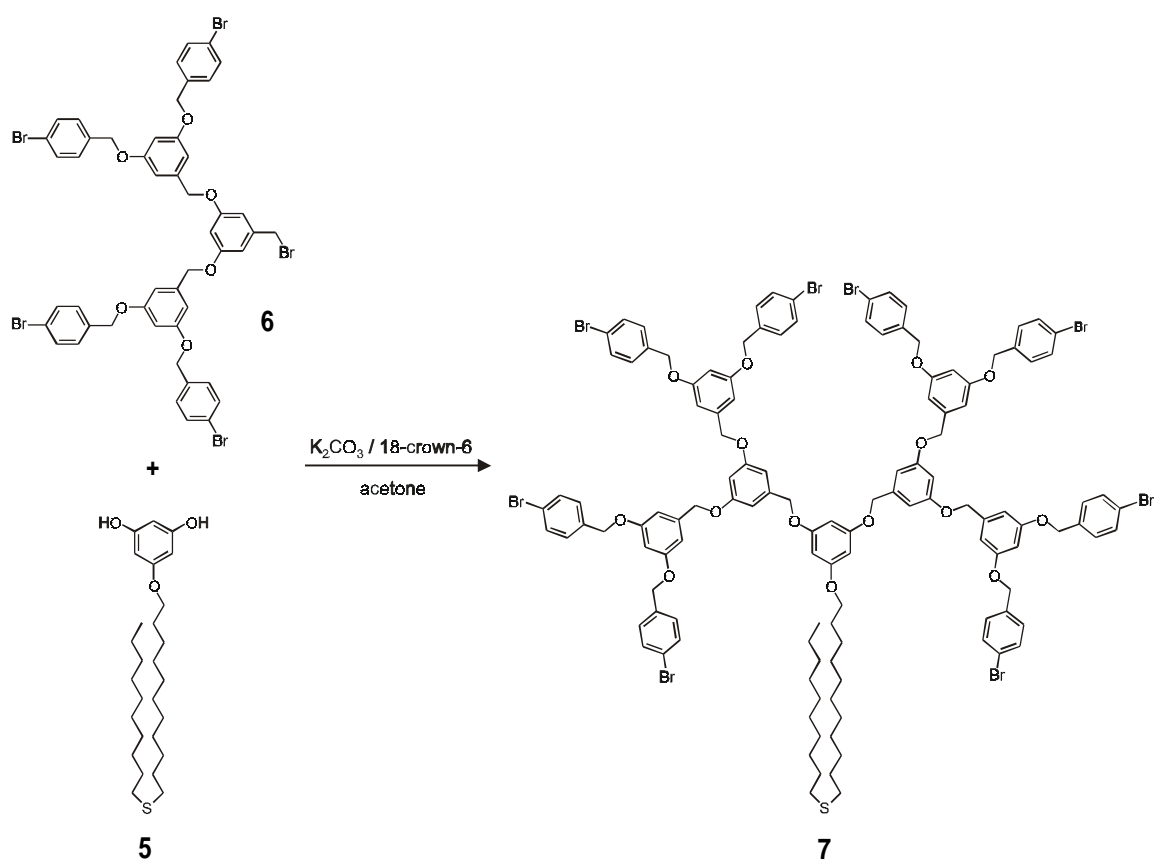


4

No features could be observed on decanethiol SAMs immersed in solutions of these control dendrimers, proving that the sulfide is essential as the anchoring point to gold. As a mechanism of the insertion process, it was hypothesized that the creation of defects in the monolayer upon exposure of the SAM to solvent is the rate-determining step.⁵⁴ The vacant sites created in this manner can be filled subsequently with the dialkylsulfide chain of the dendritic adsorbate. This hypothesis is consistent with the observation that the number of inserted features was found to be dependent on the immersion time of the SAM in the adsorbate solution. Moreover, a concentration dependence was later established by *in situ* contact mode AFM experiments.^{46c,47}

7.3.1.3 Synthesis of a covalent dendritic adsorbate

In order to perform a detailed mechanistic study on the insertion process of dendrimers into preformed SAMs *via* a thiol-sulfide exchange, a third generation covalent dendritic wedge containing a focal dialkylsulfide moiety was synthesized as outlined in Scheme 7.2. The aryl ether dendrimers first reported by Hawker and Fréchet⁵⁵ are easy to synthesize and purify, and their solubility in a range of apolar organic solvents facilitates comparison of the SAM insertion process with literature studies.



Scheme 7.2. Synthesis of third generation covalent dendritic wedge 7.

Sulfide diol **5**, which was prepared in low yield (32%) by monoalkylation of 1,3,5-trihydroxybenzene with 11-bromoundecyldecyl sulfide, was alkylated with 2 equiv of known⁵⁶ second generation dendritic wedge **6** under conventional dendritic growth conditions (K_2CO_3 and 18-crown-6 in refluxing acetone)⁵⁵ to afford adsorbate **7** in 79% yield after purification by column chromatography. Conversion of the focal benzylic bromide in **6** to the corresponding ether moieties in **7** was evidenced by a shift of the CH_2 signal from 4.40 to 4.90 ppm in the 1H NMR spectrum. Moreover, a strong signal at m/z 2538.6 corresponding to $[M + H]^+$ was observed in the positive FAB mass spectrum of **7**.

7.3.1.4 Isolation of covalent dendritic adsorbates in SAMs on gold

The insertion process of adsorbate **7** into SAMs on gold was investigated by varying the concentration of **7** in solution, the time of exposure to solvent (CH_2Cl_2) of the initial alkylthiol SAM, and the quality of the initial thiol layer. The results of these studies will briefly be summarized here.⁵⁷

An increasing number of isolated, nanometer-sized features was observed when a starting SAM of 11-mercapto-1-undecanol was exposed to solutions of increasing concentration of **7**. A representative AFM image is shown in Figure 7.2. At the maximum concentration studied (0.4 mM), the coverage⁵⁸ of dendrimer molecules was still below 1%.

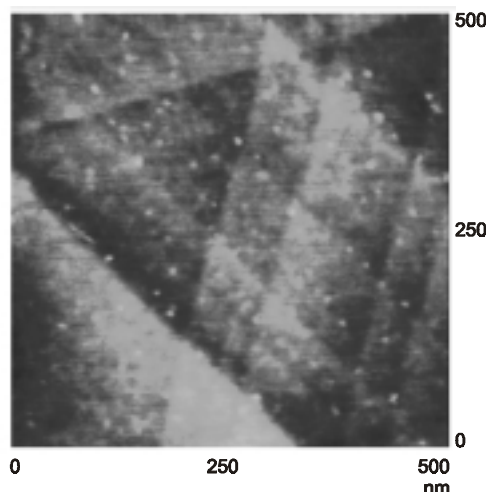


Figure 7.2. TM-AFM image (acquired in air) of dendritic wedge **7** (0.4 mM in CH_2Cl_2) inserted into a SAM of 11-mercapto-1-undecanol.

As exposure of SAMs on gold to solvent is known to cause desorption of thiols,⁴⁵ it was no surprise to find that increasing the time of exposure to solvent before insertion led to an increase in the number of inserted dendrimers. The desorption of 11-mercapto-1-undecanol from the monolayer was evidenced by electrochemical resistance measurements.

Surprisingly, the initial quality of the SAM is not a determining factor for the insertion process. With the combined available data, a mechanism for thiol-dendrimer exchange was

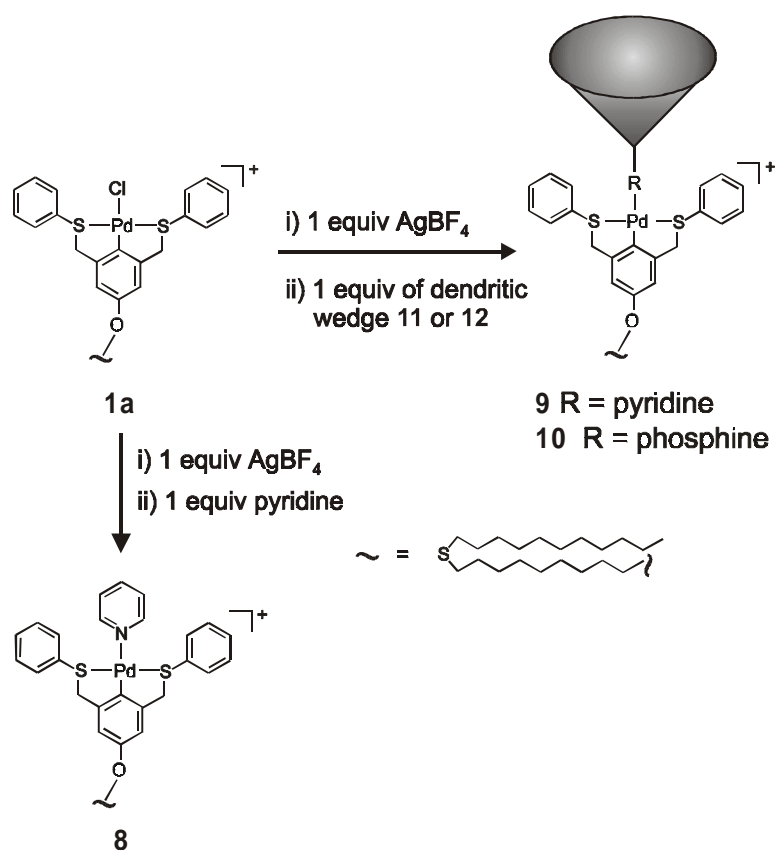
proposed which involves dissociation of the surface thiols, possibly as disulfides, followed by insertion of individual dendritic adsorbates. AFM and electrochemistry data indicate that the rate-determining step is the dendrimer insertion step, in contrast to the results described in section 7.3.1.2. However, different experimental conditions were used in that case.

7.3.2 Coordination chemistry on single SCS Pd^{II} pincers on a gold surface

7.3.2.1 Synthesis of adsorbates and solution studies

Having established favorable experimental conditions that lead to the isolation of nanometer-sized molecules on a gold surface, a next level of sophistication can be reached when dendritic growth is achieved *in situ* on the surface instead of synthesizing the adsorbates first in solution and then inserting them into monolayers. In principle metallodendritic growth should be well-suited for this purpose, since controlled dendritic growth has been demonstrated in solution by adding the required amount of silver salt and dendritic building block in cycles (see chapter 2, section 2.4.5).⁵⁹ Moreover, both chloride abstraction from Pd^{II} and subsequent coordination of dendritic building blocks to the vacant coordination site are fast processes, and this might compare favorably with often slower covalent reactions on functionalized SAMs. However, the interpretation of AFM images taken after metallodendrimer growth reactions, starting from adsorbate **3a** (Scheme 7.1) embedded as isolated molecules into a decanethiol SAM, proved to be troublesome due to the formation of insoluble residues on the monolayer (probably silver salts).

In order to avoid the use of AgBF₄ on the monolayer, the starting ligand coordinated to the Pd^{II} pincer (*i.e.* the chloride in adsorbate **1a**) should undergo replacement by other ligands *via* simple exchange reactions rather than *via* silver salt pretreatment. This excludes the commonly used chlorides as protecting ligands. However, a number of other ligands serving as temporary protecting moieties can be envisaged. Such ligands should, on one hand, be strong enough to exclude the intra- or intermolecular coordination of the dialkylsulfide moiety to Pd^{II} (which would cause polymerization in the case of intermolecular coordination), and, on the other hand, be weak enough to allow their substitution with stronger ligands. From our studies on the coordination strengths of a variety of ligands toward the SCS Pd^{II} pincer system (see chapter 3), it seems that pyridines are suitable ligands for this task. They are stronger ligands than sulfides, but at the same time they are easily substituted by phosphines. In order to test the feasibility of this strategy, adsorbates **8-10** were synthesized as shown in Scheme 7.3.



Scheme 7.3. Synthesis of adsorbates **8-10**.

Deprotection of the chloride ligand in **1a** using 1 equiv of AgBF_4 , followed by addition of 1 equiv of pyridine resulted in cationic pyridine complex **8**. The coordination of pyridine to Pd^{II} was evident from the ^1H NMR spectrum, in which a broad signal was observed at 8.11 ppm for the α -pyridyl protons, similar to analogous pyridine complexes reported in chapter 3 (section 3.4.3). No evidence for sulfide coordination was found in the ^1H NMR spectrum.⁶⁰

In order to determine by AFM whether the exchange of the pyridine ligand by another ligand could be successfully performed, second generation dendritic wedges **11** and **12** (Chart 7.1) having a focal pyridine and phosphine, respectively, were synthesized. Upon replacement of the “AFM silent” pyridine ligand of adsorbate **8**, embedded into an alkylthiol SAM, by these nanosize dendritic wedges, isolated features similar to those shown in Figures 7.1 and 7.2 should be observed.

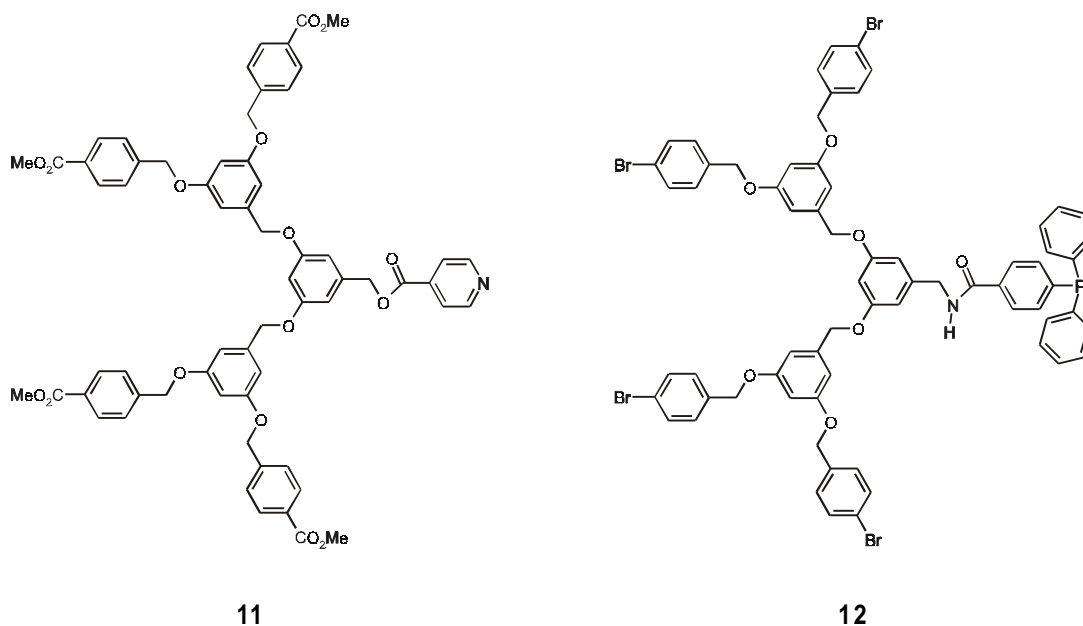
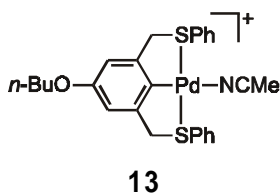


Chart 7.1.

Dendron **11** was prepared in 62% yield from the corresponding dendritic wedge containing a focal benzylic alcohol⁶¹ by esterification with isonicotinoyl chloride. Its coordination behavior toward an SCS Pd^{II} pincer system was tested with acetonitrile complex **13**, the synthesis of which was described in chapter 3. Upon mixing stoichiometric amounts of **11** and **13** in CDCl₃, the quantitative substitution of the labile acetonitrile ligand by dendron **11** was determined by ¹H NMR spectroscopy, *e.g.* a diagnostic upfield shift of the α -pyridyl protons of **11** from 8.75 to 8.42 ppm was observed upon coordination. The synthesis of dendron **12** and its successful coordination to various SCS Pd^{II} pincers was already described in chapter 4.



Besides adsorbate **8** having a pyridine ligand, adsorbates **9** and **10** (Scheme 7.3) were prepared as reference compounds. Comparing the AFM results of the growth process *on the monolayer* with results obtained from insertion of these preassembled reference compounds into alkylthiol SAMs should provide valuable information about the viability of our strategy. Compounds **9** and **10** were synthesized in solution by removal of the inert chloride ligand of **1a** with AgBF₄, followed by addition of dendritic wedges **11** and **12**, respectively. In the case of **11**, ¹H NMR spectroscopy indicated that, in addition to the pyridine wedge, the dialkylsulfide also coordinated to Pd^{II} because the binding strengths of the pyridine ester and the dialkylsulfide are similar. Two sets of signals were observed for both the pyridine α protons, the CH₂S protons of the cyclopalladated pincer system, and the CH₂S protons of the sulfide chain. From the integrals of these signals a

ratio of 4:1 was determined for coordinated pyridine wedge versus coordinated sulfide. Upon addition of excess pyridine wedge, an increasing amount of pyridine wedge was found to coordinate to the Pd^{II} pincer, however, a product free of coordinated sulfide could not be obtained. However, after insertion of adsorbate **8** into SAMs on gold, the sulfide is not available for coordination to the Pd^{II} pincer anymore, and substitution of the coordinated pyridine ligand in **8** by pyridine wedge **11** might still occur, taking into account the large excess of **11** that will be present and the fact that the distribution of different, coordinated ligands is thermodynamically controlled (see chapter 3).

When adsorbate **8** was treated with phosphine-functionalized dendritic wedge **12** *in solution*, the quantitative substitution of the pyridine ligand by the phosphine dendron (providing adsorbate **10**) was observed by ¹H and ³¹P NMR spectroscopy. Most diagnostic is the shift of the phosphorus signal from -5.6 (free **12**) to 13.6 ppm (coordinated **12**) in the ³¹P NMR spectrum upon coordination. Moreover, a signal at *m/z* 2118.6 corresponding to [M – BF₄]⁺ was observed in the positive FAB mass spectrum of **10**.

Since the exchange of coordinated pyridine in **8** by dendritic wedges proceeds partially (for **11**) and completely (for **12**), studies aiming at this exchange on adsorbate **8** *embedded in a monolayer* were undertaken using these dendritic wedges. The results will be described in the next section.

7.3.2.2 Spatial isolation of individual dendrons on gold

Insertion reactions with adsorbate **8** starting from a hydrophilic 11-mercapto-1-undecanol SAM on gold, followed by immersion of the substrates into solutions of varying concentrations of dendritic wedges **11** and **12** gave very large features, indicating physisorbed material.^{46c} TM-AFM experiments of hydrophobic decanethiol monolayers on gold subjected to the same procedure revealed also large features in the case of pyridine wedge **11**. On the other hand, experiments employing decanethiol SAMs and phosphine wedge **12** (0.01 mM solution in CH₂Cl₂, 10 min immersion time) instead of pyridine wedge **11** did reveal the presence of isolated features in the AFM images.⁶² A representative TM-AFM image of a SAM containing individual nanosize dendrons coordinated to the pincer moiety of adsorbate **8**, embedded in the decanethiol monolayer, is shown in Figure 7.3, along with a height profile.

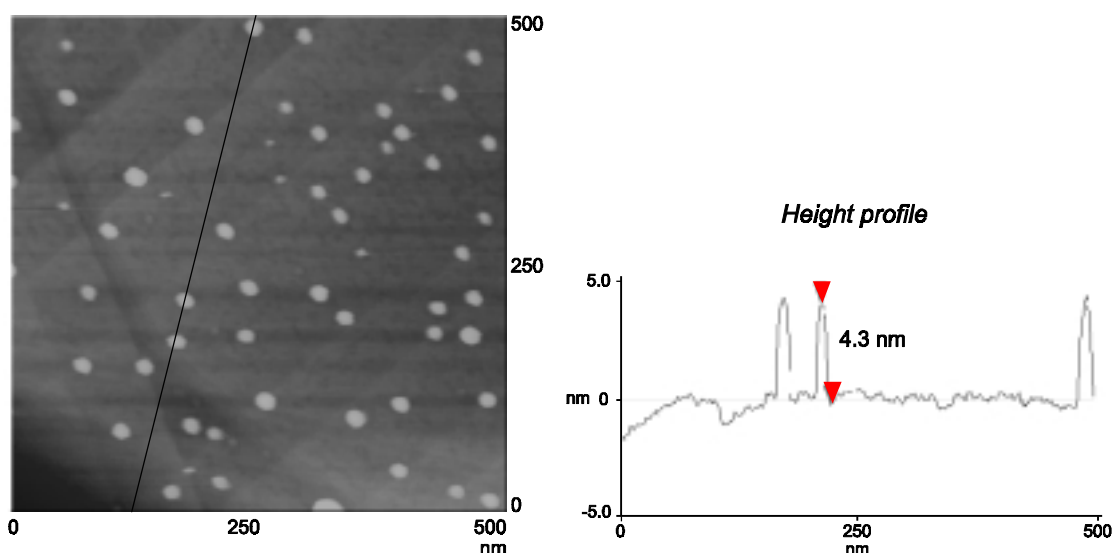


Figure 7.3. Representative TM-AFM image (acquired in air) of Pd(II) pincer-containing (**8**) decanethiol SAM after exposure to a 0.01 mM CH_2Cl_2 solution of dendrimer wedge **12** for 10 min. The height profile shown on the right corresponds to the line drawn in the AFM image (z -scale = 10 nm).

The height and width⁵³ of these features, determined by AFM, are 4.3 ± 0.2 and 15.3 ± 4 nm, respectively. From a computer-generated molecular model it was estimated that adsorbate **10** protrudes approximately 3.5 nm above the decanethiol layer, when fully stretched (Figure 7.4). Therefore, the average height determined by AFM is in reasonable agreement with the calculated value. The very soft TM-AFM conditions employed in these experiments might render the height value a good representation of the feature height.⁶³

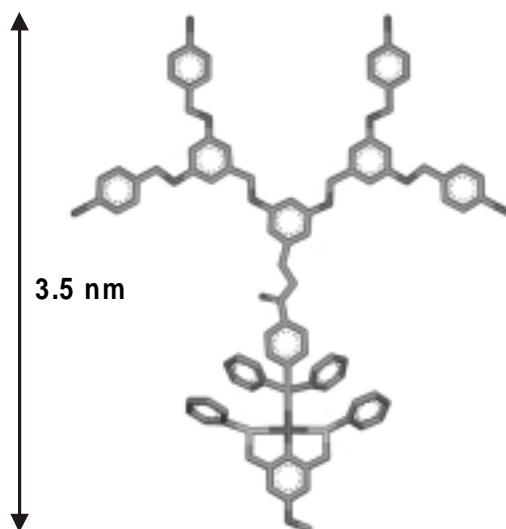


Figure 7.4. The part of adsorbate **10** that protrudes above the decanethiol monolayer, obtained by a computer-generated molecular model. Hydrogen atoms have been omitted for clarity.

To certify that the nanometer-sized features observed in Figure 7.3 are single dendritic molecules, direct insertion of dendritic adsorbate complex **10** was carried out, which should yield

similar layers as the surface reaction described above. Using the same atomic force microscopy conditions as for the previous experiments, nanometer-sized features, very similar to those observed after the single molecule growth experiments, were observed.^{46b} The height and width of the features, as determined by TM-AFM, are 4.1 ± 0.2 nm and 18.8 ± 4 nm, respectively, which corresponds very well to the dimensions of the molecules synthesized on the monolayer by reaction of isolated pincer adsorbates **8** with dendritic wedge **12**.

7.4 Conclusions

Both metallodendrimers and covalent dendrimers, functionalized with a dialkylsulfide chain for anchorage to a gold surface, have been synthesized, as described in the first part of this chapter. The successful incorporation of these dendrimers as isolated species into preassembled monolayers of alkylthiols, as determined by tapping mode AFM experiments, has briefly been discussed. In the second part, a strategy for performing coordination chemistry on isolated Pd^{II} pincer molecules inserted into alkanethiol SAMs on gold has been presented. It has been shown that the coordination of phosphines to Pd^{II} pincers can be used to successfully grow isolated molecules into nanometer-sized features which can be detected by AFM. This approach offers the possibility to isolate functional nanometer-sized objects, as shown by spatial confinement of dendritic structures.

Using the strategy presented in this chapter, a next level of complexity is obtained when the single dendritic molecules observable by AFM can be grown on the monolayer, in a controlled manner, into objects of even greater dimensions. Results concerning this topic will be described in chapter 8.

7.5 Experimental Section

General comments. For general information on instruments, procedures, and chemicals, see chapter 3. For a description of MALDI-TOF experiments, see chapter 4. Monolayer experiments were performed by A. Friggeri (metallodendrimers, covalent dendrimers, dendrimer growth reactions), and B.-H. Huisman (metallodendrimers).

Materials. Dendritic wedge (MeO₂C)₄-[G-2]-OH,⁶¹ Pd^{II} pincer adsorbate **1a**,⁶⁴ and 3,5-bis(phenylthiamethyl)phenol⁶⁵ were prepared according to reported procedures. The synthesis of dendritic phosphine wedge **12** was described in chapter 4.

General procedure for the preparation of pincer ligands containing C22 and C10 alkyl chains. 3,5-Bis(phenylthiamethyl)phenol was alkylated with docosyl (C22) and decyl (C10) bromide according to the procedure described in chapter 3 for the synthesis of 3,5-bis(phenylthiamethyl)-*n*-butoxybenzene.

C22 pincer ligand. White solid. Yield 1.30 g (73%). M. p. 67-68 °C. ¹H NMR: δ (ppm) 7.32-7.16 (m, 10 H, SPh H), 6.82 (s, 1 H, Ar H), 6.71 (s, 2 H, Ar H), 4.04 (s, 4 H, CH₂S), 3.85 (t, $J = 6.6$ Hz, 2 H, CH₂O),

1.72 (quint, $J = 7.2$ Hz, 2 H, $\text{CH}_2\text{CH}_2\text{O}$), 1.44-1.22 (m, 38 H, CH_2), 0.89 (t, $J = 6.6$ Hz, 3 H, CH_3). ^{13}C NMR: δ (ppm) 159.3, 139.0, 136.3, 129.8, 128.8, 126.3, 121.5, 113.8, 68.0, 39.0, 31.9, 29.7-29.2, 26.0, 22.7, 14.2. FAB-MS m/z 646.3 ($[\text{M}]^+$, calcd 646.4). Anal. calcd for $\text{C}_{42}\text{H}_{62}\text{OS}_2 \cdot 0.1\text{H}_2\text{O}$: C, 77.74; H, 9.66; S, 9.88. Found: C, 77.52; H, 9.61; S, 9.85.

C10 pincer ligand. Transparent oil. Yield 1.59 g (81%). ^1H NMR: δ (ppm) 7.32-7.15 (m, 10 SPh H), 6.82 (s, 1 H, Ar H), 6.71 (s, 2 H, Ar H), 4.04 (s, 4 H, CH_2S), 3.85 (t, $J = 6.6$ Hz, 2 H, CH_2O), 1.73 (quint, $J = 6.6$ Hz, 2 H, $\text{CH}_2\text{CH}_2\text{O}$), 1.46-1.30 (m, 14 H, CH_2), 0.90 (t, $J = 6.6$ Hz, 3 H, CH_3). ^{13}C NMR: δ (ppm) 159.3, 139.0, 136.3, 129.8, 128.9, 126.4, 121.5, 113.8, 68.0, 39.0, 31.9, 29.6-29.2, 26.0, 22.7, 14.2. FAB-MS m/z 477.1 ($[\text{M} - \text{H}]^+$, calcd for $\text{C}_{30}\text{H}_{37}\text{OS}_2$: 477.2).

General procedure for the preparation of Pd^{II} pincers **1b and **1c**.** The C22 and C10 pincer ligands were cyclopalladated according to the procedure described in chapter 3 for the cyclopalladation of 3,5-bis(phenylthiamethyl)-*n*-butoxybenzene, *i.e.* cyclopalladation with $\text{Pd}[\text{MeCN}]_4(\text{BF}_4)_2$ in MeCN for 1 h, followed by treatment with NaCl in $\text{CH}_2\text{Cl}_2/\text{H}_2\text{O}$. Both **1b** and **1c** were purified by column chromatography using $\text{CH}_2\text{Cl}_2/\text{acetone}$ 97:3 (v/v) as the eluent.

C22 Pd^{II} pincer **1b.** Yellow solid. Yield 0.15 g (58%). M. p. 98-100 °C; ^1H NMR: δ (ppm) 7.83-7.79 (m, 4 H, Ar H), 7.35-7.33 (m, 6 H, Ar H), 6.56 (s, 2 H, Ar H), 4.53 (br s, 4 H, CH_2S), 3.84 (t, $J = 6.4$ Hz, 2 H, CH_2O), 1.72 (quint, $J = 7.2$ Hz, 2 H, $\text{CH}_2\text{CH}_2\text{O}$), 1.40-1.20 (m, 38 H, CH_2), 0.87 (t, $J = 6.6$ Hz, 3 H, CH_3). ^{13}C NMR: δ (ppm) 157.0, 151.4, 150.1, 132.5, 131.4, 129.7, 129.6, 108.8, 68.1, 51.7, 31.9, 29.7-29.3, 26.1, 22.7, 14.2. FAB-MS m/z 751.4 ($[\text{M} - \text{Cl}]^+$, calcd 751.3). Anal. calcd for $\text{C}_{42}\text{H}_{61}\text{ClOPdS}_2$: C, 64.02; H, 7.80; S, 8.14. Found: C, 63.78; H, 7.76; S, 8.13.

C10 Pd^{II} pincer **1c.** Yellow oil. Yield 0.17 g (66%). ^1H NMR: δ (ppm) 7.82-7.79 (m, 4 H, Ar H), 7.35-7.32 (m, 6 H, Ar H), 6.56 (s, 2 H, Ar H), 4.53 (br s, 4 H, CH_2S), 3.84 (t, $J = 6.4$ Hz, 2 H, CH_2O), 1.72 (quint, $J = 6.6$ Hz, 2 H, $\text{CH}_2\text{CH}_2\text{O}$), 1.41-1.20 (m, 14 H, CH_2), 0.86 (t, $J = 6.6$ Hz, 3 H, CH_3). ^{13}C NMR: δ (ppm) 157.0, 151.4, 150.1, 132.4, 131.3, 129.7, 129.6, 108.9, 68.1, 51.6, 31.9, 29.6-29.3, 26.1, 22.7, 14.2. FAB-MS m/z 583.1 ($[\text{M} - \text{Cl}]^+$, calcd for $\text{C}_{30}\text{H}_{37}\text{ClOPdS}_2$: 583.1).

General procedure for the synthesis of metallodendrimers **3b and **3c**.** Both metallodendrimers **3b** and **3c** were synthesized according to the procedure reported for adsorbate **3a**.⁶⁴

C22 metallodendrimer **3b.** Yield 10 mg (31%). ^1H NMR ($\text{CHCl}_3/\text{CD}_3\text{NO}_2$): δ (ppm) 8.22 (br s, 6 H, pyr α H), 7.80-7.70 (br s, 15 H, pyr β H + Ar H), 7.65-7.50 (br s, 28 H, SPh H), 7.35-7.18 (br s, 42 H, SPh H), 6.70-6.50 (br s, 14 H, Ar_{Pd} H), 4.90 (br s, 12 H, CH_2O), 4.75-4.35 (br s, 34 H, $\text{CH}_2\text{S} + \text{CH}_2\text{N}$), 3.80 (br s, 2 H, OCH_2), 1.60 (br s, 2 H, OCH_2CH_2), 1.35-1.10 (br s, 38 H, CH_2), 0.78 (br s, 3 H, CH_3). MALDI-TOF MS m/z 4437.9 ($[\text{M} - \text{BF}_4]^+$, calcd for $\text{C}_{207}\text{H}_{199}\text{B}_2\text{Cl}_4\text{F}_8\text{N}_6\text{O}_{10}\text{Pd}_7\text{S}_{14}$: 4440.2).

C10 metallodendrimer **3c.** Yield 16 mg (43%). ^1H NMR ($\text{CHCl}_3/\text{CD}_3\text{NO}_2$): δ (ppm) 8.17 (br s, 6 H, pyr α H), 7.80-7.75 (br s, 15 H, pyr β H + Ar H), 7.65-7.50 (br s, 28 H, SPh H), 7.40-7.20 (br s, 42 H, SPh

H), 6.58 (s, 8 H, Ar_{Pd} H), 6.52 (s, 6 H, Ar_{Pd} H), 4.92 (s, 12 H, CH₂O), 4.70-4.35 (br s, 34 H, CH₂S + CH₂N), 3.86 (br s, 2 H, OCH₂), 1.63 (br s, 2 H, OCH₂CH₂), 1.36-1.10 (br s, 14 H, CH₂), 0.75 (s, 3 H, CH₃). MALDI-TOF MS m/z 4270.0 ([M – BF₄]⁺, calcd for C₁₉₅H₁₇₅B₂Cl₄F₈N₆O₁₀Pd₇S₁₄: 4271.9).

Sulfide pincer, pyridine complex (8). To a solution of the sulfide pincer **1a** (8.1 mg, 10.1 μmol) in CH₂Cl₂ (3 mL) were added a few drops of MeCN. Next 78 μL (10.1 μmol) of a stock solution of AgBF₄ in water (0.130 M) was added, and the resulting mixture was stirred for 10 min. A white precipitate formed, indicating the formation of insoluble AgCl. Subsequently, pyridine (90 μL of a 0.120 M stock solution in CH₂Cl₂, 10.8 μmol) was added. After the mixture was stirred at r.t. for 10 min, it was filtered through Hyflo into a 10 mL volumetric flask. The volumetric flask was filled with CH₂Cl₂ to 10 mL, providing a 1 mM solution of the pyridine complex of the sulfide pincer. For analytical investigation, this process was carried out in deuterated solvents. ¹H NMR: δ (ppm) 8.11 (br s, 2 H, pyr α H), 7.72 (br, 1 H, pyr γ H), 7.64-7.62 (m, 4 H, SPh H), 7.40-7.37 (m, 6 H, SPh H), 7.29 (d, $J = 5.7$ Hz, 2 H, pyr β H), 6.64 (s, 2 H, Ar H), 4.72 (br s, 4 H, CH₂S), 3.88 (t, $J = 6.6$ Hz, 2 H, CH₂O), 2.46 (t, $J = 7.2$ Hz, 4 H, CH₂SCH₂), 1.65 (quint, $J = 6.6$ Hz, 2 H, OCH₂CH₂), 1.55-1.45 (br m, 4 H, CH₂CH₂SCH₂CH₂), 1.40-1.14 (m, 28 H, CH₂), 0.90 (t, $J = 6.6$ Hz, 3 H, CH₃).

Sulfide pincer, pyridine wedge complex (9). The sulfide pincer **1a** (4.1 mg, 5.1 μmol) was deprotected with AgBF₄ in the same manner as described above, and subsequently (MeO₂C)₄-[G-2]-pyr (5.5 mg, 5.1 μmol) was added. After filtration of the solution through Hyflo, the solvents were evaporated *in vacuo*. ¹H NMR spectroscopy indicated coordination of both the pyridine wedge and the sulfide chain to Pd^{II}, *e.g.* δ (ppm) 8.8 and 8.4 for uncoordinated and coordinated α-pyridyl protons, respectively.

Sulfide pincer, phosphine wedge complex (10). The sulfide pincer **1a** (4.3 mg, 5.3 μmol) was deprotected with AgBF₄ in the same manner as described above, and subsequently dendritic phosphine wedge **12** (7.2 mg, 5.3 μmol) was added. After filtration of the solution through Hyflo, the solvents were evaporated *in vacuo* to give the product as a yellow solid in quantitative yield. M.p. 85-87 °C. ¹H NMR: δ (ppm) 8.02 (t, $J = 6.2$ Hz, 1 H, NH), 7.73 (d, $J = 8.3$ Hz, 2 H, Ar H), 7.48-7.10 (m, 36 H, Ar H), 6.89 (t, $J = 8.4$ Hz, 2 H, Ar H), 6.79 (d, $J = 2.4$ Hz, 2 H, Ar H), 6.69 (d, $J = 2.1$ Hz, 4 H, Ar H), 6.65 (d, $J = 2.7$ Hz, 2 H, Ar H), 6.44-6.43 (m, 3 H, Ar H), 5.00 (s, 4 H, CH₂O), 4.96 (s, 8 H, CH₂O), 4.71 (br s, 4 H, CH₂S), 4.58 (d, $J = 6.2$ Hz, 2 H, CH₂N), 3.88 (t, $J = 6.6$ Hz, 2 H, CH₂O), 2.48 (t, $J = 7.2$ Hz, 4 H, CH₂SCH₂), 1.74 (quint, $J = 6.6$ Hz, 2 H, OCH₂CH₂), 1.56 (quint, $J = 7.2$ Hz, 4 H, CH₂CH₂SCH₂CH₂), 1.46-1.25 (m, 28 H, CH₂), 0.87 (t, $J = 6.6$ Hz, 3 H, CH₃). ³¹P NMR: δ (ppm) 13.6. FAB-MS m/z 2118.6 ([M – BF₄]⁺, calcd 2119.3). Anal. calcd for C₁₀₉H₁₁₄BBr₄F₄NO₈PPdS₃·0.3H₂O: C, 59.20; H, 5.22; N, 0.63. Found: C, 58.84; H, 5.22; N, 0.68.

(MeO₂C)₄-[G-2]-pyr (11). A solution of isonicotinoyl chloride hydrochloride (0.46 g, 2.6 mmol) and NEt₃ (0.85 mL, 6.1 mmol) in CH₂Cl₂ (25 mL) was added dropwise to a solution of dendritic wedge (MeO₂C)₄-[G-2]-OH (1.00 g, 1.0 mmol) in CH₂Cl₂ (75 mL). The mixture was stirred at r.t. overnight under an argon atmosphere. After the addition of 1 M HCl (100 mL), the organic phase was separated and washed with NaHCO₃ (sat.) and brine, and subsequently dried over anhydrous Na₂SO₄. After evaporation

of the solvent *in vacuo*, the crude product was purified by column chromatography, using CH₂Cl₂/acetone 90:10 (v/v) as the eluent, affording a white solid. Yield 0.69 g (62%). Mp 79-81 °C. ¹H NMR δ (ppm) 8.75 (d, *J* = 5.7 Hz, 2 H, pyr α H), 8.02 (d, *J* = 8.1 Hz, 8 H, Ar H), 7.82 (d, *J* = 5.7 Hz, 2 H, pyr β H), 7.45 (d, *J* = 8.1 Hz, 8 H, Ar H), 6.65 (d, *J* = 2.2 Hz, 4 H, Ar H), 6.61 (d, *J* = 2.2 Hz, 2 H, Ar H), 6.54-6.52 (m, 3 H, Ar H), 5.28 (s, 2 H, CH₂O), 5.08 (s, 8 H, CH₂O), 4.97 (s, 4 H, CH₂O), 3.90 (s, 12 H, CO₂CH₃). ¹³C NMR δ (ppm) 166.2, 159.5, 159.4, 150.0, 141.3, 138.8, 137.0, 136.7, 129.4, 129.2, 126.5, 106.8, 105.9, 101.4, 101.1, 69.4, 68.9, 66.7, 51.6. FAB-MS *m/z* 1082.3 ([M + H]⁺, calcd 1082.4). Anal. calcd for C₆₃H₅₅NO₁₆·H₂O: C, 68.78; H, 5.22; N, 1.27. Found: C, 68.76; H, 5.12; N, 1.23.

7.6 References and notes

- ¹ a) Ito, T.; Okazaki, S. *Nature* **2000**, *406*, 1027; b) Walraff, G. M.; Hinsberg, W. D. *Chem. Rev.* **1999**, *99*, 1801.
- ² For a bottom-up approach to molecular computers, see: Dagani, R. *Chem. Eng. News* **2000**, *78* (42), 27.
- ³ a) *Handbook of Nanostructured Materials and Nanotechnology*; Nalwa, H. S., Ed.; Academic Press: London, UK, 2000; b) A recent issue of *Chemical Reviews* was entirely devoted to Nanostructures: *Chem. Rev.* **1999**, *99*, No. 7.
- ⁴ Ball, P. *Nature* **2000**, *406*, 118.
- ⁵ Aviram, A.; Ratner, M. A. *Chem. Phys. Lett.* **1974**, *29*, 277.
- ⁶ a) Templating, Self-assembly, and Self-organization. *Comprehensive Supramolecular Chemistry*; Lehn, J.-M., Chair Ed.; Atwood, J. L., Davis, J. E. D., MacNicol, D. D., Vögtle, F., Exec. Eds.; Pergamon: Oxford, UK, 1987-1996; Vol. 9.
- ⁷ a) Wiesendanger, R. *Scanning Probe Microscopy and Spectroscopy: Methods and Applications*; Cambridge University Press: Cambridge, 1994; b) *Scanning Probe Microscopy: Analytical Methods*; Wiesendanger, R., Ed.; Springer-Verlag: Berlin, 1998
- ⁸ a) *Introduction to Molecular Electronic Devices*; Petty, M. C.; Bryce, M. R.; Bloor, D., Eds.; Oxford University Press: New York, 1995; b) *Molecular Electronics*; Jortner, J.; Ratner, M., Eds.; Blackwell Science: Oxford, 1997; c) *Molecular Electronics: Science and Technology*; Aviram, A.; Ratner, M., Eds.; New York Academy of Sciences: New York, 1998.
- ⁹ For reviews see: a) Ishii, Y., Yanagida, T. *Single Mol.* **2000**, *1*, 5; b) Anderson, H. L. *Angew. Chem. Int. Ed.* **2000**, *39*, 2451; c) McCarthy, G. S.; Weiss, P. S. *Chem. Rev.* **1999**, *99*, 1983; d) Weiss, S. *Science* **1999**, *283*, 1676; e) Takano, H.; Kenseth, J. R.; Wong, S.-S.; O'Brien, J. C.; Porter, M. D. *Chem. Rev.* **1999**, *99*, 2845; f) Dunn, R. C. *Chem. Rev.* **1999**, *99*, 2891.
- ¹⁰ a) Hla, S.-W.; Bartels, L.; Meyer, G.; Rieder, K.-H. *Phys. Rev. Lett.* **2000**, *85*, 2777; b) Meyer, G.; Repp, J.; Zöphel, S.; Braun, K.-F.; Hla, S.-W.; Fölsch, S.; Bartels, L.; Moresco, F.; Rieder, K.-H. *Single Mol.* **2000**, *1*, 79; c) Shigekawa, H.; Miyake, K.; Sumaoka, J.; Harada, A.; Komiyama, M. *J. Am. Chem. Soc.* **2000**, *122*, 5411; d) Gimzewski, J. K.; Joachim, C. *Science* **1999**, *283*, 1683; e) Mehta, A. D.; Rief, M.; Spudich, J. A.; Smith, D. A.; Simmons, R. M. *Science* **1999**, *283*, 1689; f) Nyffenegger, R.; Penner, R. M. *Chem. Rev.* **1997**, *97*, 1195; g) Avouris, P. *Acc. Chem. Res.* **1995**, *28*, 95; h) Stroschio, J. K.; Eigler, D. M. *Science* **1991**, *254*, 1319.
- ¹¹ a) Tans, S. J.; Verschueren, A. R. M.; Dekker, C. *Nature* **1998**, *393*, 49; b) Reed, M. A.; Zhou, C.; Muller, C. J.; Burgin, T. P.; Tour, J. M. *Science* **1997**, *278*, 252; c) Klein, D. L.; McEuen, P. L.;

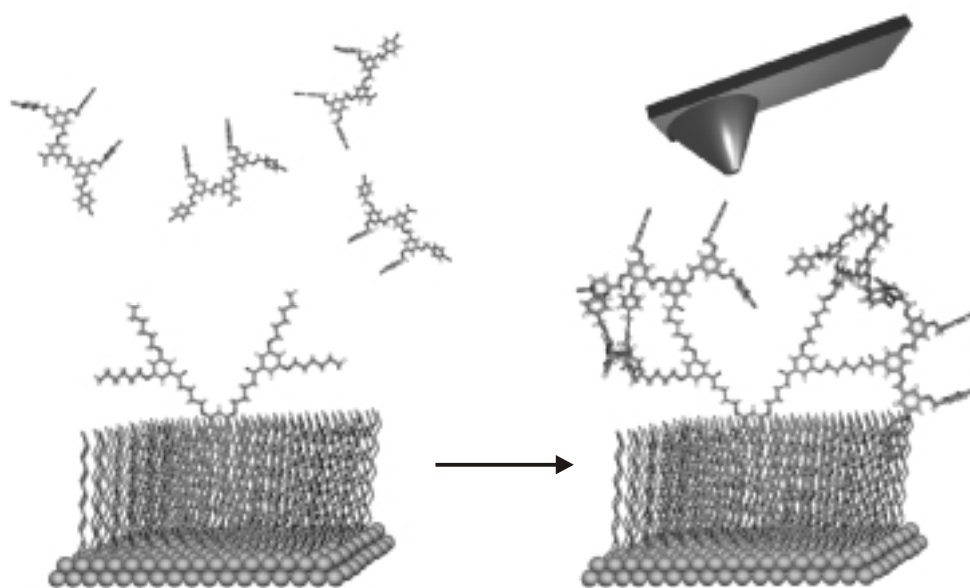
- Katari, J. E. B.; Roth, R.; Alivisatos, A. P. *Appl. Phys. Lett.* **1996**, *68*, 2574; d) Joachim, C.; Gimzewski, J. K.; Schlittler, R. R.; Chavy, C. *Phys. Rev. Lett.* **1995**, *74*, 2102.
- ¹² a) Gittins, D. I.; Bethell, D.; Schiffrin, D. J.; Nichols, R. J. *Nature* **2000**, *408*, 67; b) Collier, C. P.; Mattersteig, G.; Wong, E. W.; Luo, Y.; Beverly, K.; Sampaio, J.; Raymo, F. M.; Stoddart, J. F.; Heath, J. R. *Science* **2000**, *289*, 1172; c) Chen, J.; Reed, M. A.; Rawlett, A. M.; Tour, J. M. *Science* **1999**, *286*, 1550.
- ¹³ a) Schreiber, F. *Progr. Surf. Sci.* **2000**, *65*, 151; b) Ulman, A. *An Introduction to Ultrathin Organic Films: From Langmuir-Blodgett to Self-Assembly*, Academic Press: San Diego, CA, 1991; b) Ulman, A. *Chem. Rev.* **1996**, *96*, 1533.
- ¹⁴ Chechik, V.; Crooks, R. M.; Stirling, C. J. M. *Adv. Mater.* **2000**, *12*, 1161.
- ¹⁵ a) Sagiv, J. *Israel J. Chem.* **1979**, *18*, 339; b) Sagiv, J. *J. Am. Chem. Soc.* **1980**, *102*, 92; c) Maoz, R.; Sagiv, J. *J. Coll. Interface Sci.* **1984**, *100*, 465.
- ¹⁶ Nuzzo, R. G.; Allara, D. L. *J. Am. Chem. Soc.* **1983**, *105*, 4481.
- ¹⁷ a) Biebuyck, H. A.; Bain, C. D.; Whitesides, G. M. *Langmuir* **1994**, *10*, 1825; b) Offord, D. A.; John, C. M.; Griffin, J. H. *Langmuir* **1994**, *10*, 761; c) Schönherr, H.; Ringsdorf, H. *Langmuir* **1996**, *12*, 3891; d) Jung, C.; Dannenberger, O.; Xu, Y.; Buck, M.; Grunze, M. *Langmuir* **1998**, *14*, 1103.
- ¹⁸ a) Nuzzo, R. G.; Zegarski, B. R.; Dubois, L. H. *J. Am. Chem. Soc.* **1987**, *109*, 733; b) Porter, M. D.; Bright, T. B.; Allara, D. L.; Chidsey, C. E. D. *J. Am. Chem. Soc.* **1987**, *109*, 3559; c) Bain, C. D.; Whitesides, G. M. *Science* **1988**, *240*, 62; d) Bain, C. D.; Troughton, E. B.; Tao, Y.-T.; Evall, J.; Whitesides, G. M.; Nuzzo, R. G. *J. Am. Chem. Soc.* **1989**, *111*, 7164.
- ¹⁹ a) Troughton, E. B.; Bain, C. D.; Whitesides, G. M.; Nuzzo, R. G.; Allara, D. L.; Porter, M. D. *Langmuir* **1988**, *4*, 365; b) Steinberg, S.; Rubinstein, I. *Langmuir* **1992**, *8*, 1183; c) Hagenhoff, B.; Benninghoven, A.; Spinke, J.; Liley, M.; Knoll, W. *Langmuir* **1993**, *9*, 1622; d) Zhang, M.; Anderson, M. R. *Langmuir* **1994**, *10*, 2807; e) Beulen, M. W. J.; Huisman, B.-H.; van der Heijden, P. A.; van Veggel, F. C. J. M.; Simons, M. G.; Biemond, E. M. E. F.; de Lange, P. J.; Reinhoudt, D. N. *Langmuir* **1996**, *12*, 6170.
- ²⁰ a) Wetterer, S. M.; Lavrich, D. J.; Cummings, T.; Bernasek, S. L.; Scoles, G. *J. Phys. Chem. B* **1998**, *102*, 9266; b) Lavrich, D. J.; Wetterer, S. M.; Bernasek, S. L.; Scoles, G. *J. Phys. Chem. B* **1998**, *102*, 3456.
- ²¹ Cleavage of disulfides on gold: a) Biebuyck, H. A.; Whitesides, G. M. *Langmuir* **1993**, *9*, 1766; b) Ishida, T.; Yamamoto, S.; Mizutani, W.; Motomatsu, M.; Tokumoto, H.; Hokari, H.; Azehara, H.; Fujihira, M. *Langmuir* **1997**, *13*, 3261; c) Heister, K.; Allara, D. L.; Bahnck, K.; Frey, S.; Zharnikov, M.; Grunze, M. *Langmuir* **1999**, *15*, 5440; d) Noh, J.; Hara, M. *Langmuir* **2000**, *16*, 2045.
- ²² a) Thoden van Velzen, E. U.; Engbersen, J. F. J.; de Lange, P.; Mahy, J. W.; Reinhoudt, D. N. *J. Am. Chem. Soc.* **1995**, *117*, 6853; b) Friggeri, A.; van Veggel, F. C. J. M.; Reinhoudt, D. N.; Kooyman, R. P. H. *Langmuir* **1998**, *14*, 5457.
- ²³ Huisman, B.-H.; Rudkevich, D. M.; van Veggel, F. C. J. M.; Reinhoudt, D. N. *J. Am. Chem. Soc.* **1996**, *118*, 3523.
- ²⁴ a) Beulen, M. W. J.; Bügler, J.; Lammerink, B.; Geurts, F. A. J.; Biemond, E. M. E. F.; van Leerdam, K. G. C.; van Veggel, F. C. J. M.; Engbersen, J. F. J.; Reinhoudt, D. N. *Langmuir* **1998**, *14*, 6424; b) Beulen, M. W. J.; Bügler, J.; de Jong, M. R.; Lammerink, B.; Huskens, J.; Schönherr, H.; Vancso, G.

- J.; Boukamp, B. A.; Wieder, H.; Offenhäuser, A.; Knoll, W.; van Veggel, F. C. J. M.; Reinhoudt, D. N. *Chem. Eur. J.* **2000**, *6*, 1176.
- ²⁵ For a review, see: Flink, S.; van Veggel, F. C. J. M.; Reinhoudt, D. N. *Adv. Mater.* **2000**, *12*, 1315.
- ²⁶ a) Offord, D. A.; John, C. M.; Linford, M. R.; Griffin, J. H. *Langmuir* **1994**, *10*, 883; b) Tamada, K.; Hara, M.; Sasabe, H.; Knoll, W. *Langmuir* **1997**, *13*, 1558; c) Hayes, W. A.; Kim, H.; Yue, X.; Perry, S. S.; Shannon, C. *Langmuir* **1997**, *13*, 2511.
- ²⁷ For a review on microcontact printing and other soft lithographic techniques, see: Xia, Y.; Whitesides, G. M. *Angew. Chem. Int. Ed.* **1998**, *37*, 550.
- ²⁸ a) Liu, G.-Y.; Xu, S.; Qian, Y. L. *Acc. Chem. Res.* **2000**, *33*, 457; b) Gorman, C. B.; Carroll, R. L.; He, Y.; Tian, F.; Fuierer, R. *Langmuir* **2000**, *16*, 6312; c) Mizutani, W.; Ishida, T.; Tokumoto, H. *Langmuir* **1998**, *14*, 7197.
- ²⁹ a) Piner, R. D.; Zhu, J.; Xu, F.; Hong, S.; Mirkin, C. A. *Science* **1999**, *283*, 661; b) Hong, S.; Zhu, J.; Mirkin, C. A. *Science* **1999**, *286*, 523.
- ³⁰ Friebel, S.; Aizenberg, J.; Abad, S.; Wiltzius, P. *Appl. Phys. Lett.* **2000**, *77*, 2406.
- ³¹ Dulcey, C. S.; Georger, J. H.; Krauthamer, V.; Stenger, D. A.; Fare, T. L.; Calvert, J. M. *Science* **1991**, *252*, 551.
- ³² Yang, X. M.; Peters, R. D.; Kim, T. K.; Nealey, P. F. *J. Vac. Sci. Technol. B* **1999**, *17*, 3203.
- ³³ Yang, X. M.; Peters, R. D.; Kim, T. K.; Nealey, P. F.; Brandow, S. L.; Chen, M. S.; Shirey, L. M.; Dressick, W. J. *Langmuir* **2001**, *17*, 228.
- ³⁴ Lercel, M. J.; Whelan, C. S.; Craighead, H. G.; Seshadri, K.; Allara, D. L. *Appl. Phys. Lett.* **1996**, *68*, 1504.
- ³⁵ Ada, E. T.; Hanley, L.; Etchin, S.; Melngailis, J.; Dressick, W. J.; Chen, M. S.; Calvert, J. M. *J. Vac. Sci. Technol. B* **1995**, *13*, 2189.
- ³⁶ Xia, Y.; Rogers, J. A.; Paul, K. E.; Whitesides, G. M. *Chem. Rev.* **1999**, *99*, 1823.
- ³⁷ Magonov, S. N.; Whangbo, M.-H. *Surface Analysis with STM and AFM*, VCH: Weinheim, 1996.
- ³⁸ For more information, see:
<http://www.di.com/AppNotes/TapMode/TapModeMain.html>.
- ³⁹ Radmacher, M.; Tillmann, R. W.; Fritz, M.; Gaub, H. E. *Science* **1992**, *257*, 1900.
- ⁴⁰ Hierlemann, A.; Campbell, J. K.; Baker, L. A.; Crooks, R. M.; Ricco, A. J. *J. Am. Chem. Soc.* **1998**, *120*, 5323.
- ⁴¹ Li, J.; Piehler, L. T.; Qin, D.; Baker Jr., J. R.; Tomalia, D. A. *Langmuir* **2000**, *16*, 5613.
- ⁴² Zhang, H.; Grim, P. C. M.; Foubert, P.; Vosch, T.; Vanoppen, P.; Wiesler, U.-M.; Berresheim, A. J.; Müllen, K.; De Schryver, F. C. *Langmuir* **2000**, *16*, 9009.
- ⁴³ Bumm, L. A.; Arnold, J. J.; Cygan, M. T.; Dunbar, T. D.; Burgin, T. P.; Jones II, L.; Allara, D. L.; Tour, J. M.; Weiss, P. S. *Science* **1996**, *271*, 1705.
- ⁴⁴ Ishida, T.; Mizutani, W.; Tokumoto, H.; Choi, N.; Akiba, U.; Fujihira, M. *J. Vac. Sci. Technol. A* **2000**, *18*, 1437.
- ⁴⁵ a) Hickmann, J. J.; Ofer, D.; Zou, C.; Wrighton, M. S.; Laibinis, P. E.; Whitesides, G. M. *J. Am. Chem. Soc.* **1991**, *113*, 1128; b) Schlenoff, J. B.; Li, M.; Ly, H. *J. Am. Chem. Soc.* **1995**, *117*, 12528; c) Koega, R. R.; Schlenoff, J. B. *Langmuir* **1998**, *14*, 5469; d) Kondoh, H.; Kodama, C.; Sumida, H.; Nozoye, H. *J. Chem. Phys.* **1999**, *111*, 1175.

- ⁴⁶ a) Friggeri, A.; Schönherr, H.; van Manen, H.-J.; Huisman, B.-H.; Vancso, G. J.; Huskens, J.; van Veggel, F. C. J. M.; Reinhoudt, D. N. *Langmuir* **2000**, *16*, 7757; b) Friggeri, A.; van Manen, H.-J.; Auletta, T.; Li, X.-M.; Zapotoczny, S.; Schönherr, H.; Vancso, G. J.; Huskens, J.; van Veggel, F. C. J. M.; Reinhoudt, D. N. *J. Am. Chem. Soc.* **2001**, *123*, in press; c) Friggeri, A. *Ph.D. Thesis*, University of Twente, The Netherlands, 2000; d) Huisman, B.-H. *Ph.D. Thesis*, University of Twente, The Netherlands, 1998.
- ⁴⁷ Schönherr, H. *Ph.D. Thesis*, University of Twente, The Netherlands, 1999.
- ⁴⁸ Huck, W. T. S.; Prins, L. J.; Fokkens, R. H.; Nibbering, N. M. M.; van Veggel, F. C. J. M.; Reinhoudt, D. N. *J. Am. Chem. Soc.* **1998**, *120*, 6240.
- ⁴⁹ However, it was found that the pyridine ligands of **BB_{pyr}-Cl** are not strong enough to completely suppress sulfide coordination to the Pd^{II} pincer moiety, the ratio of pyridine over sulfide coordination being approximately 95:5 (as determined by ¹H NMR spectroscopy).
- ⁵⁰ Test reactions showed that SCS Pd^{II} pincers were depalladated upon addition of thiols, indicating the exchange of the chelate sulfides for thiols which led to a disruption of the pincer chelate rings.
- ⁵¹ Before SAM preparation, gold substrates are usually annealed with a hydrogen flame. This reproducibly yields large atomically flat Au(111) terraces of a few μm in size. The atomic steps and triangular terraces can be easily imaged with AFM (Figure 7.1). For more details, see ref. 46d.
- ⁵² The low height value obtained here may be caused by flattening of the dendrimer or compression by the tip. Moreover, the absolute height value can deviate from the expected size of the dendritic wedges if the interaction between the AFM tip and the dendrimer is different from the interaction of the tip with the surrounding thiol monolayer. With very soft tapping conditions the height value can be considered a good representation of the feature height: Brandsch, R.; Bar, G.; Whangbo, M.-H. *Langmuir* **1997**, *13*, 6349.
- ⁵³ The width of the features appears to be much larger than the expected dendrimer size due to tip convolution.
- ⁵⁴ Especially the presence of nitromethane causes the formation of a large number of defects, as was shown by electrochemical resistance measurements: Ref. 46d.
- ⁵⁵ Hawker, C. J.; Fréchet, J. M. J. *J. Am. Chem. Soc.* **1990**, *112*, 7638.
- ⁵⁶ Wooley, K. L.; Hawker, C. J.; Fréchet, J. M. J. *J. Chem. Soc., Perkin Trans. 1* **1991**, 1059.
- ⁵⁷ For a complete discussion, see Ref. 46a,c.
- ⁵⁸ The dendrimer coverage was calculated by assuming that the area occupied by one sulfide molecule is twice that of a thiol molecule (*i.e.* $2 \times 21.7 \text{ \AA}^2$), and considering that a homogeneous alkylthiol SAM corresponds to 100% surface coverage with approximately 10^{14} molecules per cm². See Ref. 45b.
- ⁵⁹ a) Huck, W. T. S.; van Veggel, F. C. J. M.; Reinhoudt, D. N. *Angew. Chem. Int. Ed. Engl.* **1996**, *35*, 1213.
- ⁶⁰ Upon coordination of a dialkylsulfide to the SCS Pd^{II} pincer system, a shift in the signal from the methylene protons next to the sulfide is observed. Such a shift was not observed in **8**.
- ⁶¹ Hawker, C. J.; Wooley, K. L.; Fréchet, J. M. J. *J. Chem. Soc., Perkin Trans. 1* **1993**, 1287.
- ⁶² Similar isolated features were also observed when monolayer-protected gold nanoclusters (diameter 2.0 ± 0.5 nm as measured by transmission electron microscopy) ω-functionalized with phosphines were employed instead of phosphine dendritic wedge **12**. A height of 3.5 ± 0.7 nm was measured for the individual features in that case.

- ⁶³ Brandsch, R.; Bar, G.; Whangbo, M.-H. *Langmuir* **1997**, *13*, 6349.
- ⁶⁴ Huisman, B.-H.; Schönherr, H.; Huck, W. T. S.; Friggeri, A.; van Manen, H.-J.; Menozzi, E.; Vancso, G. J.; van Veggel, F. C. J. M.; Reinhoudt, D. N. *Angew. Chem. Int. Ed.* **1999**, *38*, 2248.
- ⁶⁵ Huck, W. T. S.; van Veggel, F. C. J. M.; Reinhoudt, D. N. *J. Mater. Chem.* **1997**, *7*, 1213.

Chemistry on isolated, surface-confined dendrimers



Impression of dendritic growth on a self-assembled monolayer on a gold surface (AFM tip not to scale).

This chapter deals with the generation of large dendritic structures on gold, starting from dendritic wedges that have been embedded in self-assembled monolayers. A second generation dendritic adsorbate, functionalized at the focal point with a dialkylsulfide chain and containing 4 pyridines at the periphery, has been synthesized and characterized. TM-AFM experiments revealed isolated features of 3.3 ± 0.5 nm in height when decanethiol SAMs were exposed to a solution of this dendritic adsorbate. Subsequently, the peripheral pyridines were employed as the anchoring points for the non-covalent attachment of second generation dendritic wedges having a focal SCS Pd(II) pincer moiety. A substantial increase in feature size was observed by TM-AFM experiments after metal-ligand coordination, demonstrating the feasibility of non-covalent growth reactions on surface-confined dendritic molecules.

8.1 Introduction

In the previous chapter it was demonstrated that nanometer-sized dendrimers, functionalized with a dialkylsulfide chain, can be incorporated as isolated species into preassembled alkylthiol monolayers on gold. Moreover, a strategy was developed for performing coordination chemistry on SCS Pd^{II} pincers, isolated as single molecules on a gold surface, as discussed in the second part of that chapter.

Taking single, surface-confined dendrimers as a starting point, a next step in our “bottom up” methodology would be the incorporation of reactive groups at the dendrimer periphery and employ these on the surface as anchoring sites for subsequent growth reactions. A major advantage of this strategy is that both starting and end point of the growth process can be visualized by atomic force microscopy (AFM), since the dimensions of the starting dendrimers already allow them to be imaged by routine AFM experiments. This is in contrast to the methodology reported in chapter 7, where only the end point of the process could be imaged by AFM.

The confinement of dendrimers to surfaces by other research groups was already briefly discussed in chapter 7. However, dendritic *growth* on surfaces has been studied in much less detail. Zhang *et al.* prepared polyamidoamine (PAMAM) dendrimers on surfaces using the same chemistry as in bulk PAMAM preparations.¹ Hyperbranched polymers were grown by Crooks, Bergbreiter, and their coworkers from a carboxylic acid-terminated SAM on gold using amino-terminated oligomers of protected acrylic acid as branching units.² In general, surface-attached polymers are of interest because of their (potential) applications in the areas of chemical sensing, nonlinear optical materials, corrosion inhibition, adhesion, etc. Weiss, Grubbs, and their coworkers embedded rigid, linear thiols ω -functionalized with a norbornene moiety as isolated species into a dodecanethiol SAM and studied the ring-opening metathesis polymerization (ROMP) initiated by the surface-bound norbornenes using Grubbs' catalyst and a norbornene monomer.³ The polymerization process was followed by scanning tunneling, atomic force, and scanning electron microscopy, revealing polymer brushes ranging from 10 to several hundred nm.

8.2 Aim and scope of this chapter

In this chapter a strategy for performing growth on isolated, surface-confined dendrimers is presented. The synthesis of dendritic adsorbate **1** (Chart 8.1), possessing both a dialkylsulfide moieties for anchorage to gold and peripheral pyridines for non-covalent metal-ligand coordination, is described. After insertion of the adsorbates into decanethiol monolayers on gold, the pyridines are coordinated to dendritic wedges containing a focal SCS Pd^{II} pincer moiety. Both the starting and end points of the growth process are visualized by TM-AFM experiments.

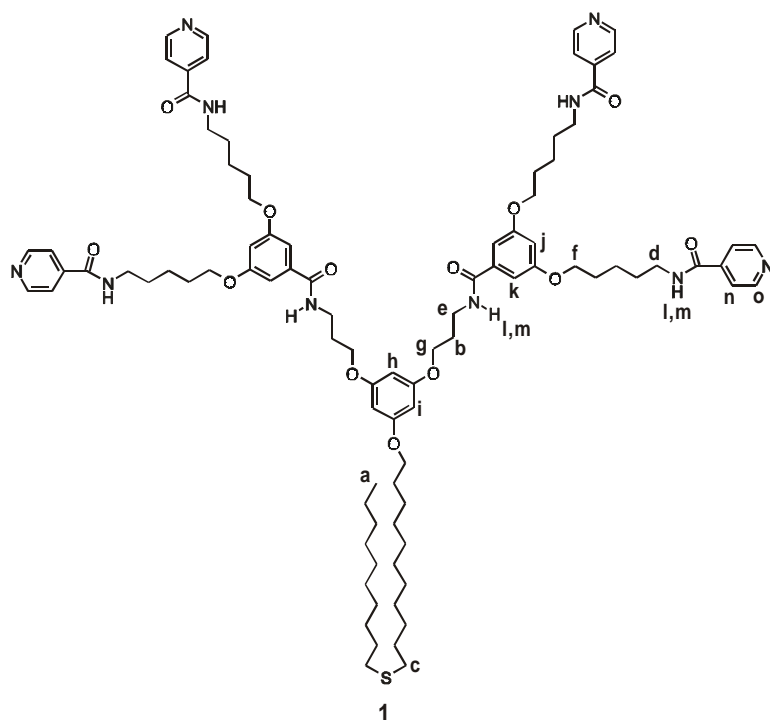
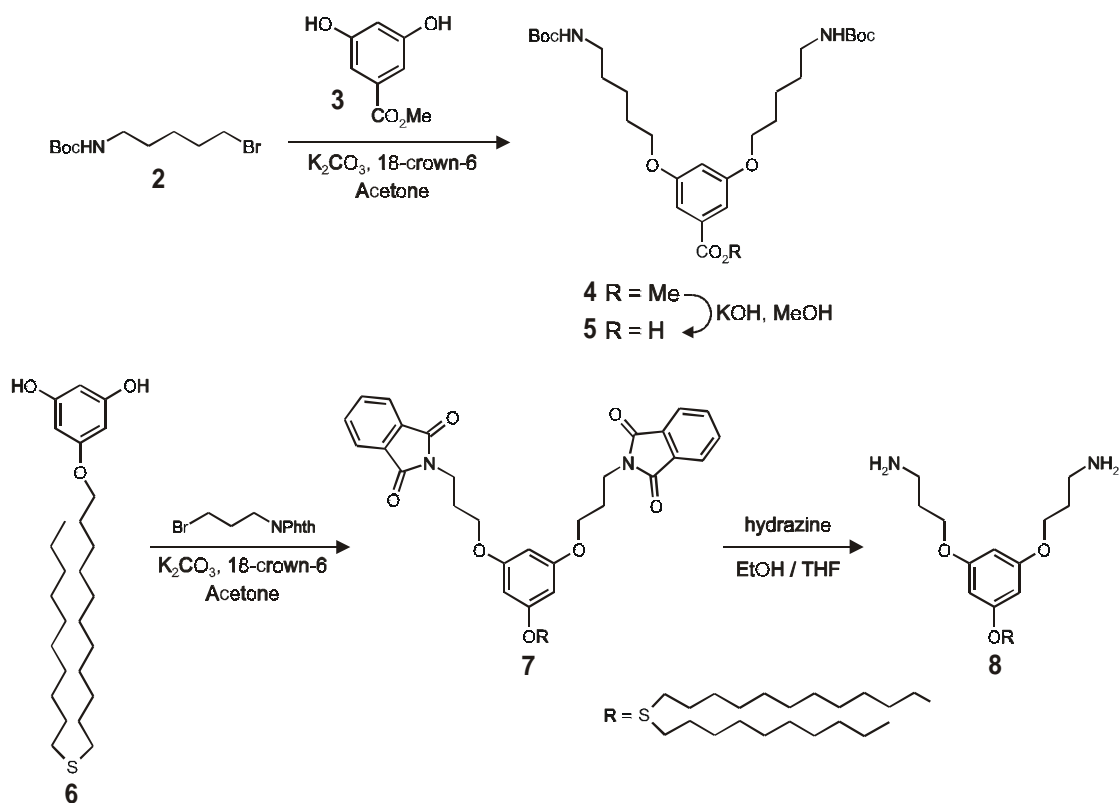


Chart 8.1. Structure of second generation pyridine-functionalized dendritic adsorbate **1**. The designations *a*, *b*, *c*, etc. are used for ^1H NMR spectroscopic signal assignments in Figure 8.1.

8.3 Results and discussion

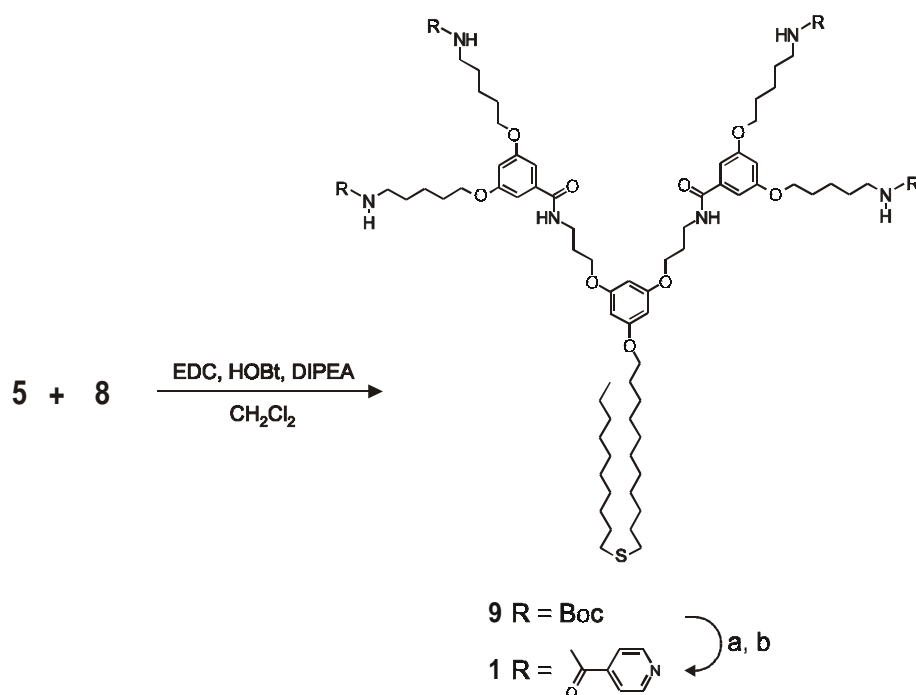
8.3.1 Synthesis of dendritic adsorbate **1**

In order to employ isolated molecules for both anchorage to gold and as starting points for further growth, a dendritic wedge containing peripheral pyridines and a focal dialkylsulfide chain was designed. In chapter 7 it was shown that dendrimers can be inserted as isolated molecules into preformed alkylthiol monolayers by chemisorption of their dialkylsulfide moieties. Pyridines were chosen as the dendrimer peripheral groups since they strongly bind to SCS Pd^{II} pincer moieties *via* metal-ligand coordination (see chapter 3).⁴ The synthetic strategy leading to dendritic adsorbate **1** is outlined in Schemes 8.1 and 8.2. A slightly adapted version of the convergent dendritic routes reported by Schlüter and coworkers⁵ and Liskamp and coworkers⁶ was used for the construction of the dendritic framework. First, dendron **4** having 2 Boc-protected amines at the periphery and a reactive carboxylic acid at the focal point was synthesized as shown in Scheme 8.1 (top).



Scheme 8.1. Synthesis of first generation dendron **5** and bis(amino) sulfide **8**.

5-[(*tert*-Butoxycarbonyl)amino]-1-pentyl bromide **2** was prepared in two steps, according to a literature procedure,⁷ by reaction of 5-amino-1-pentanol with di-*tert*-butyl dicarbonate, followed by conversion of the alcohol to the bromide with CBr₄/PPh₃. Methyl resorcyate **3** (obtained by esterification of resorcylic acid with MeOH/H₂SO₄) was alkylated with 2 equiv of **2** to afford the first generation dendron **4** in 85% yield. Saponification of the focal methyl ester with KOH in MeOH furnished carboxylic acid **5** in 88% yield. Second, dialkylsulfide **8** containing two primary amines was prepared from diol **6** (chapter 7) by alkylation with 3-bromopropylphthalimide (65% yield), followed by quantitative removal of the phthalimide protecting groups in EtOH/THF (Scheme 8.1 bottom). Third, coupling of 2 equiv of dendron **5** to diamine **8** was performed using 1-(3-dimethylaminopropyl)-3-ethyl-carbodiimide hydrochloride (EDC) and 1-hydroxybenzotriazole (HOBt) as the coupling reagents to provide second generation adsorbate **9** in 66% isolated yield after purification by column chromatography (Scheme 8.2).



Scheme 8.2. Synthesis of pyridine-terminated, second generation adsorbate **1**; a) $\text{CH}_2\text{Cl}_2/\text{TFA}$ 95:5 (v/v), r.t., 10 min, quant.; b) isonicotinic acid, EDC/HOBT/DIPEA, $\text{CH}_2\text{Cl}_2/\text{MeOH}$, r.t., 10 h, 52%.

All Boc groups of dendron **9** could be smoothly removed using very mild conditions (5% TFA in CH_2Cl_2 , 10 min at r.t.). After removal of volatiles, pure products were obtained as the corresponding ammonium salts (with trifluoroacetate anions), as inferred from ^1H NMR spectroscopy (in $\text{DMSO}-d_6$). The Boc signal at 1.4 ppm had disappeared, and the three protons of each ammonium moiety gave a signal at 7.76 ppm. No sign of decomposition was observed, implying that complete Boc deprotection can be accomplished without destroying the dendritic framework. Conversion of the peripheral ammonium groups of the deprotected dendron to neutral amines was achieved by adding an excess of DIPEA as a base. Coupling of the 4 terminal amines with isonicotinic acid using EDC and HOBT as the coupling reagents provided pyridine-terminated adsorbate **1** in 52% yield after purification. Both adsorbates **9** and **1** were isolated as colorless viscous oils and characterized by ^1H and ^{13}C NMR spectroscopy and FAB mass spectrometry. The ^1H NMR spectrum of adsorbate **1** is shown in Figure 8.1. Assignment of all signals except the methylene region between 1.8-1.2 ppm was performed with the aid of $^1\text{H}-^1\text{H}$ COSY NMR spectroscopy.

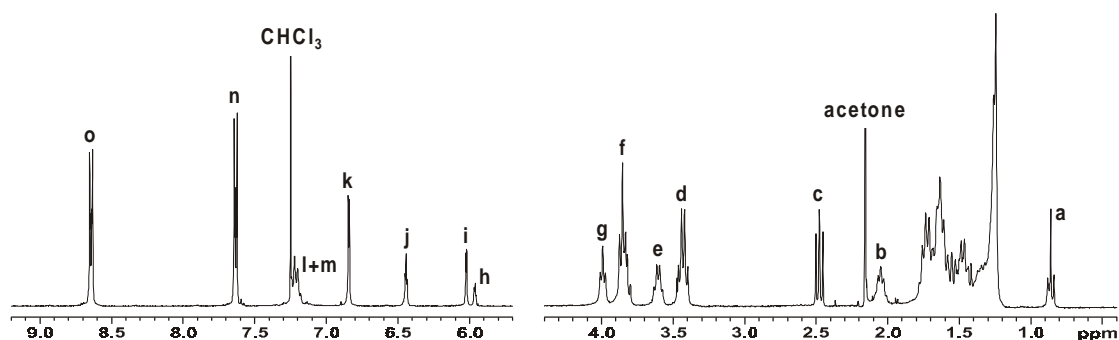
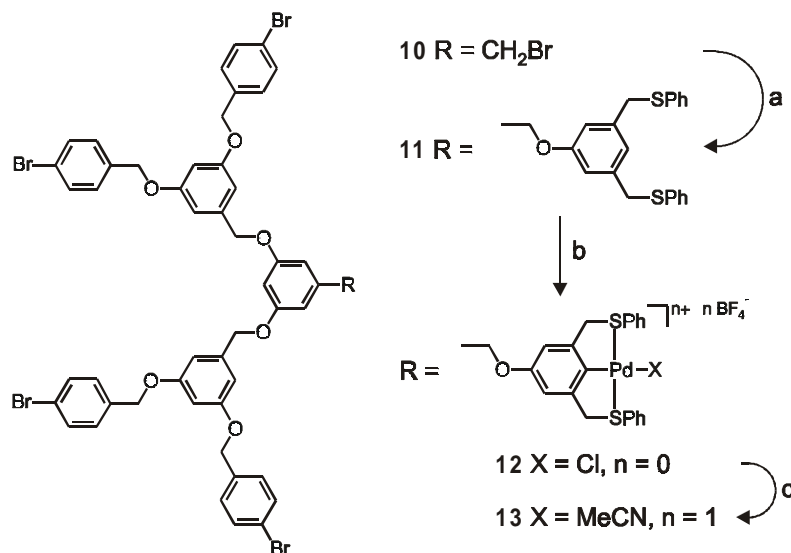


Figure 8.1. ^1H NMR spectrum (300 MHz, CDCl_3 , 298 K) of dendritic adsorbate **1**. For signal assignment, see Chart 8.1.

8.3.2 Synthesis of a dendritic wedge containing an SCS Pd^{II} pincer group

In order to employ the pyridine end groups of adsorbate **1** as starting points for further growth, a second generation Fréchet dendron was functionalized with a focal SCS Pd^{II} pincer moiety (Scheme 8.3).⁸ Coordination of each pyridine group of **1** to the Pd^{II} center of dendron **13** (by substitution of the labile acetonitrile ligand) converts second generation dendritic wedge **1** into a fourth generation metallodendron in one step. The accompanying increase in feature size should be readily observed by AFM.



Scheme 8.3. Synthesis of second generation dendritic wedge **13** containing a focal SCS $\text{Pd}(\text{II})$ pincer moiety; a) 3,5-bis(phenylthiomethyl)phenol, $\text{K}_2\text{CO}_3/18\text{-crown-6}$, acetone, reflux, 10 h, 93%; b) $\text{K}_2\text{PdCl}_4/\text{NaOAc}$, $\text{CHCl}_3/\text{H}_2\text{O}$, reflux, 2 h, 84%; c) AgBF_4 , $\text{CH}_2\text{Cl}_2/\text{CH}_3\text{CN}$, r.t., 10 min, quant.

The known⁹ dendritic wedge **10** containing a focal benzyl bromide was alkylated with 3,5-bis(phenylthiomethyl)phenol¹⁰ to give dendritic pincer ligand **11** in 93% yield. The conversion of the benzylic bromide in **10** to the benzylic ether in **11** was evident from the ¹H NMR spectrum of **11**, in which a singlet at 4.87 ppm was found for the benzylic ether protons. The benzylic bromide protons of **10** display a singlet at 4.40 ppm. Dendritic pincer ligand **11** was cyclopalladated in 84% yield using the two-phase procedure described in chapter 4 (K₂PdCl₄/NaOAc in refluxing CHCl₃/H₂O). The chloride complex **12** obtained in this manner was characterized by ¹H and ¹³C NMR spectroscopy, FAB mass spectrometry, and elemental analysis. In the ¹H NMR spectrum of **12** a broad signal at 4.51 ppm, corresponding to four CH₂S protons, indicates the presence of the two chelate rings of the SCS Pd^{II} moiety (in agreement with the SCS Pd^{II} pincers reported in chapter 3). Finally, the chloride complex **12** was converted to the acetonitrile complex **13** by treatment with 1 equiv of AgBF₄ in CH₂Cl₂/CH₃CN.

8.3.3 Coordination chemistry of dendritic wedge **13** in solution

The coordination of a variety of pyridines to SCS Pd^{II} pincer systems has been well studied in our group (see chapter 3) and by others.¹¹ In general, pyridine complexes of SCS Pd^{II} pincers are synthesized from the corresponding acetonitrile complexes by a fast and quantitative exchange. It was reasoned that quantitative exchange of the acetonitrile ligand in **13** by the *p*-amide-substituted pyridine end groups of adsorbate **1** might be inhibited for both steric and electronic reasons. Therefore the coordination of isonicotinoyl benzylamide to the pincer moiety of dendron **13** was first investigated as a model for the pyridine end groups of adsorbate **1**. As shown in Figure 8.2, significant shifts in the ¹H NMR spectrum are observed upon addition of 1 equiv of isonicotinoyl benzylamide to dendritic wedge **13** in CDCl₃. Diagnostic for pyridine coordination is the large upfield shift of the α-pyridyl protons upon coordination to the SCS Pd^{II} pincer (see also chapter 3). The absence of a signal around 8.6 ppm in the bottom spectrum of Figure 8.2 indicates the quantitative substitution of the acetonitrile ligand for isonicotinoyl benzylamide.

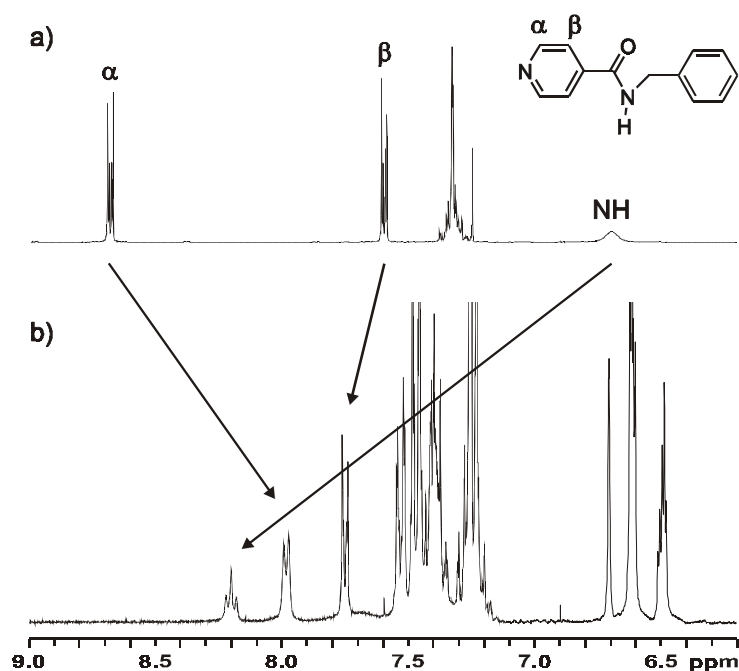


Figure 8.2. ¹H NMR spectra (300 MHz, CDCl₃, 298 K) of isonicotinyl benzylamide before (a) and after (b) addition of 1 equiv of acetonitrile complex **13**.

Next, it was determined whether adsorbate **1** can accommodate four dendritic wedges around its periphery (by coordination of the pyridyl groups of **1** to the pincer moieties of acetonitrile complex **13**). To that end, **1** was titrated to **13** in CDCl₃ solution. ¹H NMR spectroscopy showed that 4 equiv of **13** can indeed be coupled to adsorbate **1**. Upon coordination, similar shifts for the pyridyl groups of **1** were observed as displayed in Figure 8.2. However, a minor interference (\pm 5%, as judged from the NMR integrals) from coordination of the sulfide moiety of **1** to the pincer system of **13** was observed. As already discussed in chapter 7, the coordination strengths of pyridine and sulfide groups toward Pd^{II} pincers are in the same range. Sulfide interference is absent when the pyridine coordination is carried out on a gold surface, since in that case the sulfide group is already bound to the substrate.

It must be realized that coordination of four dendritic wedges to adsorbate **1** is sterically more demanding on a gold surface than in solution. Whereas the conformation of adsorbate **1** can be freely adjusted in solution in order to accommodate all four dendrons, the space available for coordination to isolated molecules of **1** inserted into SAMs is restricted to approximately half a sphere.

8.3.4 Coordination chemistry of pyridine-terminated adsorbate **1** inserted into decanethiol SAMs

Confinement of dendritic adsorbate **1** to gold was achieved by exposing a decanethiol SAM to a 0.1 mM solution of **1** in CH₂Cl₂ for 3 h. After rinsing, TM-AFM experiments in air

revealed isolated features, well separated and randomly distributed over the surface, with an average height of 3.3 ± 0.5 nm (Figure 8.3).

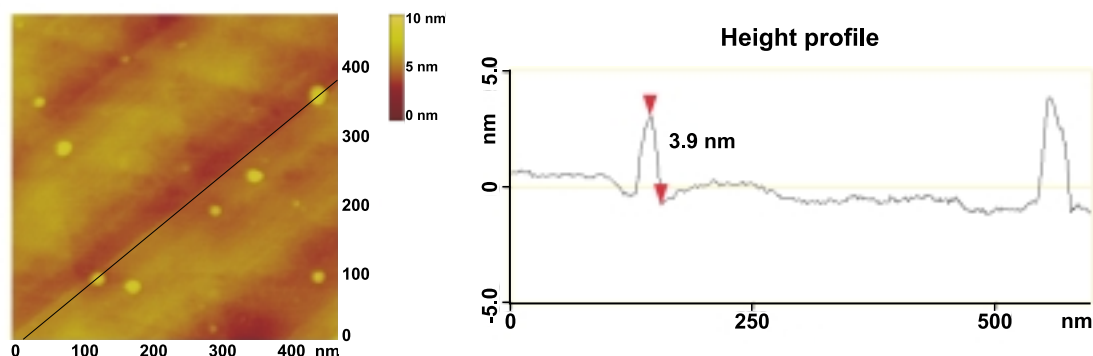


Figure 8.3. Representative TM-AFM image (acquired in air) of a decanethiol SAM exposed to a 0.1 mM solution of **1** (in CH_2Cl_2) for 3 h. The height profile shown on the right corresponds to the line drawn in the left image.

The maximum protrusion of adsorbate **1** above the decanethiol monolayer was estimated at 2.8 nm from a computer-generated model.¹² Thus the average height, as determined by TM-AFM, is in reasonable agreement with the calculated value for the single dendritic molecules. Direct comparison of the two values can be made due to the very soft tapping conditions employed in the TM-AFM experiments (see also section 7.3.2.2). The width of the dendrimers was not systematically evaluated due to problems related to tip convolution (section 7.3.1.2). The average number of nanometer-sized features counted in a 500×500 nm² area of the decanethiol SAM exposed to adsorbate **1** is 15 ± 5 , which is in the same order of magnitude as we have found for insertion of the dendritic adsorbates described in chapter 7.

Dendritic growth on gold was achieved by exposure of a decanethiol monolayer containing single molecules of **1** to a 0.1 mM solution of acetonitrile complex **13** in CH_2Cl_2 for 10 min. After rinsing, TM-AFM experiments showed that the average feature dimensions had increased significantly (Figure 8.4). By comparing Figures 8.3 and 8.4, it is seen that both the lateral width and the height of the features have increased after growth. However, the size distribution after growth is much broader than before growth, and feature heights from 3.1 to 7.5 nm are found on the monolayer.

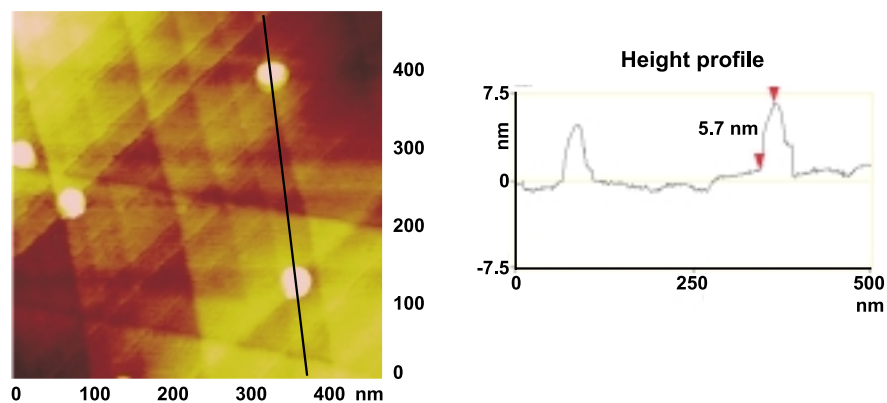


Figure 8.4. TM-AFM image (acquired in air) of a decanethiol SAM exposed to a 0.1 mM solution of **1** for 3 h, followed by exposure to a 0.1 mM solution of dendritic wedge **13** for 10 min. The height profile shown on the right corresponds to the line drawn in the left image.

There are even features which appear not to have grown at all. This indicates that not all inserted adsorbates have four molecules of **13** coordinated to them. It is most likely that a distribution of dendrimers complexing zero to four wedges of **13** has been obtained. This is different from solution where adsorbate **1** can coordinate four wedges of **13** (*vide supra*). As stated in the previous section, coordination of four dendritic wedges to adsorbate **1** is sterically more demanding on a gold surface than in solution. It is probable that coordination of **13** to **1** becomes progressively more difficult in going from the first to the fourth coordination event, and the complexation of the final wedges might be sterically and kinetically unfavorable.

8.3.5 Covalent growth reactions

In section 8.3.1 the synthesis of dendritic adsorbate **1** from adsorbate **9** was described. After deprotection of the Boc groups from adsorbate **9**, conversion of the peripheral ammonium groups to neutral amines can be achieved by addition of excess DIPEA as a base. In principle, the resulting dendritic adsorbates containing peripheral amines could be applied on a surface in *covalent* growth reactions with dendritic wedges having reactive focal groups. To that end, a second generation dendritic Fréchet wedge **14** (Chart 8.2) functionalized with a focal isothiocyanate moiety was synthesized, since the isothiocyanate group is known to react cleanly with primary and secondary amines to give thioureas. The less reactive nature of isothiocyanates compared to isocyanates prevents their reaction with alcohols and water.¹³ Dendritic wedge **14** was prepared in 66% yield from the corresponding benzylic amine (see chapter 4) by reaction with thiophosgene.

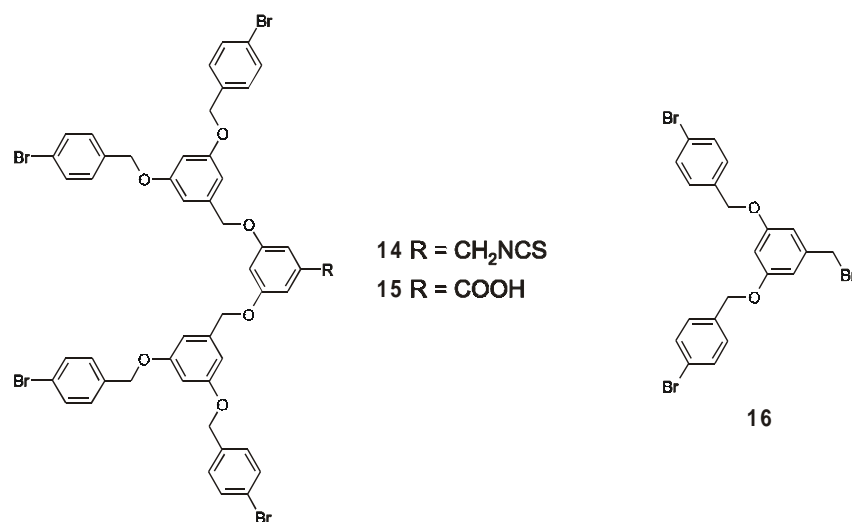


Chart 8.2.

Unfortunately, the reactivity of isothiocyanate **14** was found to be very low. In order for reactions with primary amines to go to completion, extended reaction times (10 h and more) and heating were required. These conditions are not suitable for monolayer reactions, and therefore work on this topic was discontinued. Alternatively, adsorbates having peripheral amines might be coupled to dendritic wedge **15** containing a focal carboxylic acid. On SAMs, coupling between carboxylic acids and amines has been achieved using a variety of methods.¹⁴ Carboxylic acid **15** was synthesized by alkylation of methyl resorcyate **3** (Scheme 8.1) with first generation dendritic bromide **16** (Chart 8.2) in 59% yield, followed by saponification of the focal methyl ester with KOH in 84% yield. In solution, the adsorbate obtained after deprotection of **9** could be coupled to dendritic wedge **15** using EDC/HOBt/DIPEA as the coupling reagents to form the fourth generation adsorbate **17** (Chart 8.3).

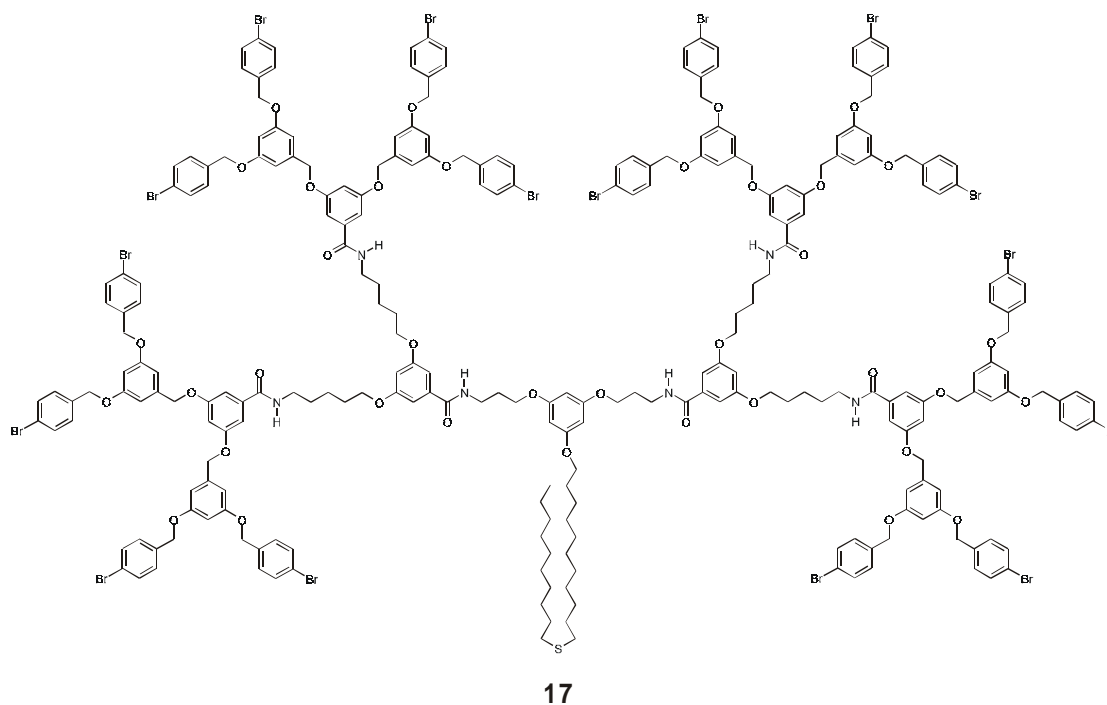


Chart 8.3. Fourth generation dendritic adsorbate **17** formed by coupling the deprotected analog of adsorbate **9** with carboxylic acid **15**.

Dendritic adsorbate **17** displays broader signals in the ^1H NMR spectrum than the components from which it was synthesized. This is probably due to the significant size increase, leading to slow tumbling of the dendrimer and/or restricted mobility inside the dendritic wedge in solution. The increase in dendritic size was also inferred from the chemical shift of the *ortho*-protons of the terminal bromo-substituted phenyl rings. In going from second generation **15** to fourth generation **17**, this chemical shift changes from 7.56 to 7.49 ppm, reflecting an increase in steric and ring current interactions between the peripheral phenyl rings as the dendritic size increases.¹⁵

Initial growth reactions on gold using the deprotected analog of adsorbate **9** and the acid chloride generated from dendritic wedge **15** were not successful. Adsorbate **9** was inserted into a decanethiol monolayer in the usual manner. TM-AFM experiments showed very small features after insertion. The Boc groups were removed by exposure of the monolayer to a 5% TFA solution in CH_2Cl_2 . After rinsing with a DIPEA solution to convert the quaternary ammonium salts to neutral amines, the monolayer was exposed to a solution of the acid chloride of **15** in CH_2Cl_2 . After growth, clean features could not be distinguished by TM-AFM experiments, suggesting the presence of a significant amount of physisorbed material on the monolayer. By changing the coupling procedure (by using, for example, an activated ester of carboxylic acid **15**), the quality of the monolayer after growth might be improved.

From this section, it can be concluded that covalent growth on a surface employing dendritic isothiocyanates or acid chlorides is much more troublesome than non-covalent metal-ligand coordination. It has been pointed out in the literature that the (covalent) reactivity of

molecules in a self-assembled monolayer may differ dramatically from that in solution.¹⁴ In contrast, metal-ligand coordination is usually a fast process.

8.4 Conclusions

In this chapter the successful growth of isolated, surface-confined dendrimers into metallodendrimers of higher generation has been demonstrated. A second generation dendritic adsorbate having 4 peripheral pyridines and a focal dialkylsulfide chain was synthesized in a convergent manner. The non-covalent coordination of second generation dendritic wedges containing a focal SCS Pd^{II} pincer moiety to this dendritic adsorbate was studied both in solution and on a monolayer. In solution, 4 dendritic wedges could be accommodated around the periphery of the dendritic adsorbate, as evidenced by ¹H NMR spectroscopy. On a decanethiol SAM on gold, isolated, surface-confined dendrimers with an average height of 3.3 nm (as determined by TM-AFM) could be grown by metal-ligand coordination into larger dendritic structures with heights ranging from 3.1 to 7.5 nm. Considering the broad range of heights obtained, it is likely that not all isolated dendritic adsorbates have 4 dendritic wedges coordinated around them.

Covalent coupling of a dendritic adsorbate having peripheral amines with dendritic wedges having a focal isothiocyanate or carboxylic acid was also investigated. It was found that the conditions needed for successful coupling in solution would be unfavorable for coupling on a monolayer.

The strategy presented in this chapter is a step forward in the “bottom up” scenario toward the confinement of nanosize functional architectures to surfaces. Current research in our group is being aimed at the laterally controlled positioning of dendritic structures on a gold surface.

8.5 Experimental Section

General comments. For general information on instruments, procedures, and chemicals, see chapter 3. Monolayer experiments were performed by T. Auletta (University of Twente).

Materials. 5-[(*tert*-Butoxycarbonyl)amino]-1-pentyl bromide **2**,⁷ sulfide diol **6**,¹⁶ Br₄-[G2]-NH₂ (chapter 4), Br₂-[G1]-Br,⁹ and Br₄-[G2]-Br⁹ were synthesized according to reported procedures.

Methyl 3,5-bis[5-(*tert*-butyloxycarbonylamido)pentyl]benzoate (4). 5-[(*tert*-Butoxycarbonyl)amino]-1-pentyl bromide **2** (3.86 g, 14.50 mmol), methyl resorcyate **3** (1.22 g, 7.26 mmol), K₂CO₃ (4.00 g, 28.94 mmol) and 18-crown-6 (0.38 g, 1.44 mmol) were refluxed overnight in acetone (250 mL) under an argon atmosphere. After evaporation of the solvent *in vacuo*, the resulting paste was taken up in CH₂Cl₂ and washed with brine (2 ×). The organic layer was dried over anhydrous Na₂SO₄ and subsequently evaporated *in vacuo*. The crude product was purified by column chromatography using CH₂Cl₂/CH₃OH 98:2 (v/v) as the eluent, which afforded the product as a colorless oil. Yield 3.33 g (85%). ¹H NMR: δ (ppm) 7.13 (d, *J* = 2.4 Hz, 2 H, Ar H), 6.60 (t, *J* = 2.4 Hz, 1 H, Ar H),

4.52 (br s, 2 H, NH), 3.96 (t, $J = 6.4$ Hz, 2 H, CH₂O), 3.88 (s, 3 H, CO₂CH₃), 3.13 (q, $J = 6.2$ Hz, 4 H, CH₂N), 1.78 (quint, $J = 6.6$ Hz, 4 H, CH₂CH₂O), 1.58-1.46 (m, 8 H, OCH₂CH₂CH₂CH₂CH₂N), 1.43 (s, 18 H, CMe₃). ¹³C NMR: δ (ppm) 166.4, 159.1, 155.4, 131.3, 107.1, 106.0, 78.6, 67.5, 51.6, 40.0, 29.3, 28.3, 27.9, 22.8. FAB MS m/z 539.4 ([M + H]⁺, calcd for C₂₈H₄₇N₂O₈: 539.3).

3,5-Bis[5-(*tert*-butyloxycarbonylamido)pentyl]benzoic acid (5). A solution of ester **4** (1.98 g, 3.68 mmol) and KOH (0.31 g, 5.52 mmol) in a mixture of methanol (75 mL) and water (25 mL) was refluxed for 3 h. After cooling to r.t., acetic acid was added (until pH = 5). The mixture was extracted with CH₂Cl₂, and the organic phase was dried over MgSO₄. After evaporation of the solvent *in vacuo*, pure product was obtained as a white solid. Yield 1.69 g (88%). M.p. 116-117 °C. ¹H NMR (CDCl₃/DMSO-*d*₆): δ (ppm) 7.04 (d, $J = 2.4$ Hz, 2 H, Ar H), 6.51 (t, $J = 2.4$ Hz, 1 H, Ar H), 5.41 (br s, 2 H, NH), 3.88 (t, $J = 6.7$ Hz, 4 H, CH₂O), 3.00 (q, $J = 6.2$ Hz, 4 H, CH₂N), 1.70 (quint, $J = 6.7$ Hz, 4 H, CH₂CH₂O), 1.46-1.39 (m, 8 H, OCH₂CH₂CH₂CH₂CH₂N), 1.35 (s, 18 H, CMe₃). ¹³C NMR (DMSO-*d*₆): δ (ppm) 167.1, 159.6, 155.5, 133.1, 107.2, 105.4, 77.3, 67.6, 29.1, 28.2, 22.7 (two carbon signals not resolved). FAB MS m/z 523.2 ([M - H]⁻, calcd 523.3). Anal. calcd for C₂₇H₄₄N₂O₈·0.5H₂O: C, 60.77; H, 8.50; N, 5.25. Found: C, 60.52; H, 8.79; N, 5.40.

Bis(phthalimido) sulfide (7). A mixture of bis(hydroxy) sulfide **6** (0.51 g, 1.13 mmol), 3-bromopropylphthalimide (0.60 g, 2.24 mmol), K₂CO₃ (0.39 g, 2.82 mmol), and 18-crown-6 (0.06 g, 0.23 mmol) in acetone (40 mL) was refluxed overnight under an argon atmosphere. After evaporation of the solvent under reduced pressure, the resulting paste was taken up in CH₂Cl₂ (100 mL) and washed with brine. The organic phase was dried over anhydrous Na₂SO₄ and subsequently evaporated *in vacuo*. The crude product was purified by column chromatography using CH₂Cl₂ as the eluent, affording a white solid. Yield 0.61 g (65%). M.p. 74-75 °C. ¹H NMR: δ (ppm) 7.85-7.80 (m, 2 H, NPhth), 7.73-7.69 (m, 2 H, NPhth), 5.93 (d, $J = 2.2$ Hz, 2 H, Ar H), 5.83 (t, $J = 2.2$ Hz, 1 H, Ar H), 3.94-3.85 (m, 8 H, CH₂O + CH₂N), 3.78 (t, $J = 6.6$ Hz, 2 H, CH_{2,chain}O), 2.49 (t, $J = 7.3$ Hz, 4 H, CH₂S), 2.13 (quint, $J = 6.4$ Hz, 4 H, OCH₂CH₂CH₂N), 1.71 (quint, $J = 6.6$ Hz, 2 H, CH_{2,chain}CH₂O), 1.56 (quint, $J = 7.3$ Hz, 4 H, CH₂CH₂S), 1.42-1.33 (m, 28 H, CH₂), 0.87 (t, $J = 6.8$ Hz, 3 H, CH₃). ¹³C NMR: δ (ppm) 167.8, 160.3, 159.9, 133.3, 131.7, 122.7, 93.5, 93.1, 67.4, 65.1, 35.0, 31.7, 31.4, 29.2-28.7, 28.4, 27.7, 25.5, 22.1, 13.6. FAB MS m/z 827.5 ([M + H]⁺, calcd 827.5). Anal. calcd for C₄₉H₆₆N₂O₇S·0.6H₂O: C, 70.24; H, 8.08; N, 3.34. Found: C, 69.96; H, 8.15; N, 3.49.

Bis(amino) sulfide (8). Bis(phthalimido) sulfide **7** (0.51 g, 0.62 mmol) was dissolved in a mixture of EtOH (20 mL) and THF (10 mL) and the solution was heated to reflux. Hydrazine monohydrate (1 mL) was added and the solution was refluxed for 2 h. After cooling to r.t., the solvents were evaporated under reduced pressure. The resulting paste was taken up in CH₂Cl₂ (100 mL) and washed with 1 M HCl, sat. NaHCO₃, and brine. After drying over Na₂SO₄, the organic phase was evaporated *in vacuo* to afford the product as a colorless oil. Yield 0.35 g (quant.). ¹H NMR: δ (ppm) 6.06 (s, 3 H, Ar H), 3.99 (t, $J = 6.0$ Hz, 4 H, CH₂O), 3.88 (t, $J = 6.6$ Hz, 2 H, CH₂O), 2.88 (t, $J = 6.6$ Hz, 4 H, CH₂N), 2.49 (t, $J = 7.5$ Hz, 4 H, CH₂S), 1.89 (quint, $J = 6.6$ Hz, 4 H, OCH₂CH₂CH₂N), 1.74 (quint, 6.6 Hz, 2 H, OCH₂CH₂), 1.56 (quint, $J = 7.5$ Hz, 4 H, CH₂CH₂S), 1.41-1.25 (m, 28 H, CH₂), 0.87 (t, $J = 6.6$ Hz, 3 H, CH₃). FAB MS m/z 567.5 ([M + H]⁺, calcd for C₃₃H₆₂N₂O₃S: 567.4).

Adsorbate 9. Carboxylic acid **5** (0.37 g, 0.71 mmol), 1-hydroxybenzotriazole hydrate (0.10 g, 0.74 mmol), 1-(3-dimethylaminopropyl)-3-ethyl-carbodiimide hydrochloride (EDC, 0.15 g, 0.78 mmol), and *N,N*-diisopropylethylamine (0.31 mL, 1.78 mmol) were mixed in CH₂Cl₂ (50 mL). A solution of bis(amino) sulfide **8** (0.20 g, 0.35 mmol) in CH₂Cl₂ (10 mL) was added dropwise. The resulting mixture was stirred overnight at r.t., and subsequently washed with NaHCO₃ (sat.), citric acid (0.6 M), and brine. After drying over Na₂SO₄, the organic phase was evaporated under reduced pressure. The crude product was purified by column chromatography using CH₂Cl₂/CH₃OH 97:3 (v/v) as the eluent, affording adsorbate **9** as a colorless viscous oil. Yield 0.38 g (66%). ¹H NMR: δ (ppm) 6.86 (d, *J* = 2.1 Hz, 4 H, Ar H), 6.71 (t, *J* = 5.4 Hz, 2 H, NH), 6.51 (t, *J* = 2.1 Hz, 2 H, Ar H), 6.05-6.03 (m, 3 H, Ar H), 4.57 (br s, 4 H, NH), 4.02 (t, *J* = 5.4 Hz, 4 H, CH₂O), 3.92 (t, *J* = 6.0 Hz, 8 H, CH₂O), 3.84 (t, *J* = 6.0 Hz, 2 H, CH₂O), 3.59 (q, *J* = 5.4 Hz, CH₂N), 3.11 (t, *J* = 6.3 Hz, 8 H, CH₂N), 2.48 (t, *J* = 7.5 Hz, 4 H, CH₂S), 2.06 (quint, *J* = 6.0 Hz, OCH₂CH₂CH₂N), 1.80-1.24 (m, 94 H, CH₂), 0.86 (t, *J* = 6.6 Hz, 3 H, CH₃). ¹³C NMR: δ (ppm) 174.7, 166.9, 160.6, 159.9, 159.7, 155.5, 136.2, 104.8, 103.9, 93.8, 93.4, 78.7, 67.5, 66.0, 40.1, 37.5, 31.7, 31.4, 29.3-28.3, 27.9, 25.5, 22.8, 22.1, 13.6. FAB MS *m/z* 1580.5 ([M + H]⁺, calcd for C₈₇H₁₄₆N₆O₁₇S: 1580.0).

Adsorbate 1. Adsorbate **9** (100 mg, 0.063 mmol) was dissolved in CH₂Cl₂ (35 mL) and TFA (1.75 mL) was added. The solution was stirred at r.t. for 15 min, and subsequently the solvent was evaporated *in vacuo*. The crude deprotected product (obtained as the trifluoroacetate salt) was thoroughly dried under reduced pressure for 3 h. After dissolving it in a mixture of CH₂Cl₂ (40 mL) and MeOH (5 mL), *N,N*-diisopropylethylamine (170 μL, 0.976 mmol) was added in order to convert the quaternary ammonium salts into amines. Subsequently, isonicotinic acid (47 mg, 0.382 mmol), 1-hydroxybenzotriazole hydrate (52 mg, 0.385 mmol), and 1-(3-dimethylaminopropyl)-3-ethyl-carbodiimide hydrochloride (EDC, 73 mg, 0.381 mmol) were added. After stirring this mixture overnight at r.t., the solvents were evaporated *in vacuo*, the crude product was taken up in CH₂Cl₂, washed with brine, and dried over Na₂SO₄. The crude product was purified by preparative thin layer chromatography using CH₂Cl₂/MeOH/NH₄OH (25% aq. solution) 91:9:0.5 (v/v/v) as the eluent, affording the pure product as a colorless thick oil. Yield 53 mg (52%). ¹H NMR: δ (ppm) 8.63 (d, *J* = 6.0 Hz, 8 H, α-pyr H), 7.64 (d, *J* = 6.0 Hz, 8 H, β-pyr H), 7.37 (t, *J* = 5.7 Hz, 4 H, NH), 7.33 (t, *J* = 5.7 Hz, 2 H, NH), 6.84 (d, *J* = 2.1 Hz, 4 H, Ar H), 6.43 (t, *J* = 2.1 Hz, 2 H, Ar H), 6.01 (d, *J* = 2.1 Hz, 2 H, Ar H), 5.95 (t, *J* = 2.1 Hz, 1 H, Ar H), 3.97 (t, *J* = 5.4 Hz, 4 H, CH₂O), 3.85-3.81 (m, 10 H, CH₂O), 3.59 (q, *J* = 5.7 Hz, 4 H, CH₂N), 3.41 (q, *J* = 5.7 Hz, 8 H, CH₂N), 2.47 (t, *J* = 7.5 Hz, 4 H, CH₂S), 2.04 (quint, *J* = 5.7 Hz, 4 H, OCH₂CH₂CH₂N), 1.76-1.24 (m, 58 H, CH₂), 0.86 (t, *J* = 6.6 Hz, 3 H, CH₃). ¹³C NMR: δ (ppm) 167.2, 165.2, 159.9, 159.7, 149.8, 141.3, 136.2, 120.6, 104.9, 104.0, 93.6, 67.2, 66.0, 39.5, 37.6, 31.7, 31.3, 29.2-28.0, 25.5, 22.8, 22.1, 13.6. FAB MS *m/z* 1600.3 ([M + H]⁺, calcd for C₉₁H₁₂₇N₁₀O₁₃S: 1599.9).

Br₄-[G2]-pincer ligand 11. A mixture of Br₄-[G2]-Br **10** (0.80 g, 0.71 mmol), 3,5-bis(phenylthiomethyl)phenol (0.24 g, 0.71 mmol), K₂CO₃ (0.20 g, 1.45 mmol), and 18-crown-6 (0.02 g, 0.08 mmol) in acetone (150 mL) was refluxed overnight under an argon atmosphere. After evaporation of the solvent *in vacuo*, the residue was taken up in CH₂Cl₂ (200 mL) and washed with brine (200 mL). After drying over Na₂SO₄ and evaporation of the solvent *in vacuo*, the crude product was purified by column chromatography (eluent: CH₂Cl₂/hexane 70:30 (v/v)), to afford a white solid. Yield 0.91 g (93%).

M.p. 79-80 °C. ^1H NMR: δ (ppm) 7.48 (d, $J = 8.4$ Hz, 8 H, Ar H), 7.26 (d, $J = 8.4$ Hz, 8 H, Ar H), 7.23-7.15 (m, 10 H, SPh H), 6.82 (s, 1 H, Ar_{pinc} H), 6.78 (s, 2 H, Ar_{pinc} H), 6.64 (d, $J = 2.2$ Hz, 4 H, Ar H), 6.62 (d, $J = 2.4$ Hz, 2 H, Ar H), 6.51-6.49 (m, 3 H, Ar H), 4.96 (s, 12 H, CH₂O), 4.87 (s, 2 H, CH₂O), 4.01 (s, 4 H, CH₂S). ^{13}C NMR: δ (ppm) 159.44, 159.38, 158.3, 138.9, 138.7, 135.2, 131.2, 129.4, 128.6, 128.3, 125.9, 121.6, 121.4, 113.6, 105.9, 101.1, 69.5, 68.8, 38.5. FAB MS m/z 1381.1 ($[\text{M} + \text{H}]^+$, calcd 1381.0). Anal. calcd for C₆₉H₅₆Br₄O₇S₂: C, 60.01; H, 4.09; S, 4.64. Found: C, 59.72; H, 4.05; S, 4.64.

SCS Pd^{II} pincer dendron 12. To a solution of the Br₄-[G2]-pincer ligand **11** (0.40 g, 0.29 mmol) in CHCl₃ (50 mL) was added a solution of K₂PdCl₄ (104 mg, 0.32 mmol) and NaOAc (26 mg, 0.32 mmol) in H₂O (50 ml). The two-phase mixture was refluxed for 3 h and subsequently filtered over Hyflo. The organic phase was washed with brine and dried over Na₂SO₄. After evaporation of the solvent *in vacuo*, the crude product was purified by column chromatography (eluent: CH₂Cl₂/acetone 97:3 (v/v)), to afford a yellow solid. Yield 0.37 g (84%). M.p. 86-88 °C. ^1H NMR: δ (ppm) 7.83-7.79 (m, 4 H, SPh H), 7.47 (d, $J = 8.4$ Hz, 8 H, Ar H), 7.36-7.34 (m, 6 H, SPh H), 7.25 (d, $J = 8.4$ Hz, 8 H, Ar H), 6.62-6.58 (m, 8 H, Ar H + Ar_{Pd} H), 6.49-6.48 (m, 3 H, Ar H), 4.96 (s, 8 H, CH₂O), 4.94 (s, 4 H, CH₂O), 4.88 (s, 2 H, CH₂O), 4.51 (br s, 4 H, CH₂S). ^{13}C NMR: δ (ppm) 159.5, 159.4, 156.1, 151.6, 149.6, 138.8, 138.7, 135.2, 131.8, 131.2, 130.9, 129.3, 129.1, 128.5, 121.5, 108.6, 105.9, 105.8, 101.1, 69.5, 69.3, 68.8, 51.3. FAB MS m/z 1486.9 ($[\text{M} - \text{Cl}]^+$, calcd 1486.4). Anal. calcd for C₆₉H₅₅Br₄ClO₇S₂Pd: C, 54.46; H, 3.64; S, 4.21. Found: C, 54.20; H, 3.53; S, 3.99.

Isothiocyanate dendron 14. To a solution of Br₄-[G2]-NH₂ (0.45 g, 0.42 mmol) in CH₂Cl₂ (50 mL) were added thiophosgene (0.04 mL, 0.52 mmol) and NEt₃ (0.08 mL, 0.58 mmol). After stirring at r.t. for 1.5 h, the solution was washed with brine and dried over Na₂SO₄. After evaporation of the solvent *in vacuo*, the crude product was purified by column chromatography using CH₂Cl₂/hexane 60:40 (v/v) as the eluent to afford dendron **14** as a slightly yellow solid. Yield 0.31 g (66%). M.p. 82-83 °C. ^1H NMR: δ (ppm) 7.48 (d, $J = 8.4$ Hz, 8 H, Ar H), 7.26 (d, $J = 8.4$ Hz, 8 H, Ar H), 6.62 (d, $J = 2.2$ Hz, 4 H, Ar H), 6.51-6.49 (m, 5 H, Ar H), 4.98 (s, 8 H, CH₂O), 4.96 (s, 4 H, CH₂O), 4.61 (s, 2 H, CH₂NCS). ^{13}C NMR: δ (ppm) 159.6, 159.4, 138.6, 136.0, 135.2, 131.2, 128.6, 121.4, 105.8, 105.4, 101.4, 101.2, 69.4, 68.8, 48.1. FAB MS m/z 1102.2 ($[\text{M} + \text{H}]^+$, calcd 1102.6). Anal. calcd for C₅₀H₃₉Br₄NO₆S: C, 54.42; H, 3.57; N, 1.27; S, 2.91. Found: C, 54.37; H, 3.62; N, 1.40; S, 2.61.

Br₄-[G2]-CO₂Me. A mixture of Br₂-[G1]-Br **16** (0.83 g, 1.53 mmol), methyl resorcyate **3** (0.13 g, 0.77 mmol), K₂CO₃ (0.27 g, 1.95 mmol), and 18-crown-6 (0.04 g, 0.15 mmol) in acetone (100 mL) was refluxed overnight under an argon atmosphere. After evaporation of the solvent under reduced pressure, the crude solid was taken up in CH₂Cl₂ and washed with brine, followed by drying over Na₂SO₄. After evaporation of the solvent, the crude product was purified by column chromatography using CH₂Cl₂/hexane 70:30 (v/v) as the eluent to afford Br₄-[G2]-CO₂Me as a white solid. Yield 0.50 g (59%). M.p. 118-119 °C. ^1H NMR: δ (ppm) 7.49 (d, $J = 8.4$ Hz, 8 H, Ar H), 7.26 (d, $J = 8.4$ Hz, 8 H, Ar H), 7.26 (d, $J = 2.4$ Hz, 2 H, Ar H), 6.73 (t, $J = 2.4$ Hz, 1 H, Ar H), 6.64 (d, $J = 2.1$ Hz, 4 H, Ar H), 6.50 (t, $J = 2.1$ Hz, 2 H, Ar H), 4.99 (s, 4 H, CH₂O), 4.97 (s, 8 H, CH₂O), 3.91 (s, 3 H, CH₃). ^{13}C NMR: δ (ppm) 166.1, 159.4, 159.1, 138.5, 135.2, 131.6, 131.2, 128.6, 121.4, 107.9, 106.6, 105.9, 101.2, 69.5, 68.8, 51.8. FAB

MS m/z 1089.1 ($[M + H]^+$, calcd 1089.5). Anal. calcd for $C_{50}H_{40}Br_4O_8$: C, 55.17; H, 3.70. Found: C, 55.10; H, 3.70.

Carboxylic acid dendron 15. A solution of Br_4 -[G2]-CO₂Me (0.42 g, 0.39 mmol) and KOH (0.11 g, 1.96 mmol) in a mixture of THF (20 mL), MeOH (30 mL), and H₂O (10 mL) was refluxed for 2.5 h. After cooling, acetic acid was added until pH = 5. The solvents were evaporated under reduced pressure, and subsequently the crude solid was taken up in EtOAc and washed with brine. After evaporation of the solvent, the product was purified by trituration with MeOH, affording a white solid. Yield 0.35 g (84%). M.p. 181-183 °C. ¹H NMR (DMSO-*d*₆): δ (ppm) 13.05 (br s, 1 H, CO₂H), 7.56 (d, *J* = 8.4 Hz, 8 H, Ar H), 7.37 (d, *J* = 8.4 Hz, 8 H, Ar H), 7.14 (d, *J* = 2.4 Hz, 2 H, Ar H), 6.89 (t, *J* = 2.4 Hz, 1 H, Ar H), 6.71 (d, *J* = 2.1 Hz, 4 H, Ar H), 6.61 (t, *J* = 2.1 Hz, 2 H, Ar H), 5.07 (s, 12 H, CH₂O). ¹³C NMR (DMSO-*d*₆): δ (ppm) 166.8, 159.3, 159.2, 139.2, 136.3, 132.8, 131.2, 129.7, 120.9, 108.0, 106.5, 101.1, 69.1, 68.4. FAB MS m/z 1075.2 ($[M + H]^+$, calcd 1075.5). Anal. calcd for $C_{49}H_{38}Br_4O_8$: C, 54.78; H, 3.56. Found: C, 54.95; H, 3.41.

8.6 References and notes

- ¹ Zhang, L.; Bo, Z. S.; Zhao, B.; Wu, Y. Q.; Zhang, X.; Shen, J. C. *Thin Solid Films* **1998**, *329*, 221.
- ² a) Zhou, Y. F.; Bruening, M. L.; Bergbreiter, D. E.; Crooks, R. M.; Wells, M. J. *Am. Chem. Soc.* **1996**, *118*, 3773; b) Zhao, M.; Zhou, Y. F.; Bruening, M. L.; Bergbreiter, D. E.; Crooks, R. M. *Langmuir* **1997**, *13*, 1388.
- ³ Weck, M.; Jackiw, J. J.; Rossi, R. R.; Weiss, P. S.; Grubbs, R. H. *J. Am. Chem. Soc.* **1999**, *121*, 4088.
- ⁴ van Manen, H.-J.; Nakashima, K.; Shinkai, S.; Kooijman, H.; Spek, A. L.; van Veggel, F. C. J. M.; Reinhoudt, D. N. *Eur. J. Inorg. Chem.* **2000**, 2533-2540.
- ⁵ Klopsch, R.; Koch, S.; Schlüter, A. D. *Eur. J. Org. Chem.* **1998**, 1275.
- ⁶ a) Mulders, S. J. E.; Brouwer, A. J.; van der Meer, P. G. J.; Liskamp, R. M. J. *Tetrahedron Lett.* **1997**, *38*, 631; b) Brouwer, A. J.; Mulders, S. J. E., Liskamp, R. M. J. *Eur. J. Org. Chem.* **2001**, 1903.
- ⁷ Lee and Miller *J. Org. Chem.* **1983**, *48*, 24.
- ⁸ While this work was in progress, dendritic Fréchet wedges having focal NCN pincer complexes were reported: Albrecht, M.; Hovestad, N. J.; Boersma, J.; van Koten, G. *Chem. Eur. J.* **2001**, *7*, 1289.
- ⁹ Wooley, K. L.; Hawker, C. J.; Fréchet, J. M. J. *J. Chem. Soc., Perkin Trans. 1* **1991**, 1059.
- ¹⁰ Huck, W. T. S.; van Veggel, F. C. J. M.; Reinhoudt, D. N. *J. Mater. Chem.* **1997**, *7*, 1213.
- ¹¹ a) Kickham, J. E.; Loeb, S. J.; Murphy, S. L. *Chem. Eur. J.* **1997**, *3*, 1203; b) Cameron, B. R.; Loeb, S. J.; Yap, G. P. A. *Inorg. Chem.* **1997**, *36*, 5498; c) Kickham, J. E.; Loeb, S. J. *Inorg. Chem.* **1995**, *34*, 5656.
- ¹² Determined with WebLab Viewer 4. For a demo version of this molecular visualization program, see: <http://www.msi.com>.
- ¹³ *The Chemistry of Cyanates and Their Thio Derivatives; The Chemistry of Functional Groups*; Patai, S. (Ed.); John Wiley & Sons: Chichester, 1977.
- ¹⁴ Chechik, V.; Crooks, R. M.; Stirlin, C. J. M. *Adv. Mater.* **2000**, *12*, 1161.
- ¹⁵ Using the chemical shift of the *ortho*-protons of the peripheral phenyl rings as a probe for steric interactions was first discussed by Fréchet and coworkers, see ref. 9.

- ¹⁶ Friggeri, A.; Schönherr, H.; van Manen, H.-J.; Huisman, B.-H.; Vancso, G. J.; Huskens, J.; van Veggel, F. C. J. M.; Reinhoudt, D. N. *Langmuir* **2000**, *16*, 7757.

Summary

This thesis deals with the synthesis of functional metallodendrimers constructed *via* non-covalent metal-ligand interactions. Metallodendrimers that exhibit a particular function *in solution* have been described in the first part of this thesis, whereas the second part is devoted to the isolation, visualization, and growth of (metallo)dendrimers *on a gold surface*.

Chapter 1 briefly outlines the need for “bottom up” strategies in miniaturization of devices. In particular the role of self-assembly as a paradigm in nanotechnology has been discussed. In addition, the contents of every chapter of this thesis have been summarized.

A literature overview of metallodendrimers has been provided in chapter 2. Dendrimers in which the metals are not essential for maintaining the branched dendritic architecture have been excluded from this review. Properties that may provide future applications have been emphasized.

Chapter 3 starts with an overview of transition metal pincer systems in supramolecular chemistry and catalysis. Subsequently, the coordination chemistry of SCS Pd^{II} pincer systems has been discussed in depth. It was found that the relative coordination strengths of several ligands to SCS Pd^{II} pincers are as follows: MeCN < (substituted) pyridines < thioureas < phosphines. The electronic effect of pyridine *para*-substituents on the coordination strength can be described adequately by the Hammett equation. The knowledge obtained from the work described in this chapter has been of crucial importance in the research that has been discussed in subsequent chapters.

A brief overview of the role of coordination chemistry in self-assembly has been given in chapter 4, followed by a detailed discussion of the construction of hybrid covalent-noncovalent “layer block” metallodendrimers. First, the synthesis of covalent Fréchet dendrons functionalized at the focal point with phosphines has been described. Starting from these hydrophobic dendritic wedges, convergent dendritic growth using building blocks with ligands of different coordination strength led to the desired “layer block” metallodendrimers. The structural integrity of the synthesized metallodendrimers was proven by a combination of NMR spectroscopy and MALDI-TOF mass spectrometry. NMR relaxation time constants (T_1) were shown to be effective probes for the mobility of methyl protons located in the dendrimer core. The introduction of a hydrophobic shell around the metallodendrimers dramatically enhances their solubility in apolar solvents and facilitates their characterization.

The encapsulation of a fluorescent switch by a metallodendritic shell has been discussed in chapter 5. The switching behavior originates from the ring opening of a rhodamine B spirolactam moiety and the ring closure of the corresponding rhodamine B amide by acid and base, respectively. Four rhodamine B spirolactam derivatives of varying size were synthesized, and their trifluoroacetic acid-induced ring opening, as followed by UV-Vis and fluorescence

spectroscopy, was studied. Both ring opening and closure can be described by a first order reaction. The rate of ring opening depends on the dendrimer size, the first order rate constants ranging from 10.9×10^{-4} to $1.8 \times 10^{-4} \text{ s}^{-1}$ in going from the smallest to the largest dendrimer. The increasing hydrophobicity of the environment around the rhodamine B core, as imposed by the dendrimer framework, is probably responsible for this. The corresponding triethylamine-induced ring closure is much faster for all four rhodamine B derivatives. Finally, tapping mode atomic force microscopy (TM-AFM) experiments of the rhodamine B dendrimers, deposited on a surface, have briefly been discussed. Isolated features with heights up to 8 nm (for the largest dendrimer) were observed after evaporation of dilute dendrimer solutions on a silicon oxide substrate.

Water-soluble, non-covalent Pd^{II} pincer assemblies form the subject of chapter 6. The strategy for rendering the hydrophobic pincer systems water soluble relies on the introduction of peripheral ligands that contain carbohydrate or tetraethyleneglycol chains. Both pyridine and phosphine ligands were functionalized with such chains, and their coordination to mono-, di-, tri-, and hexapincers has been described in detail. The assemblies were characterized by NMR spectroscopy and MALDI-TOF mass spectrometry in acetonitrile and water. In one case an aqueous gel was obtained. In general, assemblies having peripheral tetraethyleneglycol chains display a higher solubility in water than those containing carbohydrates. A possible application for these systems is as recyclable, water-soluble catalysts, to be separated from reaction mixtures *via* nanofiltration methods.

The isolation and visualization of (metallo)dendrimers on a gold surface has been described in chapter 7. The functionalization of (metallo)dendrimers with a dialkylsulfide chain enables them to be inserted into preformed alkylthiol self-assembled monolayers (SAMs) on gold. In this way the dendrimers were spatially isolated from each other, as demonstrated by TM-AFM experiments. Reference experiments confirmed that the dialkylsulfide chain is essential for surface-confinement. Pyridine complexes of SCS Pd^{II} pincers, embedded as isolated species into decanethiol SAMs, were visualized by exchange of the pyridine ligands for nanosize dendritic wedges having focal phosphine groups. Before the exchange no features bulging out of the monolayer were found by TM-AFM, whereas after exchange features with heights of approximately 4 nm were observed.

A next level of sophistication in the growth of large dendritic assemblies on gold has been described in chapter 8. In contrast to the strategy reported in chapter 7, the *starting* molecules for growth on a surface are nanosize dendrimers. Therefore they could already be imaged by TM-AFM. These isolated dendrimers were grown on the surface into larger dendritic structures by coordination chemistry. The peripheral pyridines of the starting dendrimers were coordinated to dendritic wedges having focal SCS Pd^{II} pincer moieties. TM-AFM experiments after growth showed that the isolated features had indeed increased in size, although a wide distribution of heights (3.1 to 7.5 nm) was obtained. This suggests that the number of wedges coordinated to the starting adsorbates may vary among the surface-confined dendrimers.

The results described in this thesis show that the SCS Pd^{II} pincer moiety is a versatile motif in coordination chemistry. The advantages of employing metal-ligand interactions instead of covalent reactions in the growth of nanosize architectures are evident. Both the pincers and the ligands coordinated to them are conveniently functionalized (with, for example, fluorescent dyes or dialkylsulfides and water-solubilizing ethyleneglycol chains, respectively), and this combination leads to functional (dendritic) assemblies which may be used as “bottom up” alternatives in nanotechnology.

Samenvatting

Dit proefschrift beschrijft de synthese van functionele metallodendrimeren die zijn opgebouwd via niet-covalente metaal-ligand interacties. Metallodendrimeren die een bepaalde functie *in oplossing* bezitten zijn in het eerste deel van dit proefschrift beschreven, terwijl het tweede deel de isolatie, visualisatie en groei van (metallo)dendrimeren *op een goudoppervlak* omvat.

De noodzaak voor “bottom up” strategieën in de miniaturisatie van apparaten is kort in hoofdstuk 1 uiteengezet. In het bijzonder is de rol van zelf-assemblage in nanotechnologie besproken. Ook is de inhoud van elk hoofdstuk van dit proefschrift kort samengevat.

Hoofdstuk 2 geeft een literatuuroverzicht van metallodendrimeren. Dendrimeren waarin de metalen niet essentieel zijn voor het handhaven van de vertakte dendritische structuur zijn uit dit overzicht gelaten. Eigenschappen die tot toekomstige toepassingen kunnen leiden zijn benadrukt.

Een overzicht van de rol van “pincersystemen”, gebaseerd op overgangsmetalen, in de supramoleculaire chemie en katalyse is in het begin van hoofdstuk 3 gegeven. Daarna is de coördinatiechemie van SCS Pd^{II} pincersystemen in detail besproken. De relatieve coördinatiesterkte van verscheidene liganden ten opzichte van SCS Pd^{II} pincers is als volgt: MeCN < (gesubstitueerde) pyridines < thioureums < fosfines. Het elektronische effect van *para*-substituenten op de coördinatiesterkte van pyridines kan adequaat door de Hammettvergelijking beschreven worden. De kennis vergaard met het werk dat in dit hoofdstuk is beschreven is onontbeerlijk gebleken in het onderzoek dat in de volgende hoofdstukken is beschreven.

Een kort overzicht van de rol die coördinatiechemie speelt in zelf-assemblage is in hoofdstuk 4 gegeven, gevolgd door een uitgebreide bespreking van de opbouw van hybride covalente/niet-covalente “laag blok” metallodendrimeren. De synthese van covalente Fréchet-dendrimeren die aan het uiteinde uitgerust zijn met fosfines is eerst beschreven. Convergente dendritische groei, uitgaande van deze hydrofobe dendrimeren en gebruik makend van bouwstenen met liganden van verschillende coördinatiesterkte, heeft tot de gewenste “laag blok” metallodendrimeren geleid. De structurele integriteit van de gesynthetiseerde metallodendrimeren is bewezen met een combinatie van NMR spectroscopie en MALDI-TOF massaspectrometrie. Aangetoond is dat NMR relaxatietijdconstanten (T_1) effectieve sondes zijn om de mobiliteit van methylprotonen in de kern van de dendrimeren vast te stellen. De introductie van een hydrofobe laag om de metallodendrimeren vergroot hun oplosbaarheid in apolaire oplosmiddelen en vergemakkelijkt hun karakterisering.

Hoofdstuk 5 beschrijft de inkapseling van een fluorescente schakel in een metallodendritische structuur. Het schakelgedrag ontstaat door de ringopening van een rhodamine B spirolactamderivaat en de ringsluiting van het resulterende rhodamine B amide

door middel van behandeling met respectievelijk zuur en base. Vier rhodamine B derivaten van verschillende grootte zijn gesynthetiseerd, en hun ringopening met trifluorazijnzuur is gevolgd met UV-Vis en fluorescentiespectroscopie. Zowel de ringopening als ringsluiting kunnen worden beschreven met een eerste orde reactie. De ringopeningsnelheid hangt af van de dendrimeergrootte, waarbij de eerste orde snelheidsconstante varieert van 10.9×10^{-4} voor het kleinste tot $1.8 \times 10^{-4} \text{ s}^{-1}$ voor het grootste dendrimeer. De toenemende hydrofobiciteit om de rhodamine B kern, opgelegd door de dendritische architectuur, is waarschijnlijk verantwoordelijk voor dit gedrag. De ringsluiting met triethylamine is veel sneller voor alle derivaten. Tot slot zijn de rhodamine B dendrimeren op een oppervlak bestudeerd met atomairekrachtmicroscopie. Geïsoleerde deeltjes met hoogtes tot 8 nm (voor de grootste dendrimeren) zijn waargenomen na verdamping van verdunde dendrimeeroplossingen op een siliciumoxidesubstraat.

Wateroplosbare, niet-covalente Pd^{II} pincerassenblages zijn het onderwerp van hoofdstuk 6. De strategie om de hydrofobe pincersystemen wateroplosbaar te krijgen berust op de invoering van liganden die suiker- of tetraethyleenglycolketens bevatten aan de buitenkant van de assemblages. Zowel pyridine- als fosfineliganden zijn gefunctionaliseerd met dergelijke ketens, en hun coördinatie aan mono-, di-, tri-, en hexapincersystemen is in detail beschreven. De assemblages zijn gekarakteriseerd met NMR spectroscopie en MALDI-TOF massaspectroscopie in acetonitril en water. Een gel in water is verkregen door een hexapincersysteem uit te rusten met 6 suikerketens. Over het algemeen zijn de assemblages met tetraethyleenglycolketens beter in water oplosbaar dan degene met suikerketens. Een mogelijke toepassing voor dit soort systemen is hun gebruik als herwinbare, wateroplosbare katalysatoren die van reactiemengsels gescheiden kunnen worden door middel van nanofiltratie.

De isolatie en visualisatie van (metallo)dendrimeren op een goudoppervlak is beschreven in hoofdstuk 7. Door (metallo)dendrimeren uit te rusten met een dialkylsulfideketen kunnen ze opgenomen worden in voorgevormde monolagen van alkylthiolen op goud. Op deze manier worden de dendrimeren van elkaar geïsoleerd, hetgeen door atomairekrachtmicroscopie is aangetoond. Controle-experimenten hebben bevestigd dat de dialkylsulfideketen noodzakelijk is voor de verankering aan het oppervlak. Pyridinecomplexen van SCS Pd^{II} pincers die als geïsoleerde moleculen in een decaanthiolmonolaag gezet waren, zijn aangetoond door uitwisseling van de pyridineliganden met dendrimeren gefunctionaliseerd met fosfinegroepen. Voor uitwisseling werden er geen uitstulpende deeltjes van nanometerafmetingen waargenomen met atomairekrachtmicroscopie, terwijl na uitwisseling wel deeltjes met een hoogte van ongeveer 4 nm aangetroffen werden.

Een volgende stap in de ontwikkeling van grote dendritische structuren op goud is in hoofdstuk 8 beschreven. In tegenstelling tot de strategie die in hoofdstuk 7 is toegepast, zijn de moleculen waarmee hier de groei werd begonnen al dendrimeren met nanometerafmetingen. Deze konden met atomairekrachtmicroscopie aangetoond worden (geïsoleerde deeltjes met een hoogte van gemiddeld 3.6 nm). De geïsoleerde dendrimeren zijn op het goudoppervlak met

behulp van coördinatiechemie uitgebouwd tot grotere dendritische structuren. Pyridines aan de buitenkant van de beginnende dendrimeren zijn gecoördineerd aan dendrimeren met SCS Pd^{II} pincergroepen. Atomaire-krachtmicroscopie liet zien dat de geïsoleerde deeltjes inderdaad groter geworden waren, hoewel een brede distributie van hoogtes (3.1-7.5 nm) werd waargenomen. Dit suggereert dat het aantal dendrimeren dat gecoördineerd is aan de beginnende adsorbaten kan variëren.

De resultaten beschreven in dit proefschrift laten zien dat de SCS Pd^{II} pincergroep een veelzijdige functionaliteit in de coördinatiechemie is. De voordelen van het gebruik van metaal-ligand interacties in vergelijking met covalente reacties in de groei van architecturen met nanometerafmetingen zijn evident. Zowel de pincersystemen als de liganden waarmee ze coördineren kunnen eenvoudig gefunctionaliseerd worden (met respectievelijk fluorescente groepen of dialkylsulfides en met ethyleenglycolketens, bijvoorbeeld). Deze combinatie leidt tot functionele (dendritische) assemblages die mogelijk als geschikte “bottom up” alternatieven in de nanotechnologie gebruikt kunnen worden.

